

# Remote assessment of Varroa presence in honey bee colonies using vibration measurements

Harriet Hall



A thesis submitted in partial fulfilment of the requirements of  
Nottingham Trent University for the degree of Doctor of Philosophy

This research programme was carried out in collaboration with  
the University of Warwick

September 2022

## **Copyright statement**

*This work is the intellectual property of the author. You may copy up to 5% of this work for private study, or personal, non-commercial research. Any re-use of the information contained within this document should be fully referenced, quoting the author, title, university, degree level and pagination. Queries or requests for any other use, or if a more substantial copy is required, should be directed in the owner(s) of the Intellectual Property Rights.*

## **Resulting publications**

Hall, H., Bencsik, M., Newton, M., Chandler, D., Prince, G., and Dwyer, S., 2021. *Varroa destructor* mites regularly generate ultra-short, high magnitude vibrational pulses. *Entomologia generalis*, **43**(2), pp.375-388.

Hall, H., Bencsik, M., Newton, M., 2022. Automated, non-invasive *Varroa* mite detection by vibrational measurements combined with machine learning. Submitted for peer review.

## **Digital information**

All video and audio data associated with this thesis have individual DOI links for online access.

## **Collaboration information**

I declare that this thesis was composed by myself and that the work contained herein is my own.

The University of Warwick contributed to the completion of this work by offering additional, *Varroa* infested honey bee colonies at an apiary at their Wellesbourne Campus site. They organised the building of a shed to house a second observation hive. These colonies were used by me for the collection of individual honey bee and full colony behavioural and vibrational data, which contributed to chapter 4 in this thesis. The collaborating partners, David Chandler, Gillian Prince, and Scott Dwyer also offered their thoughts and advice on the first publication that resulted from the work carried out in this thesis.

# Abstract

Honey bee colony monitoring techniques that use hive-based sensors to continuously and remotely measure a range of parameters are increasingly being published. Non-invasive surveillance methods for the identification of *Varroa destructor* presence and infestation levels are, however, not as well-studied. Varroa mites adversely affect honey bees in several ways, and regular monitoring of their population is critical for successful control.

The work carried out in this thesis explores the use of accelerometer sensors and vibration measurements as a non-invasive Varroa detection method. The capture of honey bee vibrations associated with infections of a bee virus (Chronic bee paralysis virus (CBPV)) is also investigated, as Varroa are known to vector approximately 20 honey bee diseases and their associated variants. The answers to three main questions are sought throughout this work: 1) can accelerometers be used to detect vibrations originating from Varroa?, 2) if so, can these vibrations be used as a remote mite monitoring tool?, and 3) do observable honey bee virus symptoms produce detectable vibrations?

To conduct this investigation, accelerometers were attached to a variety of substrates and linked to a camera, for simultaneous video and vibration capture, allowing the characterisation of numerous Varroa and honey bee vibrations. The waveform data was transformed into spectrogram and two-dimensional-Fourier-transform (2DFT) images, which were used as a main analysis tool for vibrational feature identification. Principal component and discriminant function analyses were implemented for the purpose of discriminating between groups of vibrational signals and for automatic detection using machine learning within long-term recordings of freshly collected, capped brood-comb.

This work demonstrates that accelerometers can detect vibrations generated by minute (1-2mm, 0.42mg) mite individuals, and in the process has enabled the discovery of a novel Varroa behaviour (jolting) that produces a unique vibrational trace. Pulses of interest were carefully characterised in terms of their visible features, periodicity, strength, and time duration. These were then used as search tools for mite detection purposes. The exciting discovery of the jolting behaviour strongly suggests that Varroa can transmit functional vibrations. Continuing to investigate and understand this phenomenon may lead, amongst other things, to novel methods of mite control in the future. These explorations showcase the potential for Varroa vibration capture in remote mite monitoring, laying the groundwork for future analysis.

This thesis also demonstrates the many advantages of the lesser used 2DFT image in animal vibration research, promoting its use. In relation to question 3 and the capture of vibrations associated with viral symptoms, no specific vibrational features were identified that could be linked to honey bee trembling, an observable symptom of CBPV. Nevertheless, the results of this chapter (4) promoted the use of 2DFTs in honey bee vibrational monitoring and endorsed solutions for future improvement to this analysis. The 2DFT was also successfully implemented following the discovery of a novel honey bee vibration, here coined the 'purr' (chapter 5).

This work encompasses the pursuit of knowledge in the recently evolved subject of biotremology, to compliment the growing field of remote honey bee colony monitoring, and particularly that of non-invasive *Varroa* detection. A better understanding of both honey bee and *Varroa* behaviours and biology has been established, promoting the importance of vibration research in these closely entwined species. The value and scope of accelerometer use has here been strengthened through the detection of *Varroa* vibrations, supporting its growing application in colony monitoring.

**Key words:** *Varroa destructor*, vibration, honey bee, colony monitoring, automatic detection, 2DFT

# CONTENTS

CHAPTER 1: INTRODUCTION	12
<b>1.1.0. Thesis overview</b>	<b>12</b>
1.1.1. A breakdown of the thesis	12
1.1.2. Core questions	14
<b>1.2.0. Literature review: The study species</b>	<b>14</b>
1.2.1. The biology and life cycle of <i>Varroa destructor</i>	14
1.2.2. Varroa sensory systems and their importance in life cycle regulation	17
1.2.2.1. Chemoreception	17
1.2.2.2. Temperature reception	19
1.2.2.3. Comb structure and its influence on the sensory systems	19
1.2.2.4. Mechanoreception	21
1.2.3. The three types of honey bee in a colony	22
1.2.4. Why the European honey bee is particularly at risk from Varroa infestation	24
<b>1.3.0. Literature review: Mite detection in honey bee hives</b>	<b>27</b>
1.3.1. Current methods of detecting Varroa in honey bee hives	27
1.3.1.1. Sugar roll/shake	27
1.3.1.2. Washing	28
1.3.1.3. Natural mite-fall counts	28
1.3.1.4. Brood uncapping	28
1.3.1.5. CO <sub>2</sub>	28
1.3.2. The advantages and disadvantages of current mite detection methods	28
1.3.3. The move towards the remote monitoring of mites in honey bee colonies	31
1.3.3.1. Gas sensors	31
1.3.3.2. Video detection	32
1.3.3.3. Audio detection	33
1.3.4. Current methods of honey bee colony health status monitoring	33
1.3.4.1. Temperature monitoring	33
1.3.4.2. Hive weight monitoring	34
1.3.4.3. Video monitoring	34
1.3.4.4. Acoustic monitoring	35
1.3.4.5. Lesser-studied monitoring parameters	35
1.3.5. The importance of monitoring vibrations in honey bee colonies	36
1.3.6. How our research group is pioneering honey bee colony monitoring via their vibrations	37
<b>1.4.0. Literature review: The novelties and methodologies of this research</b>	<b>38</b>
1.4.2. How accelerometer sensors can benefit honey bee colony monitoring	38
1.4.1. Measuring vibration: What is an accelerometer?	42
1.4.3. How accelerometers can benefit Varroa monitoring research	44
1.4.4. What this thesis achieves with accelerometer sensors	45
1.4.5. Analysis techniques used in this thesis	46
1.4.5.1. Spectrograms	46
1.4.5.2. Two-dimensional-Fourier-transform (2DFT)	49
1.4.5.3. Principal component analysis	49
1.4.5.4. Discriminant function analysis	50

<b>CHAPTER 2: ACCELEROMETER DETECTION OF VIBRATIONAL PULSES ORIGINATING FROM VARROA INDIVIDUALS</b>	<b>52</b>
<b>2.1.0. Chapter overview</b>	<b>52</b>
<b>2.2.0. Introduction</b>	<b>52</b>
2.2.1. Vibration perception and transmission in Acari	53
2.2.2. Measuring the muscular power required to produce transmitted vibrational signals	54
2.2.3. The potential for Varroa mite engagement in the honey bee colony vibrational environment	55
2.2.4. Main outcomes of this chapter	55
2.2.5. Aims of the chapter	56
<b>2.3.0. Methods</b>	<b>56</b>
2.3.1. Mite collection	56
2.3.2. Measuring the vibrations emitted from Varroa individuals	57
2.3.2.1. The substrates chosen for experimentation	57
2.3.2.2. Accelerometer recording and video set-up	58
2.3.2.3. Examining the video recordings for behaviours of interest	59
2.3.3. Measuring vibrations emitted from other species for comparison against Varroa	60
2.3.3.1. Woodlouse vibration recording	60
2.3.3.2. Honeybee individual and colony recording	60
2.3.4. Estimating the power required by Varroa to produce the jolting pulse	61
2.3.5. Signal analysis of Varroa jolting and walking vibrational pulses	61
2.3.5.1. Method 1: Using the accelerometer waveform	64
2.3.5.2. Method 2: Using individual spectrograms	65
2.3.6. Signal to noise ratio analysis/successful detection of jolting pulses	66
2.3.7. Accelerometer and Petri-dish resonance analysis	66
<b>2.4.0. Results</b>	<b>67</b>
2.4.1. A description of the jolting behaviour	67
2.4.2. Synchronous vibrational/visual assessments of the jolting behaviour	69
2.4.3. The effect of different substrates on the frequency spectrum of the jolting pulse	70
2.4.3.1. Petri-dish	73
2.4.3.2. Brood-comb	74
2.4.3.3. Honeycomb	75
2.4.3.4. Gelatine capsule	76
2.4.4. The effect of different substrates on the acceleration, time duration and decay rates of the jolting pulse	76
2.4.5. Within substrate variations observed in jolting pulses	80
2.4.5.1. Brood-comb	80
2.4.5.2. Petri-dish	81
2.4.5.3. Honeycomb	81
2.4.5.4. Gelatine capsule	82
2.4.6. Comparison of the jolting pulse with the vibrational traces of other species and mite walking behaviour	83
2.4.6.1. Honeybee individual and colony	83
2.4.6.2. Varroa mite walking vibrations	85
2.4.6.3. Woodlouse walking	88
2.4.7. Estimation of pulse power output	90
2.4.8. How detectable are jolting pulses, using accelerometer sensors?	90
2.4.9. Periodicity of the jolting behaviour	91

<b>2.5.0. Discussion</b>	<b>93</b>
2.5.1. Substrate dependent jolting pulse features	95
2.5.2. Successful accelerometer detection of mite signals	96
2.5.3. Application of jolting pulse detection in a real hive	96
2.5.4. Is the jolting pulse a functional signal?	98
2.5.5. Conclusion	99
<b>CHAPTER 3: DETECTION AND DISCRIMINATION OF VARROA VIBRATIONAL PULSES IN THE SPECIES' REPRODUCTIVE PHASE</b>	<b>101</b>
<b>3.1.0. Chapter overview</b>	<b>101</b>
<b>3.2.0. Introduction</b>	<b>102</b>
3.2.1. Why choose the capped brood cell environment for remote detection in a hive?	102
3.2.2. Observing Varroa behaviour in the reproductive phase of its life cycle	103
3.2.3. Two routes of study	103
3.2.4. Aims of the chapter	104
<b>3.3.0. Methods: Study 'a', the discrimination and detection of Varroa vibrational pulses in natural brood cells</b>	<b>105</b>
3.3.1. Brood sample collection	105
3.3.2. Video/accelerometer recordings of the brood samples	105
3.3.3. Signal analysis	106
3.3.3.1. Method 1: Training database creation and discrimination of spectrogram features specific to mite jolting and walking vibrational traces	106
3.3.3.2. Method 1: Principal component/discriminant function analysis of mite jolting and walking spectrograms	108
3.3.3.3. Method 2: Training database creation and discrimination of temporal features specific to mite jolting and walking vibrational traces	109
3.3.3.4. Method 3: Training database creation and discrimination of emerging honeybee and mite vibrational traces (spectrogram)	109
3.3.3.5. Method 4: Training database creation and discrimination of emerging honeybee and mite vibrational traces (2DFT)	110
3.3.3.6. Method 4: Testing the accuracy of the training database (2DFT)	111
3.3.3.7. Method 4: Detecting mite, bee and background vibrations using the brood sample recordings	114
3.3.3.8. Method 4: Trialling additional methods of TDB improvement	114
<b>3.4.0. Methods: Study 'b', observation of Varroa within an artificial brood cell</b>	<b>115</b>
3.4.1. Specimen collection and artificial brood cell creation	115
3.4.2. Visual/vibrational measurement collection	118
3.4.3. Additional video data of a Varroa and a developing bee in a cell	120
3.4.4. Signal analysis	120
3.4.4.1. General analysis of the vibrations captured by the accelerometer	120
3.4.4.2. Video analysis of mite walking vibrations	121
3.4.4.3. Additional video analysis	121
<b>3.5.0. Results: Study 'a', the discrimination and detection of Varroa vibrational pulses in natural brood cells</b>	<b>122</b>
3.5.1. Method 1: Training database creation and discrimination of spectrogram features specific to mite jolting and walking vibrational traces	122

3.5.2. Method 2: Training database creation and discrimination of temporal features specific to mite jolting and walking vibrational traces	123
3.5.3. Method 3: Training database creation and discrimination of emerging honey bee and mite walking vibrational traces (spectrogram)	123
3.5.4. Method 4: Training database creation and discrimination of emerging honey bee and mite walking vibrational traces (2DFT)	126
3.5.5. Method 4: Testing the success of the training data by using recordings that contributed to it	132
3.5.6. Method 4: Testing the success of the training data with novel recordings	134
3.5.7. Method 4: Trialling improvements to the TDB	135
3.5.7.1. Increasing the time window of the 2DFTs	135
3.5.7.2. Background noise removal from the long-term recordings	136
3.5.7.3. Investigation into the anomalous recording	136
<b>3.6.0. Results: Study ‘b’, observation of Varroa within an artificial brood cell</b>	<b>138</b>
3.6.1. Jolting vibrations	138
3.6.2. Mite walking and larval vibrations	138
3.6.3. Other Varroa vibrations observed in the artificial brood cells	142
<b>3.7.0. Discussion</b>	<b>144</b>
3.7.1. The benefits to further investigating Varroa walking vibrations and using 2DFTs	144
3.7.2. Question 1: Can Varroa vibrations be detected in the brood cells?	147
3.7.2.1. The potentially negative impact of walking vibration strength	147
3.7.2.2. The advantage to detecting novel mite vibrations in the artificial cell	148
3.7.2.3. The advantage of optimising the TDB	148
3.7.3. Question 2: Does jolting occur in the reproductive phase?	149
3.7.4. An alternative future direction	150
3.7.5. Conclusion	150
<b>CHAPTER 4: CHARACTERISATION OF CHRONIC BEE PARALYSIS VIRUS VIBRATIONS IN HONEY BEE INDIVIDUALS</b>	<b>152</b>
<b>4.1.0. Chapter overview</b>	<b>152</b>
<b>4.2.0. Introduction</b>	<b>153</b>
4.2.1. Current methods of CBPV diagnosis and the opportunity for its remote detection	154
4.2.2. Aims of the chapter	155
<b>4.3.0. Methods</b>	<b>155</b>
4.3.1. The hive set-up	155
4.3.2. Video/vibrational data collection from the CBPV infected observation colony	158
4.3.3. Visual/vibrational data collection from individually observed bees	159
4.3.4. Defining trembling behaviour	161
4.3.5. Signal analysis: Investigation into the vibrational features of trembling behaviour	162
4.3.5.1. 2DFT images	163
4.3.5.3. Reshaping the 2DFT for further feature extraction	164
4.3.5.4. Stacked 2DFT background subtraction for improved visualisation	166
4.3.5.5. Inspection of 2DFT images for all bee individuals	168
4.3.6. Investigation into the vibrational features of trembling at low frequencies	169
<b>4.4.0. Results</b>	<b>170</b>
4.4.1. A description of CBPV trembling behaviour based upon visual observations	170

4.4.2. The likelihood of observing a CBPV infected bee on the lifted frame of the observation hive	172
4.4.3. Characterisation of trembling behaviour vibrations	172
4.4.3.1. Features seen in the first collection of 2DFT images and 2DFT scrolling images	172
4.4.3.2. Features observed in the stacked 2DFT images	172
4.4.3.3. Inspection of 2DFT images for all bee individuals	175
4.4.4. Principal Component and Discriminant Function analysis of the 2DFT data	177
4.4.5. Investigating the vibrational features in the lowest, missing frequency band	178
<b>4.5.0. Discussion</b>	<b>179</b>
4.5.1. The capture of a new honey bee vibration	180
4.5.2. Why trembling vibrations may not have been captured in this study	181
4.5.3. Identifying trembling bees on the frame of the observation hive	182
4.5.4. Future prospects	183
4.5.4. Conclusion	184
<b>CHAPTER 5: CHARACTERISING THE FEATURES OF A NOVEL HONEY BEE VIBRATIONAL SIGNAL</b>	<b>186</b>
<b>5.1.0. Chapter overview</b>	<b>186</b>
<b>5.2.0. Introduction</b>	<b>187</b>
5.2.1. What vibrational signals have already been captured and characterised?	187
5.2.2. Improving the list of known honey bee vibrational signals	188
5.2.3. Aims of the chapter	188
<b>5.3.0. Methods</b>	<b>188</b>
<b>5.4.0. Results</b>	<b>189</b>
5.4.1. Purr time duration	189
5.4.2. Purr spectral repetition	190
5.4.3. Purr Frequency	192
5.4.4. Purr additional features	192
<b>5.5.0. Discussion</b>	<b>192</b>
5.5.1. The benefits of characterising honey bee vibrations in detail for future research	193
5.5.2. What could the function of the honey bee purr be?	194
5.5.3. Conclusion	194
<b>CHAPTER 6: CONTRIBUTIONS, LIMITATIONS, RECOMMENDATIONS</b>	<b>196</b>
<b>6.1.0. Thesis chapter summary</b>	<b>196</b>
<b>6.2.0. What has this thesis achieved?</b>	<b>197</b>
6.2.1 Answering the core questions	197
6.2.2. The discovery of the jolting pulse	198
6.2.3. Vibration capture as a remote mite detection strategy	199
6.2.4. The implementation of 2DFT images	200
<b>6.3.0. Limitations to the work carried out in this thesis</b>	<b>200</b>
6.3.1. The accelerometer	200
6.3.2. The experimental set-up	200

6.3.3. Mite collection method	201
<b>6.4.0. Future recommendations</b>	<b>202</b>
<b>6.5.0. Conclusion</b>	<b>203</b>
CHAPTER 7: APPENDIX 1	205
CHAPTER 8: APPENDIX 2	211
CHAPTER 9: APPENDIX 3	225
CHAPTER 10: APPENDIX 4	229
REFERENCE LIST	230

# Supplementary Material DOI links

## Appendix 1

S1 = 10.5281/zenodo.7018395

S2 = 10.5281/zenodo.7017001

S3 = 10.5281/zenodo.7018409

S4 = 10.5281/zenodo.7018413

S5 = 10.5281/zenodo.7018418

S6 = 10.5281/zenodo.7018426

S7 = 10.5281/zenodo.7018444

S8 = 10.5281/zenodo.7018585

S12 = 10.5281/zenodo.7018587

S13 = 10.5281/zenodo.7018591

S14 = 10.5281/zenodo.7018613

S15 = 10.5281/zenodo.7018621

S16 = 10.5281/zenodo.7018625

S17 = 10.5281/zenodo.7018632

S18 = 10.5281/zenodo.7018638

## Appendix 2

D11 = 10.5281/zenodo.7018643

D12 = 10.5281/zenodo.7018651

D14 = 10.5281/zenodo.7018656

D18 = 10.5281/zenodo.7018660

D19 = 10.5281/zenodo.7018666

D20 = 10.5281/zenodo.7018674

D21 = 10.5281/zenodo.7018680

D23 = 10.5281/zenodo.7018690

D24 = 10.5281/zenodo.7018694

D25 = 10.5281/zenodo.7018698

D26 = 10.5281/zenodo.7018702

### Appendix 3

T1 = 10.5281/zenodo.7018704

T5 = 10.5281/zenodo.7594416

T6 = 10.5281/zenodo.7594424

T7 = 10.5281/zenodo.7594433

T8 = 10.5281/zenodo.7594439

T9 = 10.5281/zenodo.7594443

T10 = 10.5281/zenodo.7594450

T11 = 10.5281/zenodo.7594467

T12 = 10.5281/zenodo.7594471

### Appendix 4

P1 = 10.5281/zenodo.7018943

P2 = 10.5281/zenodo.7018945

P3 = 10.5281/zenodo.7018947

P4 = 10.5281/zenodo.7018949

# Chapter 1: Introduction

## 1.1.0. Thesis overview

### 1.1.1. A breakdown of the thesis

The overarching aim of this thesis is to investigate whether the *Varroa destructor* mite (Varroa, from here on), a highly important parasite of the European honey bee, can be detected within beehives using accelerometer (vibration) sensors. Whilst the main scope of the Ph.D. (non-invasive detection of Varroa in honey bee hives) remains unchanged, the route of study taken to reach completion has evolved and switched direction due to an exciting behavioural discovery that occurred during the initial stages of research.

When I first embarked on this journey, the intention was to identify Varroa presence in honey bee hives via changes in the behaviour of the bees, resulting from mite infestation (i.e., identifying mite presence indirectly). It was hoped that these changes would produce detectable deviations in the colony vibrational traces picked up by the accelerometers at both population and individual levels.

However, more excitingly (and unexpectedly), I pioneered the use of these sensors in the detection of the Varroa mite itself, i.e., the identification of vibrational traces originating from one individual. Due to the miniscule mass of a mite (0.42mg), versus the mass of the accelerometer (10g), this result was completely unanticipated, and has led me to the discovery of a never-before documented Varroa mite behaviour, which produces a corresponding vibration that has features strongly indicating that it is a functional signal.

It was agreed with the supervisory team that this discovery was an important addition to the program of work that could be achieved within the timeframe of the PhD. The main focus of my research thus turned to the identification of mite infestation in honey bee colonies through the direct detection of the mites' vibrations, rather than their indirect detection resulting from bee behavioural changes.

This thesis encompasses the pursuit of knowledge related to this unexpected, vibrational phenomenon, whilst also investigating the detection of some honey bee behaviours and signals that relate to the monitoring of colony health, remotely.

In the first chapter, I provide a literature review for the thesis, covering the background of the Varroa mite and the negative effects that the species has on the European honey bee. I detail the life cycle of the two organisms: how they are intertwined and the role that mite

sensory systems play in this relationship. I further focus on the role that vibration may play in *Varroa* mechanoreception, and how there is little available research on this topic for the species.

I review the current methods of mite detection in honey bee colonies and turn the reader's attention toward remote monitoring techniques. For honey bee hives, there are a range of technologies employed to non-invasively collect data on various colony parameters, yet mite infestation is not currently well established as one of these. This then leads to a discussion on the technology used in this thesis: the accelerometer - how it has been successfully used in the field so far, and how I aim to adapt the technique to the remote detection of *Varroa* mites.

In chapter two, I discuss in detail the discovery of the novel *Varroa* behaviour and its corresponding vibrational trace. I speculate the possibility that this behaviour and its vibratory trace perform a function for the animal, based on the pulse characteristics found. The promise of detecting these pulses within a fully populated honey bee colony is also discussed, which then leads on to the following chapter.

In chapter three, I investigate whether it is possible successfully to detect the novel *Varroa* pulse of interest and *Varroa* walking vibrations in the brood comb of honey bee colonies using accelerometer sensors. Whilst the previous chapter outlines the features of the vibrational traces outside of the mites' natural environment, this study seeks the capture of mite individuals *in situ*. This endeavour also encompasses a secondary aim, which is to explore whether the novel behaviour occurs when mites are within the capped brood cells and carrying out the reproductive phase of their life cycle. The results of this are examined regarding the possible role of the currently unidentified behaviour/vibration function, alongside its detection potential in honey bee hives.

In chapter four, I discuss an investigation into the identification of honey bee trembling behaviours. Trembling in honey bees is an observable symptom of Chronic bee paralysis virus, an infection that has become more widespread in UK hives since the mid 2000's. I hypothesise that this shaking symptom will produce detectable vibrational traces that differ to those of healthy, non-trembling bee individuals. As mites are known to transmit a variety of diseases to honey bees, as well as exacerbate the negative effects of illness, the aim of this chapter is to establish if it is possible to detect honey bee viruses that result in physiological symptoms, like trembling. This could also be used as an indirect method of identifying *Varroa* presence.

Chapter five is a smaller chapter that covers the characterisation of a novel vibrational trace that is produced by honey bees. The function of this vibration is currently unknown, but I provide a foundation for further investigation into this interesting, previously un-documented pulse that may be a signal of importance to the honey bee.

Chapter six provides an overall discussion of the work covered in this thesis, the significance of the findings and the future research routes that could soon now be taken.

### 1.1.2. Core questions

The thesis aims to address the following main questions:

1. Can accelerometers be used successfully to detect *Varroa destructor* vibrations?
2. Do mite vibrations have the potential to be used as an effective tool in the identification of *Varroa* presence in honey bee colonies?
3. Can observable virus symptoms in honey bees be detected and characterised using accelerometers, and do the results have the potential to be used as an indirect method of detecting *Varroa* presence in colonies?

## 1.2.0. Literature review: The study species

### 1.2.1. The biology and life cycle of *Varroa destructor*

The *Varroa destructor* mite is an ectoparasite of honey bees (Rosenkranz et al., 2010; Nazzi & Le Conte, 2016; Evans & Cook, 2018). Prior to the year 2000, the species was referred to as *Varroa jacobsoni*, until genetic analysis confirmed that *V. destructor* and *V. jacobsoni* are, in fact, two distinct species. The former species originally parasitised the Asian honey bee, *Apis cerana*, but in recent years has successfully moved on to infest the European honey bee, *Apis mellifera* (Anderson & Trueman, 2000). A specific haplotype of the species, known as the Korean strain, is now widespread amongst *A. mellifera* colonies and is found on almost every continent (Rosenkranz et al., 2010; Nazzi & Le Conte, 2016).

*Varroa* mites live in close contact with their honey bee hosts, lacking a free-living stage. Their life cycle is divided into two phases: reproductive (occurring within the honey bee brood cells) and phoretic (where the mite is found on adult bees). During the reproductive phase, an adult female mite enters a cell that contains a honey bee larva, prior to it being capped. She becomes trapped in the larval food at the base of the cell until it is consumed by the developing bee, which triggers the mite to move on to the bee itself. Here, a feeding site is established. The mite lays eggs, and the subsequent offspring feed from the larval wound that is kept open by the mother mite. Once fully moulted, the offspring mate with one

another and the newly impregnated daughter mites leave the cell with the now fully developed bee to enter the phoretic phase and begin the life cycle again. Male mites have a short life span, preventing them from ever leaving the brood cells (Rosenkranz et al., 2010; Nazi & Le Conte, 2016) (see Figure 1.1). This second phase, however, should perhaps no longer be referred to as 'phoretic'. Mites are now known to feed on the fat body (a nutrient rich vital organ) of adult honey bees and do so for several days (Ramsey et al., 2019). As phoresy is a term provided when one species is exclusively used for transportation purposes by another (Houck & O'Connor, 1991), it may no longer be a valid terminology in the case of Varroa mites, as they remain on the adult honey bee host for prolonged periods and feed from them, rather than moving quickly into a new brood cell.

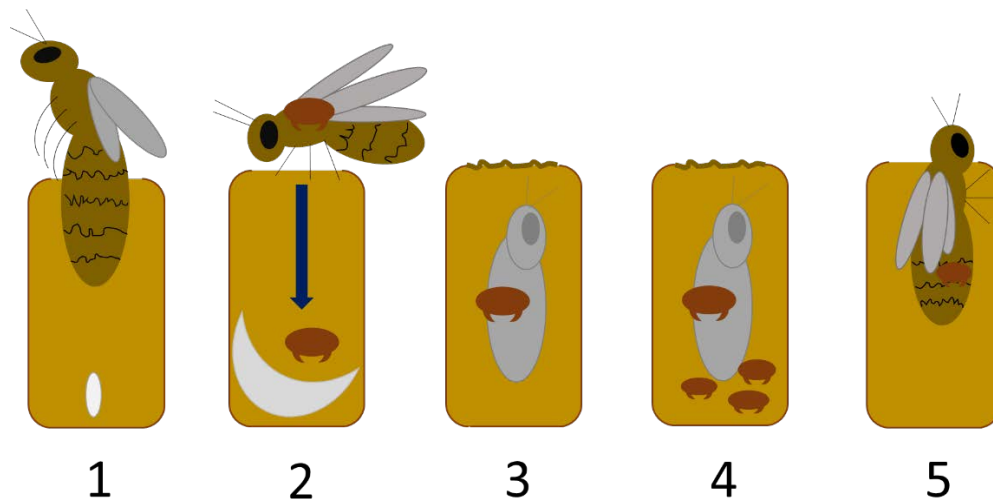


**Figure 1.1:** A simple diagram of the mite and bee life cycle. 1) the queen lays an egg in a brood cell; 2) a nurse bee carrying a female mite in the phoretic phase tends to the growing larva. The mite leaves the bee and enters the cell a few hours prior to capping; 3) now in the reproductive phase, the mite feeds from the developing bee, here shown at an early pupal stage; 4) the mite lays eggs which develop into her offspring. The offspring mate with one another; 5) the newly pregnant female mites leave the cell with the developed bee (back to the phoretic phase) to continue the life cycle. Diagram produced by Harriet Hall.

Physically, male and female mites are very different, but both possess two distinctive body parts: the gnathosoma, which contains the mouthparts, and the idiosoma, which makes up the rest of the body (Evans & Till, 1979). Females are much larger than males, reaching a body length of 1mm and width of 1.5mm (Rosenkranz et al., 2010), whereas males are 0.7mm in length and 0.8mm in width (Häußermann et al., 2015). Females also possess a highly sclerotised, red/brown idiosoma, a feature that is lacking in the softer bodied males

(Rosenkranz et al., 2010) (see Figure 1.2). The morphological features of the female mite enable successful parasitism, as the curved and flattened shape of the idiosoma allow the Varroa to closely fit to the body of the host, and the sclerotised cuticle offers protection from bees who may attempt to remove mites from their bodies (Rath, 1999; Ammar, 2015) (see Figure 1.3). It is also suggested that these features promote access to the feeding sites between the abdominal plates of the honey bee (Ramsey et al., 2019). The legs of the female mite are also adapted to gripping the bee host, although it is contested whether these structures are sucker-like or claw-like (Ramirez & Malavasi, 1991; Ammar, 2015).

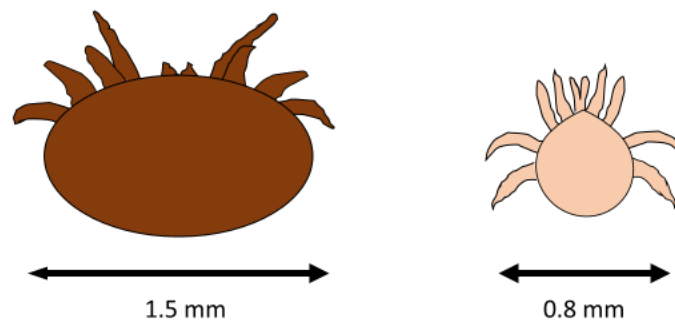


**Figure 1.2:** A simple diagram of the female mite (left) and the male mite (right). The idiosoma encompasses the majority of the Varroa body. The gnathosoma are the central protrusions in between the eight legs. Diagram produced by Harriet Hall.

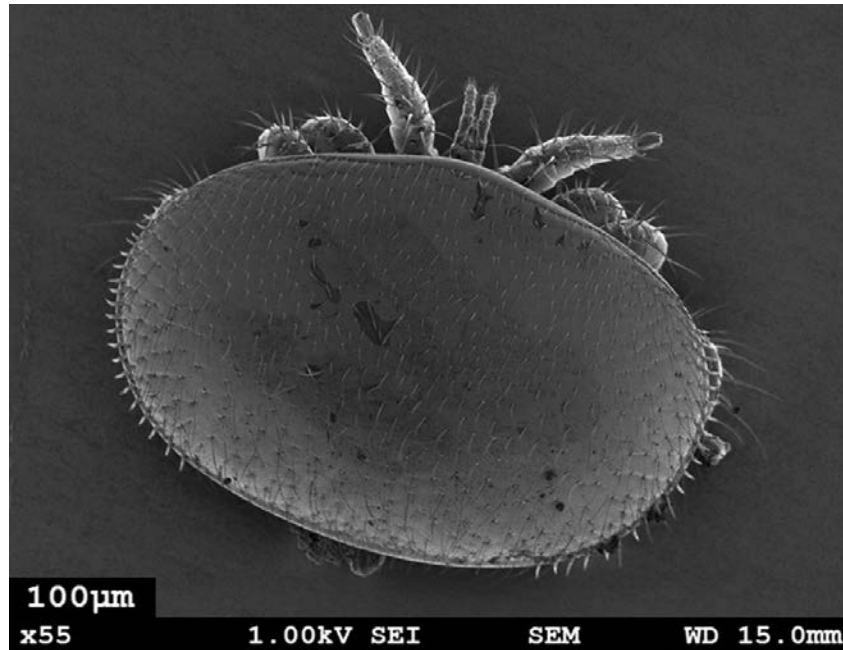


**Figure 1.3:** A scanning electron microscope image of a female Varroa mite. Here, the sclerotised idiosoma can be seen. Photo produced by Harriet Hall.

### 1.2.2. Varroa sensory systems and their importance in life cycle regulation

It is widely accepted that the sensory systems mediate the close relationship that is observed in the life cycle of mite and bee (Rosenkranz et al., 2010; Nazzi & Le Conte, 2016). The following section discusses the most widely studied stimuli that play a role in the orientation of mites to their hosts, and the subsequent regulation of successful parasitisation. Mechanoreception is focused upon as one of the least researched mite sensory modes in this field. There are no published works regarding the role of acoustic stimuli in mite orientation as the species lacks the anatomical features for sensing sound. However, the potential for sound and vibration sensing will be more thoroughly explored in the below sections. Although mites have no eyes, there is one paper that suggests their central nervous system is light sensitive as individuals moved towards sources of this type of stimulus (Kirchner, 1993a). However, this work has not yet been furthered.

#### 1.2.2.1. Chemoreception

Of the Varroa mite sensory systems, the chemical and olfactory are the most well-studied. Female mites can identify different ages, castes, and functions of bees using these systems, and orient to them appropriately. In the phoretic phase, nurse bees are chosen preferentially over other workers (Kraus, 1993; Kuenen & Calderone, 1997; Xie et al., 2016), possibly because they spend significantly more time in the brood-nest (Crailsheim et al., 1996), which

may increase opportunities for mites to move into brood cells. Host preference is also thought to be driven by differences in bee cuticular hydrocarbons and odour, as mites are known to direct themselves significantly more towards those of nurse bees over foragers, and even demonstrate a repellent reaction to forager cues (Pernal et al., 2005; del Piccolo et al., 2010).

To transition into the reproductive phase, mites must then leave the nurse bee and move into a brood cell. For successful invasion of the cell, the mite needs to enter immediately before capping occurs. Orientation to the cell at the correct time is thought to be aided by specific cuticular hydrocarbons that are emitted by the larvae. Depending on larval stage, the levels of each hydrocarbon produced differ, a parameter that is thought to induce mite entry to the cell at the appropriate time, i.e., when the larvae are at 5<sup>th</sup> instar stage (Dillier et al., 2006). *Varroa* favour drone brood, and this infestation preference is also suggested to be mediated by these compounds, as drone larvae produce higher amounts of kairomones that are attractive to mites, and for a longer period of time than worker larvae (Trouiller et al., 1992).

Once in the cell, mites follow a specific pattern of events leading to oviposition, where certain areas of the cell are used for different activities (Donzé & Guerin, 1994). This is expected to be regulated by various stimuli, including chemical (Donzé et al., 1998). Mites are also suggested to synchronise their reproduction with the development of the honey bee larva when in the cell. When introducing mites artificially to cells post-capping, i.e., not in synchrony with larval development, mite reproduction is significantly and negatively affected (Frey et al., 2013). This indicates that there is a specific, short time window during the larva life cycle that triggers the onset of reproduction, most likely linked to volatile larval extracts that positively affect mite fertility (Trouiller & Milani, 1999; Rosenkranz & Garrido, 2004; Frey et al., 2013).

*Varroa* mites also utilise chemical stimuli as a camouflage tool, likely for the purpose of avoiding detection by honey bees (Nation et al., 1992). There are many cuticular hydrocarbons that are shared by mites and their honey bee hosts (Martin et al., 2001; Le Conte et al., 2015), which alter in composition for both species as the bee moves through its developmental stages (Martin et al., 2001). Mites not only match their chemical profile to the life stage of the bee, but also to the one that is specific to the colony, as small differences occur between different colonies (Kather et al., 2015a). The flexibility observed in *Varroa* chemical mimicry is due to the method used by mites to achieve this. Passive transfer of

chemical profile is utilised, where a mite only needs contact with the host cuticular lipid layer for it to adopt the necessary hydrocarbons rapidly (Kather et al., 2015b).

It is widely accepted that Varroa achieve their chemoreceptive abilities through a sensory pit organ located on the front leg tarsi (Dillier et al., 2006; Plettner et al., 2017). This sensilla based structure is thought to be similar to the sensory Haller's organ in ticks (Dillier et al., 2006; Carr & Roe, 2016). The importance of this structure in the chemo-sensing of Varroa individuals has been demonstrated several times through the introduction of inhibitory compounds and odours (Eliash et al., 2014; Singh et al., 2015; Pinnelli et al., 2016; Plettner et al., 2017), and physical blocking of the sensilla (Häußermann et al., 2015; Nganso et al., 2020).

#### *1.2.2.2. Temperature reception*

The sensilla found on the tarsi of Varroa individuals differ from one another, so it is expected that they are not simply limited to chemo-sensing, with alternative sensilla performing different sensory functions (Liu, 1988; Zakaria & Allam, 2009). There are tarsal structures that are thought to be thermal receptors (Carr & Roe, 2016), but there is no further study into whether they do detect temperature or not. Likewise, there are only a few studies that confirm the orientation behaviour of mites towards heat sources (Dillier et al., 2006). From what is known, it appears that Varroa are sensitive to heat, even when faced with subtle temperature changes of 2°C (Le Conte & Arnold, 1988). This ability to identify temperature discrepancies is likely to influence host preference. Mites appear to prefer two day old bees over emerging ones as they produce less heat (Le Conte & Arnold, 1987), and they avoid temperatures over 40°C. This may also indicate why drone brood is chosen more frequently, as the temperature within male brood is slightly lower than that of worker brood (by approximately 0.5°C) (Levin et al., 1990; Kraus et al., 1998; Li et al., 2016), and appears to show a reduced variance in temperature fluctuation as the bee moves through the developmental stages (egg, to larvae, to pupae) when compared to worker brood (Li et al., 2016). Varroa choose temperatures that are optimum for reproduction (Le Conte & Arnold, 1987), so it is highly likely that sensing and orienting to heat sources plays a role in mite life cycle mediation.

#### *1.2.2.3. Comb structure and its influence on the sensory systems*

Chemical and temperature cues appear to be influenced by the structure of the cells that make up the comb. As the larvae develop and grow, the distance between their bodies and the rim of the brood cell decreases (Goetz & Koeniger, 1993). As this distance reduces, there

is an increase in mite attractivity to the cells (Goetz & Koeniger, 1993; Boot et al., 1995; Beetsma et al., 1999; Calis et al., 2006). Also, as the size of the cell opening decreases during capping, mite invasion rates increase (Goetz & Koeniger, 1993). It is therefore likely that there is a specific distance between larva and cell opening that is particularly attractive to mites (Boot et al., 1995), potentially mediated by the sensory systems. That is to say, the heat or volatiles produced by the larvae may be affected by the distance to the cell rim in terms of their strength (Boot et al., 1995; Beetsma et al., 1999), with mites better perceiving the signals at shorter distances.

These cues also tie-in with other structural parameter changes. Cells with rims that are elevated above the rest of the comb indicate that drone larvae are reaching maturity, as younger drone and worker cells lack this physical feature (Kuenen & Calderone, 2000; Calis et al., 2006). Mites have been shown to prefer this structure and infest elevated cells significantly more than non-elevated ones (Kuenen & Calderone, 2000).

Cell width also has an impact on brood invasion rates, with wider cells being preferred (Piccirillo & de Jong, 2003; Maggi et al., 2010a). This may explain why mites prefer to reproduce in drone larvae, as average cell width is larger for drones than workers (Maggi et al., 2010a). However, wider cells are not always chosen. Comb that is newly built from foundation wax has a larger inner cell diameter than old comb (5.15 – 5.3 mm newly built; 4.5 – 4.6 mm older comb). Yet when comparing the two, mites are known to invade the smaller cells in older comb, preferentially. It is possible that this choice is driven by the sensory systems, because old wax may absorb more larval volatiles and it is known that nurse bees spend more time tending to old comb (Piccirillo & de Jong, 2003), both of which may manipulate mite orientation toward older comb as they are attractive to the species. This may also explain why drone larvae, and therefore wider cells, are preferentially chosen. *Varroa* are highly attracted to the volatiles that are produced by drones (Trouiller et al., 1992), and therefore structural parameters such as cell width are likely to be coincidentally preferred, with the choice to invade linked to the chemosensory system rather than the mites ability to perceive cell size.

These findings indicate that there are many interacting parameters that drive the relationship between parasite and host, and these appear to be mediated by a combination of signals that can be detected by the mites' sensory systems.

#### 1.2.2.4. Mechanoreception

Whilst chemical and olfactory stimuli, and the influence of physical comb structure on these are well-studied, and temperature stimuli somewhat studied, the influence of tactile and vibratory stimuli on mite orientation behaviour is more neglected.

It has been stated that Varroa mites lack the mechanism to detect acoustic stimuli and, if it is that they could detect such cues, it would more likely be via mechanoreceptors that can pick up vibratory signals (Dillier et al., 2006). Mechanoreceptors have been identified in Varroa, often described as long, tactile hairs (Liu, 1988; Liu & Peng, 1990; Dillier et al., 2006; Zakaria & Allam, 2009); but there is no experimental evidence to establish the role that these structures play in host orientation or other behaviours.

Other mite species possess setae that are thought to have a mechanoreceptive function, hinting that Varroa mites could also be capable of utilising this sensory system. The setae described for the poultry red mite, *Dermanyssus gallinae* (Soler Cruz et al., 2005), must fulfil a mechanoreceptive purpose, as individuals are known to be receptive to vibrations. It has been demonstrated that mites become active whenever vibratory stimuli are present, linked to host orientation (Kilpinen, 2005). The northern fowl mite, *Ornithonyssus syviarum*, is a species that also uses vibration as a host orientation cue, despite carrying out its full life cycle on its host, like Varroa does. There are several reasons why a mite with this type of life history may require the need for such orientation, such as: (i) it may become dislodged during grooming, (ii) be driven by the benefits of moving to a new host for population expansion, or (iii) require directional signals to orientate on the body of the host (Owen & Mullens, 2004; Murillo & Mullens, 2017).

As with chemical and temperature cues, Varroa mites may additionally use vibrational signals as an orientation aid, not unlike the northern fowl mite. They too, are subject to similar circumstances, despite also living in such close contact with their honey bee host. For example, when grooming, bees can often dislodge mites (Pritchard, 2016) that then fall, sometimes as far as to the bottom of the hive (Fries et al., 1996). Mites may also become inclined to leave the host themselves, e.g., as a result of these grooming attempts. They will then either re-orientate to the original host (Aumeier, 2001), or move on to alternative one (Fries et al., 1996). Mites are also known to freely move between bee hosts (Le Conte & Arnold, 1987), and may even fail to attach to a bee as they emerge from the reproductive phase (Martin, 1998), which could also elicit host re-orientation behaviour. At the hive entrance, mites also frequently leave forager bees to move on to another host (Kralj & Fuchs,

2006), and are even known to leave hosts when they visit flowers, where the mite then waits for another bee to land before parasitising them (Peck et al., 2016). Under these circumstances, it is possible to theorise that Varroa mites may use the lesser-studied sensory systems (vibration/heat) to re-orient to a suitable host. As the species probably possess the suitable receptors for receiving vibratory/tactile signals, it would seem unlikely that they would not use them.

In terms of experimental evidence, there are accounts of Varroa orienting to sources of vibration and demonstrating reactions to mechanical stimuli in the form of air puffs. Mites rapidly respond to clean air puffs by quickly turning in the direction of the source, establishing that a mechanical stimulus can affect their behaviour (Kuenen & Calderone, 1998). Mites have also been shown to orient towards the vibratory signals of bees (Le Conte & Arnold, 1988), strengthening the claim that vibration may be important to this species (Le Conte & Arnold, 1987).

The evidence, albeit limited, suggests that vibration should not be dismissed as a potential regulatory system that is used in the Varroa life cycle. Mites possess hair structures that may be involved in vibratory reception and have been shown to react to mechanosensory stimuli. It would therefore seem important to research and better understand all the mechanisms that may affect the Varroa life cycle, as increased knowledge of the species' biology should lead to improved management of the pest in honey bee colonies.

### 1.2.3. The three types of honey bee in a colony

In this section, I will provide a brief overview of the honey bee colony, to promote better understanding of how and why Varroa has a destructive impact upon European honey bees.

Honey bees live in large colonies ( $\approx 40,000$  individuals) that consist of three specialised types of bee: the queen, workers, and drones (see Figure 1.4). The queen maintains the population of the colony through the laying of many thousands of eggs (up to 2000 a day in the summer months), for up to five years. The primarily sterile workers, who make up the vast majority of the colony, perform a range of tasks that include tending to the developing bee larvae and foraging for resources. Male bees, known as drones, have the primary function of mating with virgin queens and contribute to colony genetic fitness via the nuptial flight (Winston, 1987; Kraus et al., 2003). Additionally, drones also play a role in the thermoregulation of the colony (Harrison, 1987; Winston, 1987; Kovac et al., 2009).

**honeybee**  
(*Apis mellifera*)

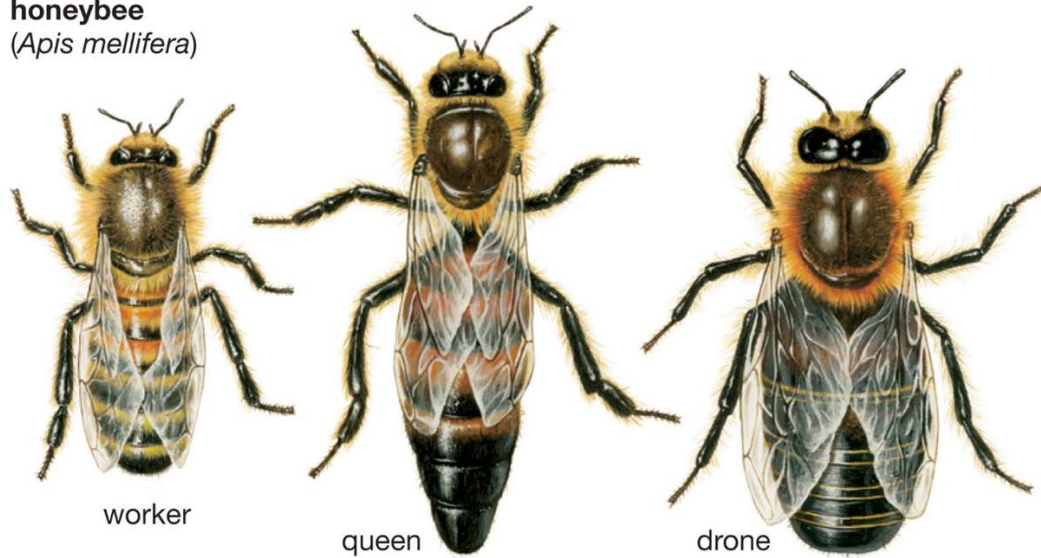


**Figure 1.4:** The three types of honey bee in a colony (Encyclopaedia Britannica, 2012).

The development of all three bee types follows the same transitional pattern from egg to larva, then pupae to adult. Dependent on the type of bee, this process differs in timescale, with queens demonstrating the shortest developmental period (16 days) and workers (21 days) and drones (24 days) exhibiting a slightly longer one. Once emerged from their cells, worker bees undergo a range of task-based changes as they progress through their lives. Highly variable age ranges have previously been documented for each of these age-based activities, but a generalised observation has been made, indicating that there are four groups. These are: (i) cell capping and cleaning, followed by (ii) brood and queen tending, then (iii) building and maintenance of the comb, before finally carrying out (iv) external hive tasks such as foraging and guarding (Winston, 1987).

Drones are only produced in large numbers for a short period of time in the colony, made to coincide with the emergence of new queens in the spring. Beyond this, the number of drones bred slowly decreases until early autumn, when their production ceases for the year. The overall percentage of comb dedicated to drone production is also lower in comparison to that of worker bees, at an average of 13 – 17% (Winston, 1987). Worker brood, on the other hand, has a consistently larger area of comb committed to its production throughout most of the active bee season, with the only exception occurring prior to swarming (colony reproduction, where the current queen leaves the hive with half of the colony, and the remaining half stay behind, where a new queen emerges from a queen cell that has been

developing prior to swarming), when drone production becomes the main energetic investment (Page & Metcalf, 1984).

#### 1.2.4. Why the European honey bee is particularly at risk from Varroa infestation

The European honey bee is not well adapted to the Varroa mite, as the species has only recently begun to infest *A. mellifera* hives. This is typical of any species that is subjected to a newly arrived threat. The original host of this parasite, *A. cerana*, is, on the other hand, well adapted, and can cope with infestation for a number of reasons.

Firstly, mites can only successfully reproduce in the drone brood of *A. cerana* (Tewarson et al., 1992; Rath, 1999; Wang et al., 2020). As drone brood is produced in limited amounts for most of the active bee season (Page & Metcalf, 1984; Winston, 1987), there is a reduction in the possible reproductive output for mites, which decreases their impact on the bee population. In European honey bees, however, Varroa can reproduce in both drone and worker brood, although with a lesser success rate than in their original host (Boot et al., 1997). Worker brood is produced from mid-winter until later autumn (Knoll et al., 2020), meaning that mites have a significantly longer time period to infest and reproduce in the cells.

Secondly, *A. cerana* carry out what is known as 'hygienic' behaviour. This is a trait that enables bees to detect mite infested brood cells, further leading to the uncapping of those cells to confirm their infestation status. If a developing worker bee is found to be parasitised, then it is removed from the colony or eaten. If no mite is found, or the occupant escapes, then the cell is simply re-capped (Rath, 1999). If a developing drone bee is found to be parasitised, then a different approach is adopted. The larva is instead 'entombed' in the cell, so that it cannot emerge. This leads to the death of the developing bee and any mites that it shares the cell with (Boecking, 1999; Rath, 1999).

Although hygienic behaviour does occur in *A. mellifera*, where they can successfully identify dead or diseased brood when uncapped (Toufailia et al., 2018), there is evidence that they do so at a slower rate in comparison to their Asian counterpart (Lin et al., 2016). It is also suggested that *A. mellifera* hygienic behaviour is more efficient towards some bee diseases than it is towards mite removal, with varying degrees of competency observed when faced with the latter task (Leclercq et al., 2017) (see Figure 1.5). Overall, the ability of *A. mellifera* colonies to carry out Varroa related removal behaviours appears to be contradicted in the literature, with varying degrees of competency observed. It is therefore difficult to draw

conclusions on the capability of this species in carrying out mite specific hygiene activities (Leclercq et al., 2017).

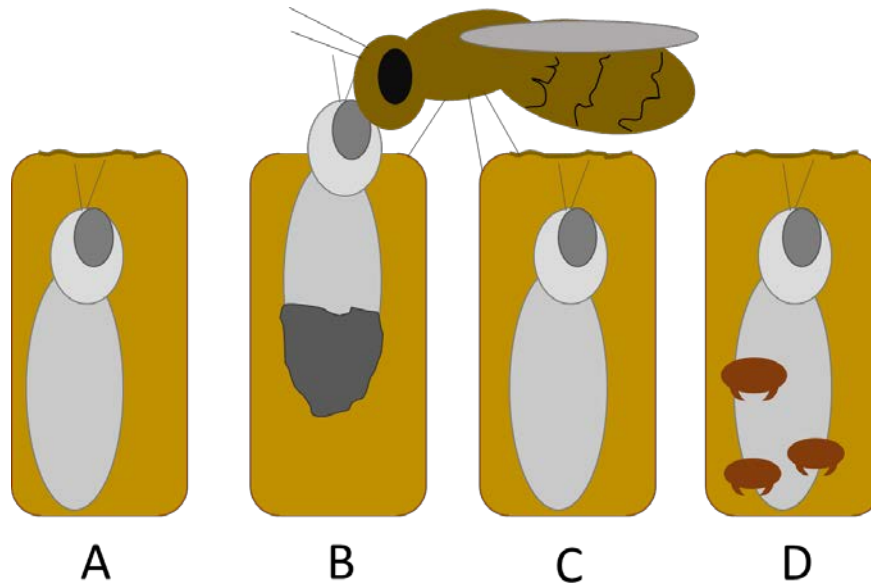


**Figure 1.5:** A simple diagram demonstrating hygienic behaviour. *A.mellifera* are better at detecting and removing diseased brood (B), than Varroa infested brood (D). A and C here show healthy capped brood. Diagram produced by Harriet Hall.

Finally, intense grooming behaviour is observed in *A. cerana*, where the bees grab the mites in their mandibles, leading to mite damage and removal from the hive (Peng et al., 1987; Pritchard, 2016). This is an attribute that is not as well developed in *A. mellifera* (Pritchard, 2016).

This reduced adaptation to mite infestation leads to increased colony vulnerability for the European honey bee. There is an extensive list of honey bee functions and biological processes that are negatively affected by Varroa, including body weight, cognition, and immune system function (Noël et al., 2020). Additionally, further impairment of a variety of other functions such as nutrition storage and metabolism can occur because of the mites feeding on the important fat body of bees, (Li et al., 2019; Ramsey et al., 2019). It is also widely accepted that as they feed, Varroa mites act as a vector of disease, mediating the transmission of several viruses. Of these, it is known that the mite is particularly effective at vectoring Deformed wing virus (causing mortality and deformities) (see Figure 1.6) and Acute bee paralysis virus (causing flight-less-ness and trembling) (Chen & Siede, 2007; Traynor et

al., 2020). These detrimental impacts can be further exacerbated when combined with additional stressors such as neonicotinoid pesticides (Blanken et al., 2015; Annoscia et al., 2020; Morfin et al., 2020; Noël et al., 2020; Schwartz et al., 2020).



**Figure 1.6:** A honey bee with Deformed wing virus, where the wings are underdeveloped (de Gelder, 2018).

If left to their own fate, i.e., without mite control measures, infested colonies will die within six months to two years from infestation onset (Le Conte et al., 2010). High mite levels in the autumn lead to colony decimation over the winter months as bees cannot survive for as long as they would if mites were not present. A shorter lifespan affects their ability to transition from a winter bee to a summer bee, which is necessary to help the colony build strength as the cold season changes to spring (Le Conte et al., 2010). Varroa mites are also thought to play a role in the phenomenon known as Colony Collapse Disorder (CCD), which is described as a rapid decrease in the population of adult bees in a colony that contains a large amount of brood. There is no single cause of CCD, as it appears to be the result of multiple stressors interacting, with pathogens likely to play an important role (vanEngelsdorp et al., 2009). As Varroa mites are known to impact upon the immune response of bees, vector a range of viruses and create exacerbated negative effects on bees when interacting with other factors

such as pesticides, it is likely that they are, in part, a cause of Colony Collapse (Le Conte et al., 2010).

### 1.3.0. Literature review: Mite detection in honey bee hives

The introduction so far has covered the life cycle of Varroa mites and how its sensory systems play a vital role in maintaining its two phases. European honey bees are at risk from the adverse effects of mite parasitism, which leads to an urgency for beekeepers to successfully detect and manage the pest before it gets out of hand.

The following sections detail the current methods used in mite detection, as well as those utilised in the monitoring of health status in honey bee hives. There is value in the implementation of these tasks in terms of Varroa and virus detection in hives, for reasons discussed in the previous sections. However, I further discuss the disadvantages of the current methodologies and comment on the requirement to turn to remote mite detection. This leads on to an explanation of the methodology of choice in this thesis: what it is, and why it has been chosen.

#### 1.3.1. Current methods of detecting Varroa in honey bee hives

Currently, the presence and number of Varroa mites in honey bee hives are established using sampling methods that require physical input from people and cause some disruption to the colony. All the techniques involve examining a sample of mites from the hive. These samples are then used to calculate a whole colony infestation estimate. I will now describe each practice, before detailing their advantages and disadvantages.

##### 1.3.1.1. *Sugar roll/shake*

This is a commonly used method, requiring a wide mouthed jar with a partially mesh-covered lid and powdered (icing) sugar. A sample of approximately 300 adult bees are taken from the colony and placed in the jar with a spoonful of the sugar. They are then rolled in the sugar so that they become fully coated (Barlow & Fell, 2006; Dietemann et al., 2013; Gregorc & Sampson, 2019). The sugar particles adhere to the ambulacrum (tarsal pads) of Varroa legs, causing them to become dislodged from the bees (Fakhimzadeh et al., 2011; Gregorc & Sampson, 2019). They can then be separated from the bees by shaking them through the mesh lid. The bees are subsequently placed back into the hive to be groomed free of the sugar (Dietemann et al., 2013).

#### *1.3.1.2. Washing*

Around 300 bees are again needed for this technique, and they are also placed in a jar, but with alcohol or soapy water instead of sugar. As the bees are rolled around, the mites adhere to the side of the glass. The number of mites and bees in the sample are divided by one another to determine the proportion of infested bees in the sample. This value is then multiplied by 100 to gain an estimate of the number of mites found per 100 bees in the entire colony (Dietemann et al., 2013). Detergent solution has been found to be slightly more reliable than alcohol for dislodging mites from bees (Rinderer et al., 2004).

#### *1.3.1.3. Natural mite-fall counts*

This method involves counting the number of mites that fall to the bottom of the hive with other colony debris. Infestation levels in the whole colony can then be estimated by multiplying the mite drop count by 250 – 500 when the hive is absent of brood, or 20 – 40 when brood is present (Dietemann et al., 2013; Gregorc & Sampson, 2019). To be able to count the mite-fall, a hive base is needed that can fit a screened board to allow Varroa to be collected, but bees to be retained in the hive (Barlow & Fell, 2006; Dietemann et al., 2013).

#### *1.3.1.4. Brood uncapping*

A portion of brood is cut from the comb or opened whilst still in the frame using a capping scratcher, which lifts out the caps and pupae found within the wax cells (Barlow & Fell, 2006; Dietemann et al., 2013). The number of cells that contain mites are counted and this value is then divided by the overall number of cells opened. Multiplying this figure by 100 provides an estimate of the number of mites found per 100 cells (Dietemann et al., 2013). Drone brood is preferably used for this method as Varroa are more likely to be found in these cells (Barlow & Fell, 2006).

#### *1.3.1.5. CO<sub>2</sub>*

This method appears to be less commonly used and is not as effective as other detection techniques (Pietropaoli et al., 2021). Like the other adult bee sampling techniques, it involves the collection of a large proportion of individuals, who are anaesthetised with CO<sub>2</sub> and then shaken to detach the mites (who also become anaesthetised and as such, loosen their grip on bees for easier detachment) from their bodies (Gerula et al., 2017).

### *1.3.2. The advantages and disadvantages of current mite detection methods*

The purpose of detecting Varroa mites in honey bee colonies is to provide beekeepers with knowledge of when to treat with acaricides, so that numbers are kept under control. It is important to time treatments correctly and not just 'blindly' use chemical mite control

without knowing the extent of the infestation and whether it is truly necessary to treat at that time. This is because acaricides are known to have various negative effects on different honey bee processes, physiological and biological functions, and the colony as a whole – the impacts of which vary from study to study and between treatment types (Tihelka, 2018; Gashout et al., 2020a; Gashout et al., 2020b; Glavan et al., 2020; Colin et al., 2021). As well as this, mite populations around the world are documented as being resistant to some acaricides (Elzen et al., 1999; Milani, 1999; Martin, 2004; Pettis, 2004; Sammataro et al., 2005; Maggi et al., 2010b; Kamler et al., 2016; Higes et al., 2020). This could be avoided by checking mite levels before choosing to treat, as well as rotational use of different treatments and use of non-acaricidal forms of control (Milani, 1999; Pettis, 2004). Therefore, treating a hive at the right time so as to not ‘over-treat’ should be of high importance for the wellness of the colony and successful eradication of the pest.

To achieve this, regular monitoring is required to identify trends in the mite population (Gregorc & Sampson, 2019). However, because all current monitoring methods necessitate visiting an apiary, this is potentially burdensome as frequent trips will be needed to accurately assess infestation levels. Furthermore, both adult bee and brood samples need to be scrutinised for Varroa in tandem to provide an accurate full colony estimate. If done alone, an estimate would only be provided for the number of phoretic mites in the hive (adult bee samples) or the number of mites in the brood cells (brood samples). The necessity for both types of sampling can therefore be demanding on both the sampler and the colony (Branco et al., 2006).

Natural mite-fall count can overcome this disadvantage, as it only requires counting the mites that fall to the bottom of the hive. It is suggested to be a very good indicator of within-colony infestation levels and can be reliably used even when the mite population is low, which is not possible with adult bee sampling techniques (Gregorc & Sampson, 2019). However, there are certain colony conditions that must be met for the whole colony estimate to be accurate when using this technique, e.g., the colony must be “brood-right” and not in a state of collapse (Branco et al., 2006). To establish if these conditions are true or not, the beekeeper must take time to inspect the colony, which adds to the time spent assessing their condition.

For increased accuracy of natural mite-fall counts, Varroa numbers also need to be noted every day for a prolonged period. A few days is not sufficient to achieve a good level of accuracy due to natural fluctuations in mite mortality (Bieńkowska & Konopacka, 2001;

Pietropaoli et al., 2021). Again, this highlights the time-consuming nature of this technique, which is also exacerbated by the need for careful, detailed examinations of the mite boards to identify *Varroa* individuals (see Figure 1.7). However, more recently, an automated system for counting mite numbers on boards has begun to be investigated, using an image based classification system that would require beekeepers to simply photograph their boards with a smartphone (Picek et al., 2022).

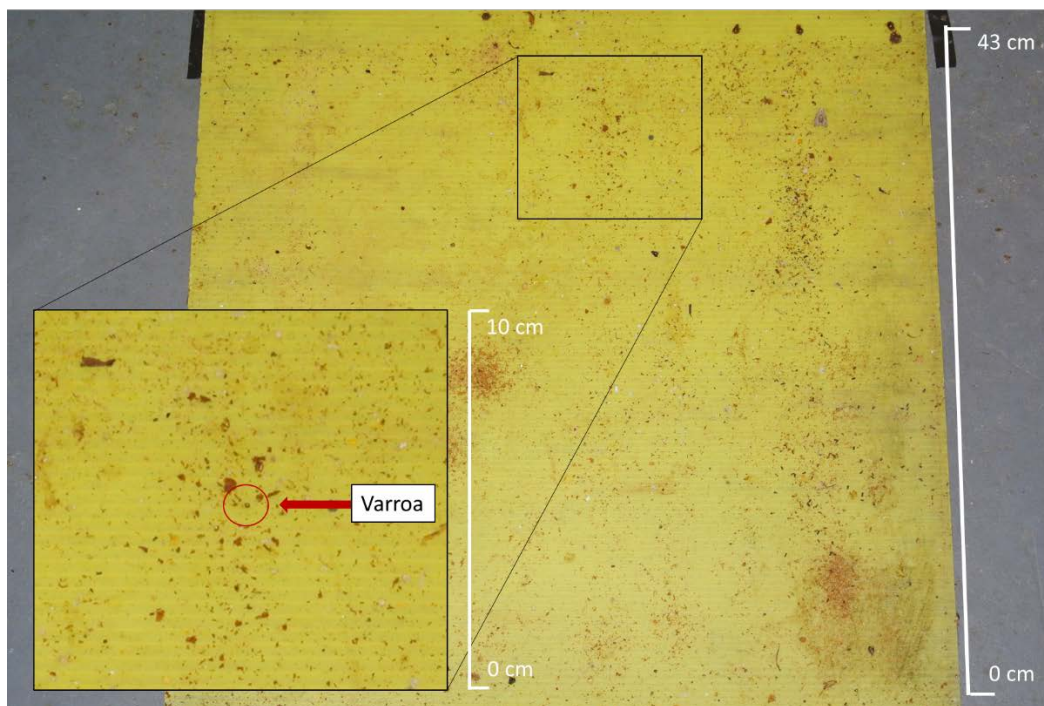


**Figure 1.7:** A mite-fall board, taken from beneath a honey bee hive. A large amount of hive debris is found on the board (43cm length) from the natural activities of the colony. The box shows a zoomed in area of the board (10cm length) to showcase the small size of a *Varroa* mite (1 – 2mm length) in comparison to the debris. A thorough, careful search of the board is needed to identify individuals. Figure produced by Harriet Hall.

The sugar roll technique is suggested to be quicker than others (Gregorc et al., 2017), but this does not demonstrate sufficient improvement when considering that the hive still needs to be opened, and that brood samples still need to be taken alongside the adults to gather a whole colony estimate. As well as this, although powdered sugar has been identified as a particularly effective substance for dislodging mites from bees (Macedo et al., 2002; Fakhimzadeh et al., 2011), it does exhibit variability in mite removal percentages (Gregorc et al., 2017). Quality of the sugar, alongside sensitivity to high temperatures and humidity, can

also have adverse effects on the success of this technique (Fakhimzadeh et al., 2011; Gregorc et al., 2017).

It is, however, far less destructive than the other methods of adult and brood sampling (brood uncapping, washing), as the bees can be placed back into the hive after being coated and rolled in sugar, whereas the other techniques involve the removal and decimation of brood cells, and the killing of all collected adults (Barlow & Fell, 2006; Dietemann et al., 2013). Alcohol wash is also an expensive, environmentally unfriendly approach that requires a careful disposal procedure (Rinderer et al., 2004; Dietemann et al., 2013).

The carbon dioxide method, like the sugar roll, allows the bees to be placed back into the hive after sampling, so may also be less detrimental in the short-term. But, whilst the other jar-based techniques involve gently rolling the bees to coat them in the substance of choice, carbon dioxide requires more intense shaking to remove mites (Gerula et al., 2017). This is surely more disruptive for the sampled honey bees, who may take longer to recover. As well as this, carbon dioxide also has the potential to adversely affect a wealth of bee processes and functions, including memory, spatial orientation, foraging behaviour, and longevity (Ribbands, 1950; Tustain & Faulke, 1979; Stec & Kuszewska, 2020). This method is also the least efficient for establishing infestation levels, as a smaller percentage of mites are dislodged from bees (Pietropaoli et al., 2021).

### 1.3.3. The move towards the remote monitoring of mites in honey bee colonies

The current methods employed by beekeepers and researchers to detect and monitor Varroa levels are generally reliable and simple to carry out. Nevertheless, there is room for improvement to reduce the number of apiary visitations and disruption to honey bee colonies. More recently, there has been a move toward researching remote monitoring techniques, which would lessen the disadvantages observed in current mite detection practices. These work-in-progress methods, at present, are mostly focused on the identification of mite presence using visual and olfactory sensors, although there is one study that investigates sound.

#### 1.3.3.1. Gas sensors

Gas sensors are currently under investigation as a potential remote mite detection tool using olfactory cues. These sensors are known as electronic noses and can identify volatile substances, with success in human, animal, and plant disease recognition (Bağ et al., 2020). They work by recognising odours that have been defined using a pattern-recognition engine and supervised learning (Gardner & Bartlett, 1994). Presently, each of the sensor

technologies tested are in a prototype phase, producing preliminary results that discriminate between mite infected and healthy colony odours (Bağ et al., 2020; Szczurek et al., 2020a; Szczurek et al., 2020b; König, 2021). One research group has, however, taken this to the next stage and tested colonies for different levels of Varroa infestation, but demonstrated poor discrimination (König, 2022). Generally, the sensors are placed in the centre of the hive through tubing and, in most instances, can be left to carry out continuous measurements with remote access to the data (Szczurek et al., 2020a; Szczurek et al., 2020b; König, 2021). However, these devices are prone to error if not cleaned regularly, which does limit their continuous monitoring possibilities as they need to be removed from the hive for this (Szczurek et al., 2020a; Szczurek et al., 2020b).

Up to six different sensors have been simultaneously tested, each chosen to identify different odours that are likely to be found in honey bee hive air. However, the composition of beehive air, and that of Varroa infested hives is still largely unknown, so it is expected that multiple devices would be needed per colony as most sensors are only sensitive to one type of compound (Szczurek et al. 2020a; Szczurek et al. 2020b). Although there appears to be a consensus that a single sensor is not sufficient in accurately assessing mite infestation (Szczurek et al. 2020b; König 2021), there are different opinions on the maximum number of sensors required (Szczurek et al. 2020b; Bağ et al. 2020).

#### *1.3.3.2. Video detection*

Visual/video detection is also in the early stages of research. The current methods that have been tested involve various types of training software and image processing to identify the presence or absence of a Varroa mite on a honey bee or within an artificial brood cell using video recordings (Ramírez et al., 2012; Elizondo et al., 2013; Chazette et al., 2016; Bjerger et al., 2019; Bilik et al., 2021). At present, there are limitations to this type of monitoring, such as requirements for powerful hardware and issues with video clarity, and that in the field, video processing has only been attempted at the hive entrance (Chazette et al., 2016; Bjerger et al., 2019). This last practical issue in particular highlights the flaws of video detection. Within the dark hive, which has limited space between frames, it would be extremely difficult to successfully video record bees and mites. It appears that this method could only work at the hive entrance, currently, which limits the success of capturing mites visually as they are most commonly found on nurse bees who do not leave the hive, or within the brood cells in their reproductive phase.

#### *1.3.3.3. Audio detection*

Microphone recordings have been used to identify differences in the acoustic signature of a healthy colony compared to a mite infested one (Qandour et al., 2014). Although this method could discriminate between the two colonies, this may not be due to the differences in the *Varroa* infestation levels. The training data used was taken from a small number of low-quality recordings. For the infested colony, the data was particularly poor, with use of only one sample which was recycled to generate multiple recordings for the training database. Only two individual hives were compared, with a third of unknown status tested later (Qandour et al., 2014). This work has not yet been followed up with further investigation.

Acoustic data collection and analysis is now becoming well-studied in the field of honey bee colony monitoring (see section 1.3.4.), but at present, this route of research has not focused any further on *Varroa* related sounds, aside from one proposed, but not tested, monitoring system (Sharif et al., 2020).

#### *1.3.4. Current methods of honey bee colony health status monitoring*

Remote monitoring systems that are used to indicate general colony status are more advanced than for those specifically involving the detection of *Varroa* mites. A variety of parameters can be non-invasively monitored, and many systems have even been commercialised for beekeeping use. This type of apiary monitoring is referred to as Precision Beekeeping, a management tool that aims to minimise colony stress and resource waste that would otherwise occur from more invasive beekeeping practices. These monitoring systems can act as an early warning for beekeepers, alerting them to colony activities such as swarming or queen-less-ness, and providing indication of when specific hive tasks need completing (Zacepins et al., 2015). I will now discuss each of the major parameters that are currently monitored in honey bee colonies, before moving on to justify the importance of vibration measurements in this field, a technique which is far less studied.

##### *1.3.4.1. Temperature monitoring*

Temperature measurements are perhaps the most common and well-established form of colony monitoring. Such systems have been made available commercially to beekeepers, who benefit from low costs and robust hardware that can be easily maintained within a hive (Zacepins et al., 2015). Various colony states can be monitored based on internal hive temperature, such as pre-swarming (linked to a hive temperature increase of 1.5 – 3.4°C), brood volume (heat fluctuations that correspond to known changes in brood rearing temperature over the year), and colony death (a decrease in temperature to ambient levels)

(Stalidzans & Berzonis et al., 2013; Zacepins et al., 2015; Zacepins et al., 2016; Kviesis et al., 2020a). The monitoring of temperature patterns within a hive also provides data that can be linked to external temperature changes, indicating if a colony is likely to overheat, which can increase the risk of bees absconding (nest abandonment) (Kridi et al., 2016).

#### *1.3.4.2. Hive weight monitoring*

Hive weight monitoring systems have also been developed into a range of commercialised products for beekeeping use, which can remotely inform the user of weight information via their mobile phones, for example (Zacepins et al., 2015). Forager population, food consumption, productivity, nectar flow timings (all established by corroborating regularly taken weight measurements with known data on average comb (honey-filled, brood-filled) and bee weights over the year), and swarming (a decrease in colony weight) can all be identified using hive weight as an information tool (Lecocq et al., 2015; Zacepins et al., 2015; Terenzi, et al., 2019a). However, there are several downsides, as the available measuring systems are both expensive and unfit for purpose in some scenarios, e.g., during winter when resources are not foraged, which leads to smaller changes in daily hive weight that cannot be detected (Zacepins et al., 2015). It is known that beekeepers are not particularly interested in, or able to, invest in these products (Zacepins et al., 2015; Zacepins et al., 2017), and work towards better weight monitoring systems to overcome these problems is now being done (Zacepins et al., 2017; Kviesis et al., 2020b; Bratek & Dziurdzia, 2021).

#### *1.3.4.3. Video monitoring*

Video data obtained from un-manned cameras placed at the hive entrance can provide a large amount of information on colony activity, as well as the presence and effects of abiotic and biotic stressors on the bees (Zacepins et al., 2015; Ngo et al., 2019). More recently, cameras and image processing techniques have also been used to identify the number of bees returning to the hive with pollen, which can help determine pollination efficiency and colony food store levels (Babic et al., 2016; Yang & Collins, 2019; Ngo et al., 2021). Visual data therefore supplies a wealth of information. A downside is, however, that it is perhaps not economically viable to set-up this type of system on every hive in an apiary, as a huge amount of raw data is produced which limits the time that can be spent filming, if the data is first stored before it is analysed (Zacepins et al., 2015). For example, bees are often fast moving, and better video detection results have been found when filming at a higher frame rate (60 frames-per-second (FPS), in comparison to 30 FPS) (Magnier et al., 2018), which creates larger files due to more data being recorded.

#### *1.3.4.4. Acoustic monitoring*

It is easy to acquire sound data, which is then used to predict and assess bee behaviours. However, the data analysis and processing involved is complicated, which may be the reason for few sound measuring devices in the field at present (Zacepins et al., 2015). Yet it is suggested that sound as a measured parameter shows good promise for the future (Zacepins et al., 2015), and many researchers have been working towards the improvement and increased scope of acoustic based measurements, particularly in recent years (Zacepins et al., 2015; Robles-Guerrero et al., 2017; Nolasco et al., 2019; Robles-Guerrero et al., 2019; Terenzi et al., 2019b; Imoize et al., 2020; Zgank, 2020; Zhao et al., 2021; Ruinga et al., 2021; Underwood & Tashakkori, et al., 2022; Zgank, 2021; Tashakkori, 2022; Terenzi et al., 2022; Yu et al., 2022).

#### *1.3.4.5. Lesser-studied monitoring parameters*

The above four current methods using temperature, weight, video, and sound, are the most well-studied parameters in honey bee colony monitoring. There are other parameters that can be remotely monitored, but these have not yet received as much research interest. Humidity, gas content, and vibrations are listed as additional promising measurements. Combined monitoring of several honey bee colony parameters is likely to be better for Precision Beekeeping success, as different hive states vary in their optimum detection method (Zacepins et al., 2015). It has also been found that highly accurate monitoring results can be achieved when combining information from multiple sources using classification algorithms (Braga et al., 2020). Several studies have investigated and implemented the remote monitoring of more than one hive measurement simultaneously with success (Murphy et al., 2015; Howard et al., 2018; Cecchi et al., 2019; Cecchi et al., 2020).

The progress that has been made so far on remote honey bee colony measurement systems, particularly in terms of the commercial systems already available for use, demonstrate that such non-invasive beekeeping techniques are possible and successful. The methods that have been (and are still being) investigated enable a huge variety of honey bee colony statuses to be assessed and monitored. The authors of Zacepins et al. (2015) highlight that it would be particularly advantageous to be able to remotely monitor honey bee diseases, indicating that detection systems for Varroa presence and Varroa-vectoring viruses would be a welcome addition to the colony state measurements that are already in place. As multi-sensor systems are also recommended, there is great hope in researching lesser-studied hive parameters, such as vibration, to allow a more detailed picture of a colony to be built.

The following section discusses the importance of vibration in the honey bee colony, which therefore highlights why the study of remote vibration monitoring could be useful in Precision Beekeeping. I later go on to discuss the inclusion of Varroa detection methods in this branch of beekeeping, and how the marriage of the two research avenues (vibration and remote Varroa surveillance) is advantageous.

### 1.3.5. The importance of monitoring vibrations in honey bee colonies

One of the most ancient and widespread forms of communication is known to be via substrate-borne vibrations, documented in many species, and estimated to be used by thousands more (Cividini & Montesanto, 2020). This form of communication enables animals to gather information from their environment, as well as use it to carry out multiple activities that are critical to their survival, such as courtship, foraging, and parental care (Cividini & Montesanto, 2020).

Sound is an alteration in pressure that propagates through a medium and is perceived via morphological structures such as ears (pressure receivers), whereas substrate-borne vibrations move through solid media and are detected by mechanoreceptors (Cividini & Montesanto, 2020). Vibration propagation is complex, and one behaviour can produce a range of vibrational waveforms types, although when considering substrate-borne vibrations, the wave type is usually a boundary wave (produced at the boundary of a solid media and another media type, such as air) (Hill & Wessel, 2016) (see Figure 1.8).

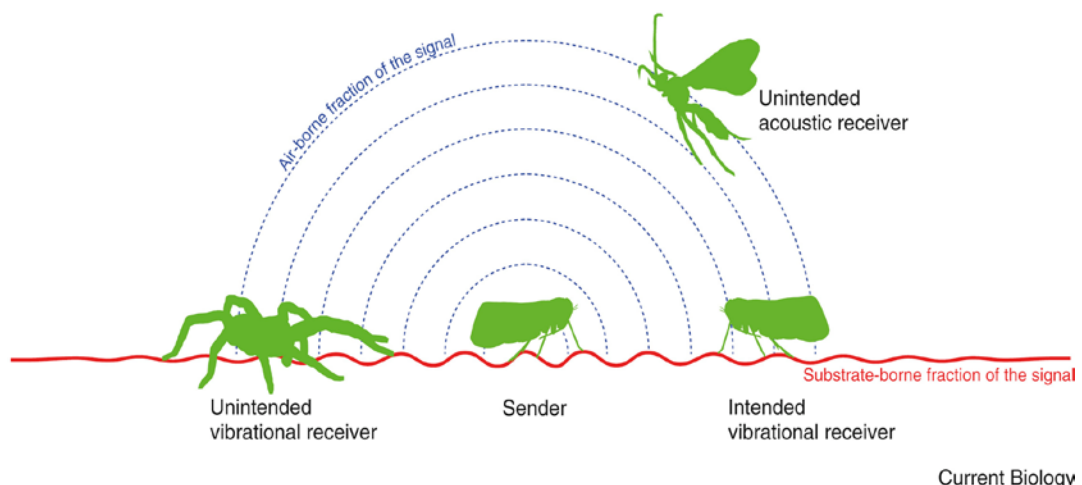


**Figure 1.8:** An example of communication types that can be formed by animal that produces a vibration (Hill & Wessel, 2016).

Honey bees engage in vibrational communication via the transmission and reception of both substrate and airborne vibrations. Substrate-borne vibrational signals are detected by the subgenual organs in the legs, and airborne signals are thought to be perceived as air particle movements by the Johnston's organ in the antennae (Hrncir et al., 2005). Sound, therefore, is not sensed in the same way for bees as it is for humans. This may lead to restrictions in our understanding of meaningful honey bee signals, as we fall victim to perceiving them only as sounds, as this is how we hear many of them (Hrncir et al., 2005). Perhaps this is why sound and microphone use have been focused upon to a greater degree than vibrations in honey bee colony monitoring.

Honey bees are thought to have a larger frequency perception range for substrate-borne vibrations (150 – 900 Hz) than airborne ones (200 – 300 Hz) (Hrncir et al., 2005). Perhaps there are a greater number of signals that can be transmitted and received via the honeycomb that could go unnoticed if focusing only on airborne sound, because even when acoustic signals are produced, there are vibrations that propagate through the substrate on which the signalling individual is stood, as well as through the air (Caldwell, 2014). The honeycomb itself is built to be reciprocally interactive with the colony, with vibrational signals transmitting faster and more locally than other types of stimuli such as chemical, which spread more widely and slowly (Hepburn, 1998). The colony builds, shapes, and actively improves the comb for the purpose of successful vibration transmission (Tautz, 1996; Sandeman et al., 1996; Smith & Chen, 2017).

#### 1.3.6. How our research group is pioneering honey bee colony monitoring via their vibrations

To better understand the world that honey bees live in, in this program of research we are monitoring colonies through a sensory mode that is of importance to them. This should therefore provide us with more detailed information on their behaviours, activities, and reactions to stressors. Our research group is unique in its investigation of honey bee vibrational signals, detecting them using accelerometer sensors. This technology has been successful in recording continuous, long-term data within honey bee colonies, which has provided vibrational information on the daily changes within the colony and of their brood cycle, as well as identifying and monitoring and predicting swarming events (Bencsik et al., 2011; Bencsik et al., 2015; Bencsik & Newton, 2018; Ramsey et al., 2020). It has also been possible to successfully characterise and identify individual honey bee signals amidst the continuous noise of the colony (Ramsey et al., 2017; Ramsey et al., 2018).

#### 1.4.0. Literature review: The novelties and methodologies of this research

I have now introduced Varroa and the negative impacts of mite infestation on honey bee colonies. Further to this I have discussed the current solution to managing their effects: physical mite detection methods that allow infestation levels to be monitored, so that mite control can be implemented at suitable times.

I now propose an advancement to the current mite detection techniques that are in place, which will investigate a less invasive, remote method for identifying Varroa infestation. Honey bee colony monitoring has progressed further in performance than Varroa monitoring. Multiple colony states and events are non-invasively monitored using a variety of techniques, and it would appear logical and valuable to both develop and include the detection of mites and measurements of their infestation levels. Honey bee colony monitoring would benefit not only from the inclusion of remote mite detection, but also from measurements of vibration, a sensory mode that is particularly relevant to bees.

At present, there are a limited number of parameters and detection methods being employed in non-invasive mite monitoring. I here aim to progress the field of remote mite detection, which in turn would build upon the honey bee colony monitoring techniques that are already available. I aim to do so using vibration as a measurable parameter and discuss the advantages of this technology in the following sections.

#### 1.4.2. How accelerometer sensors can benefit honey bee colony monitoring

For successful Precision Beekeeping, it is critically important that the measured colony data is correctly interpreted so that hive status can be accurately identified, and suitable beekeeping actions taken. This means that 'blind' measurements, i.e., those without visual evidence to confirm what is being perceived, such as temperature or sound, need to first be corroborated with physical, visual evidence of the colony/honey bee behaviour or state. Future 'blind' measurements that are acquired can then be interpreted without the need for cross-referencing the data with observational evidence, so long as there is a fixed ratio relationship between the given state/behaviour and a given data feature (Zacepins et al., 2015). This may appear to be a disadvantage to non-invasive monitoring because hives and individuals must initially be physically inspected alongside the remotely collected data. However, in the long run, it is extremely useful. For the method to be successful, a 'library' of honey bee behaviours, states and activities must first be linked to their corresponding

measurement, so that they can be correctly recognised when captured by the detection software in the field (Zacepins et al., 2015).

Accelerometers are enabling us to form such a library of individual and colony vibrational signals/states. Initially working in tandem with visual evidence, honey bee behaviours and activities are identified and can, in favourable circumstances, be linked to their corresponding vibrational trace. These vibrational signals can then be searched for, detected, and identified in long-term accelerometer datasets. Further study that utilises these sensors will therefore continue to build a more complex picture of a honey bee colony, by enabling the identification of novel vibrational signals that can then be further scrutinised to identify, visibly, what behaviour or state they correspond to. Greater knowledge of a larger number of signals will support better understanding and improved monitoring of honey bee colony life.

For this research program, a specially designed observation hive was used so that honey bee behaviours could be visually captured alongside accelerometer data. This particular hive design reduces the effect of observer intrusion on the bees, by allowing the researcher to mechanically lift just one frame out of a standard sized hive and into a clear Perspex box for temporary viewing (see Figure 1.9). Other types of observation hive force the colony to be permanently in view behind glass for favourable viewing of their activities and are often designed so that the colony cannot build the combs in their optimum configuration, thus, creating unnatural conditions (Ramsey, 2018). The new observation method has been successfully implemented in previous honey bee vibration studies (Ramsey et al., 2017; Ramsey, 2018; Ramsey et al., 2018) and allows the bees to go about their daily activities in a natural setting when they are not in view. Short observation periods (approximately 20 minutes at a time) can then be carried out, which cause minimal interference, i.e., behavioural data is captured that is highly natural and non-manipulated. In this research, for honey bee vibration capture, videos were taken of either side of the lifted frame (which had accelerometer sensors embedded in the comb) to aid the confirmation of visible behaviours with their corresponding accelerometer traces.

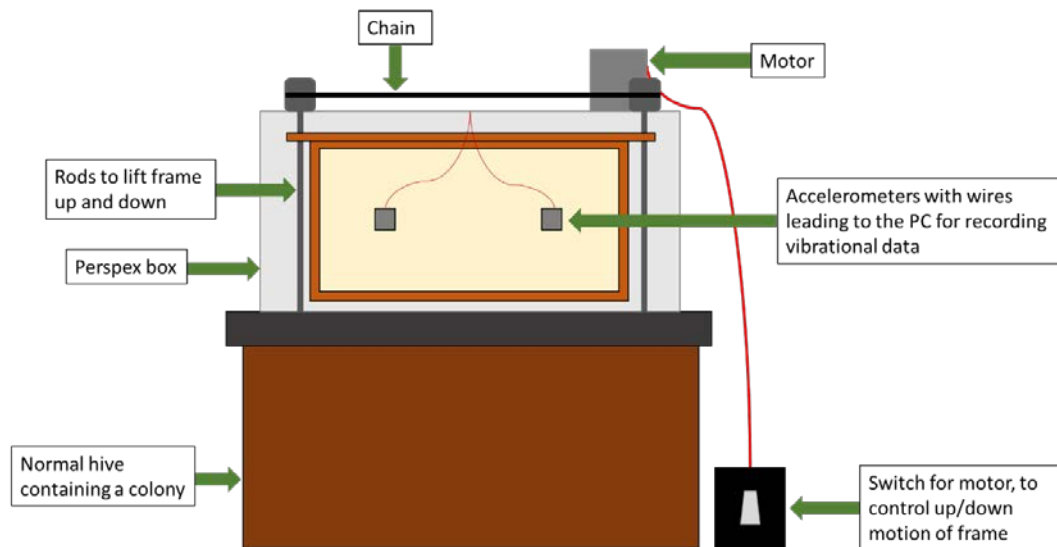


**Figure 1.9:** The specially designed observation hive. A standard, British National hive was altered to fit the observation platform on top. The lid of the hive is made of wood, with a space in the centre for the Perspex box to sit. The central frame of the hive is attached to two metal rods that link to a motor system at the top of the hive. When switched on, the motor pulls a chain that is attached to the rods, rotating them either clockwise or anticlockwise (for up or down motion). This rotation smoothly pulls the frame up into the Perspex box for viewing, and then back downwards again into the hive. After the observation period, when the frame has been returned to its normal position in the hive, a cover is placed over the Perspex box to maintain a dark and warm environment for the bees. Diagram produced by Harriet Hall.

However, to capture the trembling behaviour that is a typical symptom of Chronic bee paralysis virus (see chapter 4), as well as video data from the observation hive, additional visual evidence was required. As trembling is an uncontrolled viral symptom, rather than a purposefully produced behaviour, it was expected that a distinctive vibrational trace with clearly identifiable features may not be produced, i.e., the bee is not trying to convey a communicatory signal, so the vibration may suffer low signal-to-noise-ratio that impacts upon the clarity its features. This is unlike other detected honey bee vibrations that correspond to a functional behaviour, where the signals are strong with clear features (Ramsey et al., 2017; Ramsey et al., 2018). Also, to avoid the vibrations of the whole colony from interfering with the successful capture of trembling traces, additional video evidence of the symptom was deemed important to explore. By doing so, the vibrational signature captured from each bee could absolutely be attributed to that individuals' motions, i.e., the risk that the vibrational trace could have been produced by various other bee activities was

removed. Therefore, trembling and non-trembling honey bees were filmed when in a similar set-up to Varroa mites (see section 1.4.1.) in a Petri-dish with an attached accelerometer.

Beyond this pre-requisite of visually identifying the honey bee behaviours that correspond to vibrational traces, accelerometer sensors offer a non-invasive monitoring method that accrues richly detailed data. The model of accelerometer used in this thesis has low sensitivity to environmental factors (Brüel & Kjær), which makes it highly suitable for application within honey bee colonies. Although a delicate piece of instrumentation, they are particularly robust when faced with the challenges of a hive. They can be inserted directly into the wax of a comb (see Figure 1.10) and endure propolisation by the bees (propolis is also known as bee glue and is used by bees to seal gaps in the hive, amongst other purposes (Oršolić, 2010)) - a feature that is lacking in acoustic microphones, which need to be protected from this (Ferrari et al., 2008; Mezquida & Martinez, 2009; Pérez et al., 2016; Robles-Guerrero et al., 2017; Robles-Guerrero et al., 2019; Terenzi et al., 2020; Zhao et al., 2021). Once in the hive, accelerometers can be left for prolonged periods, and they record the vibrations of the colony continuously by transmitting the data to an external recording device (an external soundcard processes the data from an analog to a digital format, which is then saved continuously on hard drives using automatic software). This provides detailed, long-term datasets that are recorded remotely, without the need for regular human interaction.

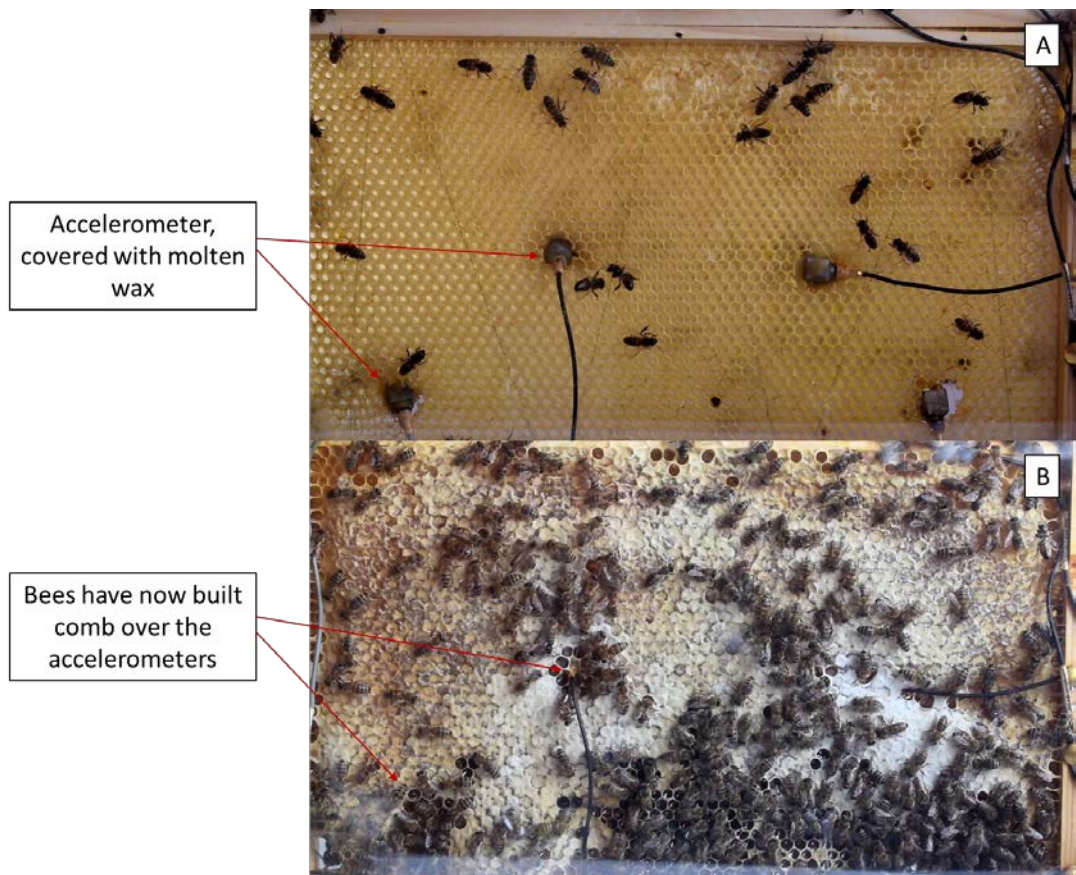


**Figure 1.10:** A frame that has four accelerometers embedded in the comb. The accelerometers are covered with a small amount of molten wax to secure them in place when they are first introduced to the frame (A). The wires that are attached to the sensors lead out of the hive to a computer set-up, which records and saves the vibrational data that is collected. Over time, the colony builds comb around and over the sensors (B). Photographs and diagram by Harriet Hall.

This thesis, therefore, utilises a valuable technology that, in the long run, could well reduce the requirement for physical inspections of the colony. Accelerometers provide highly detailed data, as they pick-up the vibrations of the entire colony over long periods of weeks, months, years. This has the potential to advance what has already been achieved in the non-invasive monitoring of colonies, and in turn would do so by recording vibrations, which are of high importance to bees.

#### 1.4.1. Measuring vibration: What is an accelerometer?

Piezoelectric accelerometers are small devices that measure acceleration, by converting one type of energy into another. An electrical signal is produced by the accelerometer, as a response to the vibration that is being measured. They contain elements made of piezoelectric material, which develops an electric charge when subjected to a force. The electrical output of the accelerometer is proportional to the vibratory acceleration that is

applied to the device (Serridge & Licht, 1987) (see Figure 1.11). When compared to other vibration sensors, piezoelectric accelerometers offer the optimum means to measure vibration (Serridge & Licht, 1987).

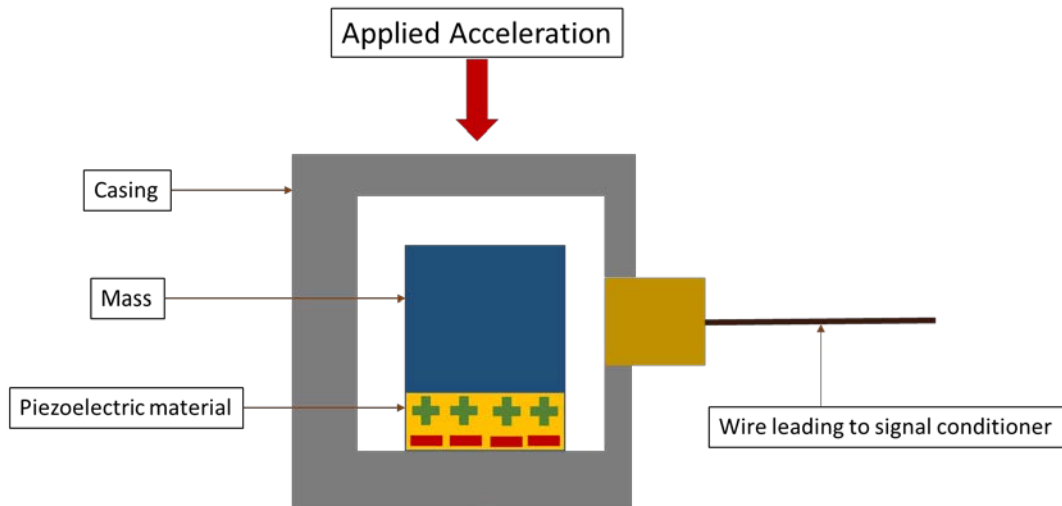


**Figure 1.11:** A simple diagram of an accelerometer. The sensor has a mass (blue). When vibratory force is applied to the casing, it causes the mass to stress the piezoelectric crystal (yellow), which has a negative and positive polarity output. When the crystal is stressed, it generates an electrostatic charge output that is proportional to the applied acceleration. A signal conditioner is used to convert the charge output that is generated by the crystal into a voltage signal that can be used for analysis (diagram adapted by Harriet Hall from industrial-electronics.com).

The model of accelerometer sensor used throughout this thesis (4507-B-002, Brüel & Kjær) has been deemed the best for its purpose, as it can detect low level vibrations with a high sensitivity to weight ratio (Brüel & Kjær). This is ideal for measuring minute organisms, as it is the smallest physical device available with such a large sensitivity. As Varroa mites are small, lightweight animals, this accelerometer model is presently the best for measuring the vibrations that they emit. In this thesis, the optimum experimental method was to directly place individuals in the vicinity of the accelerometer (on a small Petri-dish glued to the sensor, or on honeycomb that had a sensor secured to the wax, or on a piece of brood-comb, placed on the Petri-dish with attached sensor). As it was initially unknown whether the vibrations of Varroa mites could even be captured, this set-up was ideal for testing the ability of the accelerometer in detecting mite pulses. A reduction in interference from vibrations produced by background noise (by placing the accelerometer set-up onto cotton wool, and in a sound isolated room) also benefited this methodology during this investigation.

#### 1.4.3. How accelerometers can benefit Varroa monitoring research

Previous work into the remote detection of Varroa mites has focused on visual and olfactory data, with just one study that investigated acoustic data captured from the overall honey bee colony soundscape (see section 1.3.3.3.). The direct detection of the Varroa themselves has also been neglected, aside from (i) a paper that investigates walking vibrations in the brood cells but lacks detail other than a few brief sentences on the time duration, frequency and interval between pulses, and demonstrates poorly produced figures that lack y axis quantification. It also incorrectly refers to the sensory mode as 'acoustic' (Es'Kov et al., 2003), and (ii) video capture at the hive entrance, where mites that reside on adult bees have been recognised using algorithms (see section 1.3.3.2. for the discussion on video capture). Accelerometers overcome the challenges faced by video monitoring as they can reside in the darkness of the hive and still collect useful data. They also offer benefits over the gas sensor methodologies that have been employed so far (see section 1.3.3.1.), as they can remain in hives for prolonged periods without suffering from propolisation, and do not need to be removed for cleaning in order to collect data without error.

Accelerometers have proven to be highly successful for non-invasive honey bee signal capture, residing in the hive without interfering with bee behaviour or requiring human input. As previously discussed, specific honey bee behaviours that produce detectable vibrational signals have been visually identified using an observation hive (see section 1.4.2.). For Varroa mites, this method was not possible. At any given time, 65% of mites in a colony are found in the sealed brood cells, and the remainder are found on the adult bees, often squeezed between their abdominal plates, out of direct view. Therefore, direct observation of mites in their natural environment (the full honey bee colony) could not be successfully achieved. Instead, mite behaviours have here been visually corroborated with their vibrational traces by filming the mites during their time on the Petri-dish/honeycomb set-up, previously described in section 1.4.1. This way, mite vibrational traces could be clearly related to their specific movements. This method enabled the identification of vibrational traces that are specific to Varroa, so that I could then progress to automatic detection of these pulses in long-term datasets (see sections 1.4.5.3. and 1.4.5.4.).

Using accelerometers to detect mites is both beneficial and novel for two under-researched areas: (i) direct mite detection, (ii) mite detection via substrate-borne vibration capture. Identifying mite presence directly, rather than indirectly, i.e., differences in colony/individual honey bee vibrations, could be a more advantageous and reliable method for remote monitoring. Detecting vibrations that are related to the mites themselves would provide

stronger evidence for their presence, rather than an increase in honey bee grooming request vibrations, or vibrations related to hygienic behaviour, for example.

Substrate-borne vibrations have been neglected when considering mediation of the mite-bee relationship. Sound and vibration are closely intertwined sensory stimuli (Caldwell, 2014), strongly indicating that the monitoring of hive vibrations could be indicative of just as many, if not more, colony events and states than have already been established using acoustic methods alone. That said, the investigation into Varroa vibrations should be highly appropriate for the development of future sound and vibration monitoring within apiaries. Varroa vibration detection could also lead to new knowledge into the vibratory world of mites, such as the potential function and importance of vibration to this species.

Additionally, differences in the acoustic signature of mite infested and healthy honey bee colonies have been documented (Qandour et al., 2014). This indicates that it is perhaps also possible to identify dissimilarities between colonies infected with certain viruses, such as Deformed wing virus which causes wing abnormalities and Chronic bee paralysis virus which causes body trembling. The different buzzing (or lack thereof) caused by deformed wings, and the trembling of bees, are likely to produce alternative vibrational signatures that have the potential to be detected by accelerometers. As Varroa mites vector numerous honey bee viruses (see section 1.2.4.), the characterisation of these vibrational traces could act as an indirect method of remote mite detection. Remote honey bee disease recognition is not well explored, with only one study researching non-invasive American Foulbrood identification using hyperspectral imaging (Yones et al., 2019). The use of accelerometers and vibration in virus detection is a novel method that can perhaps begin to address this large gap in knowledge, to the benefit of honey bee colonies and the beekeepers who care for them.

#### 1.4.4. What this thesis achieves with accelerometer sensors

The focus of this thesis is to build upon remote honey bee colony monitoring techniques. Varroa and virus detection are currently not remotely monitored, although exploration into the possibility of achieving this has recently begun (see section 1.3.3.). Vibration as a measured parameter in remote honey bee management is also not widely studied, aside from our own research groups' endeavours. In this thesis, I combine these two under-studied areas with the use of accelerometer technology to achieve the following novel outcomes:

- 1) The direct detection of Varroa mite individuals through the capture of vibratory traces originating from their activity on a variety of substrates.

- 2) The identification of a novel Varroa behaviour that has a corresponding vibrational trace, and an examination into the prospect of searching for this specific vibrational signature within the mites' natural environment.
- 3) An exploration into the possibility of using accelerometers to identify vibratory traces that are specific to honey bee viral symptoms.
- 4) The identification and characterisation of a novel honey bee vibration, termed the honey bee 'purr', which adds to the library of known honey bee signals, for improved understanding of the colony.

Overall, this thesis will provide insight into the practicality of using accelerometers to measure vibration as a remote monitoring tool for both Varroa and honey bee viral expression, expanding upon what can already be achieved using this technology.

I will now discuss the main analysis techniques that investigated the outputs from accelerometers in this research, closing the literature review section of this thesis.

#### 1.4.5. Analysis techniques used in this thesis

##### 1.4.5.1. Spectrograms

Any accelerometer waveform can be analysed using the Fast Fourier Transform (FFT), which identifies the frequency components present in that waveform (Bergland, 1969). A Fourier transform Fourier spectra show the amplitude of each frequency component over a specified time period (see Figure 1.12). The FFT allows spectrograms to be computed by stacking a collection of spectra alongside one another. A spectrogram is a 2-Dimensional matrix, which can conveniently be shown as an image, exhibiting time on the x axis, frequency on the y axis and signal amplitude as pixel intensity (colour) (Ramsey, 2018) (see Figure 1.12). In the case of this thesis, for most spectrograms, I chose a colourmap in which a dark red colour indicates the highest magnitude of acceleration ( $m/s^2$ ) at any given point in time, and a dark blue colour shows the minimum of this (see Figure 1.12).

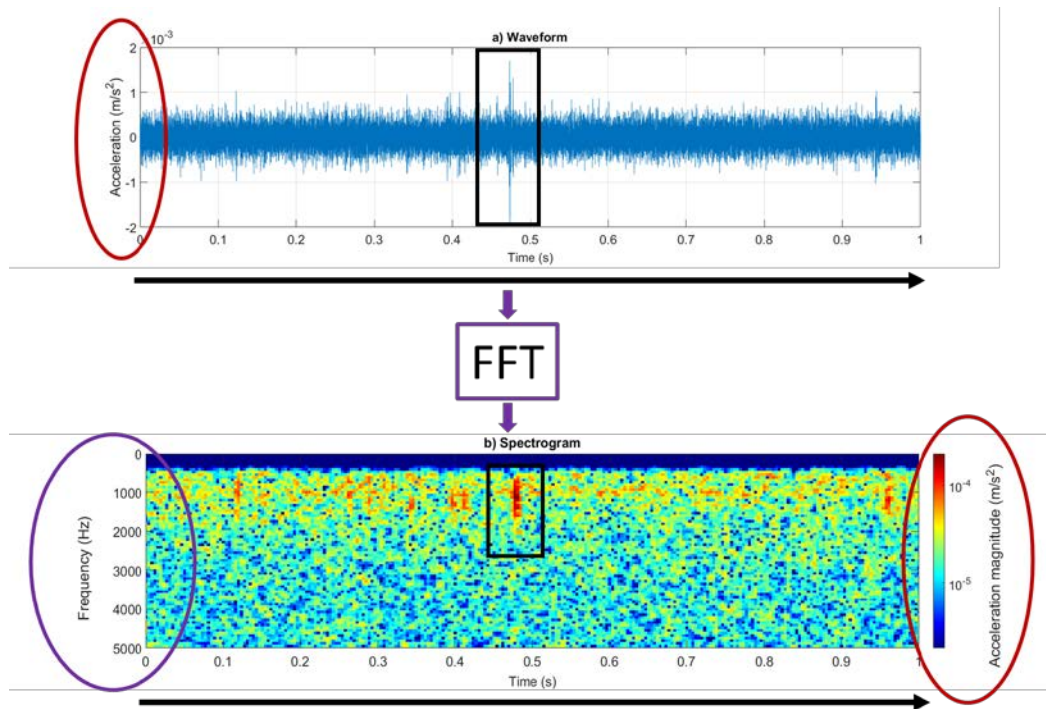


**Figure 1.12:** A graphic to demonstrate the transformation of a waveform into a spectrogram. Both the waveform ('a') and the spectrogram ('b') here illustrate the same 1 second of vibrational data, with a vibrational trace of interest at approximately 0.5 seconds. In the waveform panel ('a') the amplitude (strength) of the signal is visualised over the y axis as acceleration  $m/s^2$  (red circle). The x axis demonstrates time (s). Following FFT analysis, in the spectrogram ('b') the x axis remains the same, showing time (s) (black arrows) (here the vibrational trace of interest can be seen at the same time stamp in both the waveform and spectrogram panels in the black boxes). Acceleration is now showcased as colour (red circle), with dark red representing areas of high amplitude signal and dark blue representing areas of low amplitude signal. The vibrational trace of interest is here seen in red, as it is louder than the general background noise captured elsewhere in the window. FFT analysis reveals the frequency components that are present in a waveform. These cannot be seen in the waveform panel ('a') but are represented in the output of the spectrogram ('b'), as a result of FFT, along the y axis (purple circle). Diagram produced by Harriet Hall.

Each spectrogram image will benefit from appropriate tweaking of the image resolution, which will affect the clarity and detail of any vibrational traces present in the window. The time duration of the section of the waveform that is used to calculate one spectrum will firstly influence the horizontal resolution of the spectrogram image. This first parameter is known as the temporal resolution. The shorter the time duration, the higher the horizontal resolution of the image. Secondly, a higher resolution will also show more detail on the y axis, i.e., an improved visualisation of the frequency of the signal over time (Ramsey, 2018). A second parameter, known as the multiplication factor, is the number of spectra that are

interleaved between two consecutive spectra, vertically. Tweaking this parameter has an effect on the visualisation of the data over the x axis (see Figure 1.13)

The multiplication factor is particularly important for this thesis. Varroa vibrational signals are short in time duration (approximately 3ms). If the multiplication factor had a value of one, the ultra-short pulse would risk being lost between two consecutive spectra. A multiplication factor with a value of three, however, ensures that there are additional interleaved spectra to increase the number of vertical lines (see Figure 1.13). Therefore, the pulse can be seen in one vertical line of the spectra, in between the two original consecutive spectra.

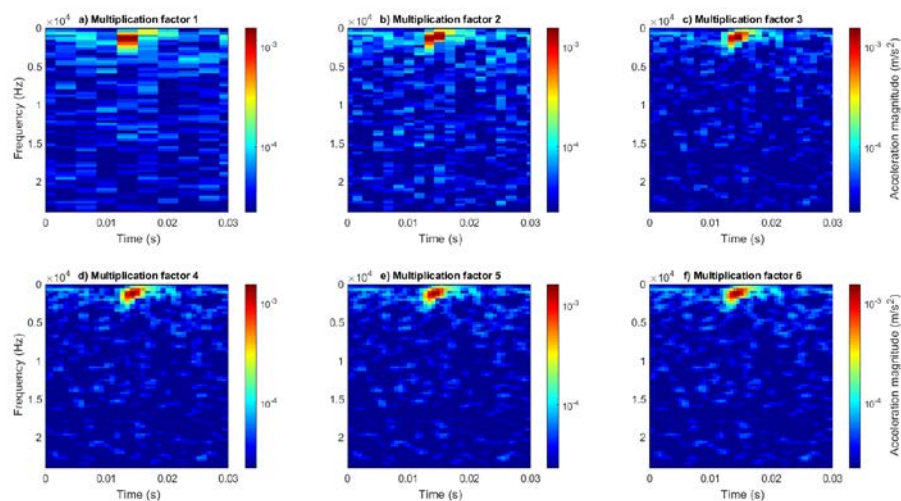


**Figure 1.13:** A set of images to demonstrate the influence of the multiplication factor on a spectrogram. Each of the six spectrograms showcase the same Varroa vibrational pulse. Panel ‘c’ shows the ideally chosen multiplication factor of three. When the multiplication factor is reduced, the number of spectra in the image is also reduced, and details and features of the vibration become lost (panels ‘a’ and ‘b’). By increasing the multiplication factor, the number of interleaving spectra is also increased, exhibiting more data (panels ‘d’, ‘e’, and ‘f’). However, beyond a multiplication factor of three, the new data that is revealed adds little to the features of the vibration that can be seen in panel ‘c’ and therefore it is not necessary to include.

Overall, the spectrogram is a highly useful tool in this thesis. It provides a quick and effective method of visualising the details and characteristics of a waveform.

#### *1.4.5.2. Two-dimensional-Fourier-transform (2DFT)*

This thesis also uses 2DFT images to visualise accelerometer data. The spectrogram is first computed on the waveform data. Then a second series of FFTs are calculated on the horizontal lines of the spectrogram (Ramsey, 2018).

The repetition frequency of each spectral component over the course of the selected time period is thus shown over the x axis (Hz). The frequency (Hz) of each spectral component is shown on the y axis. Pixel intensity (colour) demonstrates the magnitude of acceleration ( $m/s^2$ ).

This form of analysis is useful for signals containing spectra that repeat. In this thesis, the 2DFT is not ideal for visualising Varroa jolting signals (the vibrations that correspond to the novel behaviour discovered as part of this work), as these are short, individual pulses (see chapter 2 for the full characterisation of these pulses). However, for honey bee signals, as well as for Varroa walking vibrations, they play a larger role. In this work, 2DFT images are used to characterise the features of honey bee trembling behaviour, as the bodily shaking of the bee is a repeated motion. They are also used in the chapter that investigates the novel honey bee signal here termed the 'honey bee purr'. This is a vibrational signal that comprises of repeating pulses over a short time period. The 2DFT has previously and successfully been used in the characterisation of honey bee dorso-ventral abdominal vibration signals (Ramsey, 2018; Ramsey et al., 2018). In chapter 3, the 2DFT is identified as the most suitable analysis tool for visualising and characterising Varroa walking vibrations, as these are pulses that repeat over periods of one to two seconds most commonly on brood-comb, and for longer durations on Petri-dish as the mite locomotes over the substrates. The 2DFT has therefore been useful for several different applications throughout this thesis.

#### *1.4.5.3. Principal component analysis*

Principal component analysis (PCA) is a dimensionality reduction technique often used to reduce a large set of variables into a smaller one, whilst maintaining most of the information that was found in the large dataset. This smaller set of new, uncorrelated variables are known as principal components, and they are linear combinations of the original variables. In PCA, principal components are referred to as eigenvectors, i.e., the direction of the axes where the most variance is found. Each eigenvector has a corresponding eigenvalue, which is the amount of variance found in each principal component.

The number of principal components (alternatively referred to in this work as PC scores) that are produced following PCA directly links to the number of measurements found in the

dataset (e.g., if there are 200 measurements in the dataset, there will be 200 principal components/PC scores). Maximum variance is found in principal component one (PC score 1), followed by the next largest amount of variance in principal component two (PC score 2), and so on.

Inclusion of more PC scores in a reduced dataset therefore leads to the inclusion of more features found in the data. However, the larger the number of PC scores, the higher the risk of overfitting the data, as smaller details that occur in the noise of the training data will be used by the algorithm to determine discrimination, rather than those details that are actually meaningful.

Overall, PCA provides information of the most meaningful features in the data, allowing the researcher to dismiss those components that hold less important data. This allows the dimensionality of the dataset to be reduced, without losing too much information. Therefore, a better way to visualise the data has been provided, so that only the important differences can be observed.

In this thesis, PCA is used to discriminate between three different groups of vibrational signals (those corresponding to honey bee movements, those corresponding to Varroa walking, and those corresponding to background noise). PCA is used to determine the features in the data that contain the most variance, regardless of their grouping to the three categories. The PC scores identified to be of importance are then fed to a second data analysis technique: discriminant function analysis (DFA), to further assess variance between the groups of signals, using only the data held in the selected PC scores, i.e., the reduced dataset.

#### *1.4.5.4. Discriminant function analysis*

DFA is quite similar to PCA, except that in PCA, variance is found without prior knowledge about the data (i.e., PCA does not consider if the data was already in specific groups such as red flowers, white flowers and yellow flowers). DFA on the other hand, identifies the components that have maximum variance based on groups that are defined by the researcher.

In this thesis, DFA is used following PCA to determine the differences between various complex datasets (groups of vibrational signals) that contain a very large number of variables. The data given to the analysis is in the form of PC scores, established via PCA, and the purpose is to identify discriminatory features in this new, reduced dataset, based on the

predefined groups of signals that have been provided (i.e., mite, bee, and background vibrations).

This analysis is a prerequisite for the automated detection of vibrations. By determining the features that differ between signal types, the software that is built to automatically detect vibrations can identify these differences in novel accelerometer data and provide useful information on newly detected signals (e.g., it will allow the correct identification of a detected vibration based on its features).

# Chapter 2: Accelerometer detection of vibrational pulses originating from Varroa individuals

## 2.1.0. Chapter overview

This chapter describes and analyses in detail a discovery that I made regarding Varroa mite vibrations recorded with accelerometers. Not only have I established that vibrations produced by Varroa can be detected with this technology, but in the process, I also identified a behaviour novel to science that has a corresponding vibrational trace. The behaviour that produces this vibration of interest, which I term 'jolting', was observed in multiple mite individuals. Four of these individuals were focused upon for in-depth analysis, and each resided on a different substrate. It is the results of this analysis that are included in this chapter.

The chapter begins with an introduction to the study that links to section 1.2.2.4. where vibration and its potential role in the Varroa life cycle was initially discussed. The methods are then followed by the results, which provide a description of the novel behaviour, alongside a detailed investigation into the features of the vibrational trace and how it differs dependent on the substrate upon which it is transmitted. The results are then discussed in terms of the characteristics of the vibration and speculation of its function, with further focus on the potential use of this signal as a Varroa detection tool within honey bee hives.

The main figures in this text are listed as Figure 2.1, Figure 2.2., and so on. The supplementary material for this text can be found in Appendix 1, and are referenced as S1, S2 etc. in the text. There is a large amount of video data relevant to this study. Videos are also mentioned in the text as S1, S2 and so on. The figure legends for the video data can be found in Appendix 1. The videos themselves have DOI links (see page 10) and are labelled according to their text reference (S1, S2 etc.).

## 2.2.0. Introduction

As discussed in detail in chapter one, more research is now being done into remote mite detection in honey bee hives, with a current focus on visual and olfactory based technologies. Vibration sensing methodologies have not yet been implemented in this line of investigation.

Accelerometers have been used successfully by our research group to detect and characterise a variety of honey bee vibrational signals, as well as monitor the overall status of the colony (Bencsik et al., 2011; Bencsik et al., 2015; Ramsey et al., 2017; Bencsik & Newton, 2018; Ramsey et al., 2018; Ramsey et al., 2020). Individual honey bee signals can be searched for and detected within the noise of the whole colony, based on knowledge of their vibrational features. There is potential for the vibrations of Varroa mites to be captured with accelerometer technology using the same methods.

As Varroa mite detection techniques are now beginning to evolve from disruptive, physically demanding methods towards remote, technology-reliant approaches (see section 1.3.0), it would seem only logical to investigate the potential for monitoring mite related vibrations as a hands-off supervision technique.

Vibration is also a lesser-studied sensory stimulus in the Varroa mite life cycle. Gathering new information on the features of detected mite vibrations and the behaviours that produce them could provide important insight into whether mites are capable of responding to, or transmitting, functional vibrational signals. At present, there is limited evidence for this due to a lack of research, but other mite and tick species are known to transmit and respond to vibratory stimuli, indicating that it is worth perhaps pursuing in Varroa.

#### 2.2.1. Vibration perception and transmission in Acari

The utilisation of substrates to transmit and receive vibrations can be observed in many taxa and for a variety of reasons (Hill, 2009; Mortimer, 2017). Within the subclass Acari, which includes mites and ticks, vibration reception triggers movement in individuals, and is suggested to be associated with host orientation (ectoparasitic mites) (Kilpinen, 2001; Owen & Mullens, 2004; Kilpinen, 2005), predator avoidance (spider mites) (Azandémè-Hounmalon, et al., 2016), prey detection (predatory mites) (Proctor & Pritchard, 1989; Proctor & Pritchard, 1990; Azandémè-Hounmalon et al., 2016), orientation towards conspecifics for reproduction (predatory mites) (Proctor, 1991; Proctor, 1992a; Proctor, 1992b), and egg hatching delays as a response to mechanical stimuli (predatory mites) (Fukuse & Yano, 2019). For Varroa, vibration reception has been suggested to play a role in the host orientation aspect of the life cycle (Le Conte & Arnold, 1987) as mites have been observed to preferentially enter tubes that emit vibration over controls (Le Conte & Arnold, 1988). However, despite this, vibratory cues have not been investigated any further for this species.

If receiving vibrational signals is somewhat neglected as a research topic in mites, the transmission of such signals is even more so. Yet some mites have been observed generating

vibration. There is no mention of this in the literature for *Varroa*, aside from the one paper mentioned in section 1.4.3., where walking vibrations are succinctly described without detailed quantification or discussion (Es'Kov et al., 2003). For other members of the subclass Acari, however, there are more robust examples. Male water mites of the species *Neumania papillator* exploit the prey orientation response of females by vibrating their forelegs to produce signals of a similar frequency to that of their prey species. By doing so, they attract and hold the attention of females for mating (Proctor, 1992b). Females of the tick species *Otobius megnini* have been observed to produce a vibrational signal prior to mating, suggested to attract males (Hooker et al., 1912; Diyes & Rajakaruna, 2017). There is also a species of mite that has been described as having a small group of setae that are speculated to function together as a vibration transmitter for conspecific communication (Coineau et al., 1997). Although these studies lack signal quantification and experimental evidence, they provide a foundation for further investigation into a widely untapped area of exciting research.

#### 2.2.2. Measuring the muscular power required to produce transmitted vibrational signals

The features for some other invertebrate transmitted vibrations have been carefully explored. The power output of a vibrational pulse generated by one individual insect has previously been estimated (Michelsen et al., 1982), demonstrating that a small organism, the shield bug (Heteroptera) *Sehirus impressus* (*Canthophorus impressus*) (25mg, 6 – 7mm), can produce a vibration requiring a power of 30nW, using a muscle weighing 1µg, in the context of various communicatory behaviours. The author, Michelsen, then went on to calculate the same for a honey bee 'begging signal', which required a power output of 0.02mW with a muscular weight of 0.3mg (Michelsen et al., 1986). The stridulatory distress signal of an ant species has also been demonstrated to require an output of 10 – 20nW (Markl, 1967). For vibrational signals in other species, the quantification of vibrational pulse power has not been followed up (Casas et al., 2007; Michelsen, 2014).

In this chapter, I aim to overcome this by estimating the pulse power of a *Varroa* vibration, to help determine if such a pulse is functional. A high-power output in relation to small body size and mass may indicate that the vibration is energy demanding to produce, and therefore not performed by the organism without purpose.

### 2.2.3. The potential for Varroa mite engagement in the honey bee colony vibrational environment

Honey bees utilise the wax honeycomb as a means of conveying communication signals, as vibratory signals spread effectively across the comb surface (Tautz et al., 2001). The transmission of vibrations can be altered and negatively affected by changes in comb density (caused by the natural loading and unloading of the frame, e.g., due to the brood cycle) and the presence of the wooden frames, which causes differences in signal frequency (Sandeman et al., 1996; Bencsik et al., 2015). Yet honey bees have been shown to actively improve the vibration propagation properties of the substrate by dampening background vibrations and altering the structure of the comb within their wooden frames, such as by removing the frame edge (Sandeman et al., 1996; Smith & Chen, 2017). As Varroa mites occupy the same environment as their honey bee hosts, perhaps mites too have the capacity to exploit these conditions to their advantage.

### 2.2.4. Main outcomes of this chapter

This chapter investigates the use of an ultra-sensitive (1000mV/g) accelerometer (deemed the most appropriate for this purpose, see section 1.4.1.) as a method of detecting Varroa mite vibrations. Here, I successfully capture mite-related pulses for a variety of behaviours, but focus on one in particular, which I believe is of the greatest interest to science and the most promising in terms of accelerometer detection. I characterise this previously undescribed Varroa behaviour, which produces what I hypothesise to be a deliberately transmitted signal. This behaviour, here coined 'jolting', is analysed in terms of its detectable, vibrational trace, and in the context of other discernible mite behaviours and honey bee signals. The energy required to produce this signal is estimated using a control experiment that created an artificially produced vibration with features highly similar to that of the jolting pulse.

I here show that I can detect this signal on various substrates, and that the features of the pulse change dramatically depending on the nature of the substrate onto which it is delivered. A Varroa mite is a minute organism (0.42mg average weight, in comparison to a honey bee worker, 115mg average weight (Schmolz et al., 2005), and an *S. impressus*, 25mg (Michelsen et al., 1982)). Yet, I further demonstrate through the implementation of the artificial vibration experiment that mites can produce a high-power signal relative to their body size and mass that is likely, therefore, to serve a purpose. I also show that the signal has comparable vibrational magnitude to that originating from other, much larger invertebrates, and can be

produced by one individual mite repeatedly over prolonged time periods. The features are discussed in terms of the possible function of the signal, which I believe is linked to host/environmental orientation, based on the current results.

The implication of these findings in terms of nature of substrate, pulse features and behaviour are also discussed regarding the accelerometer detection of mites in a real hive environment, which may lead to a new method of detecting and managing this important species.

#### 2.2.5. Aims of the chapter

The aims of the chapter are as follows:

- Provide evidence for the detection of Varroa mite vibrations using accelerometers.
- Describe the behaviours that produce the vibrations of interest.
- Characterise the features of the main vibrational trace of interest (jolting) and how it differs dependent on the substrate upon which it is transmitted.
- Discuss the possibility of detecting this signal within honey bee hives, as a potential search tool for Varroa.
- Discuss the potential function of the jolting signal.

### 2.3.0. Methods

#### 2.3.1. Mite collection

Measurements were undertaken at Nottingham Trent University between August 2019 and December 2019 for the honeycomb and Petri-dish data, and early summer 2020 for the artificial capsule and brood-comb data. Varroa mites were collected from the base board of a hive containing a colony of *A. mellifera* that had not been treated for mite infestation that year. The hive was housed in an observatory building, protected from the weather, with a tube that led from the hive entrance to the exterior of the building to allow honey bees to forage as normal. Live mites were identified and collected daily. They were then immediately taken to the laboratory and used for measurements within one hour of collection.

Live mites were weighed using a set of electronic scales (Kern ALJ 160-4NM) as a batch of 12 individuals, and an average taken, as a single mite was too small to register on the scales ( $n = 12, 0.42\text{mg}$ ).

### 2.3.2. Measuring the vibrations emitted from Varroa individuals

#### 2.3.2.1. *The substrates chosen for experimentation*

Mites were placed onto either (i) a plastic Petri-dish (50 x 10mm), (ii) a British standard sized frame of fully built, but empty comb (no honey, pollen, or brood), (iii) a piece of loaded brood-comb removed from a hive with a scalpel, or (iv) within a gelatine capsule (see Figure 2.1).

An ultra-sensitive accelerometer (4507 B 002, Brüel & Kjær, 1000 mV/g) was used to collect the vibrational data, glued to the base of the Petri-dish, or secured centrally to the frame of empty honeycomb by pushing the sensor into the comb and securing it with a small amount of molten wax. On the opposite side of the comb, an area was marked to indicate where the accelerometer was fixed to ensure that mites were placed within the vicinity of the sensor.

In two instances, a piece of brood-comb was removed from a hive and placed on the Petri-dish with attached accelerometer. These samples were being recorded for the purpose of another study (see chapter 3) but were included in the analysis of this experiment as the set-up was identical to the Petri-dish, gelatine capsule, and honeycomb recordings, and on each of the samples, a mite appeared during filming, perhaps from ruptured cells caused by the removal of the brood-comb specimens with a scalpel. The mite individuals were seen performing the behaviour of interest, jolting, for prolonged periods, so it was decided to include them for comparison to the other substrates. Brood-comb sample 'one' was 3.5 x 2cm in diameter and contained 2 drone larvae, 1 drone pupae, 19 worker larvae, 3 worker pupae and 6 empty cells. Brood-comb sample 'two' was 4 x 2cm in diameter and contained 7 almost fully developed worker adults, 13 purple eyed worker pupae and 17 empty cells.

In one instance, a mite was placed inside a gelatine capsule (size 3, 0.3ml volume, 5.6mm inner diameter, Agar Scientific, UK) and placed on the Petri-dish above the accelerometer, in the same way that the brood-comb samples were recorded. The mite and capsule were filmed under the same conditions as the other substrates. Again, this set-up was recorded for the purpose of another study, to mimic a brood-cell (see chapter 3) but was included in this chapter for the same reasons as the brood-comb samples.

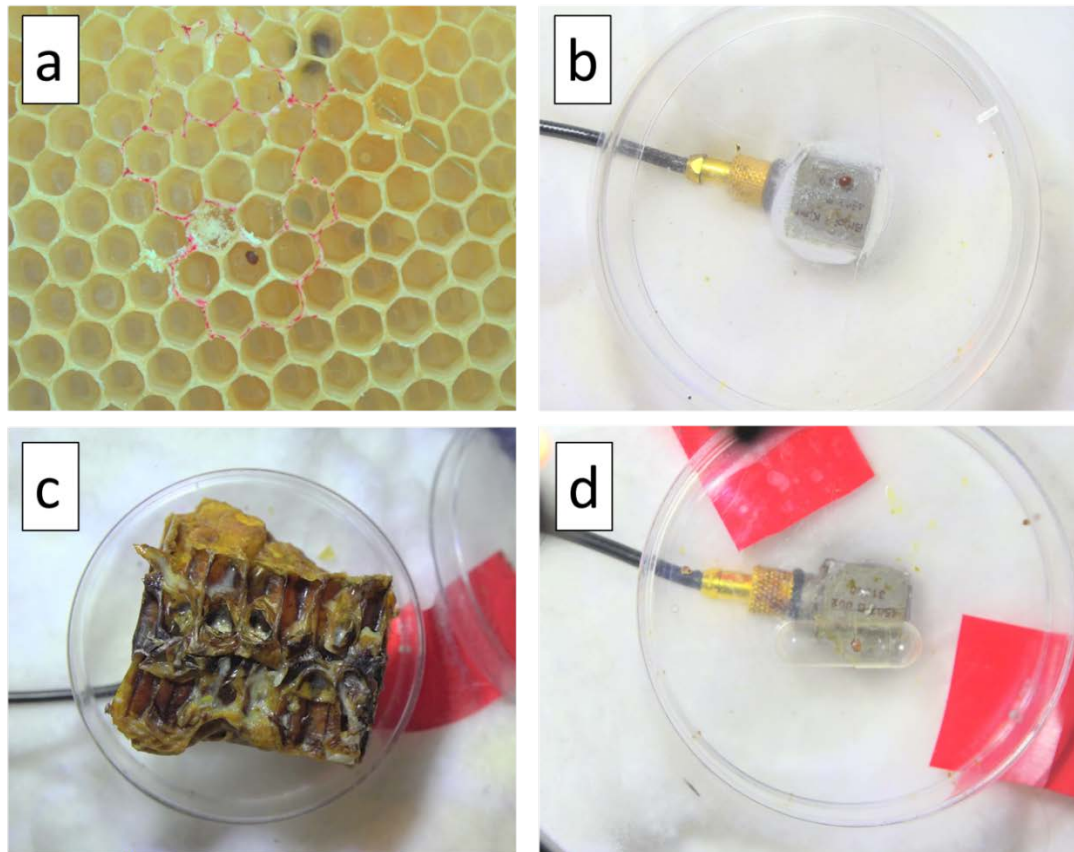


**Figure 2.1:** The four substrates used in this study. Image ‘a’ depicts the empty honeycomb. The red outlined area indicates the placement of the accelerometer, which is found on the opposite side of the comb. This image is zoomed in on a smaller area of the full, empty framed comb. Image ‘b’ shows the Petri-dish with the accelerometer glued to the underside. Image ‘c’ shows a sample of brood-comb placed on the Petri-dish. The mite can be seen on the bottom left edge of the comb. Image ‘d’ shows the transparent gelatine capsule on the Petri-dish. All images include a Varroa to demonstrate the scale of the substrate.

#### *2.3.2.2. Accelerometer recording and video set-up*

A camera (Sony 4K FDR-AX100E handy cam, China) was set-up on a tripod and positioned directly above the Petri-dish or comb for filming. A single channel conditioner (Endevco 4416, USA) at a gain of x10 fed the signal to the microphone input of the camera to capture the acceleration signal synchronously with the videos. The same conditioner was used for all measurements. A light source was placed near the vicinity of the Petri-dish/marked area of the empty comb to illuminate the mites for clearer observation.

To reduce interference from background vibrations and vibrations originating from background sound, the set-up was placed within a sound isolated room and the Petri-

dish/comb with attached accelerometer positioned on a thick wad of cotton wool (3 – 4cm in height). Ambient temperature was maintained at approximately 18 °C.

The general pattern of filming consisted of collecting 30 seconds of just background noise (required for signal analysis, see sections 2.3.5.1. and 2.3.5.2.) before adding mites to the substrate. Mites were filmed at 50 frames-per-second (FPS) in 1080 x 1920p resolution, with the audio record level set to ‘manual’ at 20% to prevent signal saturation. The audio track of the camera took place with a sampling rate of 48 000 Hz.

Each filming session lasted 10 – 20 minutes for all substrates except one video that was 60 minutes, and the brood-comb samples, which were filmed long-term, for approximately an hour and a half. The Varroa identified in these recordings were in view for about 20 minutes.

Aside from the brood-comb, mites were placed on each substrate in randomly selected groups (ranging from 1 individual to 19 individuals), dependent on the number of mites collected that day. Overall, the number of videos recorded for each substrate are as follows: (i) Petri-dish ( $n = 10$ ), (ii) honeycomb ( $n = 5$ ), (iii) brood-comb ( $n = 2$ ), (iv) gelatine capsule ( $n = 1$ ).

#### *2.3.2.3. Examining the video recordings for behaviours of interest*

The video recordings were examined to identify behaviours of interest. The initial aim of the study was to observe mite behaviour with an accelerometer sensor and deem whether it was possible to capture vibrational traces emitted from any mite activity. Several behaviours were identified that produced a detectable vibrational trace (Appendix 1, see Video S1, Video S2, Video S3, and Video S4), but I chose to focus on those that showed the most promise for yielding exciting science and for further analysis. The pulse that is the main focus of this chapter is a vibrational trace that is produced by a novel behaviour, which I term ‘jolting’. Attempts to capture sound from this behaviour with both a standard microphone (Tascam DR-05X, USA) and an ultra-sonic bat detector (Magenta Bat 5, Tutbury, UK) were unsuccessful, indicating that jolting pulses produce vibratory signals only.

For all recordings (amounting to a total of 279 minutes of footage), each individual mite was tracked for the duration of its time on the substrate to record the number of jolting pulses produced. This was for the purpose of identifying the percentage of mites that produced the behaviour of interest. In two cases, this was not possible as there were 8 and 19 mites present on the substrate, which caused difficulty in identifying specific individuals and their

jolting patterns as they moved around the substrate. Only one individual from the 19-mite video was further analysed as it remained in the same position.

For in-depth analysis of jolting pulse features, four videos comprising of a (different) jolting mite individual were chosen, one for each of the substrates of interest (Petri-dish, honeycomb, brood-comb, gelatine capsule). Focus was placed upon these individuals as they produced a remarkably high number of the pulses of interest in succession (a jolting 'trend'), with visible and hearable accelerometer traces. Four additional mites that produced a jolting trend were dismissed from further analysis as three of them lacked visible accelerometer traces and a fourth was subject to recording issues where the traces were visible but the audio saturated (clipped). The mite recorded with the saturated audio was the very first mite to be filmed. As a result of this issue, the audio was rectified immediately for all subsequent recordings.

*2.3.3. Measuring vibrations emitted from other species for comparison against Varroa*  
Varroa jolting accelerometer waveforms on the Petri-dish, honeycomb, and brood-comb substrates were compared with mite walking vibrations and the vibrations of other invertebrates (individual honey bee, full honey bee colony, a woodlouse). The jolting pulses collected on the gelatine capsule were not compared to the vibrations of the woodlouse as the data was collected at a different time, and the woodlouse individual that was used for all other substrates was no longer available. Gelatine capsule pulses were compared to walking pulses, but overall, this substrate could not be analysed in the same way as the other three substrates as only 3 of the 28 jolting pulses that were observed had visible accelerometer traces. Due to this small sample size, it was not possible to gain insightful statistics on the features of jolting pulses in capsule when compared to other vibrations. Therefore, only limited feature analysis could be carried out overall.

#### *2.3.3.1. Woodlouse vibration recording*

A woodlouse was collected and weighed. Its vibrational signal was measured using the same equipment and set-up as the mite recordings. The woodlouse was placed on each of the three substrates (Petri-dish, honeycomb, brood-comb) to provide a comparison between the signal of the Varroa mite and that of a larger invertebrate.

#### *2.3.3.2. Honeybee individual and colony recording*

'Low' and 'high' signal recordings of the honey bee colony (depending on the comb mass density load) were collected for the full colony comparison. A typical honey bee colony is distributed on ten frames, resulting in typically 1000 to 2000 honey bees per frame, and it is

expected that around 10% of these individuals contributed to the overall measured signal, as the accelerometer vibration detection range is around 4 – 5cm when the comb is loaded with contents (brood, honey, pollen), i.e., the signal is dampened. If the frame is devoid of contents, the accelerometer can detect vibrations from bees over its entirety (Bencsik et al., 2015).

A specific individual honey bee vibratory signal (a ‘whooping signal’ (Ramsey et al., 2017)) was also extracted from this data for the individual honey bee comparison. Although the ‘whooping’ signal has a much longer time duration (150ms) than that of a jolting pulse, it was chosen as an interesting reference due to it being a single pulse originating from a single bee, and very common too.

For the honey bee colony and individual honey bee comparison, the mite recording taking place only on brood-comb substrate data was chosen for visual comparison. This choice was made as the brood-comb set-up was closest to the mites’ natural environment. This allowed me to explore the possibility of detecting mites amidst the continuous honey bee signal.

#### 2.3.4. Estimating the power required by Varroa to produce the jolting pulse

The power output of the jolting pulse was estimated by an experiment aiming at replicating the vibrational trace of the Varroa jolting signal. In the sound isolated room, the same conditioner, cables, accelerometer, Petri-dish, cotton wool, and camera were set up in the same manner as for mite recordings. Glass beads (400µm in diameter) were dropped from a height of 1cm onto the Petri-dish, both directly above and slightly offset the accelerometer, to replicate the differing positions of the mites when jolting. Fifteen repeats were taken for each position. The conditioner was set to a gain of x1 as the accelerometer waveform that was produced by the impact of the falling bead clipped the digitiser. This was accounted for during the calculation to reflect the x10 gain that was used for mite recordings.

The bead velocity was measured by estimating the distance travelled by the bead frame-by-frame as it was dropped, using video captured at 240 FPS. The average weight of a collection of glass beads was taken as a single bead was too light to be detected by the scales (8028-series professional digital jewellery scale, China), resulting in an estimate for a single bead mass being 0.07mg.

#### 2.3.5. Signal analysis of Varroa jolting and walking vibrational pulses

All signal analysis was conducted though Matlab (Refworks 2019a) using code written specifically for this study, at Nottingham Trent University.

The Sony camera audio signal was calibrated using a signal generator, by driving 10 mV at 1 kHz into the microphone input slot and recording and inspecting the response.

The vibrational trace of the jolting behaviour was analysed directly from the audio track of the video footage. For each substrate, a separate, carefully designed movie was created from the Sony video footage taken of the mite, to demonstrate the synchronicity between (i) the vibrational trace of the signal and (ii) the movement of the Varroa mite (see Figure 2.2). The spectrogram of the accelerometer data was updated continuously as a function of time (reflecting the time stamps of each frame of the original video). The spatial gradient of the image was produced to identify the mite boundaries against the background pixels (edge detection) and better determine mite movement, as pixels found at the mites' periphery exhibited the greatest changes in contrast intensity upon each instance of jolting. When the spatial gradient image is blue in colour, no movement of the mite has been detected. When the mite does move, the pixels that represent the periphery of the body flash red, indicating motion (see Figure 2.2). The difference between two such consecutive frames was computed and averaged to provide a scalar as a reliable indicator of mite movement and was superimposed on the spectrogram time window (see Figure 2.2). Each resulting peak, if it extended beyond a suitably chosen threshold (a.u.), was then given a number via a counter, and the relevant accelerometer data (a time window of 0.4 seconds around the peak) saved.

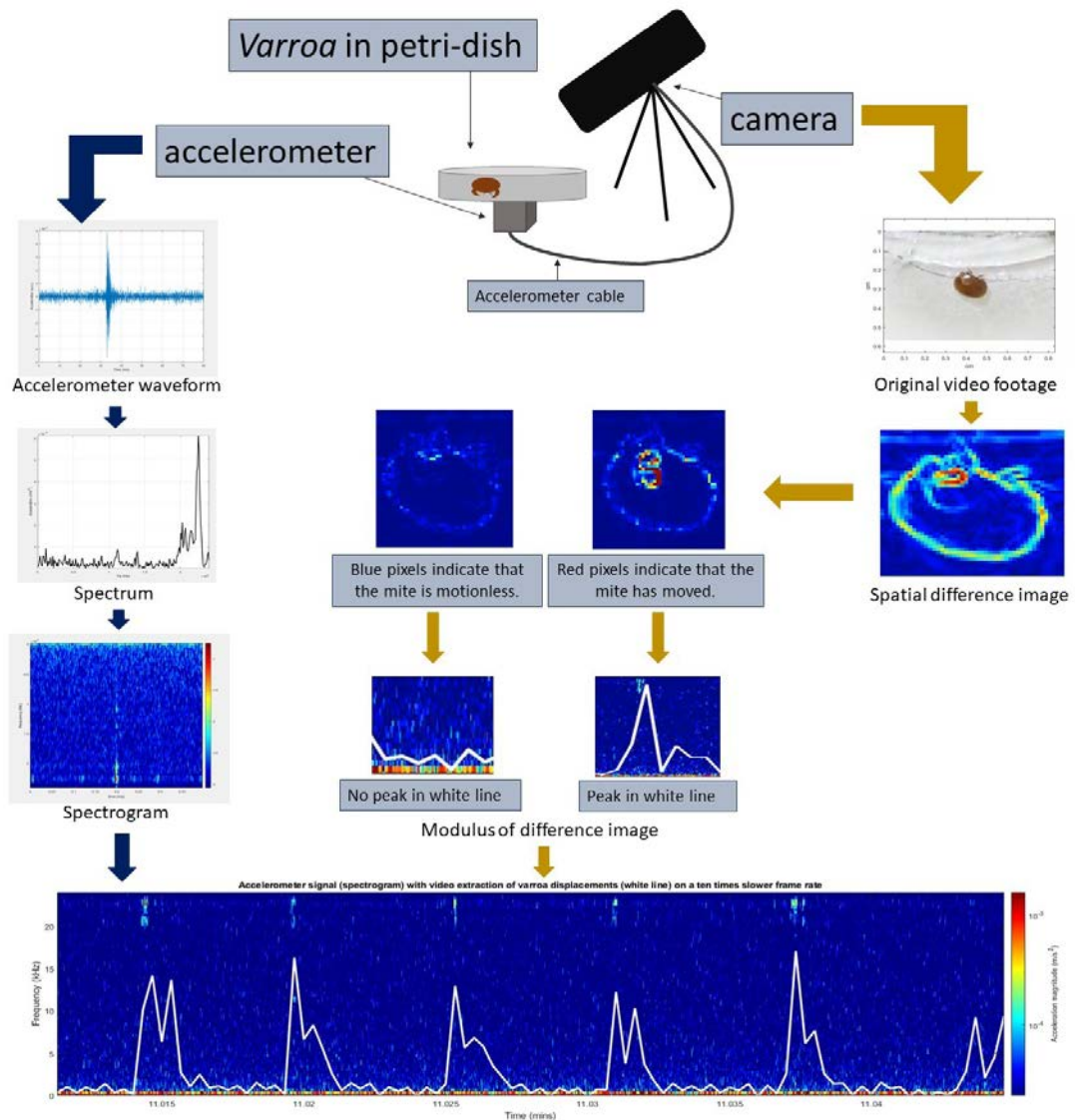


**Figure 2.2:** A diagram to demonstrate the process of analysing the jolting pulse data. All four mites on each substrate underwent the same video analysis. The mite is placed on the substrate with the accelerometer attached and is filmed with the camera, producing a movie that has synchronous audio and video. The left-hand side of this diagram demonstrates how the vibrational data are processed. The raw accelerometer waveform of the movie is transformed into a spectrum, which shows the frequency (Hz) (x axis) and magnitude of acceleration ( $m/s^2$ ) (y axis) of the vibrational data. A collection of such spectra is then stacked into a spectrogram, which shows time (seconds) (x axis), frequency (Hz) (y axis) and magnitude of acceleration (logarithmic to the base 10) (pixel intensity). Dark red shows the highest magnitude and dark blue shows  $1/70$  of this maximum. The maximum acceleration magnitude is forced to be that of the Varroa jolting pulses for better viewing, resulting in clipping of the irrelevant data at the lowest frequencies. The accelerometer recording for the entire original movie is transformed into a spectrogram, running with respect to time. The bottom panel shows a two-seconds long section of this movie. The right-hand side of the diagram demonstrates how the visual data are processed. The original video data that is collected

is further cropped to better focus on the mite for the purpose of simple edge detection (by means of the spatial gradient of the pixel intensity). The modulus (absolute value) of the difference image shows the changes in pixel intensity in two consecutive frames as seen in the spatial difference image. In the modulus of the difference image, the mite is mostly dark blue when motionless, but exhibits edges that flash red when moving abruptly. The sum of the pixel intensities in this panel are then displayed as the white line that is superimposed on the spectrogram data of the bottom panel. This demonstrates the remarkable synchronicity between video-detected mite displacement and accelerometer trace. This processing is used to create the supplementary videos (see Appendix 1, Video S5, Video S6, Video S7, and Video S8).

The peak counter was also used to record the timing of each jolting occurrence. However, the absolute timing of each jolting accelerometer trace is unknown. The displacement of the mite body lasted approximately 20ms, whereas the vibrational trace produced by the movement lasted approximately 3ms. The software did not detect the vibrational trace itself, instead saving a timing that occurred within the white peak, an area that was indicative of the entire period of mite displacement as it jolted.

As a result, the vibrational traces for each substrate were observed at slightly different time points within their 0.4 second window, and subsequently underwent further alignment using the cross-correlation product, to benefit further analysis (see sections 2.3.5.1. and 2.3.5.2.).

Any movement of the mite caused an automatic detection, whether created by jolting or not. Therefore, to ensure that only jolting behaviour was analysed, each movie was further scrutinised manually to disregard those occasional peaks that were false positives. Only the true positive jolting timings were then further analysed.

Two methods of analysis were used on the collection of extracted true positive jolting pulses, one using the accelerometer waveform, the other using spectrograms:

#### *2.3.5.1. Method 1: Using the accelerometer waveform*

This method was used to create the histogram, power spectra, and spectra figures that can be seen in the results section (see sections 2.4.3. and 2.4.6.2.). Each of the collections of jolting signals on brood-comb, honeycomb, and Petri-dish were aligned using cross-correlation product analysis. The accelerometer waveform of the strongest jolting pulse was used as a reference pulse, which was aligned to the next closest accelerometer waveform in the collection. The closest match then became the new reference pulse, and the remaining pulses were scanned for the best match to this reference. This continued until all pulses were

aligned to one another. This analysis allowed high-quality alignment despite variations found between jolting pulses. All pulses were high-pass filtered with a cut-off at 300 Hz so as to remove background noise without interfering with the frequency bandwidths that contained the signals of interest. Thermal noise (electrical noise that is produced by recording technology) was further removed by calculating the magnitude of acceleration of each pulse to produce a scalar. An area of recording that contained no signal of interest had its (high-pass filtered) spectrum averaged to produce a second scalar. These were then subtracted from one another to produce the genuine magnitude of acceleration of the pulse, i.e., free from background and thermal noise.

The histogram and spectra figures (see section 2.4.6.2.) also illustrate Varroa walking pulses. To include these, a suitable portion of accelerometer data was extracted that contained a large number of walking vibrations for each of the brood-comb, honeycomb and Petri-dish substrates. These were transformed into spectrograms and the mean of all frequencies taken for each substrate in time steps of 1ms. Walking pulses were easily identified as pronounced negative peaks in the second order time differential of the corresponding data. They were then extracted based upon the identified timings, and the overall magnitude of every pulse was calculated in the same way as for the jolting pulses, including the same filtering process and thermal noise subtraction.

#### *2.3.5.2. Method 2: Using individual spectrograms*

The jolting pulses for each collection (brood-comb, honeycomb, and Petri-dish) were also analysed as individual spectrograms, to showcase their vibrational features. Each individual jolting signal was transformed into a spectrogram. Each spectrogram was then aligned using simple cross-correlation product analysis with a reference spectrogram (a particularly clear signal chosen from each collection). The three collections of signals were then high-pass filtered to remove background vibrations that interfered with the clarity of the waveform. Appendix 1, Figure S9 demonstrates the averaged spectrogram for each collection of pulses, which was used as a guidance for where to filter the background vibrations. A second cross-correlation product alignment was then done using the time course of the filtered accelerometer signals to align them with very high temporal resolution (20 $\mu$ s). This enabled all genuine signals to be thoroughly compared for commonly shared characteristics.

For the gelatine capsule, as there were just three detectable jolting traces, the captured vibrations were transformed into spectrograms and showcased alongside their corresponding accelerometer trace. All three pulses were individually high-pass filtered with

a 500 Hz cut-off, to remove background vibrations that interfered with waveform clarity. There was no requirement to align the three pulses for further analysis due to the small sample size.

The vibrational traces recorded for the woodlouse, honey bee colony, and mite walking (on all four substrates) were all also transformed into spectrograms and scaled identically with the strongest mite jolting signal spectrogram, all in logarithmic scale. The time course of each panel was also calculated, to show the integral of the acceleration magnitude at each point in time.

#### 2.3.6. Signal to noise ratio analysis/successful detection of jolting pulses

To establish how detectable jolting pulses are, by accelerometer evidence only, the signal-to-noise-ratio (SNR) value was first estimated for each substrate (all four) and jolting pulse. The 'noise' magnitude was estimated from the standard deviation of a section of accelerometer data free from Varroa signal. The 'signal' magnitude was further estimated using the mean of the modulus of the accelerometer signal where the pulse resides, over 5ms.

Critical listening of the accelerometer recording of the signal was then undertaken, separately. Playback speeds for each substrate were chosen that best demonstrated the jolting pulse audibly. For the Petri-dish, the playback speed was reduced by a factor of ten as the pulses occur mostly at the highest (inaudible) frequency bandwidth, requiring the largest reduction in speed to bring these to as hearable a level as possible. For the brood-comb and honeycomb, the playback speed was reduced by a factor of two, as the jolting pulses naturally occur at lower frequencies that are close to human audible levels. For the capsule, the playback speed was maintained in its original form as the three jolting pulses that had visible accelerometer traces were all within human audible range.

The percentage of audible signals in each collection was finally calculated to pinpoint the (independently calculated) SNR threshold value, indicating where the method begins to detect jolting signals.

#### 2.3.7. Accelerometer and Petri-dish resonance analysis

The resonance of the accelerometer and Petri-dish were measured to establish the natural frequencies at which the sensor and substrate vibrate at higher amplitudes. It was important to determine this, so that any vibrations produced by mites could be identified in respect to

these frequencies, to establish whether they were genuinely caused by the mite and not as a result of the sensor or substrate resonant frequencies.

To measure the resonance of the accelerometer that is used in this work, a full frequency sweep (0 to 24,000 Hz) was conducted. The same accelerometer, conditioner, and camera as implemented in the rest of the study were used for this.

The accelerometer was glued centrally to a mini shaker (4810, Brüel & Kjær, Copenhagen). A conditioner with a gain of x1 fed the accelerometer signal to the Sony camera, which was used to record the response of the accelerometer to the frequency sweep. The mini shaker was driven by a PC that played back a recording of the full frequency sweep.

The magnitude of the signal driven into the mini shaker was gradually increased, and separate recordings were taken each time. Three signal sizes were explored: 3%, 6%, and 9% of the maximum volume level of the PC.

Analysis was carried out using code written in Matlab (Refworks 2019a), at Nottingham Trent University. The amplitude of the accelerometer recordings were compared to each other by plotting the difference between each of the larger signals and the smallest signal expressed as a ratio (twice bigger (6:3) and three times bigger (9:3)) (see Appendix 1, Figure S10).

The Petri-dish with attached accelerometer was secured to the same mini shaker. A conditioner with a gain of x1 fed the accelerometer signal to the PC. The full frequency sweep was driven from the PC to the mini shaker at a volume of 25%, three times: (i) Petri-dish with lid on, (ii) Petri-dish with lid off, (iii) accelerometer alone. The signal was driven to the Petri-dish both with and without the lid on as the video recordings taken of mites included both scenarios, dependent on how active the mites were (the lid was used to prevent mites from escaping in situations where they were very active). The responses of the accelerometer and the Petri-dish were recorded by the Sony camera and visualised together (see Appendix 1, Figure S11).

## 2.4.0. Results

### 2.4.1. A description of the jolting behaviour

The vibration that is the focus of this study, here termed 'jolting' pulse, chosen because of the corresponding abrupt movement of the body, is extensively illustrated and analysed. This behaviour is a rapid pulsing of the body either in a left or right direction, before returning to the original central resting position (see Figure 2.3, see also Appendix 1, Video S12).

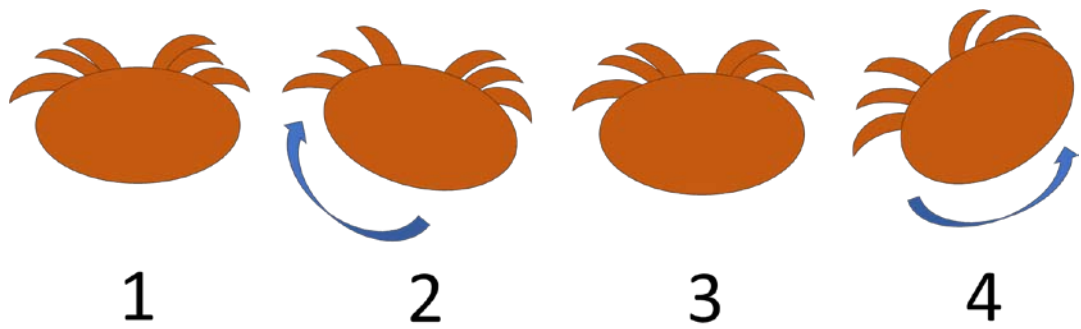


**Figure 2.3:** A simple illustration of Varroa jolting behaviour, observed from above. 1) the mite is in a stationary, resting position; 2) the mite then abruptly swings its body to the left; 3) the mite briefly returns to its original resting position; 4) the mite then swings its body to the right, before returning, again, to the resting position. Diagram produced by Harriet Hall.

When producing a jolting pulse and viewed from a sideways position, the Varroa legs can also occasionally be observed to flex, moving the body down and then back up again off the substrate (see Figure 2.4, see also Appendix 1, Video S13). During all video observations, mites were only observed to jolt when stationary.

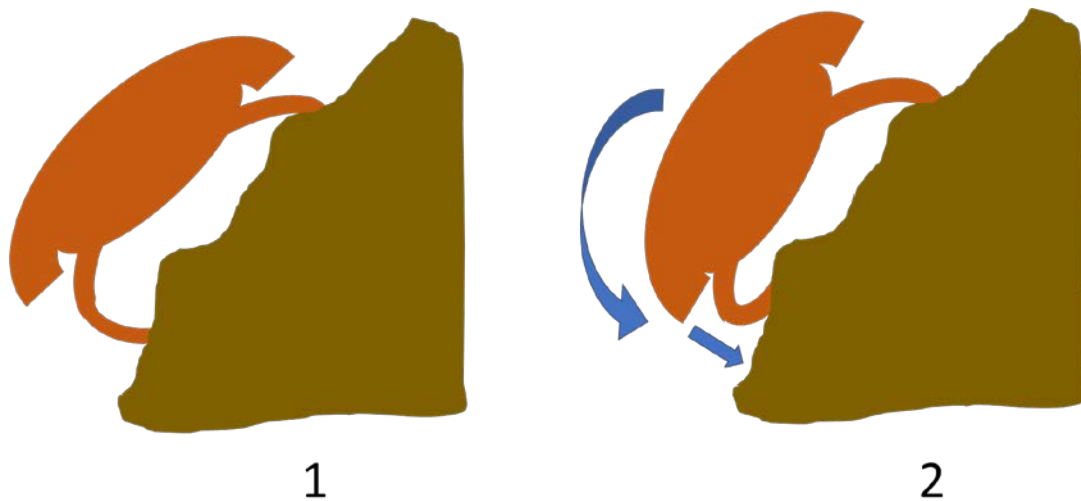


**Figure 2.4:** A simple illustration of Varroa jolting behaviour, observed from the side. Here the mite is stood on brood-comb, at an angle. 1) the mite is in a stationary, resting position; 2) the mite jolts to the left. The body swings down and leftwards and the legs bend. The mites' body and legs then move back upwards to the original position seen in 1. In some cases, both sets of legs (left and right) bend downwards as the mite jolts its body (see Appendix 1, Video S13). Diagram produced by Harriet Hall.

The jolting behaviour of mites was recorded and analysed on four substrates: Petri-dish, empty honeycomb, loaded brood-comb, and gelatine capsule. Fifty-five mites were closely inspected for jolting trends. Of these, 45.5% were never observed to jolt. The remaining 54.5% jolted at some stage during the video footage, categorised as either jolting without an obvious trend (42%), or jolting with an obvious trend (13%) (see Figure 2.5). I define ‘obvious trend’ as a mite repeatedly jolting in quick succession, with 10 seconds or less between consecutive jolts for more than one minute following commencement of the behaviour, i.e., what I deemed to be a regular occurrence of the behaviour.

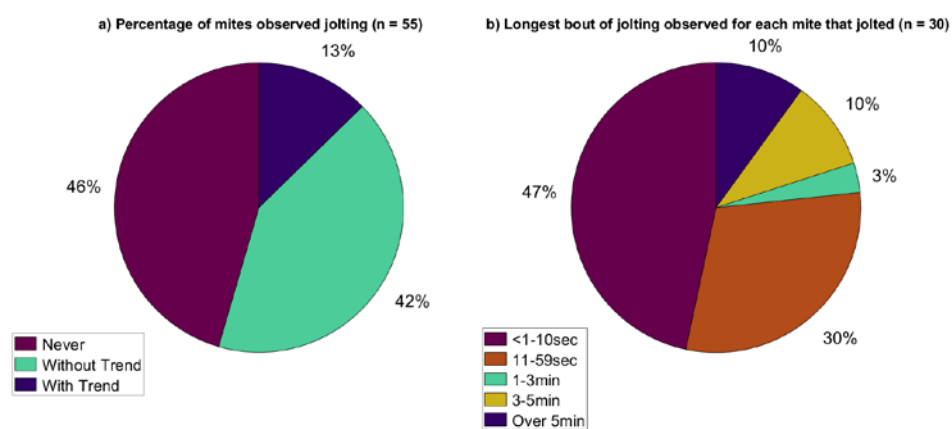


**Figure 2.5:** Pie charts demonstrating the percentage of mite individuals observed jolting (left chart) and their longest jolting time durations (right chart). Percentages have been rounded.

A substantial number of jolting vibrational pulses were measured on Petri-dish ( $n = 250$ ), and on brood-comb ( $n = 189$ ) substrates, with a smaller sample size for honeycomb ( $n = 28$ ) and gelatine capsule ( $n = 3$ ). Other vibrational traces were also detected when mites produced recognisable motions such as walking (see Appendix 1, Video S1), interacting, and undergoing the gravitational reflex response. All behaviours except one (defecation) produced measurable accelerometer traces (see Appendix 1, Video S2, Video S3, and Video S4).

#### 2.4.2. Synchronous vibrational/visual assessments of the jolting behaviour

The absolute timing of each jolt accelerometer trace is assessed within the sampling rate used for that signal, i.e., 48,000 Hz. The vibrational trace is seen (see Figure 2.2) to be produced within the time window of the video-detected mite jolting displacement, which is assessed within an interval of two successive video frames, i.e., 20ms. In spite of this large

discrepancy in the sampling rates of the two independent assessments of the jolting, my analysis clearly demonstrates (see Figure 2.2) that the observed vibrational trace and the jolting behaviour of the mite are consistently synchronous phenomena to within 20ms (see Figure 2.2, see Appendix 1, Video S5, Video S6, Video S7, and Video S8). This same figure (Figure 2.2) also demonstrates that the visually assessed time duration of the jolting (the width of the white peaks) is substantially longer than that assessed from the vibration (the spectrogram traces).

#### 2.4.3. The effect of different substrates on the frequency spectrum of the jolting pulse

The Varroa vibrational trace that exhibited the highest magnitude was extracted from each substrate specific collection of measurements (see Figure 2.6 for Petri-dish, honeycomb, and brood-comb, see Figure 2.7 for capsule). This trace varies substantially, in shape mostly, and modestly in time duration, dependent on the substrate on which the mite is residing. The substrate specific features that are seen in the strongest jolting vibrational traces can be seen in all detected pulses. As the pulses in Figure 2.6 are exceptionally strong, these Varroa jolting pulses also stimulate a collection of frequency bands rarely visible on the full collection of spectra.

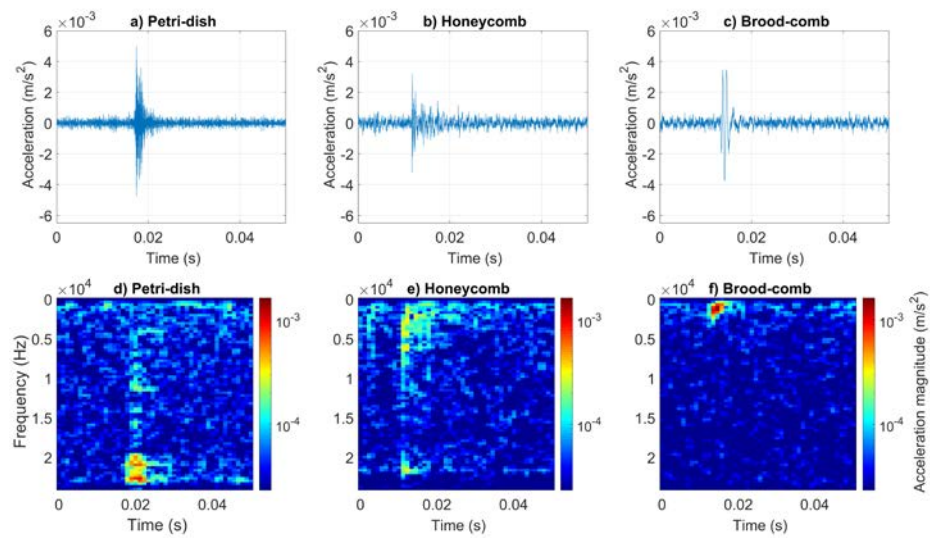


**Figure 2.6:** A series of accelerometer waveforms (top) and spectrograms (bottom) allowing the comparison of the vibration originating from the strongest Varroa jolt, detected within three separate substrates (Petri-dish ('a' and 'd'), empty honeycomb ('b' and 'e'), and brood-comb ('c' and 'f')). The accelerometer waveform has been high-pass filtered (500 Hz cut-off for all substrates) to remove irrelevant background vibrations that otherwise dominate the waveform. In the spectrogram, acceleration magnitude is logarithmic (to the base 10), where the highest magnitude is dark red ( $1.6 \times 10^{-3} \text{ m/s}^2$ ) and the lowest magnitude dark blue (and forced to  $1/70$  of the maximum). Panels found in the top, and the bottom, are scaled identically for ease of comparison.

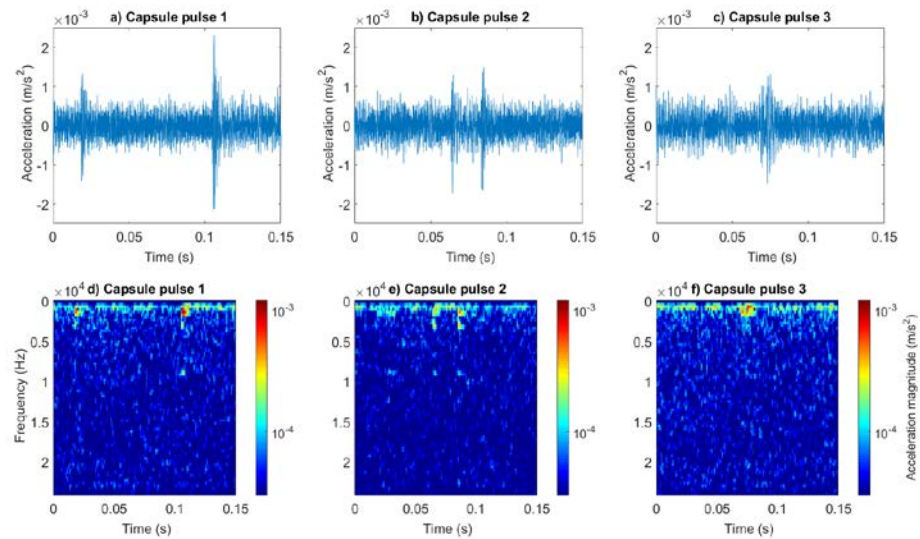


**Figure 2.7:** The three detectable jolting vibrations captured on the gelatine capsule substrate (two of which ('a' and 'b') are double waveforms that were produced during the same mite jolting motion) shown as accelerometer waveforms (top) and spectrograms (bottom). The three pulses: 1) 'a' and 'd', 2) 'b' and 'e', 3) 'c' and 'f', are all high-pass filtered with a 500 Hz cut-off to remove irrelevant background vibrations that interfere with the waveforms. In the spectrograms, acceleration magnitude is logarithmic (to the base 10), where the highest magnitude is dark red ( $1.2 \times 10^{-3} \text{ m/s}^2$ ) and the lowest magnitude dark blue (and forced to be 1/40 of the maximum). All panels are scaled identically for ease of comparison. Due to the double trace seen in panel 'a', the time axis is larger in this figure than in Figure 2.6. The SNR for these pulses is lower than that observed on Petri-dish, honeycomb, and brood-comb. The jolting pulses for these three substrates were the loudest in their collections, whereas there were only three detectable jolting pulses in capsule, and these were not as strong.

#### 2.4.3.1. Petri-dish

On the Petri-dish, the signal is mostly found at the highest measured frequencies (19,000 to 23,000 Hz), with the strongest signal contribution found between 22,000 and 23,000 Hz (see Figure 2.8 and Figure 2.8, see also Appendix 1, Video S14 for the full collection of spectrograms).

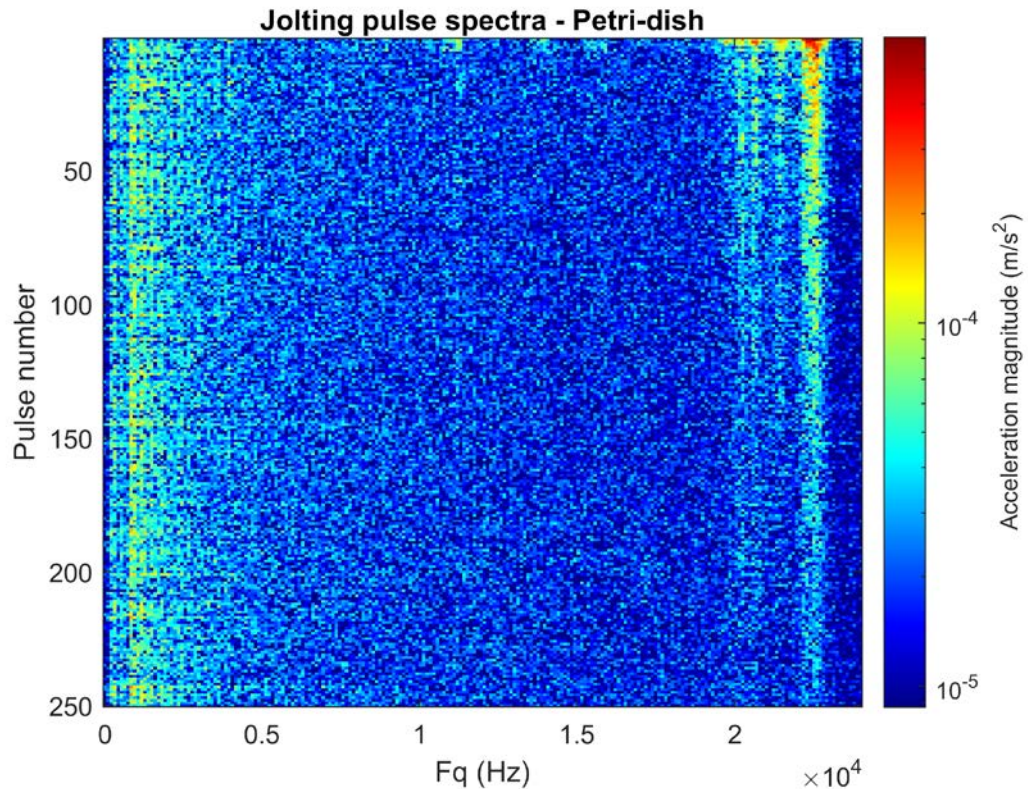


**Figure 2.8:** Jolting pulse spectra on the Petri-dish substrate, sorted by magnitude. The magnitude of acceleration is logarithmic (to the power 10) where the highest magnitude (dark red) is  $6.1 \times 10^{-4} \text{ m/s}^2$  and the lowest magnitude (dark blue) is forced to be  $1/70$  of the maximum to reduce the contribution of meaningless noise. All pulses have been high-pass filtered at 300 Hz to remove background noise without interfering with the frequency range where signal originating from the Varroa pulse is seen.

#### 2.4.3.2. Brood-comb

On the brood-comb, the opposite situation occurs, with the signal of highest magnitude found at lower frequencies, between 1000 and 1500 Hz (see Figure 2.6 and Figure 2.9, see also Appendix 1, Video S15 for the full collection of spectrograms).

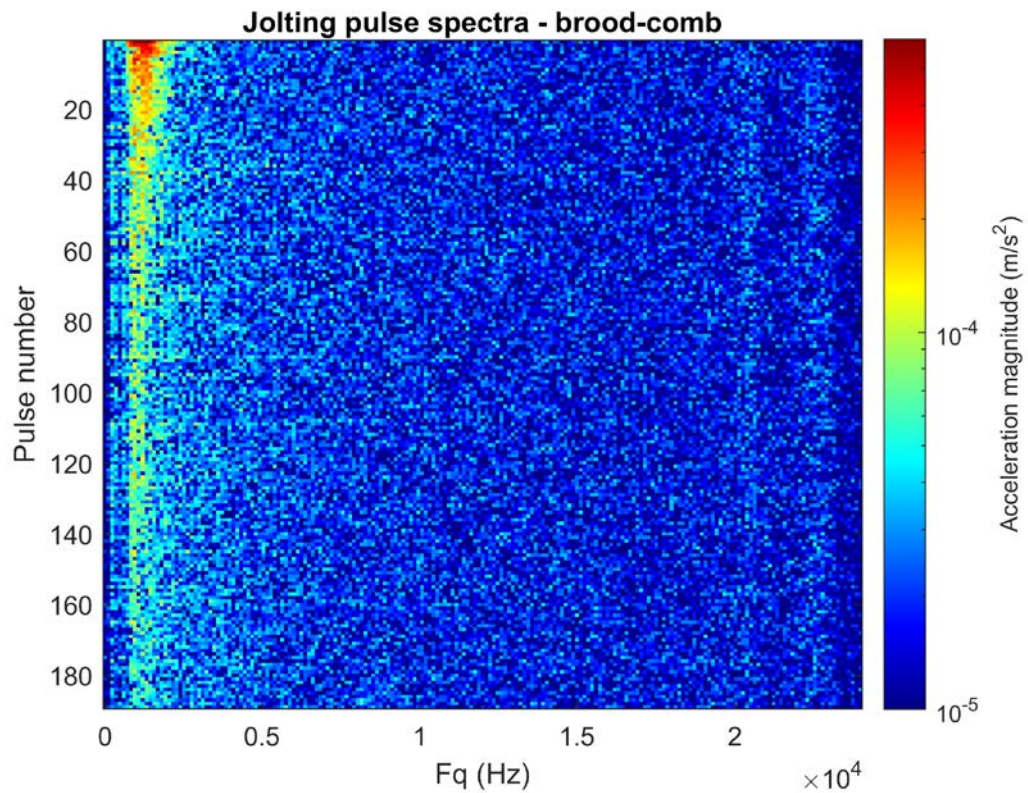


**Figure 2.9:** Jolting pulse spectra on the brood-comb substrate, sorted by magnitude. The jolting pulse spectra are sorted by magnitude in descending order. They were subject to the same analysis and filtering as the Petri-dish data in Figure 2.6 and the honeycomb data in Figure 2.8. The magnitude of acceleration is logarithmic (to the base 10) where the highest magnitude (dark red) is  $6 \times 10^{-4} \text{ m/s}^2$  and the lowest magnitude (dark blue) is forced to be  $1/60$  of the maximum to reduce the contribution of meaningless noise.

### 2.4.3.3. Honeycomb

In the honeycomb the signal is found over a much broader bandwidth between 500 and 10,000 Hz, and the individual pulses exhibit more variations in their features (see Figure 2.6 and Figure 2.10, see also Appendix 1, Video S16 for the full collection of spectrograms). The visible variation on this substrate can be seen in Figure 2.11.

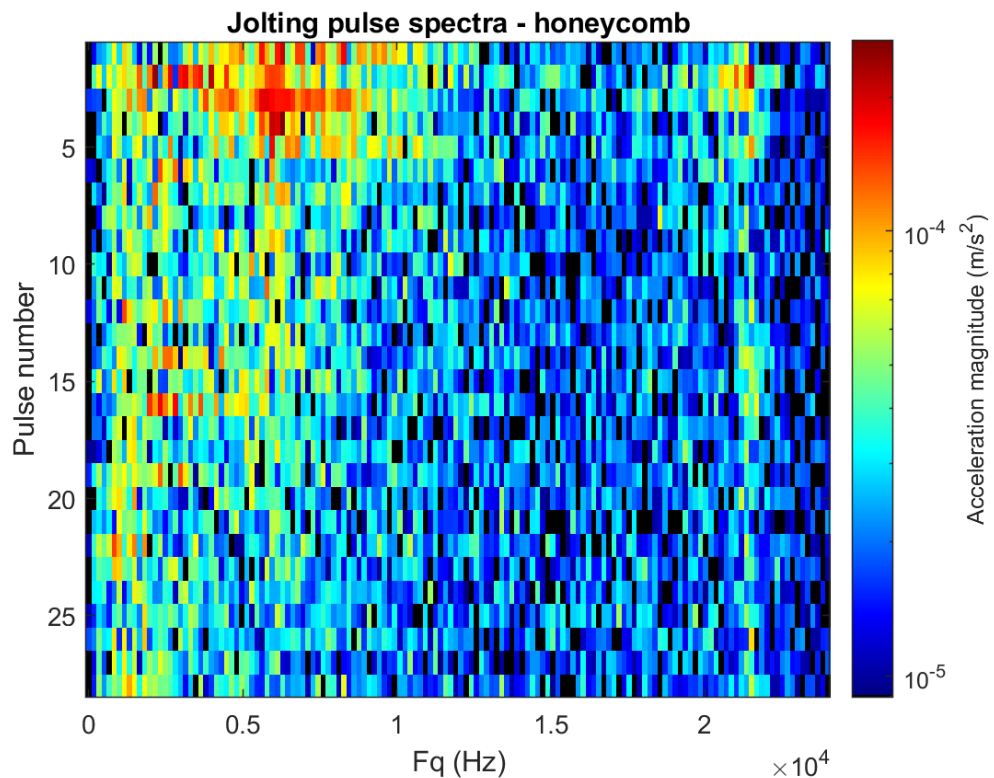


**Figure 2.10:** Jolting pulse spectra on the honeycomb substrate, sorted by magnitude. The jolting pulse spectra were analysed in the same way as those in Figure 2.6 and Figure 2.7. The magnitude of acceleration is logarithmic (to the base 10) where the highest magnitude (dark red) is  $2.7 \times 10^{-4}$  m/s<sup>2</sup> and the lowest magnitude (dark blue) is forced to be 1/30 of the maximum to reduce the contribution of meaningless noise.

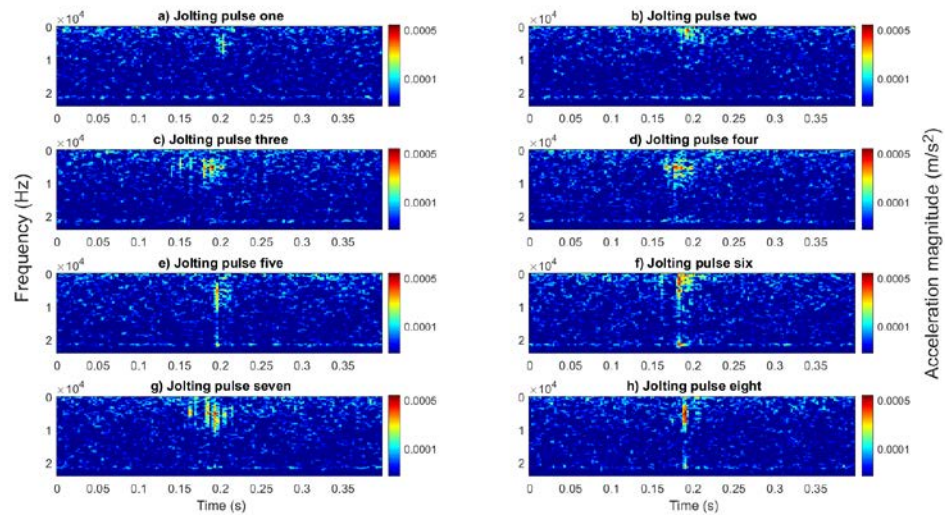


**Figure 2.11:** A series of spectrograms demonstrating the most clearly visible Varroa jolting vibrational pulses registered on honeycomb. These spectrograms showcase the larger variation that is observed in jolting pulses on this substrate in comparison to the Petri-dish and brood-comb substrates. Panels ‘e’, ‘f’ and ‘h’ provide evidence for the broad-band and generation of signal at the high-frequency bandwidth. The magnitude of acceleration is logarithmic (to the base 10), where the maximum is in red ( $5.9 \times 10^{-4} \text{ m/s}^2$ ) and the minimum blue (and forced to be 1/20 of the maximum).

#### 2.4.3.4. Gelatine capsule

In the gelatine capsule the signal is found between 500 and 900 Hz, with three clear bands specifically falling at 500 – 1850 Hz, 2200 – 3800 Hz, and 8400 – 9300 Hz in two of the three pulses. There are only three visible jolting pulses on this substrate, each is shown as a spectrogram and waveform (see Figure 2.7).

#### 2.4.4. The effect of different substrates on the acceleration, time duration and decay rates of the jolting pulse

The maximum acceleration of the strongest jolt is comparable between the honeycomb ( $3.2 \times 10^{-3} \text{ m/s}^2$ ) and brood-comb ( $3.5 \times 10^{-3} \text{ m/s}^2$ ), with a stronger acceleration for the loudest Petri-dish pulse ( $5 \times 10^{-3} \text{ m/s}^2$ ), and a lower acceleration for the loudest gelatine capsule pulse ( $2.3 \times 10^{-3} \text{ m/s}^2$ ) (see Figure 2.6 and Figure 2.7). Despite the comparable acceleration between honeycomb and brood-comb, the trace on the honeycomb spectrogram is noticeably fainter, due to the signal being spread over a very broad band.

All jolting pulses have an exceptionally short time duration, regardless of the substrate on which the Varroa is holding onto. The jolting pulse appears as a single, rapid pulse that takes

around  $50\mu$  and  $90\mu$  to grow, exponentially, from 0 to maximum acceleration on the honeycomb and Petri-dish substrates, respectively (see Figure 2.12). On the brood-comb, the growing wave front appears to be gaussian, with a 1ms time duration (see Figure 2.12).

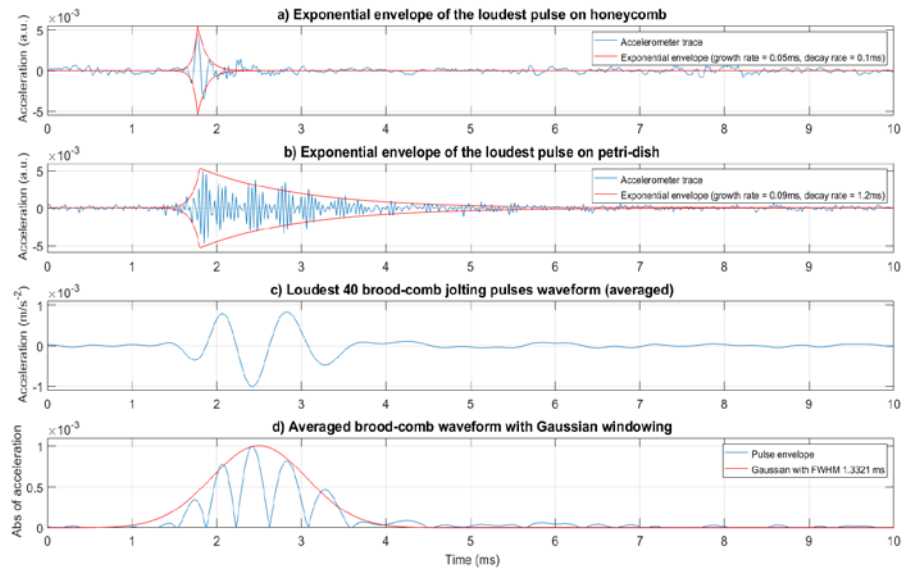


**Figure 2.12:** The growth and decay of the Varroa jolting pulse on honeycomb, Petri-dish, and brood-comb. Panel ‘a’ showcases the loudest jolting pulse waveform registered on honeycomb, and panel ‘b’ showcases the loudest jolting pulse waveform registered on Petri-dish, both of which demonstrate an exponential growth and decay that is highlighted within the red envelope. The growth rate and decay constant were estimated visually (honeycomb growth rate = 0.05ms, honeycomb decay constant = 0.1ms, Petri-dish growth rate = 0.09ms, Petri-dish decay constant = 1.2ms). The growth rate is the only element of the waveform that is caused by the animal, the decay constant on both the honeycomb and Petri-dish are likely the result of the response of the substrate. The brood-comb Varroa jolting pulse seen in panel ‘c’ is the result of the averaged accelerometer waveform for the 40 jolting pulses deemed to be loudest and are shown in panel ‘d’ to have an envelope following a gaussian function. All peaks in the vibrational trace were forced to become positive values to demonstrate the gaussian function. The negligible exponential decay can be seen, beginning at approximately 3.9ms.

The remarkable, repeatable features observed in the pulses detected within the brood-comb substrate (see Figure 2.9, see also Appendix 1, Video S15) prompted me to select the 40 traces with the highest magnitudes, and to average them to showcase the mean accelerometer waveform characteristics (see Figure 2.12). The envelope of the

corresponding brood-comb pulse is very well described by a gaussian function (see Figure 2.12), with an average full width at half-maximum of 1.33ms. It is worth noting that there is also a visible, but negligible, exponential decay of the signal.

For the gelatine capsule jolting pulses, like those on Petri-dish and honeycomb, there also appears to be an exponential growth rate. However, the background noise interferes with its clarity on this substrate, preventing detailed examination of this feature (see Figure 2.13). To that effect, the growth envelope was instead estimated using the time course, which contains the integral of all acceleration frequency components of each of the investigated Varroa pulses on this substrate (see Figure 2.14). The growth rate of the jolting pulses in capsule are 1 to 1.2ms (see Figure 2.13), the longest on any of the substrates.

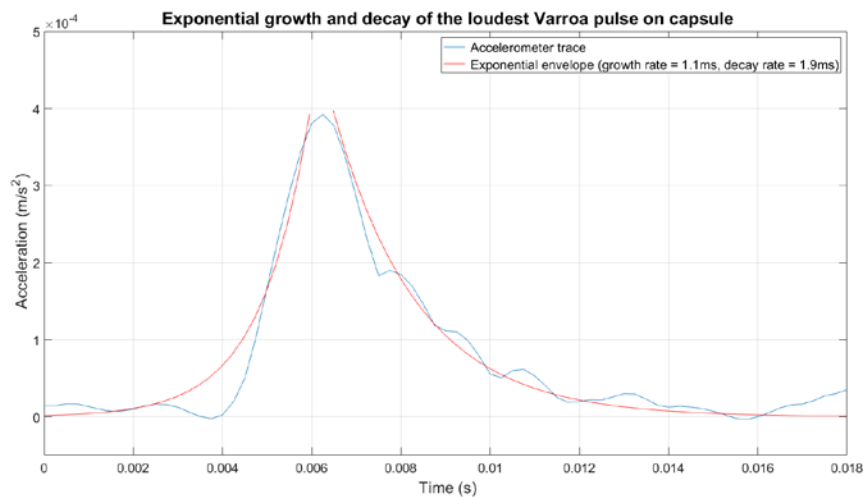


**Figure 2.13:** The growth and decay of the Varroa jolting pulse on capsule. The strongest pulse on capsule is showcased here. The integral of the magnitude of acceleration with respect to time is used to estimate the exponential envelope constants instead of the raw accelerometer waveform, due to background vibrations interfering with its clarity. The growth rate and decay constant were estimated visually and are here highlighted with the red curves. The growth constant is the only element of the waveform caused by the mite, as seen in the Petri-dish and honeycomb (see Figure 2.12). The decay constant is likely the result of the response of the substrate to the pulse.

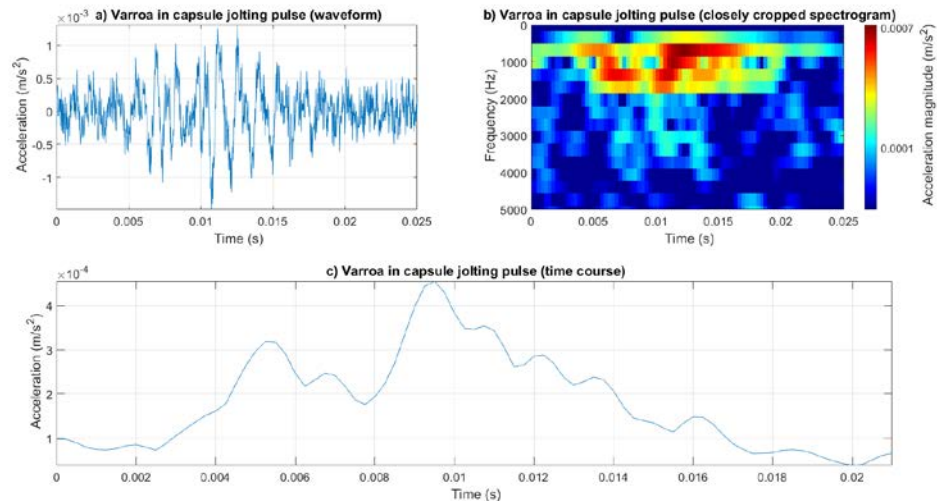


**Figure 2.14:** The Varroa jolting pulse on capsule that is shown here demonstrates a frequency spectrum with a double peak. Panel ‘a’ showcases the waveform which has been high-pass filtered with a cut-off at 0.5 kHz to remove background vibrations that were interfering with the clarity of the waveform. Despite this, the waveform is still not quite clear enough to identify the features of the trace. The spectrogram in panel ‘b’, filtered in the same way as the waveform, is closely cropped around the visible accelerometer trace to better showcase the presence of the double peak, which can be seen as the two closely located red areas. The maximum magnitude of acceleration is dark red, set as that of the Varroa pulse ( $7.3 \times 10^{-4} \text{ m/s}^2$ ) and the minimum, dark blue, is forced to be  $1/20$  of the maximum. Panel ‘c’ showcases the time course of the spectrogram, which is the integral of the magnitude of acceleration with respect to time. For this particular pulse, the growth rate was estimated from the first peak, and the decay rate from the second peak, as they are remarkably similar.

Jolting waveforms registered in the Petri-dish, honeycomb, and capsule can be described as damped sine waves, with a typical decay constant of 0.1ms, 1.2ms and 1.9ms, respectively for the strongest pulses (see Figure 2.12 and Figure 2.13). In order to assess the full pulse collections, average decay constants ( $\lambda$ ) were calculated after visual fitting on the clearest individual waveforms to quantitate the variation in the population (Petri-dish ( $n = 20$ )  $\lambda = 1.94\text{ms}$  (mean),  $1.03\text{ms}$  (s.d.), honeycomb ( $n = 5$ )  $\lambda = 0.5\text{ms}$  (mean),  $0.37\text{ms}$  (s.d.), capsule ( $n = 3$ )  $\lambda = 2.77\text{ms}$  (mean),  $1.03\text{ms}$  (s.d.)).

When considering all four substrates, the pulse attack times on honeycomb are the shortest of all. A mathematical consequence of the decreasing pulse time duration is the spectral bandwidth increase (see loudest honeycomb pulse in Figure 2.6).

## 2.4.5. Within substrate variations observed in jolting pulses

### 2.4.5.1. Brood-comb

The strongest jolting pulses are not necessarily representative of the whole collection of measurements as deviations from pulse to pulse can take place. Amongst the four substrates, jolting pulses detected within the brood-comb exhibit the highest repeatability (see Figure 2.15).

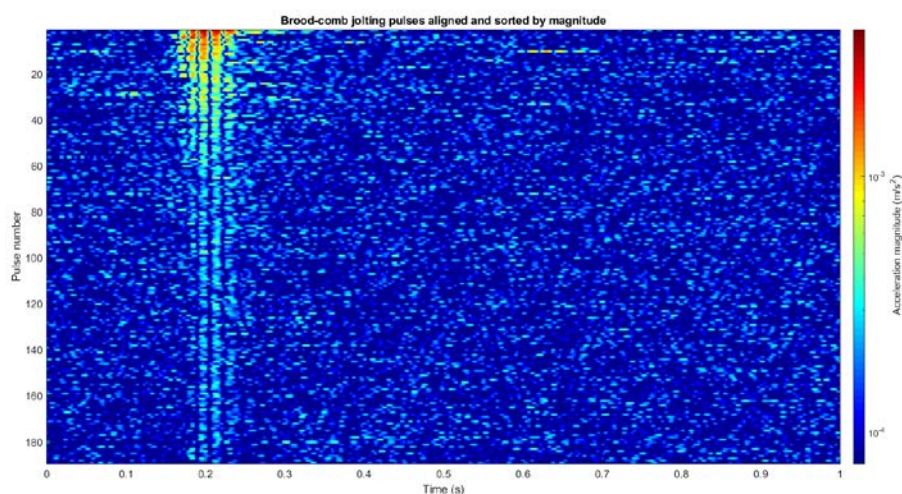


**Figure 2.15:** The collection of all 189 jolting pulses detected in the brood-comb after under-going cross-correlation alignment with the reference pulse (pulse number 1 in this instance), and further sorted by magnitude, in descending order. The similarity between pulses observed in this figure is remarkable. The polarity of acceleration has been forced to be positive to allow its magnitude to be shown on a logarithmic (log base 10) scale with dark red showing as the highest magnitude ( $3.4 \times 10^{-3} \text{ m/s}^2$ ) and dark blue showing as the minimum magnitude ( $1/50$  of the maximum).

All pulses are 4 to 10ms long, with three to five main lobes probably originating from one of the substrates' resonant mode. A few Varroa pulses (3%, based upon visual examination of the spectrograms and waveforms) exhibit a double peak (e.g., the tenth pulse on Figure 2.15), which, upon inspection of the video, appears to be produced by a matching rapid, repeated motion of the Varroa body (see Appendix 1, Video S17). When slowed down appropriately, jolting pulses in this video can be heard as 'knocking' noises, with the double trace pulses producing two separate knocks.

#### 2.4.5.2. Petri-dish

In the case of the Petri-dish substrate, the majority of the visible traces in spectrogram format are short, single peaks mostly found at the ultra-high frequency range, again with a few instances exhibiting more than one peak in quick succession (see Appendix 1, Video S14). However, for this particular substrate, careful inspection of the original Varroa jolting video does not reveal behaviour changes that could be linked to the production of multiple peaks (see Appendix 1, Video S5).

Of the 40 strongest jolting pulses on Petri-dish, 25% ( $n = 10$ ) of the spectra also exhibit lower frequency bands, additional to the ultra-high frequency band (see Figure 2.16). These are found around 10,600 – 11,300 Hz, 13,400 – 14,100 Hz, and 15,100 – 15,800 Hz. Of this 25%, seven are found in the top ten strongest of the whole sample.

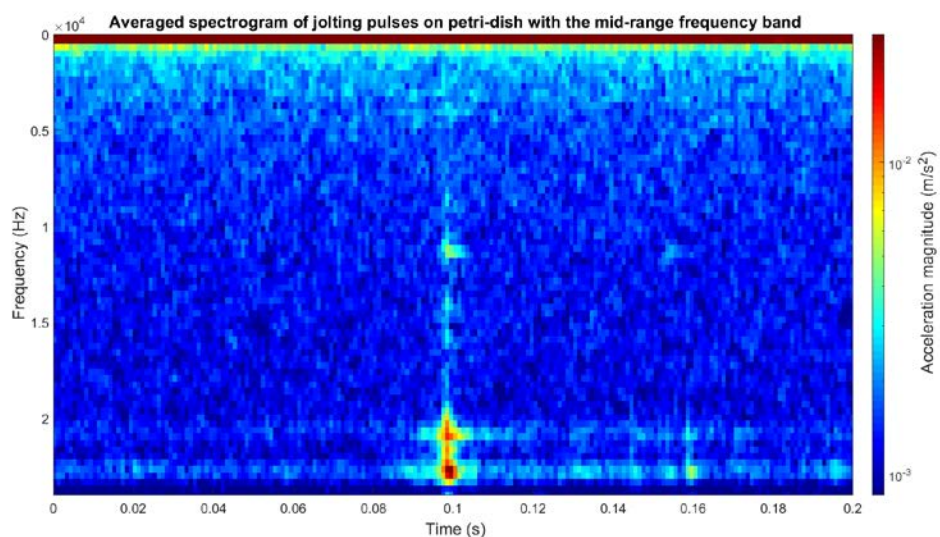


**Figure 2.16:** The average spectrogram of the ten Varroa jolting pulses registered on the Petri-dish that exhibit a mid-frequency bandwidth. The amplitude of acceleration is logarithmic (to the base 10) where the average highest magnitude is dark red ( $2.5 \times 10^{-2} \text{ m/s}^2$ ) and the lowest magnitude is dark blue (forced to be  $1/30$  of the maximum). The maximum is here forced to be that found in the averaged mite pulse, as this figure is simply to demonstrate the presence of the lower frequency bandwidth. Therefore, the absolute values of the colour coding are not relevant in this case.

#### 2.4.5.3. Honeycomb

Some of the visible honeycomb pulses comprise of a ‘train’ of several pulses in quick succession. An exceptional instance of this can be seen (see Figure 2.17) with six clear consecutive traces within 10ms of the recording. In this case, when observing the mite on

the video footage, the expected behaviour is not seen. Instead, the mite quickly jolts its body to the right, but then immediately moves the body in a forward motion, rather than returning in a leftwards motion to the original, central resting position (see Appendix 1, Video S18). This movement is exceptional and has not been seen in the other instances resulting in the production of multiple peaks, but still yields vibrational pulses with spectral features identical to that of a jolting behaviour.

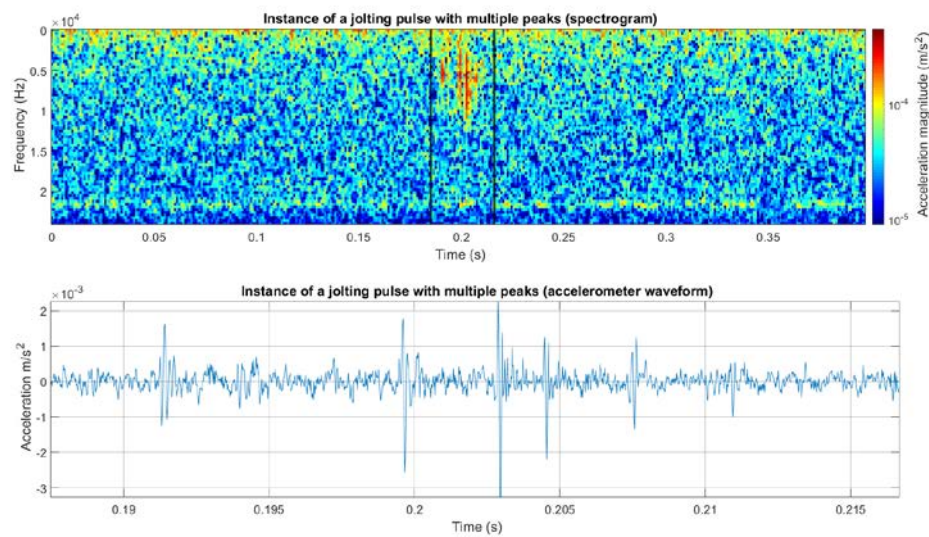


**Figure 2.17:** An instance of an accelerometer jolting pulse exhibiting multiple successive peaks, registered from within the honeycomb substrate. Six consecutive traces can clearly be seen within a short time period, lasting approximately 20ms. The black bars either side of the accelerometer trace on the top panel refer to the cropped time period seen in the bottom panel. The maximum magnitude of the pulse waveform is  $2.3 \times 10^{-3} \text{ m/s}^2$ . In the spectrogram, the magnitude of the acceleration is logarithmic (to the base 10) with a maximum acceleration of  $4.4 \times 10^{-4} \text{ m/s}^2$  and the lowest acceleration magnitude corresponding to  $1/50$  of the maximum. The maximum signal is here forced to be the maximum found in the Varroa pulse, as the purpose of this figure is to best showcase the signal peaks.

#### 2.4.5.4. Gelatine capsule

As there are only three visible accelerometer traces for the gelatine capsule, detailed analysis of variation within the collection cannot be made. Two of the three vibrations clearly exhibit a double peak, which can also be heard as two successive ‘tapping’ noises (see Appendix 1, Video S8). These two pulses also fall at the same frequency bands as one another (500 – 3500 Hz and 8600 – 9300 Hz) (see Figure 2.7). The third pulse, which is only seen at a bandwidth

of 500 – 1850 Hz, also appears to contain a double peak that is only identifiable upon more careful inspection of the trace, due to the ultra-short time duration between the peaks (see Figure 2.14). This pulse can also only be heard as a single ‘tap’ (see Appendix 1, Video S8).

#### 2.4.6. Comparison of the jolting pulse with the vibrational traces of other species and mite walking behaviour

Here, the Varroa jolting accelerometer waveforms are compared to those originating from (i) honey bees, (ii) an individual mite walking, (iii) a woodlouse.

##### *2.4.6.1. Honeybee individual and colony*

The first comparison made is between the strongest jolting pulse and the signal captured from within the centre of a honey bee hive frame, residing in a honey bee colony. The brood-comb substrate data is here used for the visual comparison (see Figure 2.18). The strongest brood-comb Varroa pulse is compared with a single honey bee ‘whooping’ signal, and the overall signal originating from the colony during two phases: low accelerometer signal (when the frame is heavily loaded with brood and/or honey, therefore attenuating vibrational signals) and high accelerometer signal (when the frame is lighter in weight and therefore less attenuation occurs).

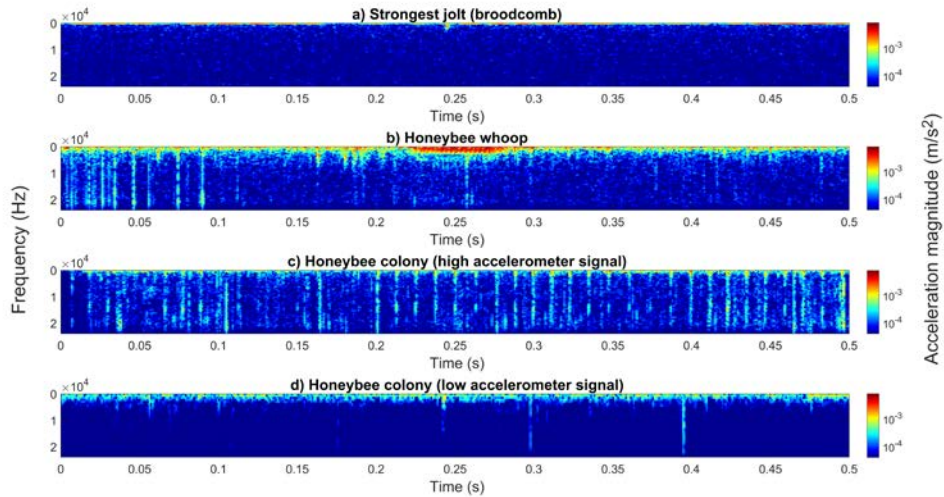


**Figure 2.18:** A series of 0.5s long spectrograms allowing the comparison of the vibration originating from the strongest Varroa jolt on brood-comb (panel ‘a’), a honey bee ‘whooping’ signal that comprises of a single pulse (panel ‘b’), and the whole honey bee colony in both low signal (panel ‘c’) and high signal periods (panel ‘d’). All recordings were carried out separately but are plotted here together for direct comparison. Variation in signal strength between ‘c’ and ‘d’ occurs mostly as a result of changes in comb mass density throughout the 21-day period of the brood cycle (Bencsik et al. 2015). In this figure, the magnitude of the acceleration is logarithmic (to the base 10), where the highest magnitude is dark red ( $7.5 \times 10^{-3} \text{ m/s}^2$ ) and the lowest magnitude dark blue (and forced to  $1/200$  of the maximum). All four panels are scaled identically for ease of comparison. In the top spectrogram, the regular background vibration inherent to the room was calculated and subtracted.

Despite the large difference in mass and size between an adult honey bee individual ( $115 \pm 7\text{mg}$  (Schmolz et al., 2005), 1.2cm) and a Varroa mite (0.42mg, 1mm), it was most surprising to find that the acceleration magnitude of the strongest pulse is comparable to that of the colony during a period of low signal (jolting pulse =  $9.4 \times 10^{-3} \text{ m/s}^2$ , low signal colony =  $1.9 \times 10^{-3} \text{ m/s}^2$ ). The jolting pulse is also found to be only 5 times smaller than (i) an individual pulsed bee signal and (ii) and the entire colony when accelerometer signal is high (see Figure 2.18) (jolting pulse =  $9.4 \times 10^{-3} \text{ m/s}^2$ , ‘whooping’ signal =  $4.5 \times 10^{-2} \text{ m/s}^2$ , high signal colony =  $4.5 \times 10^{-2} \text{ m/s}^2$ ). The quoted magnitudes of acceleration represent the integral of all acceleration frequency components for the maximum vertical point in time in each panel (see Figure 2.19).

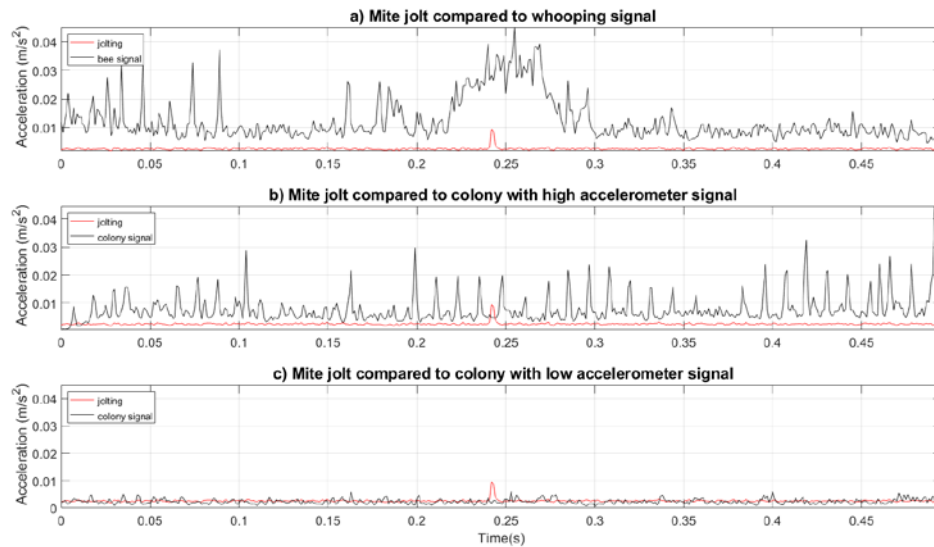


**Figure 2.19:** Time course of the loudest Varroa jolt on brood-comb with the signal from the full colony and a single bee. The signal seen here in each panel is the integral of the magnitude of acceleration with respect to time. The background vibration that is inherent to the room was calculated and subtracted from this data. The loudest jolt (red) is here compared to the signal of a single bee (black) and the vibrations of the full colony at low and high signal (black). High signal is captured when the frame containing the accelerometer is empty of brood. Low signal is captured when the frame is fully loaded with brood and/or honey. The ‘whooping’ signal (panel ‘a’) was captured during a period of high signal.

The strongest jolting pulse captured on the empty honeycomb also demonstrates the same order of magnitude as the vibrations of the honey bee colony (loudest honeycomb jolting =  $9.2 \times 10^{-3} \text{ m/s}^2$ ) (see Figure 2.20, in section 2.4.6.2.), registered from within a normally loaded frame.

#### 2.4.6.2. *Varroa mite walking vibrations*

The jolting vibrations were then compared to walking mite vibrations registered on all four substrates (see Figure 2.20 and Figure 2.21).

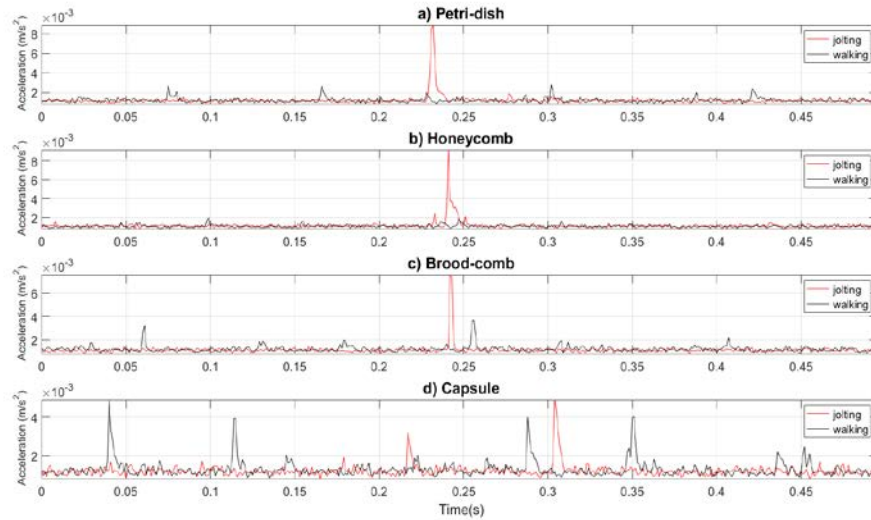


**Figure 2.20:** Time course of a Varroa jolting pulse and walking accelerometer traces. A 0.5 second accelerometer extract of mite walking behaviour (black) is here compared to a 0.5 second extract of accelerometer data containing the loudest pulse on each substrate (red).

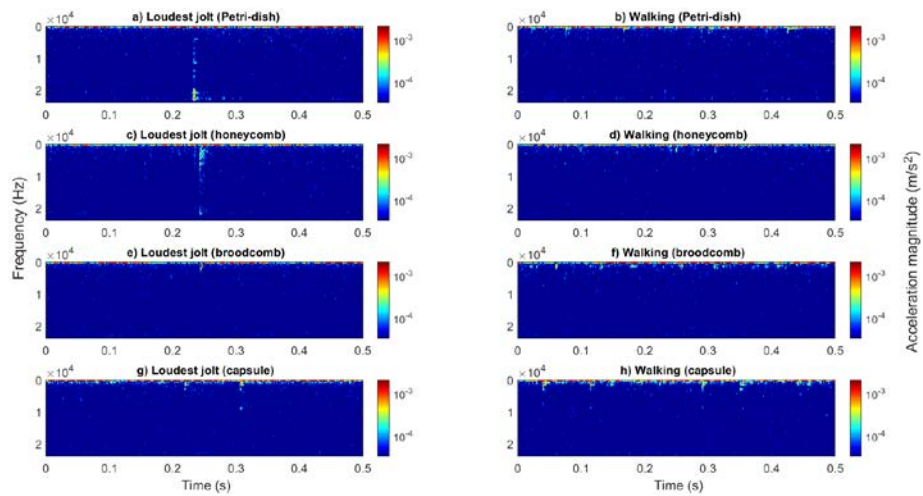


**Figure 2.21:** A series of spectrograms allowing the comparison of the vibration originating from the loudest jolt on the left column and walking behaviour on the right column, on four separate substrates (Petri-dish ('a' and 'b'), empty honeycomb ('c' and 'd'), brood-comb ('e' and 'f'), capsule (g and h)). The magnitude of acceleration is logarithmic (to the base 10), where the highest magnitude is dark red ( $2.1 \times 10^{-3} \text{ m/s}^2$ ) and the lowest magnitude dark blue (and forced to  $1/300$  of the maximum). All eight panels are scaled identically for ease of comparison. In each spectrogram, the regular background vibration inherent to the room was calculated and subtracted, but still results in red pixels on the very lowest frequency band. The data observed in each panel is that also used in Figure 2.20.

The maximum magnitude of acceleration was calculated for every jolting pulse, and a large collection of walking pulses, on each of the three substrates that contained a substantial number of jolting vibrations (Petri-dish, honeycomb, brood-comb). Although walking vibrations can be stronger than jolting pulses in rare occasions on the brood-comb, the average jolting pulse strength is systematically higher than that of the walking pulses on all three substrates (see Figure 2.22). One walking pulse does exceed the magnitude of the loudest jolting pulse on gelatine capsule, but detailed comparisons cannot be made in this instance due to the small number of visible pulses collected (see Figure 2.20).

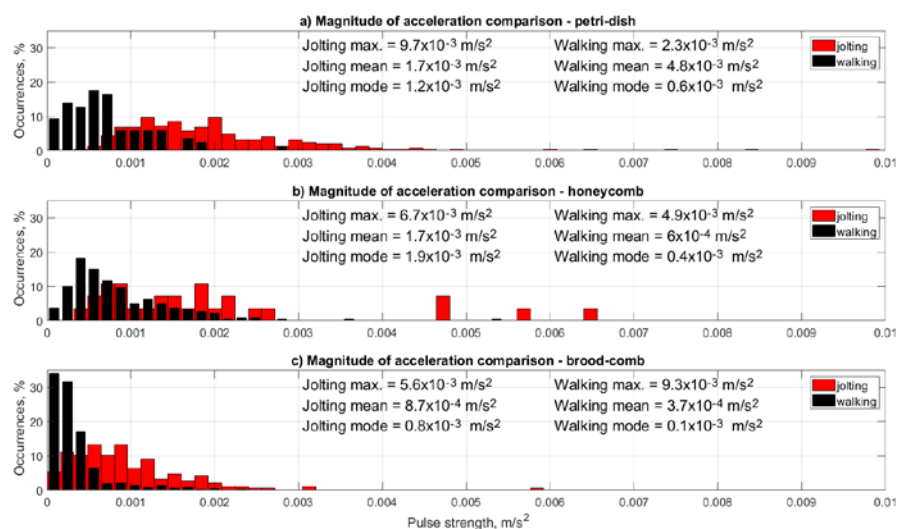


**Figure 2.22:** A series of histograms demonstrating the strength of Varroa jolting against the walking pulses on Petri-dish, honeycomb, and brood-comb. In all three panels the vertical axis is normalised to showcase the distribution probability (Petri-dish jolting/walking pulses  $n = 250/89$ , honeycomb jolting/walking pulses  $n = 28/219$ , brood-comb jolting/walking pulses  $n = 189/1272$ ). Histogram bin-width is identical for all plots – but the displayed black walking bars have been narrowed so that the red jolting bars, displayed behind, can be viewed.

The spectra of the walking and jolting pulses on the substrates that demonstrated a substantial number of visible pulses were then compared to each other to explore whether they can be discriminated (see Figure 2.23). The vibrational pulses originating from a Varroa walking on these three substrates are produced regularly at a frequency ranging from 500 – 3000 Hz. On the Petri-dish, the 500 Hz peak may be a resonance of the Petri-dish, as it is the only frequency clearly observed as a result of stimulation to this substrate (see Appendix 1, Figure S11). On the brood-comb, the vibrations produced by both behaviours share the same

frequency band, whereas the Petri-dish and honeycomb demonstrate high discrimination between walking and jolting. Both types of pulse on honeycomb stimulate the ultra-high frequency bandwidth that seems to originate from a resonant mode inherent to the accelerometer itself (see Appendix 1, Figure S10). Gelatine capsule walking pulses, although not included in this analysis, can be seen to fall between 500 and 3000 Hz, as with the other substrates (see Figure 2.21).

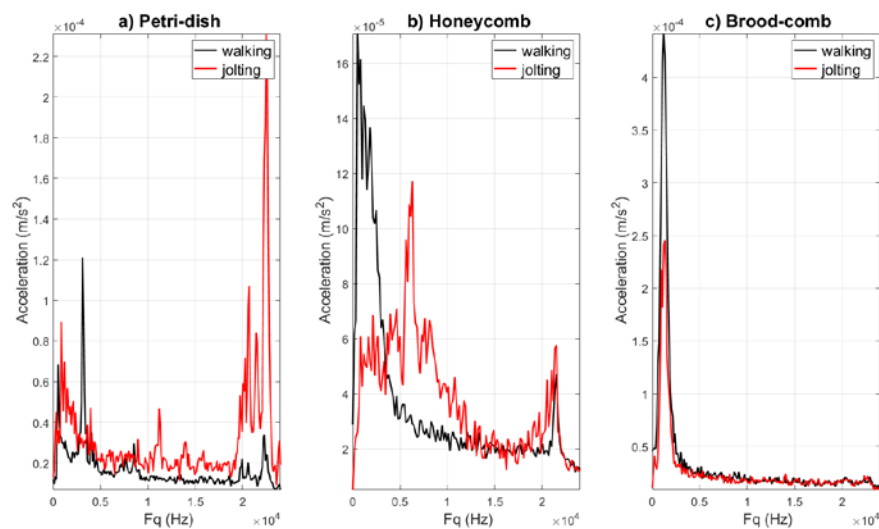


**Figure 2.23:** Comparison of the average jolting pulse spectra against the average walking pulse spectra, on Petri-dish, honeycomb, and brood-comb. Each collection of pulses (walking or jolting on each substrate) was individually sorted by magnitude and the strongest ones in the collection averaged. The purpose of this is to demonstrate a possible discrimination between the two different behaviours on each substrate on the basis of the pulse spectral features. The number of pulses chosen to be averaged for each collection differs based upon the extent of the collection of spectra and their clarity/quality (Petri-dish jolting  $n = 15$ , Petri-dish walking  $n = 40$ , honeycomb jolting  $n = 10$ , honeycomb walking  $n = 40$ , brood-comb jolting  $n = 20$ , brood-comb walking  $n = 20$ ). All averaged pulses were high-pass filtered with a cut-off at 300 Hz to remove background noise without interfering with the frequencies where the signal of interest occurs.

#### 2.4.6.3. Woodlouse walking

The strongest jolting pulses on Petri-dish, honeycomb, and brood-comb were lastly compared with vibrations originating from another, much larger invertebrate (a woodlouse = 10mm, 37mg) (see Figure 2.24 and Figure 2.25).

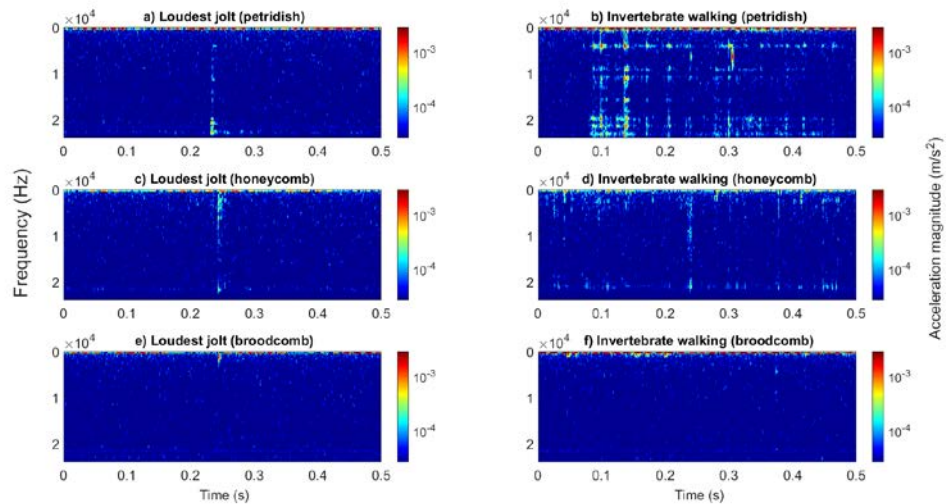


**Figure 2.24:** A series of spectrograms allowing the comparison of the vibration originating from the loudest recorded Varroa jolt, and typical vibrations originating from a walking invertebrate (woodlouse, 37mg), on three separate substrates (Petri-dish ('a' and 'b'), empty honeycomb ('c' and 'd'), brood-comb ('e' and 'f')). The magnitude of acceleration is logarithmic (to the base 10), where the highest magnitude is dark red ( $2.8 \times 10^{-3} \text{ m/s}^2$ ) and the lowest magnitude dark blue (and forced to 1/400 of the maximum). All six panels are scaled identically for ease of comparison. In each spectrogram, the regular background vibration inherent to the room was calculated and subtracted, but still results in red pixels on the very lowest frequency band.

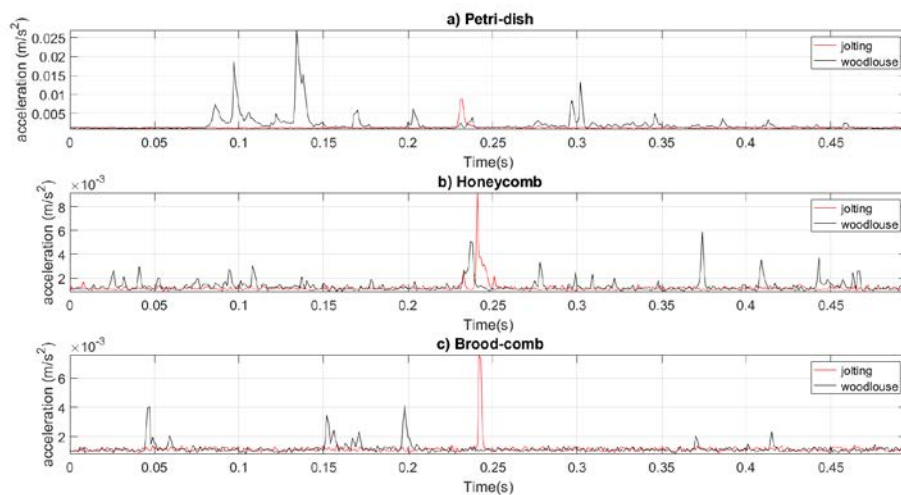


**Figure 2.25:** Time course of the Varroa jolting pulse and invertebrate walking accelerometer traces. The loudest jolt (red) is here compared to the invertebrate walking vibrations (black).

The strongest Varroa pulses on the honeycomb and brood-comb are comparable to the walking vibrations of the woodlouse (brood-comb pulse =  $7.6 \times 10^{-3} \text{ m/s}^2$ , brood-comb woodlouse =  $4.1 \times 10^{-3} \text{ m/s}^2$ , honeycomb pulse =  $9.2 \times 10^{-3} \text{ m/s}^2$ , honeycomb woodlouse =  $5.9 \times 10^{-3} \text{ m/s}^2$ ) (see Figure 2.25). For the Petri-dish, the jolting pulse exhibits a strength that is a factor two smaller than that of the woodlouse walking (Petri-dish pulse =  $8.9 \times 10^{-3} \text{ m/s}^2$ , Petri-dish woodlouse =  $2.6 \times 10^{-1} \text{ m/s}^2$ ) (see Figure 2.25). As with other previous comparisons, these values were obtained from the integral of all acceleration frequency components in the Varroa pulse and the loudest walking vibrational trace of the woodlouse on each substrate.

#### 2.4.7. Estimation of pulse power output

To estimate the power output provided by a mite delivering a jolting pulse, a well-controlled vibration was produced artificially, yielding a vibrational trace similar to that of a Varroa. To this end, a small silica sphere of known weight (0.07mg) was dropped onto the Petri-dish substrate.

Its velocity was measured at the point of impact with the Petri-dish (0.5 m/s) from a height drop of 1cm. From this, the kinetic energy of the bead hitting the Petri-dish was estimated to be 17.5nJ, which, when delivered within 0.54ms (the time taken for a jolting pulse to go from 0 to maximum on the Petri-dish (see Figure 2.12) results in a power of approximately 32 $\mu$ W. As the mite vibrational pulse is forty times weaker than the artificially produced vibration, this means that the animal must typically deliver approximately forty times less power, i.e., 810nW in each jolting pulse.

#### 2.4.8. How detectable are jolting pulses, using accelerometer sensors?

Not all video-evidenced jolting pulses produce a detectable vibrational trace. This must be due to the animal genuinely delivering vibrations with varying strength combined with the limited sensitivity of my measurements. The fraction of detected pulses decreases with the accelerometer's sensitivity, and no jolting vibration was ever detected when using a ten times less sensitive crystal (4507, Brüel & Kjær).

In order to assess the detectability of jolting vibrational pulses on each substrate, the SNR was estimated for each vibrational trace, and I also independently noted the percentage of pulses that could be picked up by critical listening, changing the playback speed as required, in order to best perceive the collection of jolting pulses. On brood-comb, 25% of pulses were hearable, corresponding to a SNR boundary of 0.7475. Petri-dish and honeycomb exhibited a higher percentage of audible pulses (Petri-dish = 47%, SNR boundary = 0.0142, honeycomb

= 68%, SNR boundary 0.2265). Gelatine capsule pulses demonstrated the lowest percentage of audible pulses at 11% (SNR boundary = 0.2492).

#### 2.4.9. Periodicity of the jolting behaviour

I now consider all the mite individuals observed for jolting behaviour (see Figure 2.5) and describe the periodicity and pattern of the jolting. Mites produced this behaviour for varying lengths of time (from as little as one single jolt up to almost 50 minutes of regular jolting behaviour), often with a few location changes between where jolting was seen to temporarily cease.

Of the mites that were observed jolting (54.5%,  $n = 30$ ), individuals were categorised based upon the greatest length of time where the behaviour was regularly produced. I call this a 'bout' of jolting, defined as a period where a mite remains in the same position and jolts with 10 seconds or less between consecutive pulses. If more than 10 seconds elapsed, or mite re-positioning occurred, then the subsequent jolt that followed this was considered to be the start of a new bout. Of these mites, 77% jolted for periods of less than one minute (see Figure 2.5, panel 'b'). Mites producing a jolting bout that lasted more than one minute (13%) were then further scrutinised to identify an overall behaviour pattern during their time spent on the substrate.

The overall duration of jolting varied between individuals, with the longest time period observed as 49 minutes and 50 seconds. The Petri-dish and brood-comb mites pulsed for approximately 8 minutes each (see Figure 2.26).

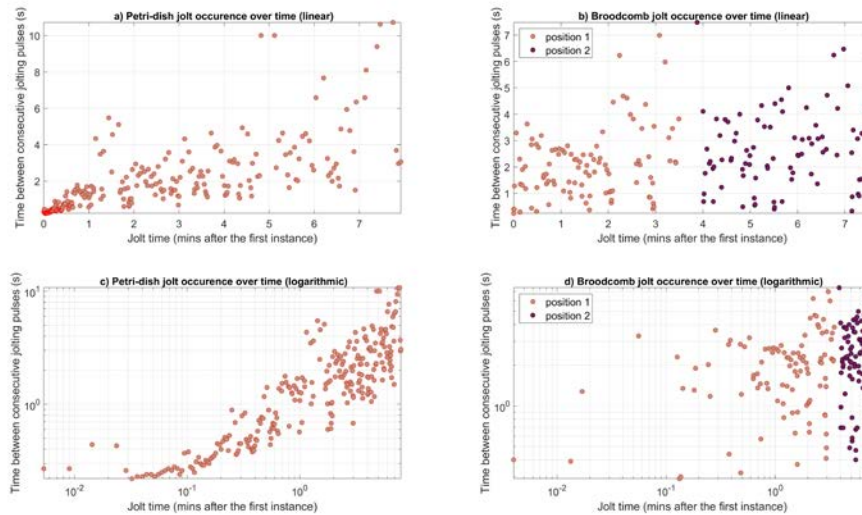


**Figure 2.26:** Jolt occurrence time intervals with respect to time. The data for the mite jolting on Petri-dish (left column) and on brood-comb (right column) are shown here. Jolt occurrence time intervals are showcased in both linear (panels ‘a’ and ‘b’) and logarithmic (panels ‘c’ and ‘d’) scales. A change in the colour of the datapoints is indicative of the mite moving to a new position on the substrate.

The periodicity of the jolting of the mite individual residing on honeycomb is also shown alongside the data from two other mites on Petri-dish and another mite on brood-comb (see Figure 2.27) with broadly varying overall pulsing time durations seen. In 50% of cases in this category, mites repositioned during jolting. This was either a minor displacement, where the mite simply stopped pulsing to turn and face another direction, or a larger motion, where it stopped then walked to another area on the substrate before continuing with the behaviour.

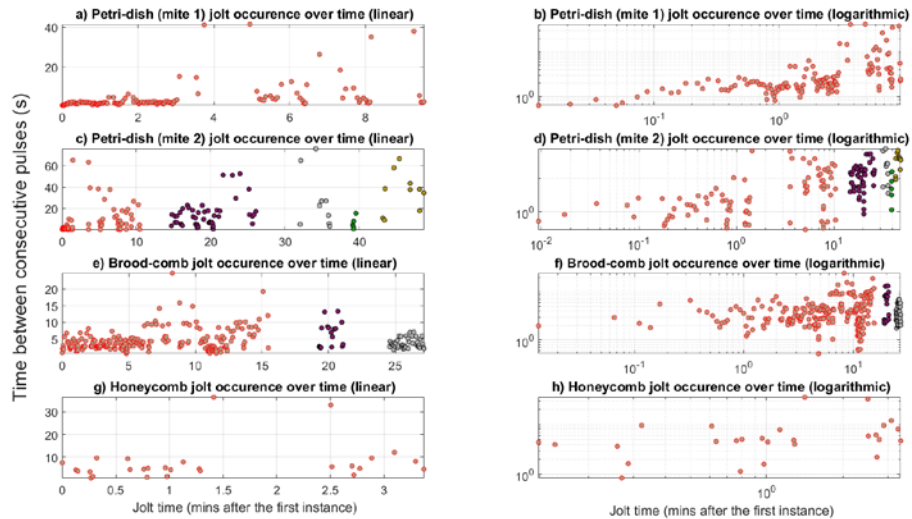


**Figure 2.27:** Jolt occurrence time intervals with respect to time. Data are shown here for a second and third mite on Petri-dish ('a', 'b' and 'c', 'd' respectively), a second mite on brood-comb ('e' and 'f') and the mite that produces audible jolting pulses on the empty honeycomb that is referred to in the main text ('g' and 'h'). Jolt occurrences and time between consecutive instances of jolting are showcased in both linear ('a', 'c', 'e', and 'g') and logarithmic ('b', 'd', 'f', and 'h') forms. A change in the colour of the datapoints is indicative of the mite moving to a new position on the substrate.

For some mites, there appears to be a trend in their jolting activity, but modest sample size prevents the drawing of interpretive comments. Some individuals jolt rapidly from commencement of the behaviour, with very short time intervals, around 0.5 seconds, between consecutive jolting pulses. As time increases, the temporal density of pulse occurrences decreases (see Figure 2.26, panels 'a' and 'c', see Figure 2.27, panels 'a' to 'd'). Other individuals produce jolting pulses at more regular intervals regardless of time, with a similar rest period between consecutive pulses (see Figure 2.26, panels 'b' and 'd', see Figure 2.27, panels 'e' to 'h'). Where repositioning occurs, identified by a change in colour on the figures, the 'trends' here described appear to continue regardless of the interruption due to movement.

### 2.5.0. Discussion

In this work, I detected vibrational signals originating from individual *Varroa* mites with accelerometer sensors. As the jolting behaviour is very common, it comes to a great surprise that it has, until now, remained unnoticed. Only one previous study describes 'jolting movements' in *Varroa* (Piou et al., 2019), however this work instead characterised the reaction of mites to electrostatic substrate discharges. In my study, more than 50% of mites

produced jolting behaviour at some stage during observation, ranging from single jolts to mites that jolted hundreds of times for several minutes.

The synchronicity between video-captured mite movement and accelerometer vibrational trace provides strong evidence that the displacements of the body in left and right directions are features of the same behaviour which also yields a detectable vibration. The critical listening of the audio of the slowed video data also further demonstrates a robust synchronicity where the jolting pulses can be heard as 'knocking', 'clapping', 'clinking', or 'tapping' noises, with a timbre clearly modulated by the nature of the substrate on which the vibration is detected.

On all four substrates investigated, double or multiple peak vibrations were occasionally found in rapid succession. On brood-comb and honeycomb, two rapid, successive body displacements can be seen alongside a double audible 'knock' or 'clap' consistent with the multiple peak vibratory trace seen. This is also seen on the gelatine capsule, although the double motion of the body is less clear in these instances, despite the corresponding 'tapping' sounds being very clear. For Petri-dish, although visible differences in the jolting vibrational traces are seen, i.e., some have double peaks, some have single peaks, there are no visual or audible differences in the production of both types of pulse when viewing the displacement of the mite. Perhaps the double motion of the body observed on the brood-comb and honeycomb is a result of the uneven comb surface interfering with the flow of the displacement, whereas the Petri-dish is homogenous and flat. This may also explain why the double motion of capsule pulse behaviour is less pronounced, as the capsule is a flatter surface than the comb.

The mechanism behind jolting vibration production can only be speculated presently. The visible motion of the body lasts approximately 20ms, but the vibrational trace itself is only 0.3 – 1ms long, followed by a decay of 1 to 4ms that is likely to result from the resonance of the substrate. This could be indicative of a 'spring' or 'click' mechanism, which is documented in a variety of species that produce ultra-short and ultra-fast movements (Gronenberg, 1996; Patek et al., 2011). The relatively slow visual jolting would correspond to the loading of the 'spring', whilst its ultrafast release would cause the remarkably short accelerometer pulse.

For those jolting pulses that are occasionally observed as a 'train' of vibrations, the mechanism behind production could be a regularly repeating anatomical feature, such as a comb. Microstridulation is described in the mite species *Grandjeanicus gabonensis*, which possess a 'toothed' hair system that can transmit vibration when stimulated (Coineau et al.,

1997). Setae of a similar structure have also been noted in the mite *Sphaerolichus lekprayoona* (Fuangarworn, 2012), although for both species, no further work has been undertaken regarding the quantification of the vibrations that they produce. I expect that if Varroa mites were to possess such a mechanism, a much higher proportion of jolting vibrations would be produced that showcase multiple peaks, whereas most featured a single pulse in the collections described here.

At this stage, visual observations are limited by the use of a 50 FPS camera; a more detailed visual investigation into the movement of Varroa as they jolt is required to begin understanding the mechanism behind vibration production, involving a camera capable of at least 1000 FPS to register a displacement that I expect is taking place within 1ms or less. Further to this, observing mites on a flat, transparent surface from various angles could help to visually establish the mechanism driving pulse production. As jolting mites have occasionally been seen to 'flex' their legs, resulting in body motion displacement towards the substrate and then back up again, this future work could also help to identify the directionality of leg movement and understand the involvement of the legs, if any, in jolting behaviour.

#### 2.5.1. Substrate dependent jolting pulse features

The jolting pulse vibrational trace varies strongly dependent on the substrate on which it is transmitted. This is a feature of any vibrational signal captured on a variety of media, exacerbated here by the short impulse nature of the signal of interest. In the honeycomb, in particular, there is a remarkably broadband trace that could be described as approaching that of a Dirac delta function. This corresponds to an ultra-fast burst of energy delivered to the substrate (Reeping & Reid, 2016). A jolting mite delivers a short burst of vibrational energy into the material on which it is stood, and the shorter this pulse is, the broader the environmental information gathered in the spectrum that the accelerometer, and probably the mite, register.

The platform on which a vibration is transmitted produces a set of resonance signals that are characteristic of the substrate (Otten et al., 2001), a strong feature seen in my results. Individuals that can produce higher intensity signals and shorter signals will benefit from a broader range of frequency perception (Otten et al. 2001). Particularly strong Petri-dish and honeycomb jolting pulses stimulated an increased number of frequency bandwidths than lower intensity ones, an indication that more resonance information is produced. Jolting pulses stimulate a larger number of frequencies than walking pulses, which can only be seen

at the frequency bandwidth of 500 – 3500 Hz (with a less intense peak at 23,000 Hz on Petri-dish and honeycomb), irrespective of the substrate upon which the pulses were delivered. It is perhaps the natural responding frequencies of the substrate that cause brood-comb jolting and walking pulses to share a similar bandwidth.

The accelerometer model used in this study has a main resonance at 17,900 Hz, which was coincidentally never stimulated by mite activities. Deviation from signal strength linearity at the moderate resonances of the crystal (11,000, 15,000, and 22,000 Hz) was less than 10%, further indicating that the frequency components of the jolting pulses were a genuine result of mite stimulation.

#### 2.5.2. Successful accelerometer detection of mite signals

Accelerometers have been used successfully by our research group to detect and characterise specific honey bee signals (Bencsik et al., 2015; Ramsey et al., 2018; Ramsey et al., 2020), and I have now demonstrated that the same sensors can also detect the vibrations of a much smaller and lighter organism, *Varroa destructor*, on four different substrates. *Varroa* signal capture is particularly successful on the Petri-dish and honeycomb substrates, but still demonstrates good efficacy at 25% on the denser brood-comb. This is still remarkably good, considering that capped brood-comb is known to be poorer at transmitting vibrational signals in comparison to open, empty cells (Bencsik et al., 2015), further evidenced by honey bee waggle dance success on this medium in comparison to capped comb (Tautz, 1996).

#### 2.5.3. Application of jolting pulse detection in a real hive

My results suggest that it might be possible to continuously, non-invasively detect live *Varroa* mites with fully populated hives using accelerometers. I have demonstrated that this signal is highly repeatable, with an identifiable shape, spectrum, and time duration, particularly for the brood-comb, which is the most similar to a real hive substrate.

The average strength of the jolting pulse is well above what would be expected for an animal of such size, which can be observed when comparing it to the vibrational signals of much larger invertebrates (honey bee and woodlouse). The vibrational strength of the honey bee colony recording, in which hundreds of bees contribute to the measurement during a period of high signal, is only one order of magnitude higher than that of a single mite jolting pulse. I can see in my data that when there are lulls in bee buzzing, jolting pulses exceed the maximum acceleration of the bee signal, providing a good opportunity for them to be detected.

The low signal data strength is, more surprisingly, comparable to that of the jolting, but there is a limitation to this result. Note that the honey bee vibrations were emanating from an entire hive's frame, which during the low signal period was loaded with brood/honey. The jolting pulse, in comparison, was delivered onto and collected from a much smaller section of brood-comb. This perhaps led to the comparable signal strength seen in the low signal data when compared to the jolting pulse. Nonetheless, I have shown that honeycomb pulses are comparable in strength to brood-comb pulses, and these were recorded on a British standard sized frame which although devoid of contents, was still fully built, in terms of the wax cells, i.e., close to the expected substrate in the hive. This is especially true for the high signal colony data, as the frame will be closer to a state of emptiness due to a lack of brood, e.g., when eggs have just been laid, after a swarm, and during winter (Bencsik et al., 2015). Success in detecting Varroa vibrational signals in the hive is therefore expected to vary throughout the year in response to the everchanging periods of high and low signal that occur as a result of the brood cycle, and therefore, shifts in frame load (Bencsik et al., 2015).

Detection success is also likely to be affected by the distance between the mite and the accelerometer. In this work, mites were always positioned within 3 to 4cm of the sensor, but in a real hive this may not always be achievable. It is most likely that mites would be successfully detected when within the brood cells, as population modelling predicts that 65% of mites in a honey bee colony will be within the sealed cells at any time (Martin, 1998). Varroa are known to often come into direct contact with the comb in the reproductive phase (Donzé & Guerin, 1994), so it is highly likely that walking will take place and it is possible that jolting may also occur. I know from experience that bees will use the cells surrounding the accelerometer with their normal content, including brood. This increases the chances of a mite inhabiting the vicinity of the sensor for many days in succession, improving its chance of detection.

Establishing jolting pulse function may be an advantage to mite detection. It is currently unknown whether this behaviour is produced in the brood cells. If I can establish when and where the behaviour is likely to occur, I can focus on more specific search times and locations for its detection. In previous studies, myself and our research group have placed two accelerometers in a central position on the frame, equidistant from one another and the frame edge. This has worked well for registering frequently occurring honey bee signals (Ramsey et al. 2018), but may not be optimum for mite signal capture. It is likely that several accelerometer sensors will be required for this exploration.

#### 2.5.4. Is the jolting pulse a functional signal?

As discussed above, better understanding of why the jolting pulse is transmitted by the mite may provide additional information on where the behaviour will occur, as well as provide further important biological information on this species.

Some of the features of the jolting vibrational trace indicate that it may serve a purpose. As mites lack the necessary structures for detecting airborne sound (Dillier et al., 2006) and have no eyes (Dillier et al., 2006; Dowling, 2015), it is presumed that other sensory systems guide the species behaviour, such as the chemosensory and olfactory systems (Dillier et al., 2006; Ziegelmann et al., 2013). Perhaps vibratory information contributes to the successful completion of the mite life cycle.

One feature that I see in my results is the exceptional strength of the jolting pulse. For an animal of its modest size and mass, the jolting vibration is remarkably strong when compared to the vibrational signals of the larger invertebrates investigated here (honey bee, woodlouse). It also requires a large power of 810nW, delivered by the mite. This is indicative that the pulse has a purpose, as other small organisms display power outputs of a similar or smaller size for functional vibratory signals ((i) leaf cutter ant stridulatory distress signals: output 10 – 20nW (Markl, 1967), organism size 1 – 10mg (Roces & Hölldobler, 1994), 3 – 16mm; (ii) *Sehirus impressus* (*Canthophorus impressus*) communication signal: output 30nW, organism size 25mg, 6 – 7mm (Michelsen et al., 1982); (iii) *Omecetrus viridulus* grasshopper courtship signal: output 61nW (Michelsen & Elsner, 1999), organism size 165 – 310mg (Kriegbaum 1997), 1 – 2cm). Therefore, *Varroa*, an animal of significantly smaller size, produces jolting vibrations that are of a much higher power output. Due to the high energy requirement of this pulse, it would seem unlikely that the vibration registered is simply a by-product of the animal's activity.

Another feature is the substrate dependent pulse characteristics, which, as previously discussed, result from the frequency response of the substrate. Some species engage in the production of probing pulses that are transmitted into a substrate so that the organism can detect the subsequent reflections and gain environmental knowledge (Wäckers et al., 1998). Parasitoid wasps, mole rats, and aye-ayes (Broad & Quicke, 2000; Kimchi et al., 2005; Sterling & McCreless, 2006) do so in order to identify hosts/prey or gather environmental knowledge on their surroundings. As jolting pulses vary as a result of the substrate on which they are transmitted, but walking pulses do not, this could be indicative of a probing function.

The time duration of the jolting pulse is perhaps also indicative of this function, as parasitoid wasp probing pulses in particular are known to be ultra-short (approximately 1ms with 2ms decay) (Wäckers et al., 1998). Mole rats, when excavating tunnels produce short taps of less than 1ms to identify the presence of obstacles such as rocks in the soil (Kimchi et al., 2005). Aye-eyes, when foraging, also produce similarly short taps to identify wood-boring larvae (Ramsier & Dominy, 2012). Varroa jolting pulses are short, demonstrating a growth rate of 0.3 – 1ms on the majority of substrates. The exponential decay observed on Petri-dish, honeycomb, and capsule does not appear to be sustained by the animal, indicating that the oscillations following on immediately from the jolting vibration must result from the remaining vibrational energy in the substrate. It is possible that this substrate reverberation is also detected by the mite, as it is by the accelerometer, which may then also provide additional probing information.

I have also established that some mite individuals jolt hundreds of times, continuously, and for prolonged periods. This indicates a large expenditure of accumulated energy, and thereby further suggests that perhaps jolting is beneficial to the animal in some way. The probing pulses of the species mentioned earlier also follow a repetitive action, with parasitoid wasps transmitting vibrations repeatedly until a host is found (Wäckers et al., 1998), mole rats producing  $198 \pm 15$  signals per metre of tunnel that they excavate (Kimchi et al., 2005), and aye-eyes tapping the material containing their prey at a consecutive rate of  $97.7 \pm 19.9$ ms over a range of a few seconds (Ramsier & Dominy, 2012). Additionally, death-watch beetles are known to repeat production of a substrate-borne vibration (up to 190 times in a 30-minute period) for sexual communication when searching for a mate (Birch & Keenlyside, 1991). Jolting pulse repetition is therefore compliant with the idea of them serving an exploratory purpose, although it remains to be explained why some individuals remain static and jolting for prolonged periods and why some only jolt a few times. Investigation into how common Varroa repetitive pulsing is, and the circumstances under which it occurs, requires a dedicated experimental protocol.

#### 2.5.5. Conclusion

The work discussed in this chapter demonstrates the successful detection of individual Varroa mite activities using accelerometers on multiple substrates and disclose a behaviour that is new to science, which I refer to as 'jolting'.

The features of the associated vibrational pulse strongly indicate that it is possible to detect mites in real hives using accelerometers, and this now requires further work to narrow down

the location of pulse production for a more lucrative search. In the following chapter, I will further build upon the results gathered here, with an experimental protocol designed to better identify the function of the jolting pulse, aiming to establish whether this behaviour is produced within capped brood or not. This chapter will also investigate the potential to detect mite vibrations within the sealed brood cells, as this has been deemed the most promising hive location to achieve Varroa vibration detection. This exploration will be the next step towards achieving mite monitoring in a fully populated hive via vibration capture, the results of which may also shed light on the function of what I believe to be a behaviourally significant signal, based upon these early findings.

# Chapter 3: Detection and discrimination of Varroa vibrational pulses in the species' reproductive phase

## 3.1.0. Chapter overview

The previous chapter detailed a never-before described behaviour and its corresponding vibrational trace, which I termed the 'jolting' pulse. The substrate dependent features of the vibration were discussed in terms of frequency, strength, time duration, and periodicity. The potential for detecting this pulse in fully populated honey bee hives was thoroughly discussed, with emphasis on an investigation into the detection of Varroa jolting vibrations in the capped brood-comb.

In this chapter, I follow up the claim that investigating mite vibration capture in capped cells is the most promising route of detection. As covered in the previous chapter, Varroa spend half of their life cycle in the brood cell, and modelling predicts that a high percentage of the individuals found in a hive will be beneath the sealed wax cells at any time during the brood rearing season. Chapter three covers the investigation into the discrimination and detection of known Varroa vibrations (jolting and walking) in this environment, as an advancement towards the remote monitoring of mites in colonies.

I further investigate whether the jolting behaviour occurs when mites are in the sealed cells. The capped brood cells have been suggested to be the most promising area of the hive to begin remotely detecting mite individuals, but it is not yet known whether the novel jolting behaviour occurs here. Here, I mimic the reproductive phase in an observational experimental set-up, to identify the presence, or absence, of this behaviour. This investigation is important as it should indicate if jolting vibrational traces are useful as a search tool in this environment. Furthermore, it should also begin to reveal why the behaviour is produced.

This chapter is therefore split into two separate studies. Study 'a' utilises the results gathered in chapter two, building a training database of known Varroa vibrations that can be used to detect and identify mites in brood-comb accelerometer recordings. Study 'b' involves the experimental set-up of an artificial brood cell, to rear a mite and larva together and observe their behaviour over time. The purpose of this is to establish whether jolting occurs during

this life phase or not. The introduction is followed by the methods, where the two separate studies are outlined. The results section follows the same consequential order, discussing the results of Study 'a' and then 'b'.

The main figures in this chapter are listed as Figure 3.1, Figure 3.2 and so on. The supplementary material can be found in Appendix 2, and are referenced as D1, D2 etc. There is some video data associated with this chapter. Videos are also referred to as D1, D2 and so on, in the main text. Their figure legends can be found in Appendix 2. The videos themselves have DOI links (see page 10) and are labelled according to their text reference (D1, D2, etc.).

### 3.2.0. Introduction

#### 3.2.1. Why choose the capped brood cell environment for remote detection in a hive?

It is now possible to identify vibrations produced by a single Varroa mite using accelerometer sensors. Although these traces have already been detected on empty honeycomb and capped brood-comb, there is a necessity to move this research forward towards an even more natural setting. For the majority of their life cycle, mites are found either within the sealed brood cells of the comb or residing on the adult bees themselves (Rosenkranz et al., 2010; Nazzi & Le Conte, 2016).

It is uncommon, although not unheard of, for mites to also be found moving around on the comb surface within a hive (Kuenen & Calderone, 2000). There are some circumstances that could lead to longer term mite contact with the comb face, such as when mites pass from bee to bee (Le Conte & Arnold, 1987). The chance of this occurring may be exacerbated in the autumn/winter months, as Varroa numbers increase (van Dooremalen et al., 2012) and individuals are forced to remain in the phoretic phase, due to a lack of brood (Bowen-Walker et al., 1997; Martin, 1998). This could lead to an increased chance of mites falling onto the comb, which is particularly likely as mites cause higher mortality in over-wintering bees, and therefore they may need to transfer more frequently from dead or dying individuals to live ones (Bowen-Walker et al., 1997).

Regardless of this, however, the most sensible route of mite vibration capture would appear to be, at present, the monitoring of the brood cell contents, as 65% of mites in a colony are suggested to reside here at any time during the brood season (Martin, 1998).

### 3.2.2. Observing Varroa behaviour in the reproductive phase of its life cycle

The brood cells are where Varroa mites carry out their reproductive phase (Rosenkranz et al., 2010; Nazzi & Le Conte, 2016). When in this phase, Varroa have been successfully observed from the moment the brood cell is sealed to the emergence of the developing bee within. This has been achieved using artificial, transparent cells that have enabled continuous observation (Donzé & Guerin, 1994; Donzé & Guerin, 1997; Calderón, et al. 2009; Calderón, et al. 2012;). Mirrors have been used to capture all angles of artificial cells during filming (Donzé & Guerin, 1994; Donzé & Guerin, 1997), and this has provided the opportunity to collect detailed information on the behaviour of both mite and bee during their period in the cell.

Meticulous observations have been recorded thanks to this experimentation. Numerous in-cell activities and behaviours have been identified and monitored, including the number of Varroa feeding and defecation occurrences, choice of oviposition sites, offspring behaviour, and larval movements (Donzé & Guerin, 1994; Donzé & Guerin, 1997; Calderón et al., 2009; Calderón et al., 2012). This method has proven to be successful in capturing the full development of both mite and bee during this phase of their life cycle (Donzé & Guerin, 1994; Donzé & Guerin, 1997). Transparent cells occupied with a developing bee and mite can therefore provide a very good representation of what happens within a sealed cell whilst enabling the extraction of detailed information.

### 3.2.3. Two routes of study

The work in this chapter links two methods of experimentation to attempt to answer two questions:

1. Can accelerometers successfully detect mite activities when they are in the reproductive phase of their cycle?
2. Does jolting behaviour occur during the reproductive phase?

This chapter first aims to detect the mite vibrations that are now known and identifiable (jolting and walking), resulting from the previous chapters work. By removing sections of capped brood from a honey bee hive and recording the vibrations that occur within, these known traces can then be searched for.

Although it is not yet known whether jolting behaviour is produced during the reproductive phase of the life cycle, a lack of jolting pulse capture would not necessarily mean that mites cannot be detected by accelerometer sensors. As I determined in the previous chapter,

walking pulses occasionally have the potential to be of similar strength to jolting pulses. Walking behaviour is common within the cells, with mites described to walk regularly on the cell wall, particularly when they are moving to and from defecation sites (Donzé & Guerin, 1994). Consequently, it is likely that walking vibrational pulses can be detected and should be an ideal indicator of mite presence within the brood cells, in the event that jolting pulses cannot be found.

To ascertain whether or not jolting occurs in the brood cells, Varroa behaviour was here observed during this phase of the mite life cycle. To do this, the transparent cell method was adapted from the work carried out by the authors, Donzé and Guerin (1994, 1997). Identification of this behaviour in the artificial cells would suggest that jolting vibrations are useful for mite monitoring. Not only this, knowledge of where and when the jolting behaviour is produced should be advantageous for narrowing down why it occurs. Other behaviours, perhaps with their own corresponding vibrations, may also be identified as a result of this work, some of which could be unique to the cell period of Varroa life.

Both routes of investigation, (i) the detection of known mite vibrational traces in natural samples of brood, and (ii) the observation of the reproductive phase within artificial brood cells, aim to strengthen the claim that Varroa mite vibrations are a useful, measurable parameter when considering the remote monitoring of Varroa populations within honey bee colonies.

#### 3.2.4. Aims of the chapter

This work aims to:

- Discriminate between the vibrational features of mite jolting, mite walking, and additional, identifiable vibrations that occur within the brood-comb, e.g., those originating from honey bees.
- Use these vibrational signals as a search tool, to detect and identify mites/bees in long-term recordings of natural capped brood samples.
- Implement a transparent cell methodology to observe the reproductive phase of Varroa and seek out instances of jolting behaviour.
- Characterise the features of additional Varroa vibrations that may be produced during the reproductive phase, when the mite is in contact with the artificial brood cell wall and when on the larva. However, it is important to note when Varroa move on the soft-bodied larvae, vibrations may be dampened and therefore more difficult to detect.

### 3.3.0. Methods: Study 'a', the discrimination and detection of Varroa vibrational pulses in natural brood cells

#### 3.3.1. Brood sample collection

Samples of capped brood were removed from 4 different colonies in the spring and summer of 2020 and 2021. Using a scalpel, each section of brood (approximately 3 x 3cm in diameter) was cut from the comb of the hive and immediately transferred to the laboratory.

#### 3.3.2. Video/accelerometer recordings of the brood samples

Each sample was recorded, individually, in a sound isolated room. The sample was placed on a Petri-dish (50 x 10 mm) in the orientation that it would naturally be found in the honey bee hive (see Figure 3.1). An accelerometer (4507 B 002, Brüel & Kjær, 1000 mV/g) was attached to the base of the Petri-dish using a thin layer of glue. This was then positioned on top of a thick wad of cotton wool to help reduce interference from background vibrations. A single channel conditioner (Endevco 4416B, USA), set at a gain of x10, fed to both the accelerometer and the Sony camera that have been used throughout this thesis (Sony 4K FDR-AX100E handy cam, China) to enable synchronous recording of the accelerometer data and video. A light source was placed near the set-up to illuminate the specimen.



**Figure 3.1:** Sample orientation of a brood specimen, viewed from above.

Long-term recordings of 90 to 120 minutes were carried out for each specimen. Once the recording had finished, the brood sample was weighed on a set of electronic scales and measured to establish its actual dimensions. The number of cells on each side of the sample were counted, and the status of each cell (capped or uncapped) noted. A set of laboratory tweezers was used to carefully uncap each sealed cell and remove the bee inside. The approximate age of each developing bee was then estimated.

The number of Varroa mites found in each sample was noted (number of samples collected that contained Varroa = 8, number of samples collected that did not contain Varroa = 10).

### 3.3.3. Signal analysis

All signal analysis was conducted through Matlab (Refworks 2019a) using code written specifically for this study, at Nottingham Trent University. As with chapter two, the audio signal from the camera was calibrated.

The purpose of this signal analysis was to build a training database (TDB) of known vibrational signals that could be used as a search tool, for detecting signals of similar features in the novel brood-comb recordings.

Sections 3.3.3.1., 3.3.3.2., 3.3.3.3., 3.3.3.4., and 3.3.3.5. describe methods that were explored to determine their success in discriminating one type of vibration from another. Method 4 (section 3.3.3.5.) was identified as showing the most promise for the purpose of this work.

#### *3.3.3.1. Method 1: Training database creation and discrimination of spectrogram features specific to mite jolting and walking vibrational traces*

Focus was initially placed on mite jolting and walking pulses. Discriminating between the features of both types of vibrational trace was deemed necessary to establish which behaviour a recorded vibration belonged to.

A TDB was built using walking and jolting pulses. The collection of jolting pulses that were detected in chapter two ( $n = 189$ ) were extracted and transformed into individual spectrograms. These were then aligned in time to a particularly clear reference jolting pulse (see Appendix 2, Figure D1) using cross-correlation product analysis. Only the strongest, clearest pulses were chosen for further analysis as part of the TDB ( $n = 39$ ) (see Appendix 2, Figure D2).

A collection of clear, strong walking pulses ( $n = 110$ ) was identified and extracted from the same accelerometer recording as the jolting pulses. The walking pulses were also aligned to

the same reference pulse as the jolting pulses, so that all traces were positioned identically in time (see Appendix 2, Figure D3).

The accelerometer data for both walking and jolting pulses was band-pass filtered (500 – 8000 Hz), to remove redundant background frequencies and improve the clarity of the pulse features for successful alignment processing.

Following this, the two groups of centred pulses then underwent a second cross-correlation product analysis using the filtered waveform of each pulse, rather than the spectrograms, for improved centring (see Figure 3.2, Figure 3.3).

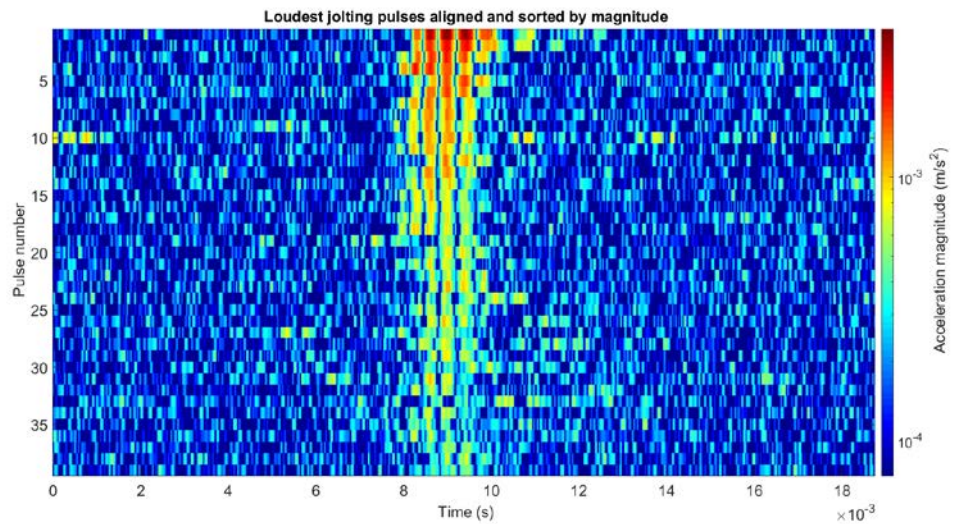


**Figure 3.2:** The loudest jolting pulses ( $n = 39$ ) viewed together. The pulses have here undergone a second alignment process and are now well aligned in time to one another. The magnitude of acceleration is logarithmic (to the base 10), where the highest magnitude is dark red ( $3.7 \times 10^{-3} \text{ m/s}^2$ ), and the minimum is dark blue (forced to be 1/50 of the maximum). All data shown here has been band-pass filtered (500 – 8000 Hz).

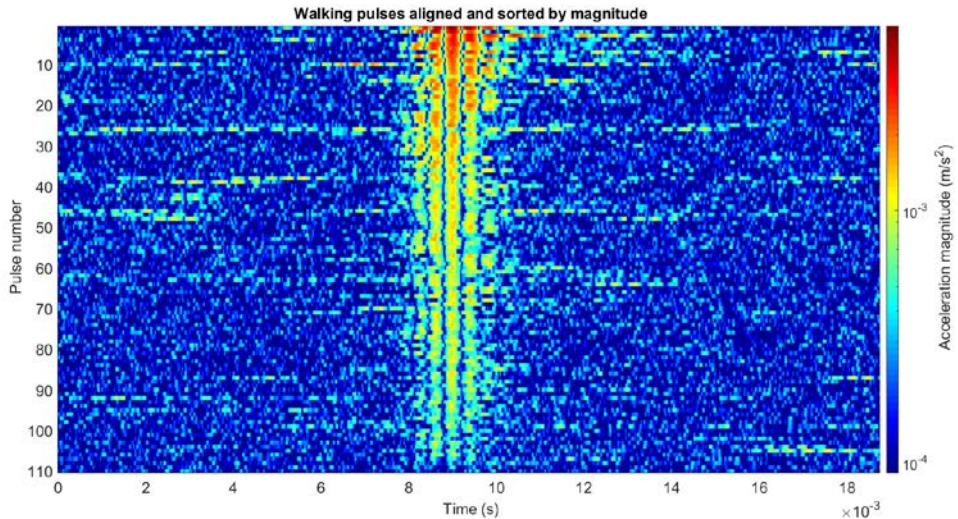


**Figure 3.3:** The full collection of walking pulses ( $n = 110$ ) viewed together. The pulses have undergone the same analysis as the jolting pulses and are now well aligned in time to one another. The magnitude of acceleration is logarithmic (to the base 10), where the highest magnitude is dark red ( $5.4 \times 10^{-3} \text{ m/s}^2$ ), and the minimum is dark blue (forced to be  $1/60$  of the maximum). All data shown here has been band-pass filtered (500 – 8000 Hz).

For the creation of the final training data, the original, unfiltered accelerometer data containing the jolting and walking pulses was used, to maintain a larger frequency bandwidth for training purposes. The data was then only high-pass filtered (500 Hz) to remove the low background frequencies that largely impacted upon the visibility and clarity of the walking and jolting vibrational traces.

The pulse waveforms within this less harshly filtered data could then be aligned in time based on the shift-in-time values that were established from the two cross-correlation product analyses (see Appendix 2, Figure D4 and Figure D5). This way, the data could be accurately aligned in time, without losing additional data (that needed to be removed for accurate alignment in the first instance).

### 3.3.3.2. Method 1: Principal component/discriminant function analysis of mite jolting and walking spectrograms

Every walking and jolting pulse was then transformed back into a spectrogram to include the frequency component features of the walking and jolting pulses for discrimination. Principal component analysis (PCA) and discriminant function analysis (DFA) (see sections 1.4.5.3. and 1.4.5.4. for full description) were then implemented to establish discriminatory features in the two groups.

*3.3.3.3. Method 2: Training database creation and discrimination of temporal features specific to mite jolting and walking vibrational traces*

When viewing the data as spectrograms, a visible difference in the temporal density of vibrational pulses could be seen. Jolting pulses, in general, exhibited just one single or double peaked trace within the spectrogram time window, whereas walking pulses demonstrated numerous traces in the same time period (see Figure 3.2, Figure 3.3). The number of vibrational traces identified in a chosen time window were then made to be the discriminatory feature of interest.

The second order time differential was calculated for each jolting and walking pulse. Each pulse time window was then scrutinised for points of steep negative inflection, which were indicative of walking/jolting pulse presence in the data. It was expected that walking behaviour would demonstrate a larger number of negative inflection points than jolting. Various parameters (window length, multiplication factor, temporal resolution, threshold value, and data normalisation) were tweaked to find optimum discrimination between the two datasets (see Appendix 2, Figure D6 and Figure D7 for full details).

The optimum TDB outcome was then tested on the accelerometer recording that contained a mite jolting and walking in view (i.e., the recording that was used to create the TDB), so that the success of the TDB could be tested and corroborated with visual evidence of mite behaviour. To do this, the recording was scanned to identify all points of negative inflection that fell beyond the chosen threshold. It was expected that periods where the mite was motionless would exhibit a lack of spikes, and that a larger number of spikes would be detected when walking than when jolting.

*3.3.3.4. Method 3: Training database creation and discrimination of emerging honeybee and mite vibrational traces (spectrogram)*

The bee signals used in this analysis were chosen from a brood-comb accelerometer recording where only developing bees resided (no mites were present in the sample). The vibrations chosen were attributed to one bee that was seen emerging from her cell. The walking signals were the same as used previously for jolting and walking discrimination.

The spectrograms of the two types of signal were first investigated in the same way as for the jolting and walking pulses (see section 3.3.3.1., see Appendix 2, Figure D8 for bee alignment, Figure 3.3 for walking alignment). A mite walking pulse was chosen as the reference pulse for aligning all data due to the repeatable features and clarity of this type of

vibration. Bee emergence signals varied substantially in time, shape, and frequency, therefore alignment to a bee signal would have provided a less optimum outcome.

The aligned spectrogram collections were scaled, and then underwent PCA and DFA. Good discrimination was only seen between the two groups (mite and bee) on the horizontal axis of the DFA scatterplot, therefore only DF score 1 was focused on for further analysis. A DF spectrum image (spectrogram) was produced, as a result, for this first DF score.

This DF spectrogram was then used as a reference image in cross-correlation product analysis, to test the suitability of the TDB (containing the aligned spectrogram collections). The full accelerometer recordings that were used to create the TDB were transformed from waveform to spectrogram image for every 1ms of data. The cross-correlation product was then calculated between this image and the DF spectrogram to produce a DF score value. The analysis then moved on by 1ms in time (short enough to reduce the chance of missing a walking pulse, typically 3ms in duration).

Once this analysis had run through the full accelerometer recording, the values that were saved for each 1ms of data were plotted as histograms, to identify the spread of the DF scores. This visualisation of the data was necessary to identify whether the mite walking pulses, and bee emergence signals were falling into their correct cluster.

#### *3.3.3.5. Method 4: Training database creation and discrimination of emerging honeybee and mite vibrational traces (2DFT)*

As well as spectrograms, 2DFT images were also tested. This method demonstrated to be the best out of the four tested methods for discriminating between the datasets.

A new TDB was built using one-second-long extracts of accelerometer data, each transformed into a 2DFT image. Alignment of the data was not necessary in this case as the purpose of the 2DFT was to identify the frequencies that occurred in the accelerometer data. This parameter is not affected by the vibrational waveforms' position in the one second time window (the frequencies in the waveform remained the same, regardless of its position), and therefore vibrational waveforms did not need to be shifted in time to align with one another, this would not influence the discrimination outcome as it would with a spectrogram. Three categories of data were used: (i) bee ( $n = 242$ ), (ii) mite ( $n = 66$ ), (iii) background ( $n = 87$ ). The 2DFTs were collected from the two brood-comb sample recordings that were used for the bee/mite spectrogram investigation, one brood comb recording that contained the vibrations of only bees, and one other recording of a mite walking visibly and audibly on a

brood comb sample. Periods of background noise were also gathered from this data (via critical listening). The purpose of this was to benefit discrimination between quieter walking vibrations and background vibrations, as walking vibrations were more likely to suffer from poor signal-to-noise-ratio (SNR) than bee pulses.

The horizontal axis of each 2DFT was interpolated to reduce the number of pixels that were unnecessarily present for this analysis. Without interpolation there would be too many unnecessary details present, which would slow down the machine learning, as well as increase the risk of overfitting the data, where small, inconsequential elements are incorrectly identified by the algorithm as meaningful and are utilised to achieve discrimination. Each 2DFT was appropriately cropped to remove frequency bandwidths along the y axis (0 – 500 Hz and 4000 – 24,000 Hz) that did not hold information related to vibrational differences between the three groups. The 2DFTs were then scaled by their maximum amplitude to reduce the impact of the signal strength variation that was observed in the dataset from interfering with the discrimination process.

This training data then underwent PCA to determine which features held maximum variance, followed by DFA, which used this reduced dataset to seek further features of high variance based on the specific groupings of the vibrations (mite, bee, and background). From this analysis, the data could be viewed as a scatterplot in DF space. Two discrimination spectrum images (2DFTs, one for DF score 1 and one for DF score 2) could also be visualised. These two images were saved so that they could be utilised in the next stage of analysis.

#### *3.3.3.6. Method 4: Testing the accuracy of the training database (2DFT)*

The long-term recordings from which the TDB was created were used for this next stage of analysis. For each recording, a one-second-long extract of accelerometer data was transformed into a 2DFT which was scaled, interpolated, and cropped in the same way as the 2DFTs that formed the TDB (see Figure 3.4).

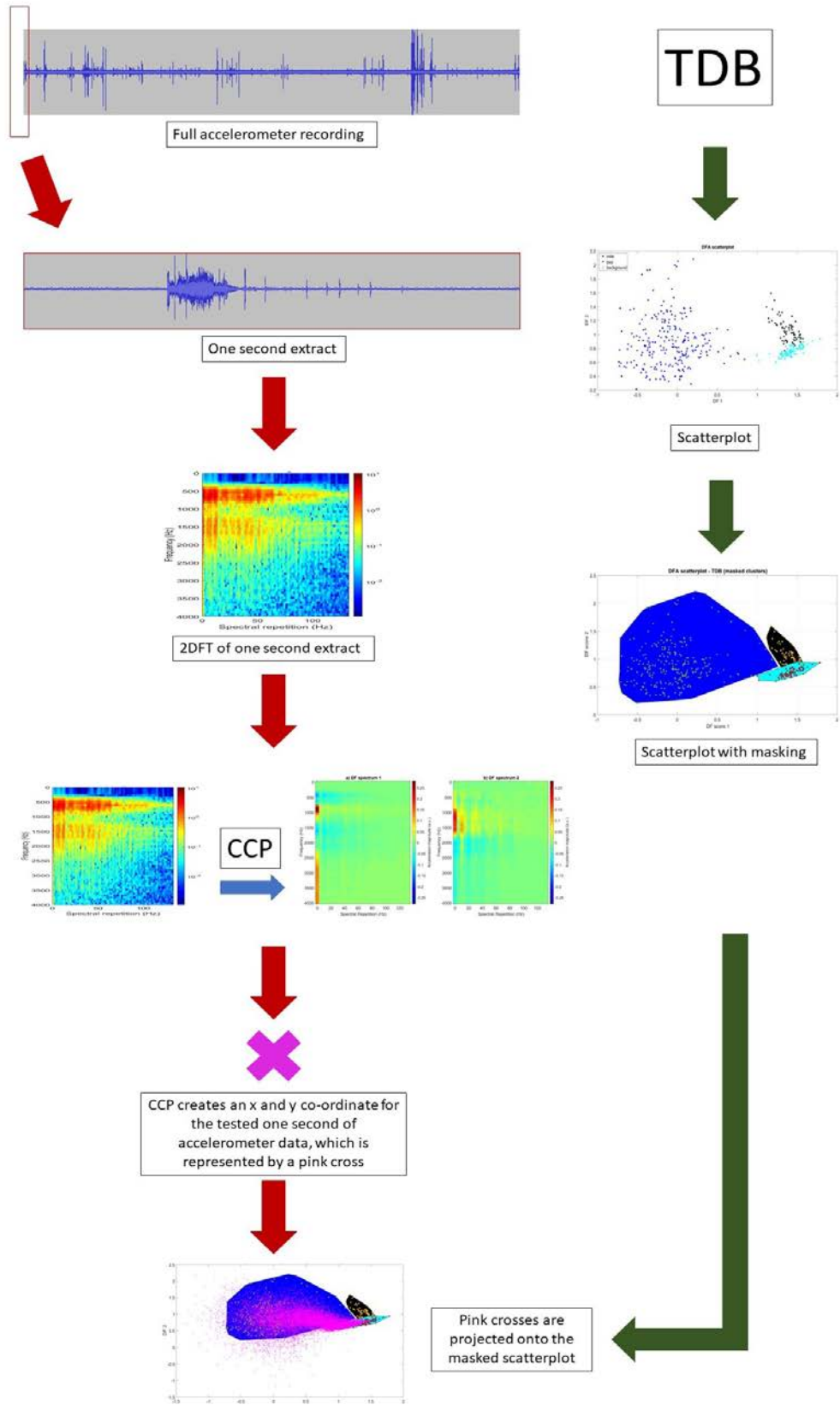


**Figure 3.4:** A figure to showcase the training database (TDB) testing process. On the left-hand side of the plot (red arrows) an accelerometer recording containing known vibrations (i.e., it has been

corroborated with video evidence of the same data to identify timings where either mite, bee, or just background vibrations are present) is tested to determine the success of the TDB. One second of the data is extracted and transformed into a 2DFT of the same dimensions as those that formed the TDB. This 2DFT then undergoes cross-correlation product analysis with the two discriminant 2DFTs that were created during PCA/DFA. This produces a set of co-ordinates for that one second of data, to be plotted onto DF space. This process is repeated in steps of time of 0.25 seconds until the full recording has been analysed. A set of co-ordinates (pink crosses) is therefore created for that recording. On the right-hand side of the plot (green arrows), the TDB undergoes PCA/DFA to produce a scatterplot, showcasing the discrimination outcome and clustering of the three groups (mite, bee, background). This scatterplot is then analysed to determine the periphery of each cluster, which produces a 'mask' for each group. The pink crosses for the analysed recording can then be projected onto this masked scatterplot, to identify where in DF they fall. In doing so, the success of the TDB can be determined.

Cross-correlation product analysis was implemented between this 2DFT and the two discrimination spectra that were created during PCA/DFA. The result of this analysis was a set of co-ordinates, on DF scores, for a single datapoint that could be plotted onto a graph alongside the TDB cluster data (see Figure 3.4).

The scatterplot data, originating from the 2DFT, underwent a 'masking' technique, to determine the periphery of each groups cluster (bee, mite, background) (see Figure 3.4). The new datapoint could then be plotted onto this graph, for the purpose of identifying where in DF space it fell, i.e., did it fall within one of the masked areas or not. The accelerometer data for that point was then visualised and critically listened to, so as to determine what the audio data contained (bee emergence signals, mite walking signals, background noise, or something else). This could then be corroborated with where the datapoint was plotted, to see if it had fallen correctly into its corresponding cluster area or not (see Figure 3.4).

The analysis then moved on in time, in steps of 0.25 seconds, and was repeated until pre-defined periods of the accelerometer data had been searched. The tested accelerometer data contained known bee emergence signals (where mites were not present) or, known mite walking signals (where bees were not present) or, known background noise. In doing so, the accuracy of the analysis could be tested as the vibrations captured were visibly/audibly recognisable (see Figure 3.4).

If a datapoint fell outside of any of the cluster masks, or into the wrong cluster mask, the training database was then updated to correctly include this new data. In doing so, the

training data, and therefore the outcome of the search analysis, could be improved for greater success the next time it was tested. The TDB initially started out with a smaller number of signals from only two long-term recordings and was repeatedly updated until the final outcome described in section 3.3.3.5.

#### *3.3.3.7. Method 4: Detecting mite, bee and background vibrations using the brood sample recordings*

The full collection of brood sample recordings (with or without Varroa) were then tested using this training data. Utilising the same method as described in sections 3.3.3.5. and 3.3.3.6., each full recording was analysed to see whether the machine learning picked up on the presence of Varroa in the selected recordings. The purpose of this analysis was to establish the accuracy of the training data and whether it was possible to determine the presence or absence of Varroa mites in each novel sample when using this method.

#### *3.3.3.8. Method 4: Trialling additional methods of TDB improvement*

Following analysis of the brood-comb samples (with or without Varroa), it was deemed necessary to test further improvements for the benefit of the discrimination process.

- 1. Increasing the time window of the 2DFT:** The length of the accelerometer data that was included in each 2DFT was increased from 1 second to 1.5 seconds. The centre point of each accelerometer extract remained the same, with the additional time data added on to the beginning and end. The purpose of this method was to determine if stronger discrimination could be found between honey bee and Varroa vibrations when additional temporal information was included. An increase in the time window was expected to become more representative of mite walking features because a larger number of pulses could be included in a larger time period.
- 2. Background noise removal:** For this method, the original one-second-long TDB was used. The Varroa present and absent brood-comb recordings were modified to remove background vibrations. It was deemed possible that differences in general background noise may be biasing the outcome of the discrimination process, as the recordings were collected on different days over the course of 12 months.

A section of background noise was identified in each recording (minimum two seconds). This area was then averaged and subtracted from the entire recording. The remainder of the analysis then continued as normal.

- 3. Adding a fourth category to the supervised machine learning:** One Varroa absent recording demonstrated an anomalous result whereby the majority of datapoints clustered the DF space area that corresponded to the mite category. The recording was critically listened to in comparison to Varroa walking vibrations to determine if there were any significant similarities between the two. In 9/10 extracts of accelerometer data from each of these recordings, the two types of vibration were successfully identified (see section 3.7.5.3.). The success of this critical listening exercise indicated that there were features present in the two types of vibration that would enable discrimination to occur should these anomalous recording vibrations (that were resulting from bee activity) be added to the TDB as a separate group.

Therefore, the TDB was then updated to also comprise of the vibrations of the unusual bee recording in a fourth, separate category. Analysis was then run as normal, to find out whether PCA/DFA could establish any discriminatory features between this dataset and the other three categories, particularly the Varroa, as the unusual bee vibrations were most similar to those of mites.

The DF space scatterplot and discrimination 2DFTs were saved for further cross-correlation product analysis, for testing of the Varroa present and absent recordings.

### 3.4.0. Methods: Study 'b', observation of Varroa within an artificial brood cell

#### 3.4.1. Specimen collection and artificial brood cell creation

This data was collected at Nottingham Trent University during the late spring and early summer of 2020. The procedure for occupying an artificial cell with both a Varroa mite and honey bee larva was adapted from the methodology used by Vincent Piou's research group (Piou et al., 2016; Piou et al., 2018; Piou & Vétillard, 2020). A full frame containing a large proportion of fifth instar larvae was removed from a colony of *A. mellifera* and brushed free of all adult bees.

Transparent gelatine capsules (size 3, 0.3ml volume, 5.6mm inner diameter, Agar Scientific, UK (chosen to improve mite reproduction in comparison to other capsule sizes (Piou, 2020)) were separated into their two halves. One half of the capsule was gently inserted into one cell containing a fifth instar larva so that the capsule was protruding out of the cell (see Figure

3.5). Once a collection of capsules had been inserted into one side of the frame, the entire frame was placed in a specially designed holder that allowed it to lie horizontally without impacting the inserted capsules. The capsule-loaded side of the frame was placed on the underside of the holder, so that gravity could aid the spinning fifth instar larvae in falling into the capsules (see Figure 3.6).



**Figure 3.5:** Clear gelatine capsules were inserted into cells containing fifth instar larvae. Following a few hours of gravity-driven displacement of the larvae into the capsules, they can be seen here at varying stages of capsule occupation.

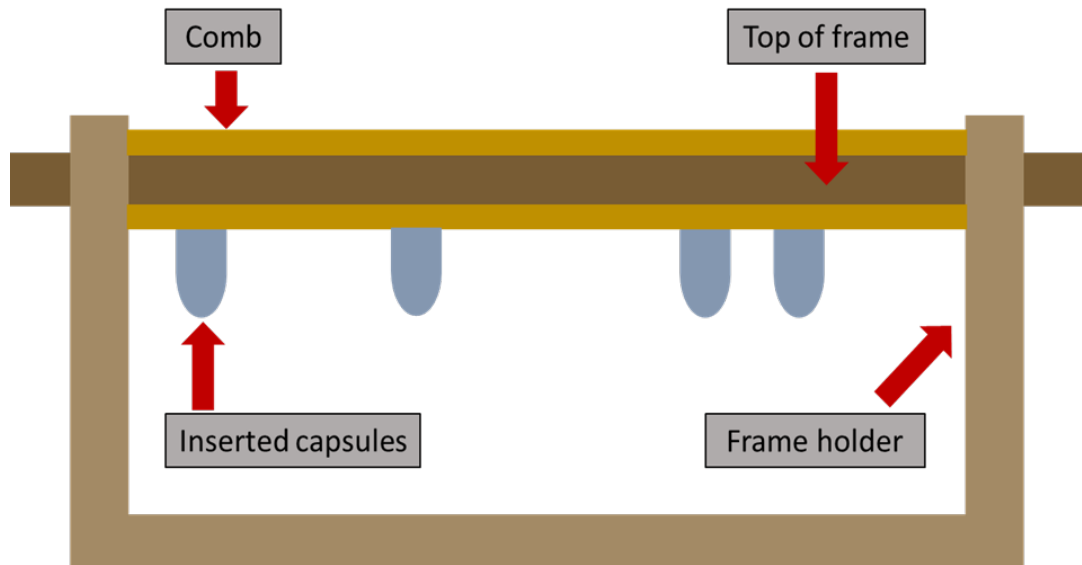


**Figure 3.6:** The set-up of the frame with inserted gelatine capsules in the frame holder. Diagram produced by Harriet Hall.

The frame set-up was then placed in an incubator set at 35°C and left overnight to give the larvae time to naturally fall into the capsules. The following morning, the frame was removed from the incubator. Those capsules containing larvae were removed from the cells and fitted back together with the other, separated half. When placed back together, there was a small gap between the two capsule halves. This benefited gaseous exchange between the capsule and the external environment. These fully assembled capsules were then placed back into the incubator. During this time, capped brood on the frame was also searched for Varroa mites by removing the brood cappings using a pair of laboratory tweezers. Any mites found under the surface were collected with a paintbrush and immediately transferred to a capsule containing a larva.

This procedure was altered later in the study to 'reset' the mite life cycle. As mites were collected from capped brood cells, it was possible that they had undergone some of the reproductive phase before removal. To reduce any such detrimental effects, mites were instead first placed on an adult bee to mimic the phoretic phase and therefore 'reset' the biological cycle of the mite.

In order to do this, adult bees were collected from a colony and placed in a sealed plastic box with airholes. Fondant was provided in the box as a food source. Once mites were collected, they were placed in the box with the bees for a three day period (Piou et al., 2016). Successful attempts to mimic the phoretic phase did not occur however, due to problems maintaining

bee longevity, as they quickly died in the box. The specimens that are subsequently described in this study were established without the honey bee host intermediate step.

#### 3.4.2. Visual/vibrational measurement collection

A capsule containing a Varroa mite and a larva were moved to a second incubator (Lucky Reptile Incubator, Lucky Reptile, Germany) that had a clear plastic door for viewing the specimen. The capsule was rested directly onto an accelerometer (4507 B 002, Brüel & Kjær, 1000 mV/g), using a small amount of petroleum jelly (Vaseline) to hold it in place. The accelerometer was secured to a wooden board with a thin layer of glue to prevent the sensor from displacing during measurements. The wooden board was placed on polystyrene to reduce the effect of vibrations that were produced by background noise. A small hole was drilled into the door of the incubator to allow the accelerometer cable to extend outside, whilst enabling the incubator door to stay shut and prevent heat escape. A small rubber bung fitted into this hole and around the accelerometer cable to further prevent any heat and humidity loss. The accelerometer cable fed to a single channel conditioner (Endevco 4416B, USA) that was set to a gain of x10 (see Figure 3.7). Accelerometer data was recorded synchronously with video footage via the camera (Sony 4K FDR-AX100E handy cam, China) that was set-up on a tripod in front of the incubator.

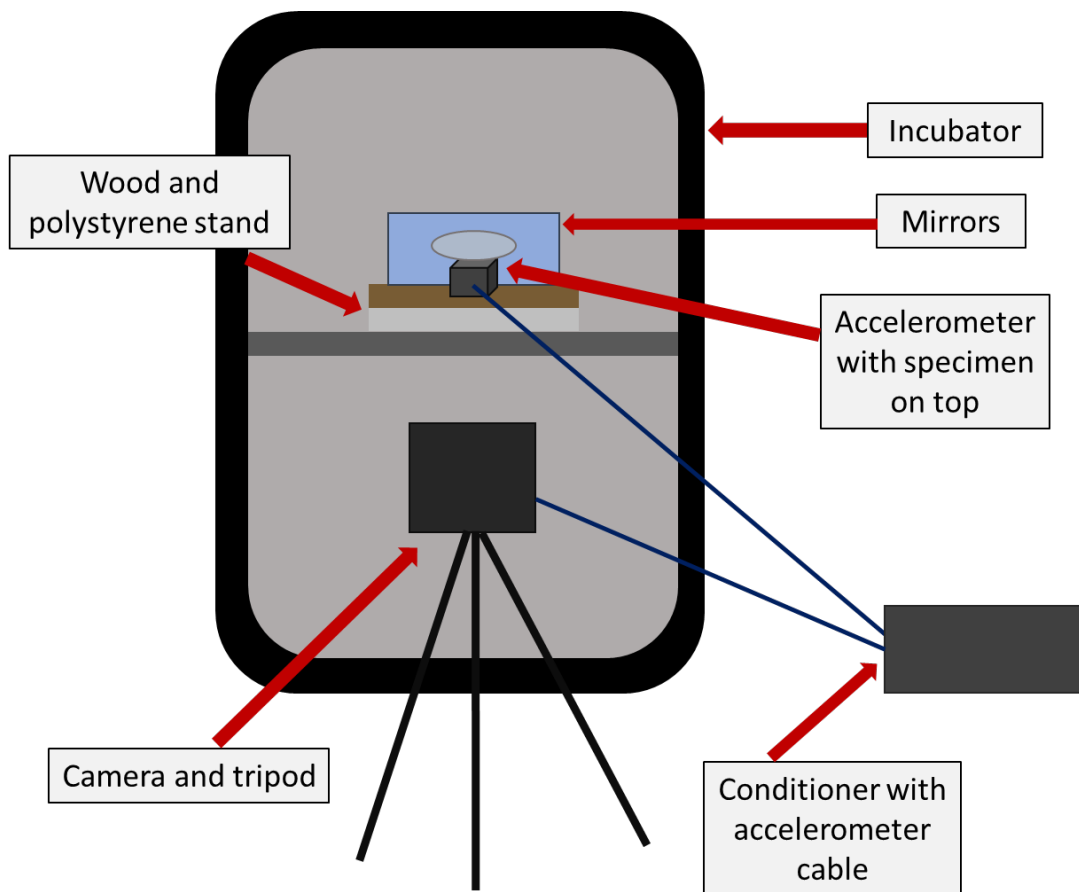


**Figure 3.7:** A diagram to show the set-up of the specimen in the incubator for filming and recording of accelerometer data. Diagram produced by Harriet Hall.

Within the artificial capsule, the *Varroa* was expected to move around the cell and behind the larva. To avoid observational data loss because of this, a set of mirrors was placed behind the specimen (a method adapted from Donzé & Guerin, 1994). Four 1 x 1cm mirrors were glued into an orientation that allowed maximum viewing of the specimen. A central mirror was glued to three peripheral mirrors at approximately 140° angles. When filming, these mirrors allowed the capture of all but the bottom edge of the capsule, which sat on the accelerometer (see Figure 3.8). Mite and larva were filmed for 2 – 3 hours at a time twice daily.

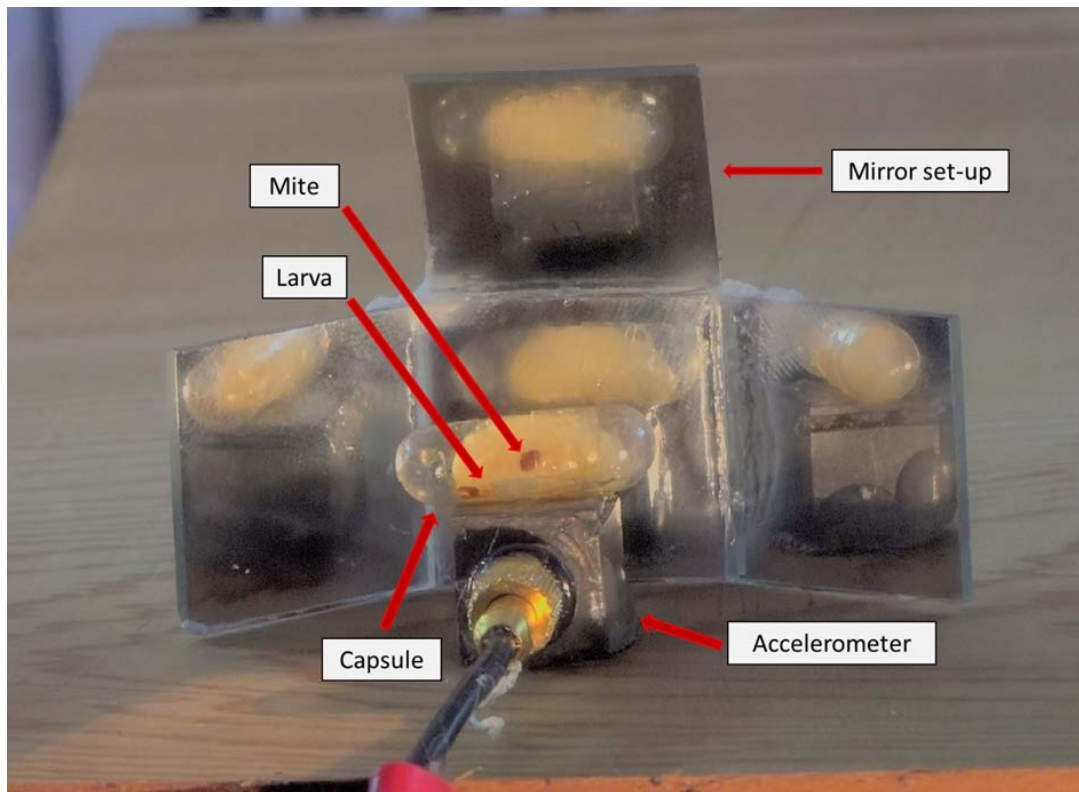


**Figure 3.8:** The specimen set-up on the accelerometer with the mirrors behind showing all possible angles for observation.

#### 3.4.3. Additional video data of a Varroa and a developing bee in a cell

One 24-hour-long video (filmed at 25 FPS) of a developing bee and three Varroa mites (two female, one male) within a capped brood cell that has a glass viewing panel along one of its lengths was kindly provided to our research group by Dr. Paul Siefert (Institut für Bienenkunde, Goethe-Universität Frankfurt), for additional visual investigation of the jolting behaviour. This video data was collected by Dr. Siefert in an experimental set-up of his own design (Siefert et al., 2020; Siefert et al., 2021). The three mites were observed in their natural environment, a sealed brood cell within a fully populated honey bee hive. The developing bee was in the last 24 hour period before emergence into the colony, which can also be observed in the video. Vibrations were not captured in this set-up.

#### 3.4.4. Signal analysis

##### 3.4.4.1. General analysis of the vibrations captured by the accelerometer

Each incubator video was scrutinised for the behaviour of interest (jolting) as well as for instances of Varroa walking behaviour and any other behaviour of interest occurring from either the mite or larva.

When a behaviour of interest was identified, the accelerometer data for that period was investigated for observable vibrational traces. Waveforms were extracted and transformed into spectrograms for feature identification.

Mite and larval vibrations were compared by means of their spectrograms, as well as to that of the background noise. The time course of the magnitude of acceleration of these vibrations was also computed, to show the integral of the acceleration magnitude at each point in time.

For a specific, unknown *Varroa* behaviour of special interest, the features of the vibrational traces were investigated in both waveform and spectrogram. The growth and decay of the strongest vibrational signals were also calculated by visibly estimating the curves.

#### *3.4.4.2. Video analysis of mite walking vibrations*

Video data of *Varroa* walking on the capsule wall when the larvae were both alive and deceased were chosen for further analysis, to demonstrate the vibrational features and audible characteristics of the walking pulses in the two different scenarios. The video analysis was also used to demonstrate synchronicity between the vibrational traces seen and the audio/video of the mite walking.

For each scenario (dead larva, and live larva) movies were created from the video footage taken of each mite and larva in the capsule. A grid was superimposed onto the original video footage so that when the *Varroa* moved around on the capsule, the co-ordinates of its movement could be logged, enabling tracking of the mite. The spectrogram of the accelerometer data was updated as a function of time continuously (reflecting the time stamps of the original video). The modulus of the difference image calculated the difference in pixel intensity between two consecutive frames, so that mite movement could be identified more clearly (when the mite was motionless the pixels in the window remained blue, whereas when the mite walked, the pixels flashed red in accordance with the change in pixel intensity).

#### *3.4.4.3. Additional video analysis*

The video provided by Dr. Paul Siefert was critically viewed for the full 24 hour period to observe whether jolting, or any other behaviour of interest, occurred.

### 3.5.0. Results: Study 'a', the discrimination and detection of Varroa vibrational pulses in natural brood cells

Here, the results follow the same chronological order as seen in the methods section. Each training database creation and discrimination method is discussed in order, leading up to the final chosen method (method 4) used in this study.

#### 3.5.1. Method 1: Training database creation and discrimination of spectrogram features specific to mite jolting and walking vibrational traces

The spectrogram images of a collection of mite jolting ( $n = 39$ ) and walking ( $n = 110$ ) vibrations were used to create a TDB for the purpose of identifying specific features that discriminated the two groups from one another.

In the case of this analysis, the use of spectrograms was not successful. The two groups (walking and jolting) did not form well defined clusters (see Figure 3.9). The inclusion of up to seven principal components (26% of deviations) was subjectively deemed suitable for this discrimination, according to the scree plot (see Appendix 2, Figure D9). However, the clustering was poor regardless of the number of principal components included. This data was therefore not suitable for further testing.

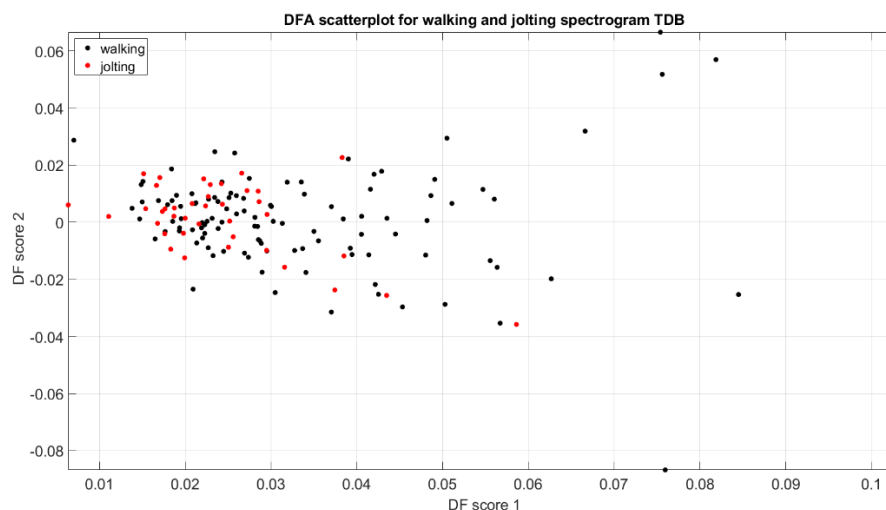


**Figure 3.9:** Discriminant function analysis outcome for the collection of Varroa walking and jolting pulses. Here, seven principal components are included in the analysis. Each point represents one walking pulse (red) or one jolting pulses (black) within accelerometer data windows of 0.018 seconds. A lack of discrimination between the two clusters can be seen.

### 3.5.2. Method 2: Training database creation and discrimination of temporal features specific to mite jolting and walking vibrational traces

Following on from the spectrogram investigation, it appeared that there was a different feature that could perhaps benefit discrimination between mite jolting and walking pulses. As introduced in the methods (section 3.3.3.3.), this feature was identified as the temporal density of pulses within a set time window. Jolting pulses most commonly demonstrated a single pulse, whereas walking vibrations, in many cases, had multiple satellites either side of the centred pulse (see Figure 3.2 and Figure 3.3).

A function designed to count the number of pulses observed per window, was optimised to identify the best parameters required for good discrimination between the groups (see Appendix 2, Figure D6 and Figure D7). When testing this function on the accelerometer recording that was used to build the TDB, the outcome was not ideal. This was because when using the chosen optimum parameters for this analysis, it was expected that for an ideal period of 0.11 seconds, between 5 and 20 points of negative inflection (spikes) would be detected when the mite was walking, and between 1 and 4 would be detected for a jolting mite (see Figure D7). Yet regardless of whether the mite was motionless, walking or jolting, spikes were detected at almost all times throughout the recording, and often at an unexpectedly high number (see Figure D10).

Although there is some basic discrimination seen when the mite was walking compared to when it was jolting (more spikes seen during walking periods, as expected) (see Figure D10), it is still difficult to identify when the mite was immobile due to spikes being consistently detected throughout the entire recording. This method was deemed too simplistic for the purpose of identifying mite activity and distinguishing jolting from walking pulses.

It appeared, at this stage, that discriminating between the two types of Varroa vibration might not be possible with good enough quality. For the purpose of moving forward with the investigation into Varroa detection beneath the capped cells, another approach was instead tested.

### 3.5.3. Method 3: Training database creation and discrimination of emerging honey bee and mite walking vibrational traces (spectrogram)

It was deemed more relevant to attempt feature discrimination between honey bee and mite vibrations (whether they be walking or jolting), as the bee vibrations were the only other signal found to occur in the brood samples (corroborated through visual evidence of a bee emerging from her cell). The two types of vibration were easily distinguishable via critical

listening, as bee vibrations were louder, and sounded 'scratchy' in nature, whereas mite vibrations exhibited a lighter 'tapping' sound (see Appendix 2, Audio D11 and Audio D12).

Both bee emergence and mite walking vibrations were known to occur in the brood cells, whereas it remained unknown if jolting pulses did. Therefore, attempting discrimination between known Varroa and honey bee brood cell signals offered a stronger approach towards mite detection success in this environment, at this time.

To begin this investigation, spectrogram images of mite walking and bee emergence vibrations were tested. The TDB that contained these two groups of signals showed good clustering when analysed using PCA and DFA (see Figure 3.10). A scree plot for this data indicated that up to approximately 20 principal components (40%) would have been suitable for discrimination (see Appendix 2, Figure D13). Nonetheless, overall, 27% of all PCA deviations were chosen for this analysis based on the clarity of the clustering outcome and discriminant 2DFT image (see 2DFT panel, Figure 3.10, see Appendix 2, Figure D13). The discriminant 2DFT for DF score 1 (horizontal axis) was chosen for further analysis only, as the majority of the discrimination between bee and mite vibrations was along the x axis (see scatterplot panel Figure 3.10), where the bee emergence cluster mostly fell between -140 and -30 and the mite walking cluster fell between -20 and 5, with some minor overlap. The discriminant 2DFT for DF score 2 (vertical axis) was not included in further analysis for this reason.

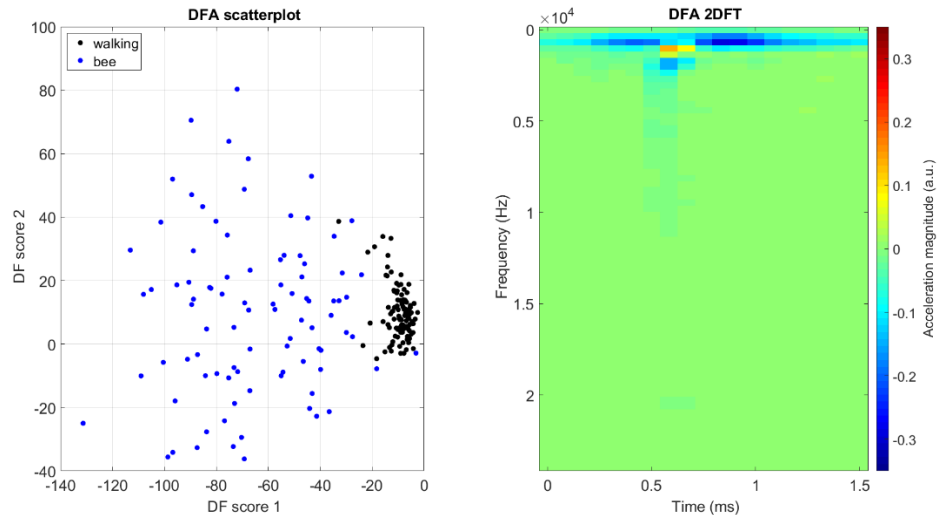


**Figure 3.10:** The machine learning outcome for the mite and bee spectrogram discrimination. Inclusion of five principal components leads to good discrimination between the two groups, mostly on the horizontal axis. The spectrum panel shows the DF spectrum for DF score 1, used as a reference image in cross-correlation product analysis. Magnitude of acceleration is in arbitrary units, where dark red and dark blue indicate spectrogram features that have the strongest influence on the discrimination between mite and bee vibrations, and green is indicative of zero, i.e., features that did not have any influence. The maximum and minimum values of the plot have been forced to -0.35 to 0.35, for easier interpretation of the colour coding.

This discriminant 2DFT image was then used as a reference for cross-correlation product analysis on the entire accelerometer data that was used to create the TDB. The purpose of this was to test that the algorithm was suitable for discriminating between walking and emergence signals (even those signals that did not contribute to its training). When testing the accelerometer recording that captured the mite walking, the spread of DF scores was similar to what was expected, based upon the DFA scatterplot (most scores fell between -20 and 5 on the x axis) (see Figure 3.11). When testing the accelerometer recording that captured the honey bee emerging from its cell, the bee data also demonstrated a number of scores that fell in the expected range (-140 to -30) (see Figure 3.11). However, the spread of DF scores skewed and overlapped strongly towards the co-ordinates of the mite cluster (-20 to 5) (see Figure 3.11).

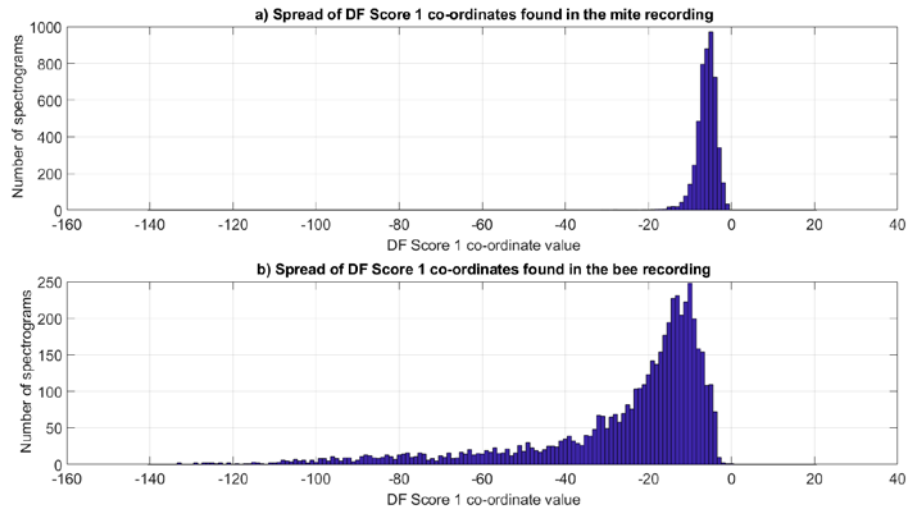


**Figure 3.11:** A histogram to demonstrate the spread of DF co-ordinates for five seconds of mite walking data (panel ‘a’) and 5 seconds of bee emergence data (panel ‘b’). The vast majority of mite DF scores fall in the -20 to 0 range. The bee DF scores are also skewed towards this range, demonstrating overlap between the two groups.

#### 3.5.4. Method 4: Training database creation and discrimination of emerging honey bee and mite walking vibrational traces (2DFT)

Method 3 showed some promise, but it was further decided to also test discrimination of the data in a different format (2DFT), to first establish whether a better outcome could be achieved before continuing with spectrogram analysis, if necessary. Therefore, a new TDB was created using 1-second extracts of mite walking and bee emergence signals. These extracts were transformed into 2DFTs.

The decision to do so was aided by critical listening. As described in section 3.5.3., bee and mite vibrations are distinguishable audibly. Both types of pulse occur repeatedly in short spaces of time, and are identifiably different in their patterns of production, with mite walking vibrations sounding more periodic in nature, in contrast to bee vibrations which were produced at more variable intervals (see Appendix 2, Audio D11 and Audio D12). For this reason, examination of the data in 2DFT format was deemed appropriate.

The unique gait of Varroa mite has, as a result of this study, been characterised (see Figure 3.12). A video that demonstrates a mite walking, a honey bee emerging from a brood cell, and general background noise demonstrates synchronous visual and vibrational evidence for the unique vibration of each category (see Appendix 2, Video D14). One second of accelerometer recording was used for obtaining a collection of walking pulses for this

discrimination, as Varroa were typically observed to walk on brood-comb in short bursts of 1 – 2 seconds.

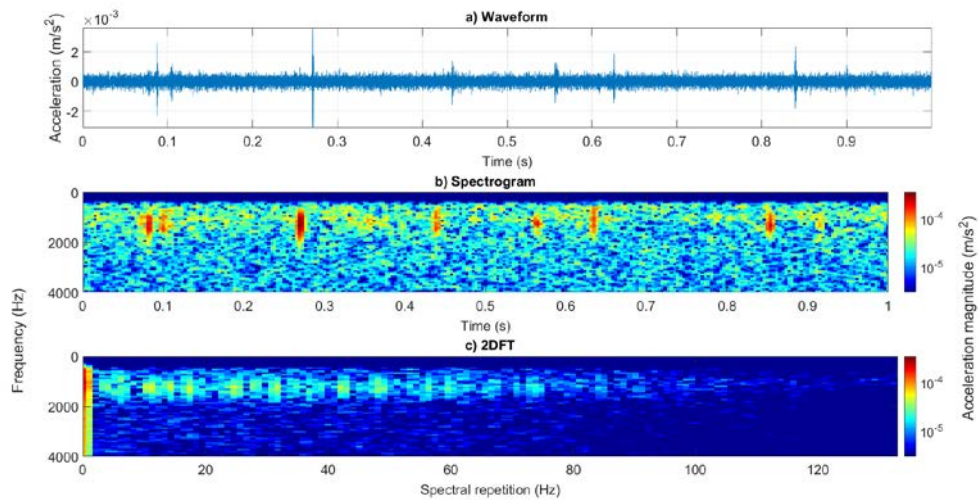


**Figure 3.12:** A typical example of one second of mite walking vibrations on brood-comb, viewed as an accelerometer waveform (panel ‘a’), spectrogram (panel ‘b’), and 2DFT (panel ‘c’). Magnitude of acceleration is logarithmic (to the base 10), where dark red is the maximum ( $3.4 \times 10^{-4} \text{ m/s}^2$ ), and dark blue is the minimum ( $1/120$  of the maximum). The spectrogram and 2DFT panels have been scaled identically and cropped to remove redundant frequencies (high-pass filtered 0 to 500 Hz, and cropped at 0 to 4000 Hz).

Honey bee vibrations did not typically demonstrate specific recurring frequency components and their spectral repetitions (see Figure 3.13). Mite walking vibrations, in contrast, exhibited specific features that were more regular. Ten one-second-long 2DFT images of mite walking vibration were scrutinised both on brood-comb and also on Petri-dish (a flat, homogenous surface, in comparison to that of brood-comb). On both substrates, multiple recurring frequency components were observed in each 2DFT, within a range of 4 and 60 Hz (see Figure 3.12, Figure 3.14). On the brood-comb, these spectral repetition frequencies demonstrated more regularity (4 Hz (60%), 14 Hz (40%) and 6 Hz (30%)), whereas on Petri-dish, there was more variation (with only 7 Hz (30%) presented more commonly) (see Figure 3.12, Figure 3.14).

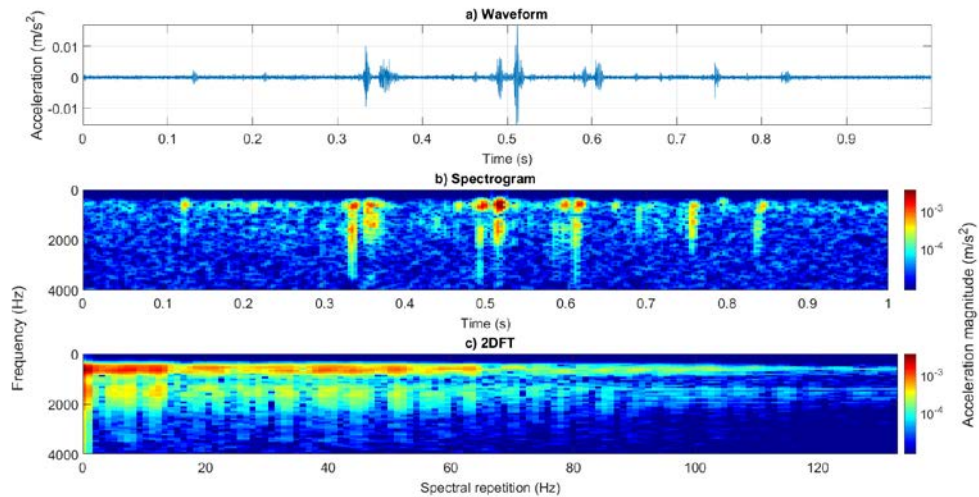


**Figure 3.13:** A typical example of one second of bee emergence vibrations in a brood cell, viewed as an accelerometer waveform (panel 'a'), spectrogram (panel 'b'), and 2DFT (panel 'c'). Magnitude of acceleration is logarithmic (to the base 10), where dark red is the maximum ( $3.6 \times 10^{-3} \text{ m/s}^2$ ), and dark blue is the minimum ( $1/500$  of the maximum). The spectrogram and 2DFT panels have been scaled identically and cropped to remove redundant frequencies (high-pass filtered 0 to 500 Hz, and cropped at 0 to 4000 Hz).

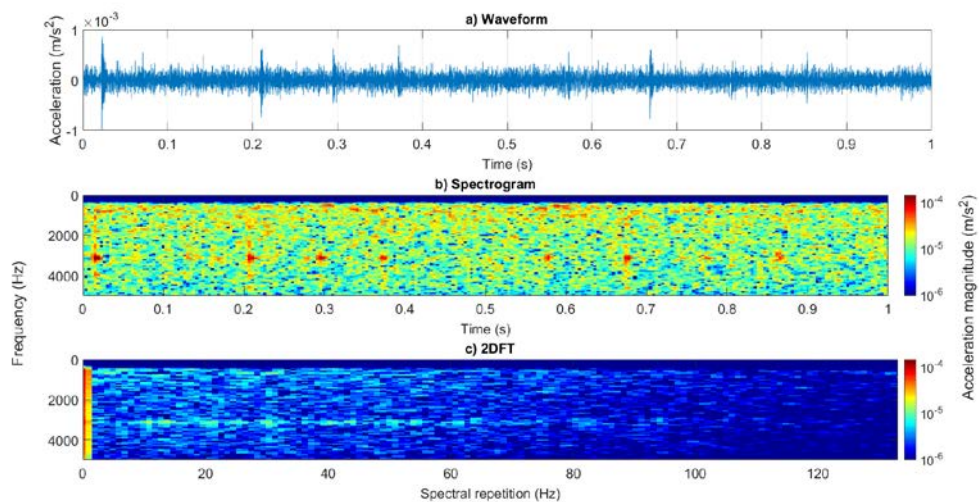


**Figure 3.14:** A typical example of one second of mite walking behaviour on Petri-dish, viewed as an accelerometer waveform (panel 'a'), spectrogram (panel 'b'), and 2DFT (panel 'c'). The data has been band-pass filtered (500 to 5000 Hz) to better showcase the vibrational pulses in the waveform panel. Magnitude of acceleration is in logarithmic (to the base 10), where dark red is the maximum ( $1.4 \times 10^{-4} \text{ m/s}^2$ ), and dark blue is the minimum (here forced to be  $1/150$  of the maximum). The spectrogram and 2DFT panels have been scaled identically for unbiased comparison.

A second method of gait quantification was also carried out, whereby the time elapsed between consecutive pulses was identified for 10 seconds of walking behaviour on brood-comb (see Appendix 2, Video D14), and 10 seconds of walking on Petri-dish (the same data that contributed to 2DFT creation). This confirmed that 0.04 to 0.08 seconds is the most common time interval between successive pulses (see Figure 3.15). There is a discrepancy observed between the results of the 2DFT and that of the time interval analysis, despite the same data being used for both, whereby the spectral repetition frequencies observed in the 2DFTs do not regularly match up with the time elapsed between consecutive pulses (only 0.07s matches the 14 Hz frequency component commonly seen in the 2DFTs). This is due to differences in the two methods employed. The 2DFT strongly emphasises periodicity in the walking rate of the mites. This feature is deteriorated in the time interval analysis, as elapsed time was calculated between consecutive vibrations, rather than two successive vibrations that were produced by each leg (it was unknown which leg produced which vibration). The 2DFT is capable of extracting and showcasing this periodicity data, whereas calculating the time between successive pulses was an additional, useful tool for determining the speed of *Varroa* leg movements.

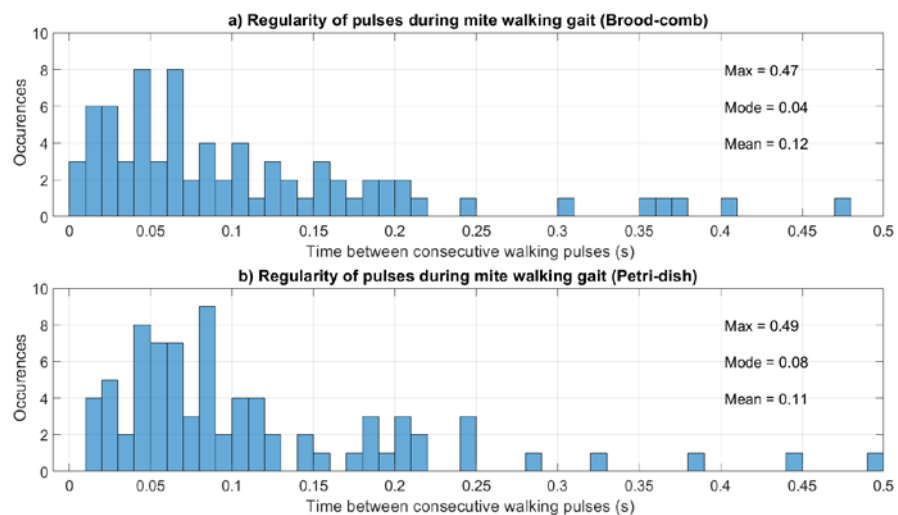


**Figure 3.15:** Two histograms demonstrating the time elapsed between consecutive walking pulses, in seconds, on both brood-comb (panel 'a') and Petri-dish (panel 'b') substrates.

Differences between honey bee and mite vibrations were also observed in frequency harmonics. Mite walking vibrations occurred within one frequency band, between 500 and 2000 Hz (see Figure 3.12 and Figure 3.16). Honey bee vibrations typically exhibited two

bandwidths, between 500 and 900 Hz, and 1250 and 2500 Hz (see Figure 3.13 and Figure 3.16). Background vibrations, as expected, lacked any clear traces (see Figure 3.16).

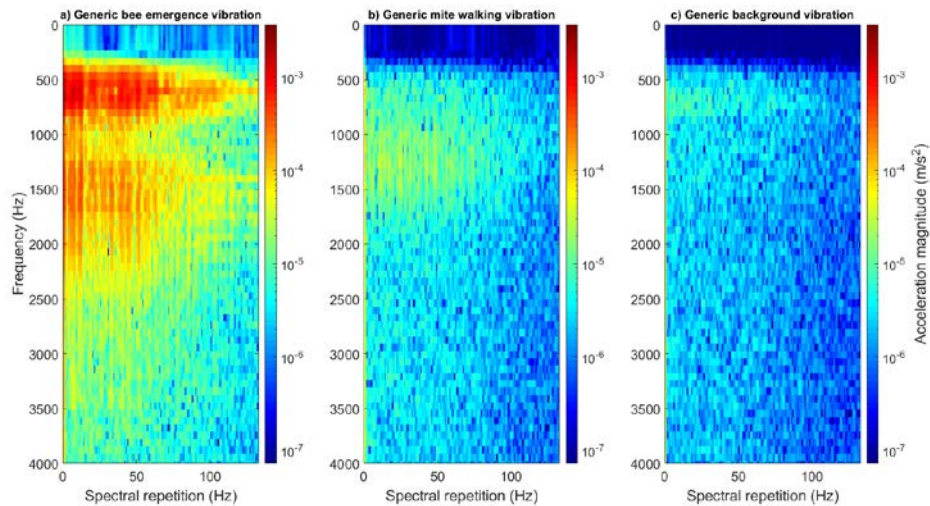


**Figure 3.16:** One-second-long extracts of bee (panel ‘a’), mite (panel ‘b’) and background (panel ‘c’) vibrations, viewed as 2DFTs, showcasing the differences between the three types of signal. All accelerometer data has been high-pass filtered (500 Hz) to reduce the impact of background vibrations on the clarity of the mite traces in particular. No traces of interest were identified beyond 3500 Hz. Magnitude of acceleration is logarithmic (to the base 10), where dark red is the maximum ( $3.6 \times 10^{-3} \text{ m/s}^2$ ), and dark blue is the minimum ( $1/50000$  of the maximum). All three panels have been scaled identically.

When viewing the full TDB, i.e., every 2DFT that contributed to the training (where each 2DFT was stretched into a single horizontal line), variation is particularly clear between the bee signals and the mite and background signals. Mite and background data are distinguishable from one another, but not as much as from the bee signals. This was expected due to the lower SNR typically seen in mite walking vibrations (see Figure 3.17).

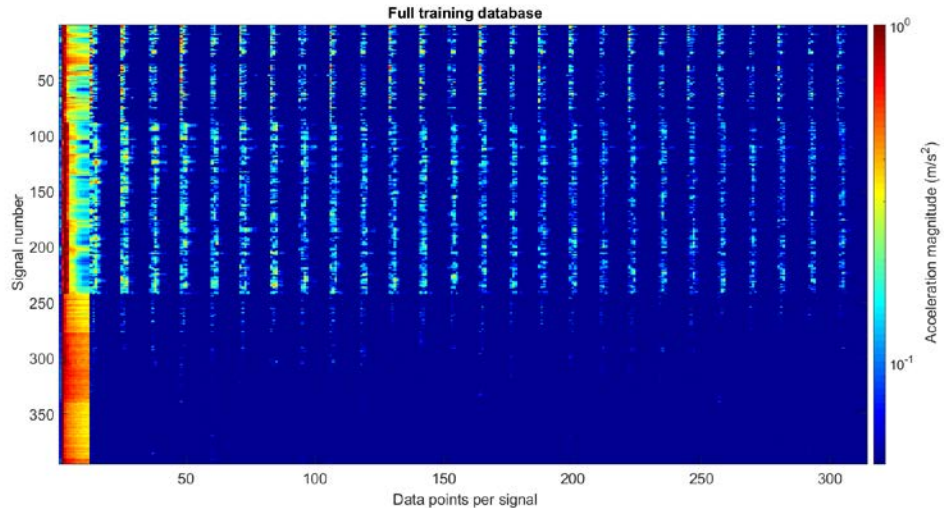


**Figure 3.17:** All data that contributed to the training database. Each 1 second extract of bee, mite and background signal can be seen here, with one signal per horizontal line of the figure. All bee data can be seen from signal number 1 until 242, mite data can be seen from 243 to 308 and background data can be seen from 309 to 395. Each signal has been interpolated and scaled identically for improved, unbiased viewing of the training data. All data has been cropped to include only the frequencies of interest. Magnitude of acceleration is logarithmic (to the base 10) with the maximum magnitude observed as dark red (forced to be  $1 \text{ m/s}^2$ ) and the minimum as dark blue, forced to be  $1/20$  of the maximum.

Following PCA and DFA, the three groups exhibited good clustering in DF space (see Figure 3.18). The mite and background clusters overlapped with one another to a degree, as expected from the low SNR of the mite's vibrations. The number of principal components chosen to be included in the analysis was six (25% of the total deviations), as this value provided optimum clustering of the groups and clarity of the discriminant 2DFT images (see Appendix 2, Figure D15 for scree plot). Both discriminant 2DFT images were necessary to include in further analysis as the clustering of the three groups occurred over both the horizontal and vertical axes (see Figure 3.18).

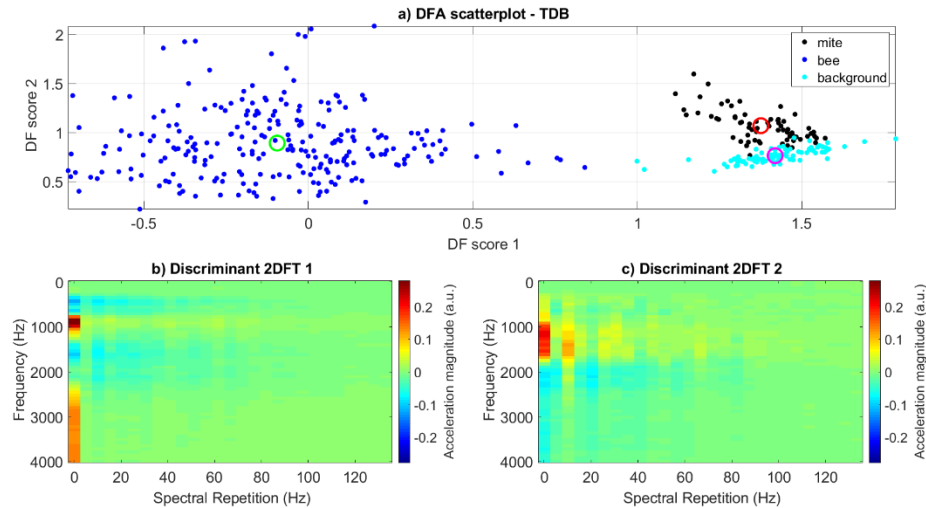


**Figure 3.18:** A figure to show the results gathered from PCA/DFA on the TDB. Panel ‘a’ exhibits the scattering of the bee (blue), mite (black), and background (cyan) data in DF space. The centroid for each data group (bee = green, mite = red, background = magenta) is shown. All three data types exhibit good clustering, with some overlap of the mite and background signals. Panel’s ‘b’ and ‘c’ show images (discriminant 2DFTs) generated from the PCA/DFA that were then used as reference images in further testing of the machine learning. Magnitude of acceleration is in arbitrary units, where dark red and dark blue indicate features of the 2DFT that have the strongest influence on the discrimination between the three groups. Green is indicative of zero, i.e., those features that did not have any influence on the discrimination. Discriminant 2DFT 1 exhibits influential features along the horizontal axis and discriminant 2DFT 2 shows those along the vertical axis. The maximum and minimum values of the plot have been forced to -0.28 to 0.28, for easier interpretation of the colour coding.

The DFA scatterplot was then altered to showcase the clustering of each group more clearly in DF space, by applying a masking technique (see Appendix 2, Figure D16). When new datapoints from long-term brood-comb recordings were projected onto this plot, the filled areas were used to provide a category to the datapoint that is being queried.

### 3.5.5. Method 4: Testing the success of the training data by using recordings that contributed to it

Each of the four recordings that contributed to the TDB were tested using the discriminant 2DFTs for cross-correlation product analysis and the scatterplot for projecting the outcome of the analysis (see Figure 3.18, see also Appendix 2, Figure D16). Not all the accelerometer data in each recording was used to form the TDB. Therefore, it was necessary to check that novel data from these recordings could be successfully classified by the software.

Projection of all data onto the cluster plot provided a successful outcome. Honey bee recordings demonstrated major clustering over the bee and background masks, and Varroa recordings exhibited strong clustering over the mite and background masks (see Figure 3.19). All four recordings showcased a negligible percentage of points that fell into the incorrect mask (see Appendix 2, Table 1). Background noise featured more prominently in the Varroa recordings as the mites were seen to walk less frequently in comparison to honey bees who produced more frequent vibrations (see Figure 3.19, see also Appendix 2, Table 1). All recordings were scrutinised via critical listening and observation of the corresponding accelerometer and video data to determine the success of the data projection.

To further evidence the success of the TDB, specific time periods of known vibration (background only, bee only, mite only) were also classified (see Appendix 2, Figure D17, see also Appendix 2, Audio D18, Audio D19, and Audio D20).

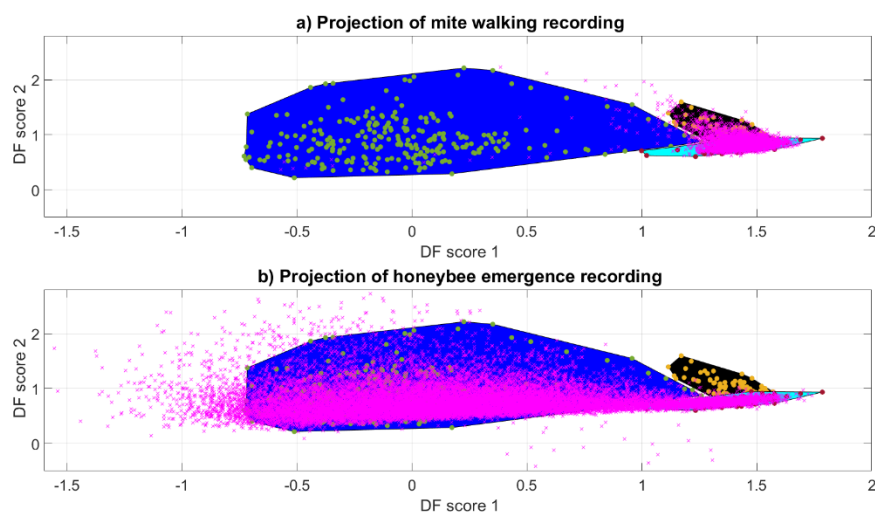


**Figure 3.19:** The classification outcome of one full recording that contained Varroa mites (panel ‘a’) and one full recording that contained honey bees (panel ‘b’) (pink crosses). The masked areas incorporate the clustered datapoints for each TDB group (bee = blue, mite = black, background = cyan). The area of each mask is determined by the peripheral datapoints of each cluster. Those that contributed to the TDB are highlighted in alternate colours (bee = green, mite = yellow, background = red). The bee cluster was extended beyond the shape achieved in the original scatterplot (see Figure 3.18). The Varroa sample contained larval stage honey bees, which do not produce any measurable vibrations of their own when naturally developing in the brood-comb (Ramsey, 2018). No Varroa mites were present in the sample that contained the honey bee. The spread of datapoints (pink crosses) strongly coincides with the known vibrations in these samples.

### 3.5.6. Method 4: Testing the success of the training data with novel recordings

The brood-comb sample recordings that did not contribute to the TDB were then tested. This dataset included eight recordings that contained Varroa mites and eight recordings that did not contain Varroa mites.

The outcome of this classification analysis was poor in terms of discrimination between the two groups (Varroa absent and Varroa present). Each recording demonstrated variation in data spread, with the majority of points clustering over the bee and background masks, and negligible overlap into the mite mask (see Figure 3.20, see also Appendix 2, Table 2).

Only one recording showcased an outcome that greatly differed from the others, whereby the main clustering of points occurred over the mite mask (see Figure 3.21). This recording did not contain mites.

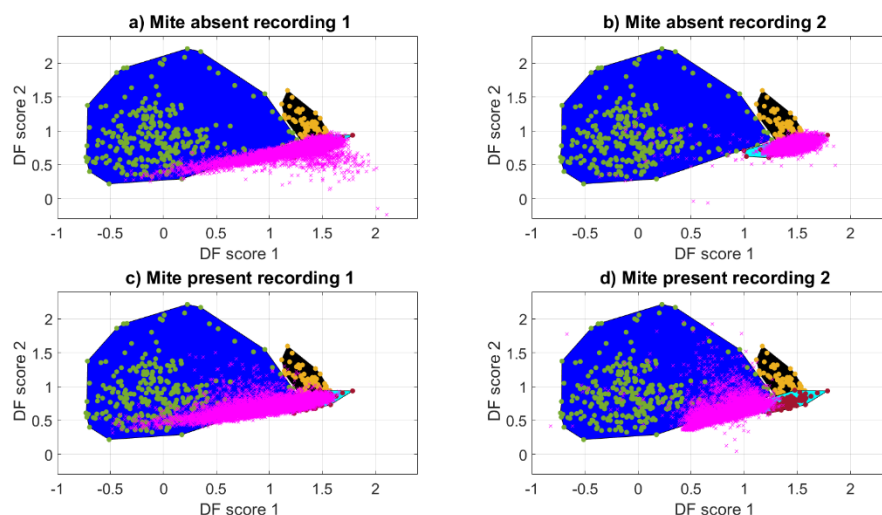


**Figure 3.20:** Classification of two recordings that contained mites (panels ‘a’ and ‘b’) and two recordings that did not contain mites (panels ‘c’ and ‘d’) (pink crosses). As with Figure 3.19, the masked areas are representative of the PCA/DFA scatterplot outcome (bee = blue, mite = black, background = cyan), and the datapoints within the masks showcase those that contributed to the TDB (bee = green, mite = yellow, background = red). These four recordings have been randomly chosen to demonstrate that both Varroa absent (panel ‘a’) and Varroa present (panel ‘c’) data were similar, i.e., discriminatory features could not be found between the two groups. All four recordings also show the variation in data spread, some of which is likely to be linked to the age of the developing bees within the samples, as larva and pupae do not produce measurable vibrations when in the natural brood-comb (Ramsey, 2018). This may explain why recordings such as that in panel ‘b’ exhibited a large amount of clustering over the background mask.

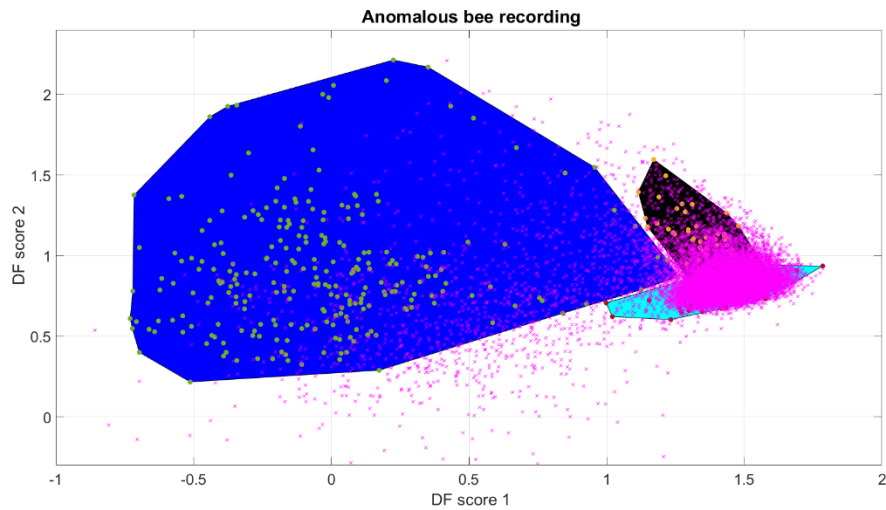


**Figure 3.21:** The classification of datapoints from the Varroa absent brood-comb sample recording where the main area of clustering occurs over the mite and background masks (pink crosses). (Masked areas: bee = blue, mite = black, background = cyan; datapoints that contributed to the TDB: bee = green, mite = yellow, background = red).

### 3.5.7. Method 4: Trialling improvements to the TDB

As a result of the poor discrimination found between the two novel groups of brood-comb recording (Varroa present and Varroa absent), the TDB and recordings were updated in an attempt to improve the discrimination outcome. Additionally, the anomalous bee recording was investigated for the same reason.

#### 3.5.7.1. Increasing the time window of the 2DFTs

Rather than using one second extracts of accelerometer data to create the TDB 2DFTs, the window was extended to 1.5 seconds. The purpose of this was to determine whether the inclusion of more vibrational data would lead to stronger discrimination between the mite walking and bee emergence vibrations.

All other analysis remained the same. PCA/DFA demonstrated that the most suitable number of principal components to include was seven.

As with the one second TDB, when projecting the classification outcome of the Varroa present and absent recordings onto DF space, discrimination between the two groups was low, with both showing negligible clustering in the mite mask (see Appendix 2, Table 3).

Additionally, a new TDB with two-second-long extracts of accelerometer recording was also trialled. This was unsuccessful as optimal clustering could not be achieved when carrying out PCA/DFA.

### 3.5.7.2. Background noise removal from the long-term recordings

The removal of the average background noise from each of the Varroa present and absent recordings was also unsuccessful.

The projected datapoints of the long-term recordings demonstrated no identifiable features that supported discrimination between the two groups.

### 3.5.7.3. Investigation into the anomalous recording

The Varroa absent recording that provided the unexpected clustering outcome was further investigated, first through critical listening and visual inspection of the accelerometer data. Varroa walking pulses occur between 500 and 3000 Hz (see chapter 2, Figure 2.23). The honey bee vibrations that occurred in the anomalous recording often fell between this frequency range (see Figure 3.22). However, upon blind, critical listening of vibrations produced by this bee compared to Varroa walking vibrations, 9/10 of the examples could be correctly identified, despite the visual similarities observed between the two (see Appendix 2, Audio D12 and Audio D21).

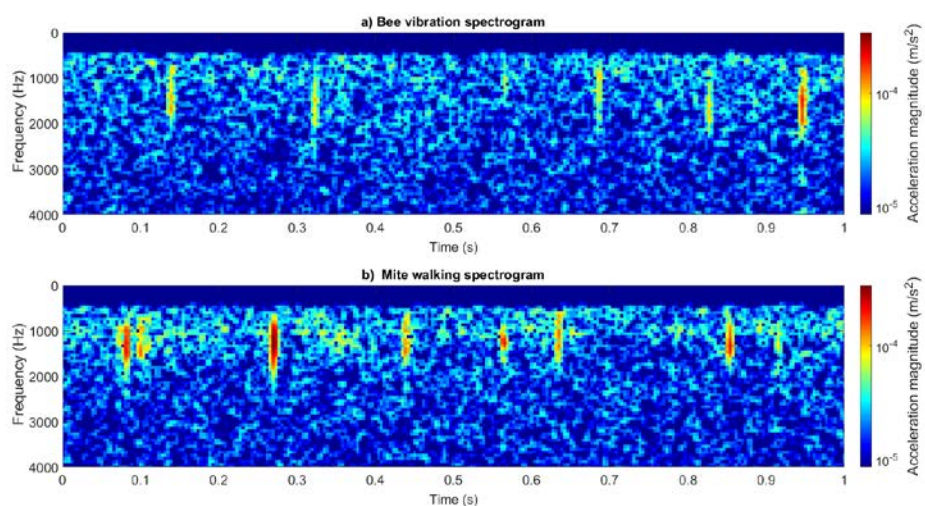


**Figure 3.22:** Accelerometer data from the anomalous bee recording (panel ‘a’) and a mite walking on brood-comb (panel ‘b’), viewed as spectrograms. Magnitude of acceleration is logarithmic, where dark red ( $3.4 \times 10^{-4} \text{ m/s}^2$ ) represents the maximum and dark blue ( $1/40$  of the maximum) the minimum. Both panels have been scaled identically.

Following this, a fourth category was added to the TDB, containing vibrations from the offending bee recording. Inclusion of 9% of all deviations in this TDB provided optimum clustering of the data and clarity of the discriminant 2DFT images, which could not be further improved (see Appendix 2, Figure D22 for scree plot).

Datapoints from all four categories (mite, bee, background, anomalous bee) clustered together strongly, but some discrimination was found between the mite, bee and anomalous bee groups, where approximately 50% of the mite vibrations clustered separately (see Figure 3.23).

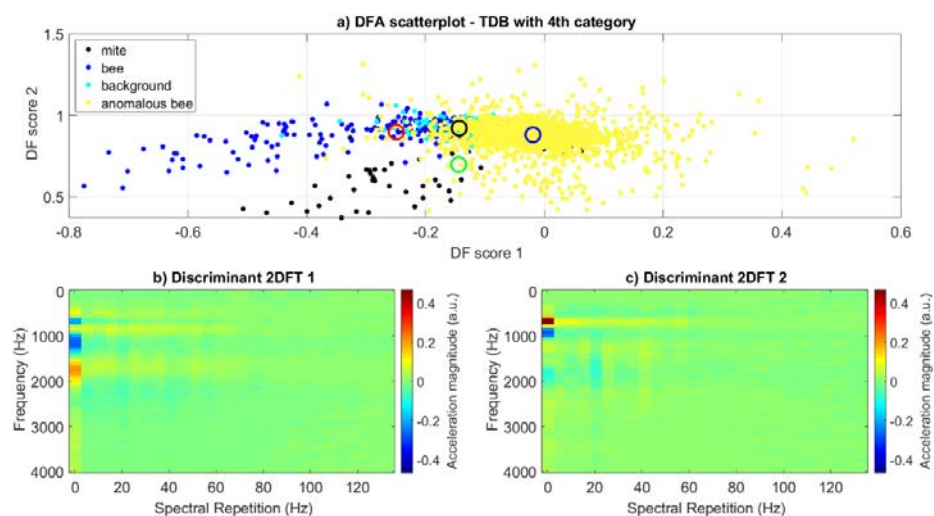


**Figure 3.23:** A figure to show the results gathered from PCA/DFA on the TDB with a fourth category. Panel ‘a’ exhibits the scattering of the four groups: mite (black), bee (blue), background (cyan), anomalous bee (yellow). The centroid for each group is plotted as a circle (mite = green, bee = red, background = black, anomalous bee = blue). Panels ‘b’ and ‘c’ show the discriminant 2DFT images that were used as reference images for cross-correlation product analysis. Magnitude of acceleration is in arbitrary units, where dark red and dark blue indicate features of the 2DFT that have the strongest influence on the discrimination between the three groups. Green is indicative of zero, i.e., those features that did not have any influence on the discrimination. Discriminant 2DFT 1 exhibits influential features along the horizontal axis and discriminant 2DFT 2 shows those along the vertical axis. The maximum and minimum values of the plot have been forced to -0.47 to 0.47, for easier interpretation of the colour coding.

When projecting all Varroa present and absent recordings onto this new scatterplot, the difference between the groups in terms of overlap into the ‘mite only’ area of the mask was

minimal (see Appendix 2, Table 4). Discrimination between the two could therefore not be achieved.

### 3.6.0. Results: Study 'b', observation of Varroa within an artificial brood cell

#### 3.6.1. Jolting vibrations

On two separate occasions, a Varroa mite individual and a honey bee larva were placed together in a capsule, in an incubator. Both attempts to rear the organisms were unsuccessful, with the larvae and mites only surviving for approximately 48 to 72 hours. It is unknown whether the larvae were affected by the presence of light in the transparent, artificial capsule, as brood-cells would be in subject to darkness in the hive, but as the larvae lack eyes, this is unlikely to have had an effect. The full life cycle was not captured, but for the two sets of specimens, approximately 19 hours of footage were recorded synchronously with the accelerometer, where the larvae and mites were alive and active.

Each video was carefully scrutinised for its full duration, following the behaviour of the mite throughout. Jolting behaviour was never seen.

Five additional videos included footage where either the mite, the larva, or both, were dead, amounting to approximately 13 hours 20 minutes. In one of these video recordings, the larva was deceased but the Varroa alive and consistently active. Two instances of jolting could be seen when the Varroa was standing on the body of the dead larva. No accelerometer trace was detected for either pulse.

In the additional video supplied by Dr. Paul Siefert, mites were regularly seen in the field of view, i.e., not hidden behind the developing bee. Defecation, and what was believed to be feeding and mating behaviour was often observed. Jolting was never seen.

#### 3.6.2. Mite walking and larval vibrations

Varroa walking behaviour was common, most often seen in short bursts of 0 – 5 seconds. The mites were observed walking on both the larva and the capsule. When on the capsule, the mite was always seen to walk (either on the larva or the capsule wall) in the space between the larva body and the capsule wall.

The vibrational traces produced by Varroa walking behaviour fell between a frequency range of 800 – 7000 Hz (see Figure 3.24). In the scenario where the larva was dead, but the mite alive, walking behaviour was seen to occur almost continuously, rather than in short bursts.

The vibrations emitted from walking in this environment were also consistently, audibly louder than those captured when the larva was alive (see Appendix 2, Video D23 and Video D24). Yet it was found that mite vibrations produced when the larva was alive can be just as strong as those when not ‘impacted’ by larval presence (live larva walking magnitude of acceleration max. =  $2.25 \times 10^{-4} \text{ m/s}^2$ , dead larva walking magnitude of acceleration max. =  $2.03 \times 10^{-4} \text{ m/s}^2$ ) (see Figure 3.24). When the mite walked between the larva and the capsule, the pulse bandwidth is between 2000 and 3000 Hz, whereas when walking on the capsule without the larva in the way, the pulses have a larger bandwidth of 2000 up to 7000 Hz in some instances (see Figure 3.24, see Appendix 2, Video D23 and Video D24).

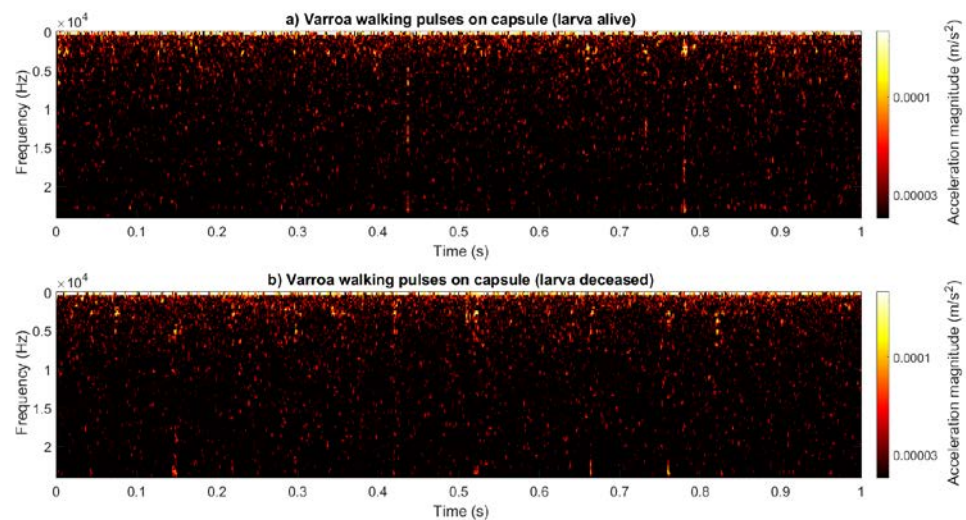


**Figure 3.24:** A spectrogram to show the walking traces of the Varroa in the capsule with the live larva in comparison to the deceased larva. Panel ‘a’ demonstrates walking pulses detected when the larva was alive. The Varroa was regularly observed walking in the space between the larva body and the capsule. Panel ‘b’ showcases walking pulses detected when the larva is deceased and occupying only one end of the capsule. The mite here was more commonly observed walking on the area of the capsule that was free of the larva. The magnitude of acceleration is logarithmic (to the base 10) where the maximum is white ( $2.3 \times 10^{-4} \text{ m/s}^2$ ), and the minimum (black) is forced to be 1/10 of the maximum. The background vibrations that are inherent to the room have been subtracted from the data for each panel.

In Figure 3.24, the spectrogram data where the larva is alive (panel ‘a’) showcases three accelerometer traces that have exceptionally large frequency bandwidths (timestamp 0.43s = 5000 – 8500 Hz, 10,000 – 15,000 Hz, 21,000 – 23,000 Hz; timestamp 0.75s = 12,000 – 14,000 Hz, timestamp 0.79s = 12,000 – 19,500 Hz, 22,000 – 24,000 Hz). It is possible that these peaks

are the result of walking behaviour, but there were difficulties in deciphering the origin of the traces as the larva also created vibrations as a consequence of it moving around within the capsule. These vibrations have been termed larval ‘clicks’ due to the nature of the sound produced, and they appear to be caused when the larva comes into contact with the capsule wall before pulling away as it continues its motions (see Appendix 2, Video D25). Although it has been demonstrated that larvae and pupae do not produce any vibrations when developing in a natural frame of brood-comb (Ramsey, 2018), this is not the case in gelatine capsules. These peaks are short, sharp and have large bandwidths, extending over most of the frequency spectrum in many cases (see Figure 3.25, see Appendix 2, Video D25). The three traces seen in Figure 3.24 are most likely caused by the larva, therefore.

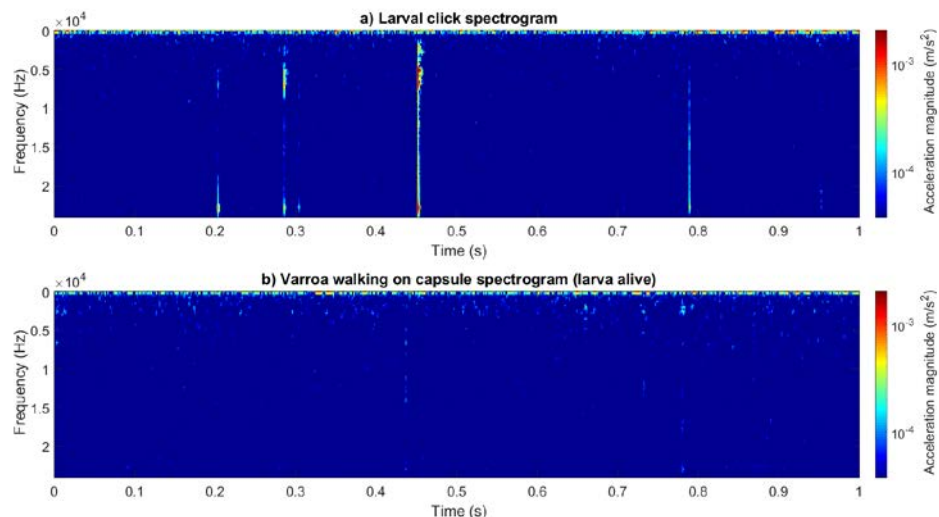


**Figure 3.25:** A spectrogram showing larval ‘click’ vibrations in comparison to the walking pulses of a mite on capsule when the larva is alive. Walking traces can be seen in panel ‘b’ as pale blue/cyan coloured traces. Magnitude of acceleration is logarithmic (to the base 10), where the maximum is dark red ( $2.1 \times 10^{-3} \text{ m/s}^2$ ) and the minimum dark blue (and forced to be  $1/70$  of the maximum). Both panels are scaled identically for ease of comparison. The background vibrations inherent to the room have been subtracted from the data.

The magnitude of acceleration of these ‘clicks’ is substantially larger than that of the Varroa walking pulses (larva maximum magnitude of acceleration =  $0.5 \times 10^{-2} \text{ m/s}^2$ , mite walking maximum magnitude of acceleration =  $0.3 \times 10^{-3} \text{ m/s}^2$ ) (see Figure 3.25 and Figure 3.26). Larval vibrations were commonly seen. In one recording where the larva was alive, but the mite dead, the average number of ‘clicks’ within a 15-minute period was 10 per 30 seconds.

A similar number of mite walking vibrations can be observed in 1 second, a timeframe 30 times shorter (see Figure 3.24 and Figure 3.25).

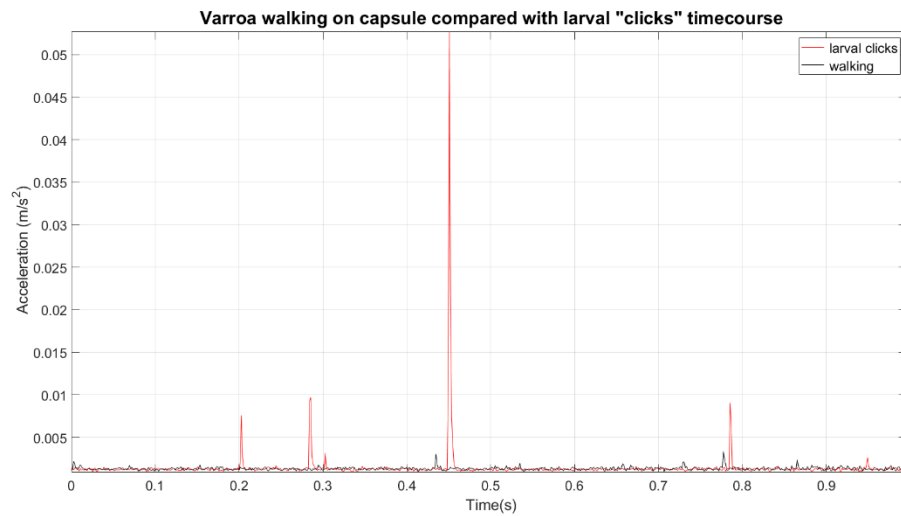


**Figure 3.26:** The time course of the larval ‘click’ vibrations (red) in comparison to the walking pulses of a mite on capsule (black). The same data that produced Figure 3.25 has been used to produce this figure. The signal seen here is the integral of the magnitude of acceleration with respect to time. The background vibration inherent to the room has been calculated and subtracted from this data.

When on the larva, mites were only observed walking for short periods, the same as when walking on the capsule. No vibrational traces were detected in any instance of walking on larva (see Figure 3.27), except for a small number of larger frequency peaks that were indicative of larval movement. To confirm that these vibrations were larvae-related, 44 accelerometer extracts (0 – 5 seconds) of mite walking on dead larvae were inspected. No accelerometer traces were observed in any of these extracts.

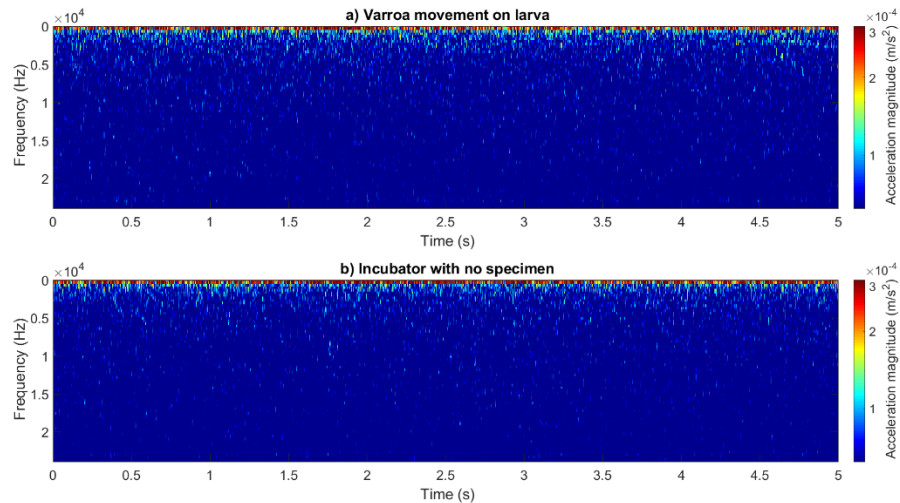


**Figure 3.27:** A spectrogram to show a typical extract of Varroa walking pulses when on the larva, in comparison to the incubator environment background noise. No traces can be seen in the data. Magnitude of acceleration is logarithmic (to the base 10), where the maximum is dark red ( $3.2 \times 10^{-4} \text{ m/s}^2$ ) and the minimum dark blue (forced to be  $1/40$  of the maximum).

### 3.6.3. Other Varroa vibrations observed in the artificial brood cells

A Varroa behaviour not yet seen during the research carried out in this thesis was observed six times. The behaviour always occurred when the mite was standing on the larva, and is a repeated, rapid up and down motion of the whole mite body (see Appendix 2, Video D26). In one instance, this movement produced a corresponding, audible vibration that was detected by the accelerometer.

The vibration is a train of pulses that are synchronous with the movement of the mite (see Appendix 2, Video D26). This pulse train lasts, in its entirety, approximately 3.9 seconds. However, the incubator fan switches on (an automatic occurrence to maintain incubator temperature) around  $2/3$  of the way through the production of this behaviour, interfering with its clarity after 2.5 seconds. The vibration can still be heard during this period (see Appendix 2, Video D26), but for the purpose of showcasing the accelerometer data, this portion of the pulse is removed, as the incubator fan vibration masks the majority of the pulse bandwidth at 1000 – 3200 Hz.

There are approximately 29 visible peaks in the train of pulses seen before the incubator fan switches on, which fall between 500 and 9200 Hz. Overall, two main frequency bandwidths are seen, at 1000 – 4000 Hz and 4400 – 7500 Hz (see Figure 3.28).

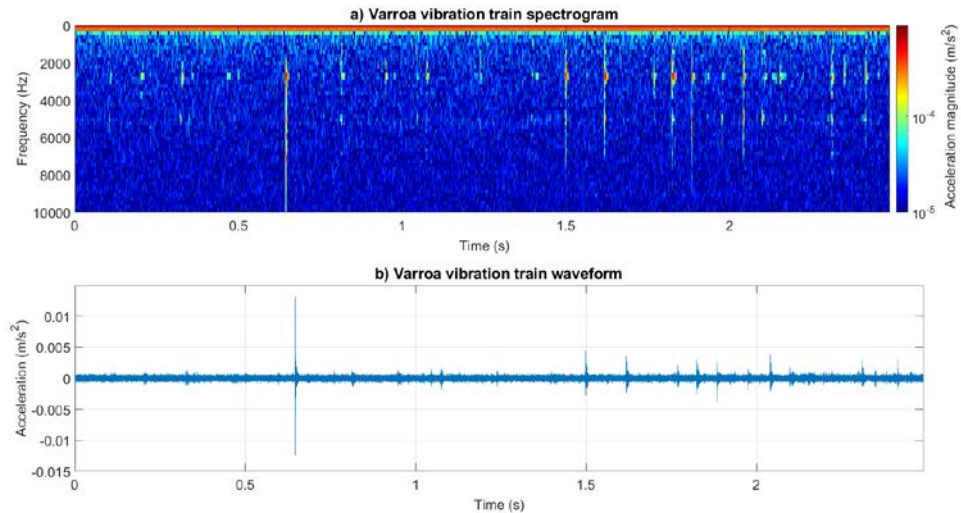


**Figure 3.28:** The Varroa multiple peak vibration showcased as both a spectrogram (panel 'a') and waveform (panel 'b'). The accelerometer trace has been high-pass filtered at 300 Hz to improve the clarity of the waveform, as background vibrations were interfering. In the spectrogram panel, magnitude of acceleration is logarithmic (to the base 10), where the highest magnitude is dark red ( $8.9 \times 10^{-4} \text{ m/s}^2$ ) and the minimum is dark blue (forced to be  $1/90$  of the maximum). At 0.65 seconds there is a spike caused by the larva ('click'), which can be heard in Video D25 and Video D26. The maximum magnitude of the Varroa vibration is  $5.2 \times 10^{-4} \text{ m/s}^2$  (panel 'b'). The regular background vibrations inherent to the room have been calculated and subtracted, resulting in an unavoidable red/orange band before the cut-off where the data has been high-pass filtered.

Of the 29 peaks, the seven that had the most visibly clear waveforms were chosen to estimate the time duration of the individual pulses (see Figure 3.28). Each pulse has an exponential growth and decay rate, which were visually fitted ( $(n = 7)$  growth rate = 0.37ms (mean), 0.28ms (s.d.),  $\lambda = 2.9\text{ms}$  (mean), 1.2ms (s.d.)). The loudest pulse of the seven selected peaks is shown in Figure 3.29.

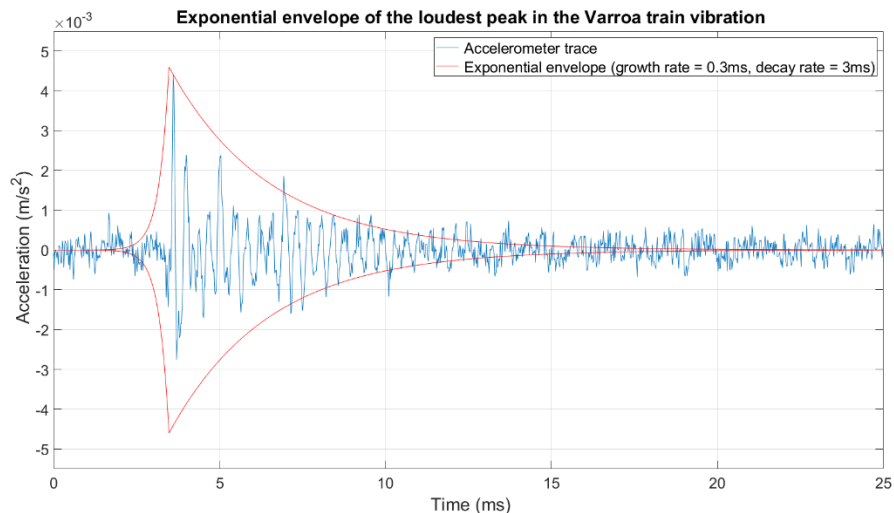


**Figure 3.29:** The growth and decay rate of the loudest Varroa pulse within the multiple peak vibration. The exponential growth and decay of the pulse is highlighted within the red envelope. The growth rate and decay constant were estimated visually (growth rate = 0.3ms, decay constant = 3ms). It is likely that the decay rate is the response of the substrate (larva body).

### 3.7.0. Discussion

This chapter set out to answer two questions: 1) can accelerometers be used to detect Varroa mite vibrations when in the brood cells? And 2) does mite jolting behaviour occur in the reproductive phase? Alongside beginning to answer these queries, this investigation has also produced some additional, exciting findings, which I will discuss first.

#### 3.7.1. The benefits to further investigating Varroa walking vibrations and using 2DFTs

In the previous chapter, individual Varroa walking pulses were discussed mostly in terms of their frequency and magnitude of acceleration. Here, the investigation into Varroa vibration characteristics has been furthered, providing additional information on the features of walking traces. The vibration that constitutes the gait of a Varroa walking is now characterised by a unique feature, as a result of its two-dimensional-Fourier transformation, which I discuss below.

In addition to the walking vibration features characterised in chapter 2, I have quantified the elapsed time between consecutive walking pulses. This, alongside the spectral repetition rate identified in the 2DFTs, has shown that walking vibrations are most commonly produced at a rate of 0.04 to 0.08 seconds. This was seen on both the flat, homogenous Petri-dish substrate and the more varied brood-comb substrate, demonstrating that Varroa are capable walkers regardless of media. This confirms other (non-quantitated) descriptions of

Varroa movement that report the behaviour to be fast and efficient (Ziegelmann et al., 2013; Sonenshine et al., 2022).

The differences observed in the spectral repetition rates of the mites walking on brood-comb and Petri-dish may be explained by the nature of the media and the speed of mite movement. The Petri-dish is a foreign substrate, and as such, Varroa may alter its gait accordingly when moving over it, as has been observed in other invertebrate species (cockroaches (Weihmann et al., 2017), caterpillars (Metallo et al., 2020), and tardigrades (Nirody et al., 2021)). Additionally, a minor flaw to the 2DFT image is that the repeating frequency components observed will alter to reflect a change in mite walking speed. This could explain why the recurring frequencies seen in Petri-dish 2DFTs were not the same as those in the brood-comb 2DFTs, i.e., mite speed was different on each substrate. However, the 2DFTs for the brood-comb showed more common repeating frequencies (4 Hz (60%), 14 Hz (40%)), and were also well clustered during the discrimination analysis, determining that mite speed was consistent on this substrate. Therefore, it is unlikely that mite velocity affected the brood-comb 2DFTs, nor therefore, the mite detection outcome. Space is restricted within the brood cells, and it is likely that speed of mite movement is more consistent in this environment.

The quantification of mite walking vibrations that I have supplied in this thesis are the first known, detailed investigation into Varroa gait. Previously, Varroa have been observed to walk using only the 2<sup>nd</sup>, 3<sup>rd</sup>, and 4<sup>th</sup> pairs of their eight legs, whilst lifting their first pair in an exploratory manner (Dillier et al., 2006; Ziegelmann et al., 2013). No further study has been carried out on the six-legged gait of Varroa beyond these observational comments. Other mite species are known to have modified forelegs that are used for a variety of purposes other than locomotion, and in the order Mesostigmata, to which Varroa belong, the function is (like Varroa) sensory in nature (Dowling, 2015). Similarly, there is lack a of research into the gait specific features of other mites, where the studies more commonly refer to speed, grasping, or jumping ability (Spagna & Peattie, 2012; Wolff, 2021).

Varroa gait may be similar to that of other mite species, or even other arachnids, some of which are also known to walk on six legs (the jumping spider *Mymarachne formicaria* mimics its ant prey by lifting its forelegs whilst walking (Shamble et al., 2017); harvestmen (Opiliones) have four different gait types and never use the 2<sup>nd</sup> pair of legs when walking, instead utilising them as environmental probes (Spagna & Peattie, 2012; Escalante et al., 2019); whip spiders (Amblypygi) and whip scorpions (Theyphonida) have antenniform forelegs that have developed a sensory function and play no role in locomotion (Santer &

Hebets, 2011; Spagna & Peattie, 2012; Schmerge et al., 2013)). However, gait variation in the arachnid class is highly varied, more so than that seen in insects (Spagna & Peattie, 2012). It is possible that *Varroa* locomotory style is entirely unique to that of other arachnids, mite or otherwise, as they have unusual anatomical features in their muscular structure, and their body plan differs substantially to other mite species (Sonenshine et al., 2022). Although I cannot comment on *Varroa* gait pattern in terms of the swing and stance phases of each leg whilst walking (a characterisation method commonly used in gait analysis (Duysens et al., 2000; Beer & Chiel, 2003; Mendes et al., 2013)), I have contributed new knowledge on *Varroa* walking behaviour in regard to its corresponding vibrational pattern, offering a novel basis for further investigation into the gait of this species.

The work carried out as part of this thesis has therefore not only supplied the discovery that *Varroa* vibrations can be detected, but it has also continued to shape knowledge of what the characteristics of those vibrations are. Individual walking pulses viewed as spectrograms provided one perspective of the vibration. In looking at a group of walking pulses as 2DFTs, I have contributed an alternate viewpoint that improves our understanding, characterisation, and detection of mites, as a combination of visualisation processes can only benefit our comprehension of a vibrational pulse (Kershenbaum et al., 2016).

Here, the 2DFT has not only offered novel representation of a mite vibration, but has also demonstrated its value as a detection tool. The use of spectrograms in the discrimination process was sub-par in comparison to that of 2DFTs, which exhibited clear feature differences between honey bee, mite, and background vibrations. Previously, in terms of animal-based sound and vibration research, 2DFT images have only been used in the characterisation of honey bee dorso-ventral-abdominal-vibrations and honey bee colony swarming vibrations (Ramsey, 2018; Ramsey et al., 2018; Ramsey et al., 2020). This work has therefore strengthened the repertoire of 2DFT use in sound/vibration feature analysis, as well as invertebrate vibro-acoustic detection, which more often rely on waveform or spectrogram images (Hopp et al., 1998; Kershenbaum et al., 2016; Banga et al., 2018; Adedeji et al., 2020). Therefore, there is an advantage to implementing alternative, lesser-used visual analyses in animal vibration research.

Although the anomalous bee recording exhibited visual similarities to *Varroa* walking pulses, the claim that a *Varroa*'s gait has a unique vibration still holds true. When critically listening to audio samples of bee and mite, 9 out of 10 could be correctly identified, strongly indicating that there are features that define one from the other. When adding the vibrations of the

bee to the TDB, this was further confirmed, as discrimination could still be found between this bee and 50% of mite walking vibrations.

### 3.7.2. Question 1: Can Varroa vibrations be detected in the brood cells?

Known honey bee, Varroa, and background vibrations were easily discriminated and classified using the training data and DFA results that were obtained when using the 2DFT images. Although the 'blind' recordings could not successfully be identified as containing mites or not, the attempts to achieve discrimination have not been fruitless. The results gathered here are now discussed in terms of potential explanations for why problems arose and how solutions can be implemented in the future.

#### 3.7.2.1. *The potentially negative impact of walking vibration strength*

It is possible that poor SNR negatively affected the discrimination process, causing difficulties in the classification of Varroa present and absent files. Mite walking vibrations typically suffered from poor SNR when compared to honey bee emergence pulses, which can be seen when viewing the TDB has a whole (see Figure 3.17). This is to be expected when considering the mass of a honey bee (115mg (Schmolz et al., 2005)) in comparison to that of a Varroa mite (0.42mg). In general, walking pulses also generate weaker magnitudes of acceleration when compared to mite jolting pulses, as outlined in chapter 2 (see Figure 2.22).

Aside from SNR, walking pulse strength is possibly further affected when the mite is within the brood cell. When observing mites in artificial gelatine capsules, mites were most often seen walking on the capsule wall or on the larva, in the space between these two, which produced vibrations that were generally of a much lower magnitude of acceleration, when compared to those of a mite walking freely (when the larva was deceased). Although mites are known to walk regularly when in the brood cell, the free space available to them for movement is restricted (Donzé & Guerin, 1994; Donzé & Guerin, 1997). It is possible that the majority of mite walking vibrations suffer attenuation under these conditions, as it appears that they are dampened by the presence of the developing bee. The mites in the brood-comb samples may also not have walked on the cell wall at all, instead remaining on the larvae/pupae, which would have likely degraded vibration propagation. Time spent on the cell wall varies dependent on the length of time that a Varroa has been in the capped cell, where individuals heavily reside on the larva following emergence from the larval food (0 to 6 hours post capping), and periods spent on the cell wall then gradually increase over time (Donze & Guerin, 1994; Donze & Guerin, 1997). As I had no visual evidence of the movements carried out by Varroa in the capped brood samples, the activity levels and the substrate that

individuals resided on were unknown, which may have contributed to the lack of detectable mite-related vibrations.

As accelerometer technology develops, it is possible that the SNR problem can be overcome, as future sensors may have the ability to capture weaker vibrations. However, for now, this work is limited to the detection range of the most sensitive model available.

#### *3.7.2.2. The advantage to detecting novel mite vibrations in the artificial cell*

When observing the mites and larvae in the artificial capsules together, walking pulses could not be detected on the larva body, but the vibration of a different behaviour was. There is potential to observing and capturing a range of Varroa behaviours in this way, should walking be more difficult to capture using accelerometers at this time.

This newly observed behaviour produced a strong vibration that comprised of a train of pulses. It is possible that this action and its corresponding vibration relate to what has previously been described as 'repetitive sampling', whereby mites produce a successive number of back-and-forth movements of the entire body, whilst remaining in place (Donzé & Guerin, 1997). This description matches that of the observed mite movement, which was also seen in the brood video supplied by Dr. Paul Seifert. It is important to further investigate and characterise this behaviour and its vibration, as well as further explore other typical mite behaviours that occur in the brood cells, as potentially useful vibrations could be discovered that benefit mite detection.

#### *3.7.2.3. The advantage of optimising the TDB*

Another benefit of this investigation is that, within the time constraints of this thesis, several optimisations of the TDB were trialled, including spectrogram use, 2DFT use, background noise removal, and increased 2DFT length. Attempts to update and improve the TDB have therefore been thorough, but not exhaustive. This repertoire of optimisation methods is now available to be built upon, so that new attempts to improve the training data and classification software can be made. The time and energy taken to investigate various TDB optimisation methods was therefore useful.

There is now scope for the TDB to be supplemented with additional data. Here, four recordings contributed to the formation of the training data, but the inclusion of more recordings and training passes would increase its chance of success, as machine learning algorithms perform better with the more information they are fed (Ayodele, 2010). A limitation to the TDB in this case was the low number of recordings that captured mites

visibly and audibly walking on brood-comb. In comparison to Petri-dish, where walking behaviour is known to occur continuously for several minutes, on brood-comb mites walk more infrequently and in shorter bursts. Data from a larger number of brood-comb recordings would better develop the machine learning algorithm.

Implementing the use of two types of features may also benefit the discrimination outcome. Facial recognition technology, for example, can benefit from the inclusion of multiple images (such as alternate poses or facial expressions for the same person), or the fusion of various features from multiple images (such as different textures or edges) (Anwarul & Dahiya, 2020; Chambino et al., 2020). In the work carried out here, the inclusion of both 2DFT and spectrogram in the training data may offer a multi-faceted view of each vibrational groups' features, advancing the discrimination.

### 3.7.3. Question 2: Does jolting occur in the reproductive phase?

Attempts to discriminate the novel jolting pulse from walking pulses was unfortunately unsuccessful. However, this does appear to be logical when considering the similarities between the two types of vibration. Both occur within the same frequency band and exhibit comparable visual features. Nonetheless, it is not improbable that the two could be differentiated with more work, particularly if focussing on the temporal differences.

The data gathered in this chapter, alongside the observations made by other researchers, upholds the current theory that jolting is mostly performed when outside of the brood cell. It is, of course, possible that jolting simply was not captured during the artificial capsule experiment, as the full, natural cycle of the Varroa was not achieved. Equally, the video supplied by Dr. Paul Siefert contained only 24 hours of brood cell activity, which may have missed jolting occurrences. It is also possible to consider that in this artificial scenario, the mites may not have experienced normal cues from the larvae or may have been behaving differently. However, the full reproductive cycle has been visibly captured several times, with detailed behavioural observation, and jolting was never mentioned (Donzé & Guerin, 1994; Donzé & Guerin, 1997; Calderón et al., 2009; Calderón et al., 2012). This not only indicates that jolting does not occur in the reproductive phase, but also that the discrimination attempted in this chapter between jolting and walking pulses is not necessarily required for mite detection in the brood cells specifically. Therefore, this work has helped to affirm that focussing on walking pulses for mite detection was a suitable choice over the continuation of jolting and walking pulse discrimination.

#### 3.7.4. An alternative future direction

An alternative experimental approach could be taken to achieve higher mite detection success in honey bee colonies. Here, I focussed on the brood cells as the most logical starting point for this investigation, as 65% of mites are theorised to reside here (Martin, 1998). However, following the challenges faced in this work, another area of the hive has been identified as potentially being even more suitable (for which I would like to thank Vincent Gallo, Ph.D., Queen Mary University, for suggesting).

Accelerometer placement on the bottom board of a hive could likely overcome several of the issues encountered in this study. Beekeepers use boards specifically for the purpose of counting mites (Barlow & Fell, 2006; Dietemann et al., 2013; Gregorc & Sampson, 2019), which makes it an ideal place to detect and quantify Varroa numbers. Mites, in my own experience, are often found on boards still alive and walking around, indicating that walking behaviour is capturable by accelerometers here. Additionally, according to our theory that jolting serves as an environmental probing tool and as jolting pulses are stronger than walking ones (see chapter 2), it could be that bottom boards provide a better chance of detecting the vibrations of this behaviour, which in turn would benefit further understanding of pulse function. Furthermore, mite vibrations on this substrate would likely exhibit higher SNR, particularly as the board is largely free from the effect of the colony's vibrations as bees are not in direct contact with the substrate.

It seems that it would be highly worthwhile to explore this alternate route and compare with that of mite detection in the brood cells, to confirm which is the more reliable method of remote mite monitoring.

#### 3.7.5. Conclusion

The capped brood cells were explored as a potential location for Varroa mite vibration capture and identification using accelerometers. Although not fully successful, this work has identified why this has perhaps been the case and offered new solutions for future improvement. The experiment utilising the bottom board appears to be the next best step for this research, not only for mite monitoring purposes, but also the continuation of jolting pulse investigations.

The results achieved in chapters 2 and 3 have laid the groundwork for future enquiries into Varroa vibrations and remote direction, as well as provided novel discoveries of importance. Chapter 4 now takes an alternate approach to vibration detection, investigating those produced as a result of honey bee symptomatic disease. As Varroa vector a variety of bee

viruses and are known to adversely affect colonies when present alongside other negative events, e.g., disease, an approach towards remote virus capture is also beneficial.

# Chapter 4: Characterisation of Chronic bee paralysis virus vibrations in honey bee individuals

## 4.1.0. Chapter overview

In the previous chapter, I investigated the direct detection of Varroa mites in samples of capped brood-comb, using vibrations originating from individual mites. In doing so, I identified novel features of Varroa gait, resulting from 2DFT analysis. This section demonstrated that it is possible to discriminate between Varroa mite walking and honey bee vibrations, but that the low signal-to-noise-ratio (SNR) of mite walking vibrations may cause difficulty in applying discrimination and detection to individuals found within the capped cells, at present. The current results also indicated that jolting behaviour may not occur in the reproductive phase of the mite life cycle, although further work is needed to fully evidence this.

There are benefits to directly detecting the presence of the Varroa themselves in honey bee colonies, but there are also advantages to their indirect detection, such as via the identification of honey bee diseases. As Varroa are capable of vectoring a large variety of honey bee viruses, remotely detecting a disease could additionally, indirectly lead to knowledge of Varroa infestation. Equally, the remote detection of Varroa, leading to the implementation of mite control methods, could reduce the chance of Varroa vectored viruses taking hold in a colony. Furthermore, the presence of multiple colony stressors (mites, viruses, pesticides etc.) can lead to exacerbated negative effects on colony strength and survival. By also focusing on disease monitoring, colonies could quickly be medicated accordingly, limiting the number of present stressors that could contribute to colony collapse.

In this chapter, I delve into the possibility of detecting honey bee vibrations that may be produced as a result of viral infection. The disease that I focus on in this study is known as Chronic bee paralysis virus (CBPV), a widely acknowledged honey bee virus. A commonly observed symptom of infection is body trembling, which I hypothesised accelerometers would be able to detect. I recorded the vibrations of bee individuals taken from these hives, to establish the validity of my hypothesis.

This chapter begins with an introduction to CBPV, where I discuss its symptoms and current forms of diagnosis. The methods are then followed by the results, which currently indicate that there are no distinct differences between the accelerometer recordings of healthy bees and trembling bees. The results of this study are discussed in terms of the methods that were implemented and how future work should include the suggestions that I make for improved chances of capturing vibrations specifically related to CBPV.

The main figures in the text are listed as Figure 4.1, Figure 4.2, and so on. The supplementary material can be found in Appendix 3, and are referenced as T1, T2 etc. There is some video data relevant to this chapter. Videos are also mentioned in the main text as T1, T2, and so on. The figure legends for the video data can be found in Appendix 3. The videos themselves have corresponding DOI links (see page 11) and are also supplied on a USB stick, labelled according to their text reference (T1, T2, etc.).

#### 4.2.0. Introduction

There are more than 20 viruses known to affect honey bees (Dittes et al., 2020a). Chronic bee paralysis virus was one of the first to be isolated and is described as an infectious disease that negatively impacts adult bees (Bailey et al., 1963; Ribière et al., 2010). In comparison to the other common viruses contracted by honey bees, CBPV is unusual as it is the only one that causes observable symptoms in the form of both behavioural and physiological changes (Ribière et al., 2010).

When the virus was first characterised, infected adult bees were described as having trembling movements, spread wings, and distended abdomens (Bailey, 1965). At the time, however, there were other researchers that had observed different signs of what they believed to be CBPV (hairlessness, a greasy appearance, dysentery, and odour) (Bailey, 1965). As a result, two syndromes have previously been referred to. Type 1 syndrome matches the original descriptions made by Bailey (1965), with the additional symptom of flight-less-ness, which causes large clusters of individuals to be found around the hive exterior. Death occurs a few days after the onset of these symptoms, with colonies often collapsing. Type 2 syndrome, otherwise known as 'hairless black syndrome', produces the alternative set of symptoms described by researchers. Hairless bees appear shiny and black, flying as normal for the first few days after symptom onset, but they then lose this ability and begin to tremble, before dying. Infected individuals may also be subject to attack from healthy nestmates (Ribière et al., 2010).

#### 4.2.1. Current methods of CBPV diagnosis and the opportunity for its remote detection

Most honey bee viruses can exist as covert infections in apparently healthy colonies (McMenamin & Genersch, 2015), and CBPV is no different (Ribi re et al., 2002; Tentcheva et al., 2004; Wu et al., 2015; Schurr et al., 2019). These studies shed light on how the virus may persist within colonies, existing as a low-level infection that is then aggravated by external stressors, causing outbreaks (Ribi re et al., 2010). Although there is not a strong link between Varroa and CBPV in terms of the mite being a viral vector (Bailey & Ball, 1991; Tentcheva et al., 2004; Chantawannakul et al., 2006; Carreck et al., 2010; Guzman-Novoa et al., 2012), Varroa could instead be an additional stressor that negatively interacts with the virus. It is known that the mite has an effect on bee immune response and exacerbates adverse colony reactions when interacting with other stressors (Le Conte et al. 2010). This highlights the importance not only of detecting Varroa mites in colonies, but also diseases, which can be directly or indirectly affected by their presence.

CBPV has characteristic, observable symptoms, which therefore provides a fairly straightforward diagnosis when the infection has taken a hold in a colony. However, as it often manifests in colonies at low levels, as well as bees appearing healthy before the onset of visible symptoms, other detection methods can offer an earlier diagnosis. One of the first tests used for CBPV detection is Agarose Gel Immunodiffusion (AGID), a quick and simple technique that can detect CBPV antigen presence (Ribi re et al., 2010). However, this is not efficient enough to detect the virus when expressed as a latent infection, unless paired with a Reverse Transcription Polymerase Chain Reaction (RT-PCR) technique. The RT-PCR confirms the presence of a covert infection, whilst the AGID test identifies the etiological agent of symptomatic colonies (Ribi re et al., 2002). Detection of CBPV in colonies focuses on the use of various RT-PCR analyses to this day (Morimoto et al., 2012; Modirrousta & Moharrami, 2015; Kim et al., 2019; Dittes et al. 2020b). An instrument used by Kim et al. (2019) to carry out PCR provides fast results and can be used in the field, which could be beneficial for quick assessment of colony health-status.

However, PCR analysis is complex and unlikely to be commercialised for beekeeper use in the field in the near future. Precision Beekeeping is now on the rise (see section 1.3.4), and remote systems to detect and alert beekeepers to the onset of symptoms may offer an alternate, more user-friendly approach to PCR. Regular monitoring and recording of colony status is important not just for when a hive is undergoing viral diagnosis, but all year round as a prevention technique (Dittes et al., 2020a). Although PCR can detect CBPV before

observable symptoms appear, this would require beekeepers to have regular inspections and tests to check if their colonies are free of the virus or not. If they could instead be alerted to symptom onset as soon as it occurs, their colonies would have a good prognosis if a management plan was then immediately put into place to save them (Dittes et al., 2020b).

As CBPV causes bees to tremble, I hypothesise that accelerometers are likely to detect the vibrations that are produced because of this behaviour. In this chapter, I investigate honey bee trembling at an apiary that was deemed to be moderately infected with CBPV, with the intention of characterising any vibrational features specific to the behaviour. Observable symptoms have previously been described, but a detailed study into the specific features of trembling and its potential vibratory trace has not yet been carried out. This work aims not only to provide a more in-depth characterisation of this symptom of CBPV, but also add to our list of known honey bee vibrations, offering the potential for remote detection of the symptoms of this virus in a fully populated hive.

#### 4.2.2. Aims of the chapter

The aims of this chapter are as follows:

- Describe the features of CBPV trembling behaviour.
- Identify whether there is a corresponding accelerometer trace for this behaviour.
- Observe if there are vibrational features specific to infected bees that can distinguish them from healthy bees.
- Characterise the features of the trembling vibrational trace.
- Collect visual and vibrational data from an entire colony of CBPV infected bees, to establish whether it is possible to detect trembling vibrations in a fully populated hive.

### 4.3.0. Methods

#### 4.3.1. The hive set-up

Experimental work was carried out at Warwick University Wellesbourne campus between July and October 2019. A honey bee hive with an observation platform (of the same design as described in section 1.4.2., see Figure 1.9) was housed in a shed with mains power supply. Honey bee outdoor access was provided via a tube leading from the hive to the shed exterior. Three standard (non-observation) hives were situated adjacent to the shed (see Figure 4.1). A regional bee inspector deemed the colony in the observation hive and one of the exterior colonies to be moderately infected with CBPV (naturally) on the 18/07/2019.



**Figure 4.1:** The shed that houses the observation hive with yellow landing board and tube that connects the hive to outdoors (circled, blue). The three standard hives can be seen adjacent. The red arrows indicate the colonies that became infected with CBPV – black, visibly trembling and visibly healthy bees were collected from these colonies for observation.

Four ultra-sensitive accelerometers (4507 B 002, Brüel & Kjær, 1000 mV/g) were embedded in the comb of the central frame of the observation hive using a small amount of molten wax to fix them in place. Two were placed at central, approximately equidistant positions, and another two placed on the lower half of the frame, to capture most of the most honey bee vibrational activity (see Figure 4.2). This choice was justified by honey bee distribution in the hive. Bees congregate in specific areas based upon their age and task. Most groups occupy large areas of the frame, whereas foragers limit themselves to the hive proximity (Baracchi & Cini, 2014). Bees performing the waggle dance are known to prefer the comb edges, alongside the central frames of the hive and the lower portions of frames (Tautz & Lindauer, 1997; Kimura et al., 2011; Ortis et al., 2019; Bozek et al., 2021). Placing two accelerometers on the lower half of the comb therefore increased the chance of capturing a larger variety of honey bee activity.

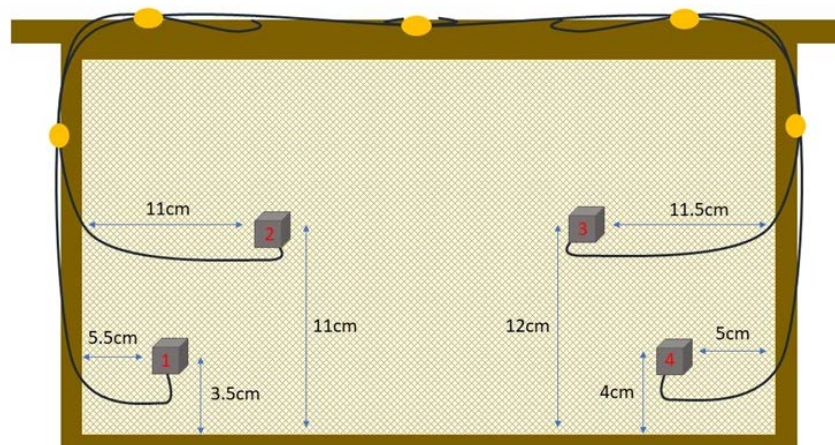


**Figure 4.2:** The layout of the central frame of the observation hive. The four accelerometers (grey cubes) were embedded in the foundation comb (chequered area) in the orientation seen above. Each of the four accelerometers were numbered 1-4 for the purpose of the full frame analysis. The distance from the edge of the frame (brown areas) to the centre of the accelerometer is shown. The accelerometer wires (dark blue lines) were secured to the frame with drawing pins (yellow circles) to reduce their interference to both the honey bee colony and the video observations. Diagram produced by Harriet Hall.

The accelerometer wires lead to four single channel conditioners (Endevco, 4416B, USA) one for each accelerometer. The conditioners were set at a gain of x1. Each conditioner fed to a soundcard (Alessis io4) that enabled the accelerometer recordings to be saved by the PC. The PC saved the accelerometer data continuously in one-hour-long folders onto a 6TB hard drive (see Figure 4.3).

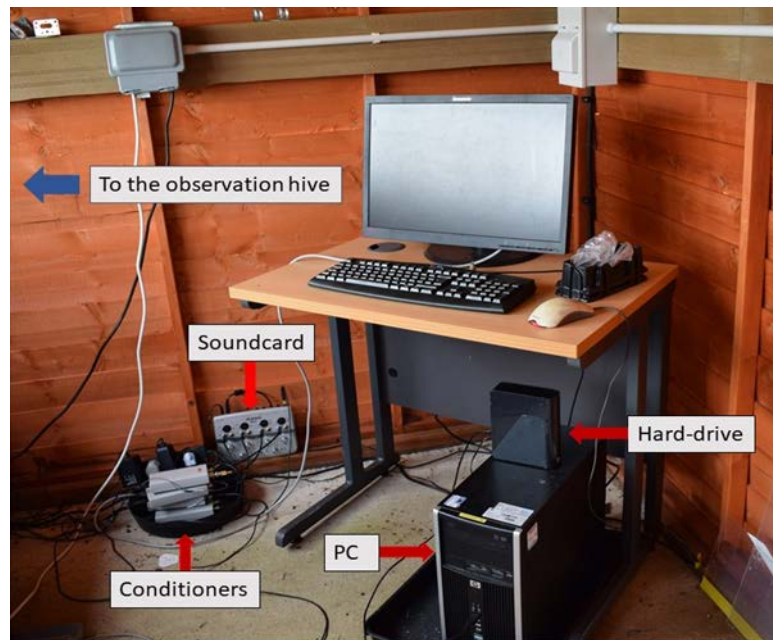


**Figure 4.3:** The hard-ware set-up inside the shed. The observation hive is out of view, the blue arrow indicates where it is outside of this image.

#### 4.3.2. Video/vibrational data collection from the CBPV infected observation colony

The frame of the observation hive was lifted twice a day, for one or two days a week over the data collection period (July to October 2019). Twenty minutes of footage was collected per filming session using a dual camera set-up (one positioned on each side of the Perspex box of the observation hive, on tripods) so that both sides of the frame could be simultaneously observed. To record the vibrations of the hive synchronously with the video data, the two cameras (Sony 4k, FDR-AX100E handy cam, China; Nikon D3300, Japan) were plugged into the soundcard (see Figure 4.3) via the microphone input using a jack-to-mini-jack cable. The cable was split, enabling both cameras to record vibrational data simultaneously. Filming was carried out at 50 frames-per-second (FPS) in 1080 x 1920p resolution.

The video data collected amounted to a total of 28 videos. To identify the presence of trembling behaviour, instantaneous scan sampling was carried out. This method of sampling was chosen as it allows the activity of many individuals to be easily noted at pre-selected timings (Altmann, 1974). As a single honey bee frame contains many hundreds of individuals, this method of sampling allowed each bee to be focused on with ease. A rectangular area of 300 x 400 pixels was cropped around accelerometer 1 (see Figure 4.4). This reduced the number of bees that required sampling, providing a 'snapshot' of the population, whilst also focusing on the areas where vibrational activity would most likely be detected (near to the

accelerometers). The video was played, allowing the observation of only this cropped area. Every two minutes, the behaviour of each bee was noted as either ‘trembling’ or ‘not trembling’. As bees can turn black and hairless, but not tremble, the morphology of each bee was also noted. Every bee was observed for five seconds before moving the video back to the start of the sampling interval time to watch the next bee. It was determined that five seconds was adequate to establish if bees were trembling. Once the video had ended, an area of the same size was cropped around the next accelerometer (see Figure 4.2), and the process repeated for each of the four accelerometers.

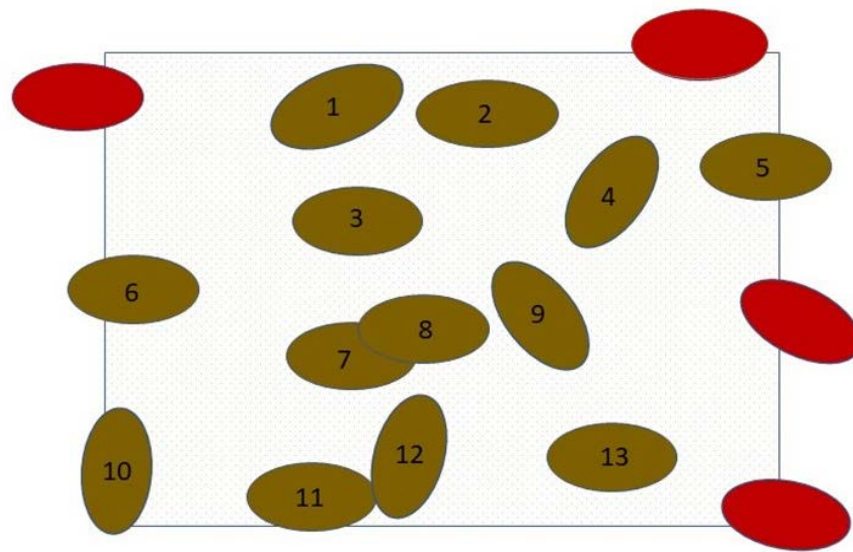


**Figure 4.4:** An image to demonstrate the pattern of instantaneous sampling. Each bee is represented by either a brown or red oval. The rectangle indicates the cropped area that was sampled. Bees were only sampled if more than half of their body was in view (brown ovals). Bees that didn't fit this description (red) were omitted from sampling. To ensure that every visible bee was sampled (and sampled only once), they were observed in a numbered sequence (e.g., as seen here), from a left to right and top to bottom direction by visually splitting the sampling area into smaller sections. Diagram produced by Harriet Hall.

#### 4.3.3. Visual/vibrational data collection from individually observed bees

Individual bees were collected from the landing board of the observation hive (see Figure 4.5) and from that of the other infected hive. Trembling bees were often seen on the grass just below the landing board and were also collected from here. A mixture of visibly healthy, black/hairless and visibly trembling bees were collected.



**Figure 4.5:** Image of the landing board that led to the observation hive within the shed.

The method of recording visual and vibrational data for each bee individual was the same as that implemented for Varroa observations in chapter 2. The only difference in the set-up was that it was here placed on the concrete floor of the shed that housed the observation hive, with cotton wool to reduce interference from background vibrations, rather than in a sound isolated room, as there was not one available at the University of Warwick Wellesbourne campus (see Figure 4.6). The vibrations that are produced by honey bees are stronger than those produced by Varroa, and as such, the concrete floor and cotton wool provided suitable dampening against background noise. The camera filmed at 50 FPS at a 1080 x 1920p resolution. Each bee was filmed for approximately five minutes.



**Figure 4.6:** The set-up for the individual bee recordings.

#### 4.3.4. Defining trembling behaviour

The morphology of each bee under observation (whether in the Petri-dish or from the full frame) was noted in terms of three categories: (i) normal, described as a healthy adult bee with hair on the abdomen and thorax; (ii) intermediate, where hair loss has started either on the abdomen, thorax, or both; (iii) black, where the bee is almost or completely hairless, described as greasy/shiny and black in the literature (Ribi re et al., 2010) (see Figure 4.7).

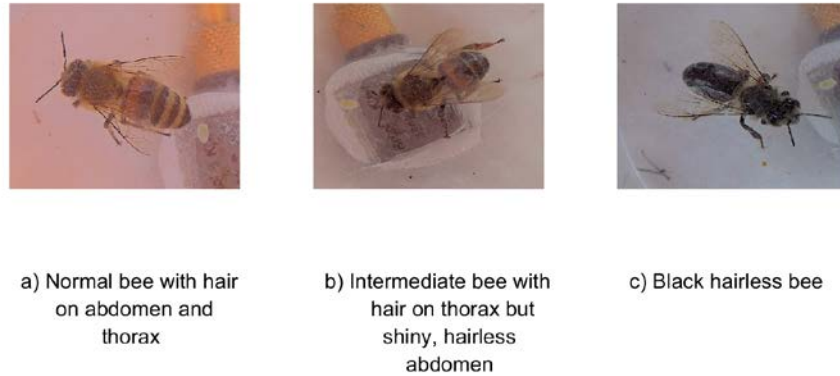


**Figure 4.7:** Representative examples of each of the bee morphologies observed. Normal bees (a) have a thick hair covering over the thorax and hair (pale orange stripes) on each of the abdominal tergites. Intermediate bees (b) lack some hair on the thorax, giving a patchy appearance. The hair on the abdomen is shorter or non-existent. In black bees (c), the hair is almost completely lost on the thorax and abdomen, giving the bee a black, shiny appearance.

In order to come up with a meaningful definition of trembling behaviour, each video was observed numerous times to build up a refined set of criteria regarding what the symptom involved. From this, a list of questions was created. Each video was then examined again to answer these questions:

1. What morphological category does the bee fit in (see Figure 4.7)
2. Is the bee always mobile, i.e., no periods of stationary trembling behaviour?
3. Does the bee tremble when walking or carrying out other activities e.g., grooming?
4. Does the bee produce behaviours that appear to be out of the bees' control?
5. Is the proboscis extended and does the bee appear unable to retract it?
6. Does the bee stumble and fall over?

This list of questions allowed specific behaviours to be identified and determine whether these behaviours were common or uncommon. A general description of the symptom could then be established. I define question four as behaviours that a bee would perhaps not normally produce, that looked as though they occurred in a way that was out of the bees' control (such as when humans are ill and cannot control when they cough, for example).

#### 4.3.5. Signal analysis: Investigation into the vibrational features of trembling behaviour

As trembling is a repeated behaviour, the 2DFT (see section 1.4.5.2.) was again chosen as a suitable tool to visualise the characteristics of the accelerometer waveform.

The exercise that was carried out to define trembling behaviour (see section 4.3.4.) also enabled a definition of severe vs. mild trembling movements to be described (see Appendix 3, Video T1). Using this information, specific bee individuals were chosen (those that trembled severely and those that did not tremble at all) for an initial 2DFT comparison. The purpose of this was to first identify any major vibrational features of trembling that are not seen in visibly healthy individuals.

Accelerometer data from the individual bee recordings was transformed into 2DFT format. Two types of analysis were implemented: (i) 2DFT images created from specific time windows of accelerometer data, (ii) videos of each bee, with the 2DFT updating with time, running synchronously with the video. The use of 2DFT images was required for clear identification of vibrational features observed in trembling and non-trembling individuals. The 2DFT videos allowed me to observe changes in vibrational features as they happened synchronously with bee movements, and were beneficial for linking behaviour to vibration in real time. The two types of analysis together helped to build a more detailed picture of trembling and non-trembling characteristics.

#### *4.3.5.1. 2DFT images*

Only stationary bees were chosen for the 2DFT image analysis, to prevent interference from other vibrations that might occur due to walking/grooming etc. Each 2DFT was created from time windows of stationary bee accelerometer data that were 0.5 to 1-second-long (suitable for capturing visually repetitive trembling motions of the body).

As trembling behaviour is visible to the human eye, it was expected that the repetition frequency of the trembling vibration would also fall within human visual range. Human vision is limited to around 50 Hz repetition frequency, therefore 2DFT parameters were chosen to mimic this (temporal resolution of 0.02s, multiplication factor of 2), providing a spectral repetition axis (x axis) with a maximum at 50 Hz.

The accelerometer data for each video was computed to produce a 2DFT over one second of data at a time. This updated with time, producing a scrolling window of eight seconds for comfortable viewing of the data (a shorter time window would scroll more quickly and cause increased difficulty in identifying vibrational features of interest). This way, the vibrational activity of each bee could be visualised alongside its corresponding video, synchronously. Each video could then be scrutinised for changes in the features of the vibrational traces seen as they happened, in time with the corresponding bee movements to identify features of interest.

#### 4.3.5.3. Reshaping the 2DFT for further feature extraction

Following on from the image and video investigation, particular features of the 2DFTs were identified as requiring further, more detailed exploration.

The first 4 horizontal pixel lines of the 2DFT were established as a bandwidth where frequency peaks of interest occurred (0 – 175 Hz) (see Figure 4.8), particularly the first two lines between 0 and 100 Hz on the y axis.

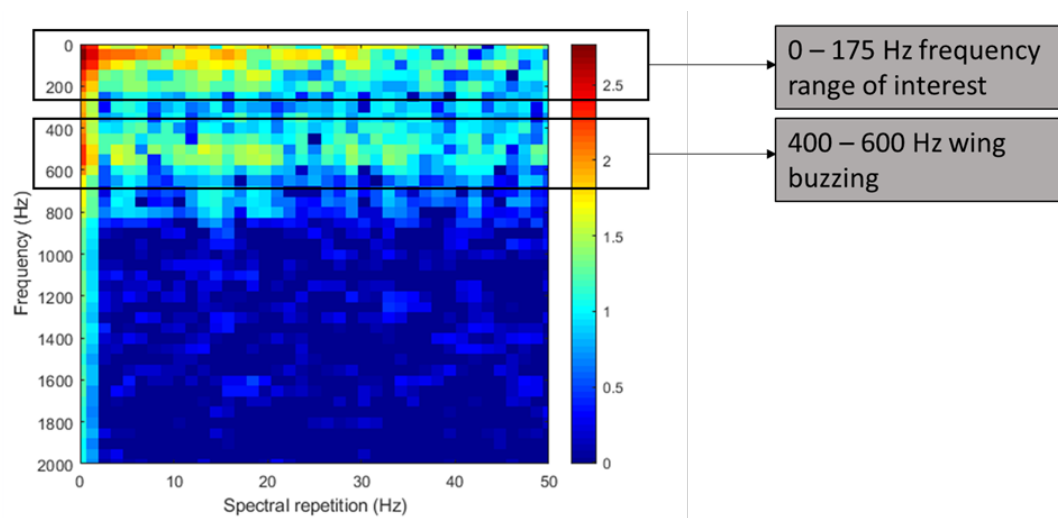


**Figure 4.8:** The 2DFT of a bee individual, demonstrating the frequency bandwidths of interest. Here, the 0 to 175 Hz frequency band was identified as an area worthy of further investigation regarding potential trembling behaviour vibrational features (the first four horizontal lines). The 400 to 600 Hz area demonstrates where bee wing buzzing occurs, regardless of the symptomatic status of the bee, and was therefore dismissed from any further analysis. Diagram produced by Harriet Hall.

All bee individuals that had stationary periods ( $n = 54$ ) were then included in this next stage of analysis. The video data for each bee was analysed in the same way as section 4.3.5.2., where the accelerometer data was transformed into a 2DFT that ran synchronously with the visual data. This time, however, the 2DFT data was coarsened four times (see Figure 4.9). This is an analysis technique that is used to reduce the amount of data present (here the number of pixels present in the 2DFT image), without losing any important information found in the data. By reducing the temporal resolution (0.005s) but maintaining the original multiplication factor (2) in the 2DFT image, the first four horizontal lines of pixels, i.e., the frequency band of interest, were combined into one line that contained the data of importance. This allowed simple data extraction of the bandwidth of interest. This line of data was then selected and saved for every frame of the video (50 FPS). Each line was then

stacked one by one, from left-to-right, and in video frame order to create a scrolling figure of the data (see Figure 4.9).

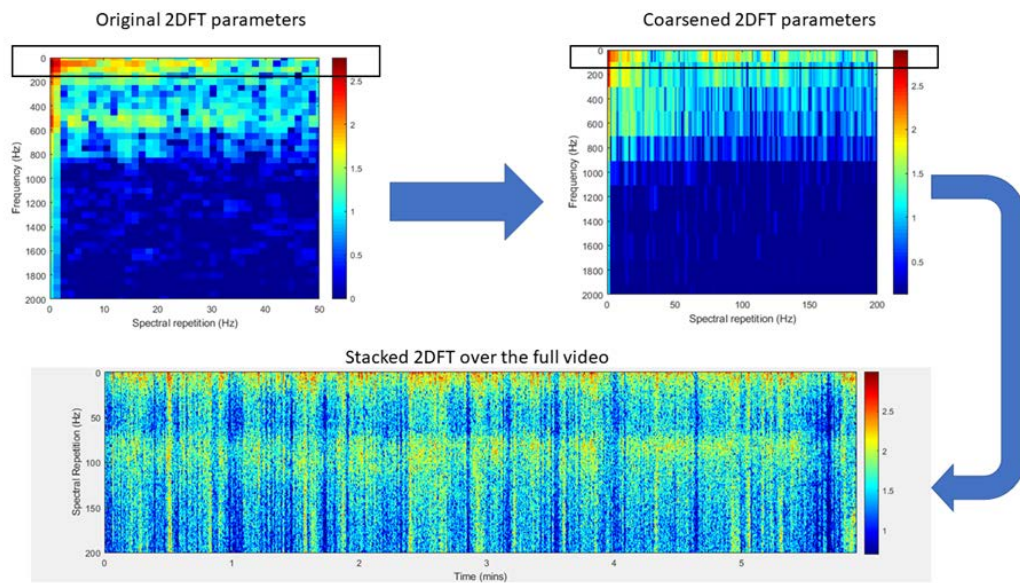


**Figure 4.9:** A diagram to demonstrate the transformation of the individual bee 2DFT into the stacked 2DFT. The top two panels show a 2DFT that encapsulates 0.8 seconds of consistent trembling behaviour as an example. The first panel shows the 2DFT with the originally chosen temporal resolution (0.02s) and multiplication factor (2), with the first 4 horizontal pixel lines of interest highlighted within the black box. This 2DFT is then coarsened (temporal resolution reduced by four times, from 0.02s to 0.005s), and this inherently makes the four lines of interest into one, highlighted again by a black rectangular box. The full range of the spectral repetition axis of the 2DFT is now 200 Hz (a four times larger value) due to the updated temporal resolution, which is four times smaller, and provides four times more spectra. This is a trade-off created by the calculation,  $range = 0.5 * \left( \frac{multiplication\ factor}{temporal\ resolution} \right)$ , that dictates the range of the spectral repetition axis. This single line, which now contains the accelerometer data for the original four lines, is then selected and displayed for every frame of the video (50 FPS). The bottom plot demonstrates the outcome of the stacking of the three lines, where each of the individual lines have been built together from the beginning to the end of the bee video. This provides an overall picture of the evolution of the relevant accelerometer data at each video frame for the area of interest only. The spectral repetition axis has now been made to be the y axis, and time (mins) becomes the x axis. The magnitude of acceleration in all three panels can be seen as the third dimension (pixel colour), where dark red is the maximum and dark blue is the minimum. The colour coding values are not relevant here as the purpose of this figure is visual demonstration of the analysis only. Diagram produced by Harriet Hall.

Each of these reshaped figures (referred to as 'stacked 2DFTs' in the text) were inspected for periods when each bee was stationary only (the same as in previous analyses), to attempt to identify features specific to mild trembling, strong trembling, and non-trembling bees.

#### *4.3.5.4. Stacked 2DFT background subtraction for improved visualisation*

A recording of the background noise alone, i.e., the Petri-dish and accelerometer without any contents, was taken under the same conditions as the honey bee recordings, in the shed. This was carried out with the same hardware and method as for the individual honey bees. The purpose of this was to provide accelerometer data for the surrounding environment, so that it could later be removed from the honey bee recordings. This was useful for three reasons: (i) after subtraction of the background noise, the vibrational traces seen should only be those caused by the honey bee itself, (ii) the clarity and definition of the honey bee related vibrations will be improved, providing a more reliable visualisation of their features, (iii) the set-up of the hardware was not placed in a sound isolated room as the University of Warwick could not provide this, therefore background removal will promote clarity of the honey bee vibrations.

Although it was not possible to control the background noise to the same degree as for the *Varroa* recordings in chapter 2 (due to the lack of sound isolated room at the University of Warwick), it is worth noting that the general ambient noise was quiet, interspersed with very occasional farm vehicle noise. As honey bees are a larger species than *Varroa* and produce louder vibrations and sounds, the necessity for a sound isolated room was reduced.

The background noise recording was analysed in the same way as the bees, to produce a stacked 2DFT.

Three methods of background removal were trialled, and one was deemed most suitable for viewing the stacked 2DFTs at their best (see Appendix 3, Figure T2, Figure T3 and Figure T4). The following paragraphs describe the chosen method.

The entire data set of stacked 2DFTs of the background noise was averaged over the horizontal dimension (time, 4 minutes 9 seconds) and subtracted from a honey bee recording. The background noise, however, had some areas of higher magnitude of acceleration than the honey bee recording, likely the result of increased vibration in the Petri-dish, which may be inherent to this substrate when there is not an object/bee in contact with it, or due to prolonged external noise, caused by a nearby farm vehicle.

In order to avoid showcasing meaningless measurements, when subtracting one from the other, any negative values seen in the honey bee recording were forced to be positive and further shown on a logarithmic scale (see Figure 4.10).

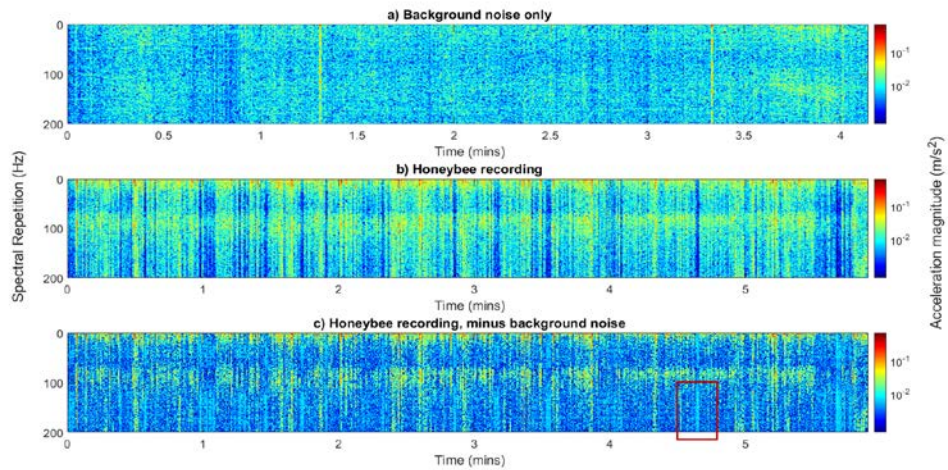


**Figure 4.10:** The subtraction of background noise from a honey bee recording. Here, the recording of the background vibrations inherent to the environment (panel ‘a’) is averaged and subtracted from a recording of a honey bee individual (panel ‘b’). The honey bee recording with subtracted background noise (panel ‘c’) exhibits an artefact, whereby the lowest magnitude areas of panel ‘b’ are now higher in magnitude on panel ‘c’, rather than lower, which is what would be expected. An example of the artefact (areas of light blue that should show as dark blue) is highlighted in panel ‘c’ in red. The features of the honey bee vibrations are much clearer following the subtraction. The magnitude of acceleration is logarithmic (to the base 10), where dark red is the maximum ( $6.8 \times 10^{-1} \text{ m/s}^2$ ) and dark blue is the minimum ( $1/1000$  of the maximum). All panels are scaled identically.

To overcome the artefact, the vertical elements (each vertical pixel line over the time axis) of the background noise were then sorted by magnitude of acceleration, so that the strongest were grouped together, in descending order (see Figure 4.11). Only an area that exhibited particularly low background signal was then selected for averaging and subtracting (330 vertical elements) (see Figure 4.11). The artefact present in the final honey bee recording for Figure 4.10 can still be seen in Figure 4.11, but is much improved as the areas that were previously higher in magnitude following background subtraction are now of a lower acceleration ( $\text{m/s}^2$ ). This result could not be enhanced any further by reducing the number of averaged vertical elements selected for averaging.

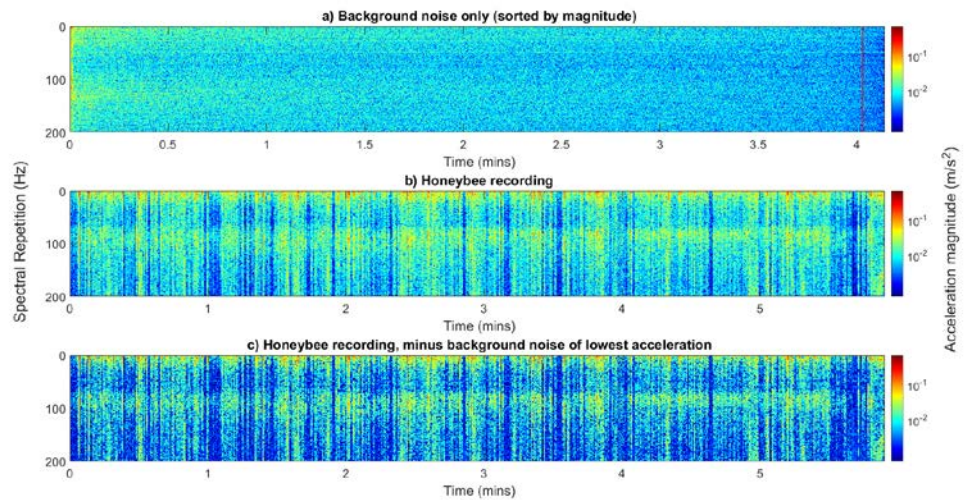


**Figure 4.11:** The subtraction of a section of background noise from a honey bee recording. The background recording has here been sorted by magnitude so that the highest magnitude spectra are found to the left of the figure (panel 'a'). A red line indicates the area to its right that was selected for averaging and subtracting (panel 'a'). The honey bee recording is seen in panel 'b', and the same recording with the subtraction of the background selection is seen in panel 'c'. The artefact seen in figure 4.10 (the light blue areas in panel 'c') is now less noticeable (the light blue is now a darker blue, closer to what would be expected). The magnitude of acceleration is logarithmic (to the base 10), where dark red is the maximum ( $6.8 \times 10^{-1} \text{ m/s}^2$ ) and dark blue is the minimum ( $1/1000$  of the maximum). All panels are scaled identically.

In hindsight, instead of undertaking a single, four-minute-long background recording on the first day of these experiments, it would have been preferable to collect 30 seconds of background noise before placing each individual honey bee on the Petri-dish. This way, environmental vibration present at that same moment in time could be subtracted from the related honey bee recording, rather than using a generic recording for all honey bees. The outcome of the background removal process outlined here was the best that could be achieved with the data.

#### 4.3.5.5. Inspection of 2DFT images for all bee individuals

Following on from the inspection of all bee videos as stacked 2DFTs, it was further decided to also look at 2DFT images (see Figure 4.8) for all bees with stationary periods, because the stacked 2DFT analysis revealed a larger spectral repetition axis due to data coarsening (0 – 200 Hz). Prior to this, only non-trembling and severely trembling bees that had stationary periods had been inspected for defining vibrational features that characterised the two groups. The larger spectral repetition axis (0 – 200 Hz) could then be scrutinised at all

relevant frequency bandwidths (0 – 2000 Hz, y axis) to seek out potential discriminatory features that might have been missed during previous analysis.

Multiple 2DFTs were created from the accelerometer data of each bee individual, where possible, dependent on the length of the time that each bee was stationary for (non-trembling  $n = 55$ , mild trembling  $n = 43$ , strong trembling  $n = 46$ ), and in the same way as they were for section 4.3.5.1.

Principal component analysis (PCA) and discriminant function analysis (DFA) were then carried out to identify any feature components that discriminated the three groups of 2DFT data from one another.

#### 4.3.6. Investigation into the vibrational features of trembling at low frequencies

The camera used in this study has an unavoidable limitation: an inability to capture vibrational data between 0 and 15 Hz. Unfortunately, this was only discovered after the collection of all trembling bee data.

To determine whether this low frequency range held vibrational information on the features of trembling, a different recording set-up was implemented. In a concrete floored room, similar to the shed set-up where the bee recordings were captured, the camera, cotton wool, conditioner, accelerometer and Petri-dish were placed in the same experimental design (see Figure 4.6).

In all previous recordings, the conditioner had fed to the camera for synchronous accelerometer and video data capture. In this case, the conditioner instead fed to a soundcard (Alessi io4), which had the capacity to record the previously missed lower frequencies. Recorded data was saved to a hard drive. The camera was used to capture video data. The vibrational data recorded by the soundcard was later synchronised with the video.

Bees were collected at the entrance of the observation hive on the Nottingham Trent University Clifton campus, and were doused in carbon dioxide to knock them unconscious. They were individually placed on the Petri-dish, and then the accelerometer and video data were recorded for each bee, as they transitioned from an unconscious to an awake state (i.e., becoming mobile as they recovered from the CO<sub>2</sub>). Bees infected with CBPV could not be used at this point in the research as the previous colony was infected naturally and had since recovered from the virus.

## 4.4.0. Results

### 4.4.1. A description of CBPV trembling behaviour based upon visual observations

The trembling that is seen as a symptom of CBPV is easily identifiable when observing bees. However, defining this trembling based upon specific characteristics is less straightforward due to the large variation seen from bee to bee.

Often, bees produced what I defined as 'uncontrolled' behaviours (see section 4.3.4.). These were seen in many individuals, but each bee performed a different number or combination of these. The uncontrolled behaviours that were observed are as follows: (i) shuddering, described as a sudden, rapid tremble of the body, similar to the shuddering motion that a human would produce when they felt a gust of cold air (see Appendix 3, Video T5), (ii) body jerking, described as rapid, singular jerks of the body that in some cases were repeated sequentially (see Appendix 3, Video T5), (iii) lifting both front legs whilst shaking (see Appendix 3, Video ), (iv) grasping a front leg in the mandibles and appearing unable to let go of it.

In some of the bees (10%), the proboscis was extended and the glossa appeared to be stuck outside of the proboscis 'tube' (see Appendix 3, Video T5).

A large proportion of bees (65%) fell over at some point regardless of trembling status, but the difference between trembling (TR) and non-trembling (NT) individuals appeared to be that NT bees righted themselves very quickly (an instant reaction to stand back up) and only fell when walking around the Petri-dish at speed. TR bees fell over more often (TR falling = 38%, TR no falling = 11%, NT falling = 26%, NT no falling = 11%) and became stuck on their back for longer time periods (several seconds), struggling to right themselves.

Additional symptoms were slow body movements and dragging of some of the legs when ambulatory.

For the vibrational analysis of trembling behaviour, because of the large variation observed between bee individuals, only bees that were stationary were scrutinised in detail. This provided a less complicated list of features to be compared between TR and NT individuals. As such, the definition that is here outlined relates only to trembling behaviour seen when bees are static.

Bees that trembled did so most commonly with a side-to-side rocking of the abdomen and thorax, although this could also be front to back motion, or a mixture of both directions. The

leg joints often rocked in synchrony with the movement of the body when the feet were in contact with the Petri-dish. Trembling could also be seen sometimes in the head and antennae as rapid shaking (see Appendix 3, Video T6).

Trembling caused bees to become unsteady on their feet. Any number of the legs could be seen repeatedly reaching out and attempting to grasp the substrate (see Appendix 3, Video T7). This regular lifting of the legs sometimes caused the bee to stumble/shuffle away from their original standing position. Therefore, although this description is based upon stationary individuals, for TR bees, complete immobility was often not possible due to the nature of the symptom. The definition of 'stationary' is here defined as a bee remaining in the immediate vicinity of the area where it was first observed, without active, purposeful movement in a specific direction.

There were a total of 54 bees with stationary periods during their time under observation. Of those, 21 (39%) were of normal morphology, 14 (26%) were of intermediate morphology, and 19 (35%) were of black/hairless morphology. A Chi-Square test of association was carried out to establish whether there was a link between the morphology of the bee and an observation of trembling behaviour, and this yielded  $X^2(2, N = 54) = 11.306$ ,  $p = 0.004$ , indicating that there is a link does exist. A larger number of intermediate/black bees were observed trembling than those of normal morphology (see Figure 4.12).

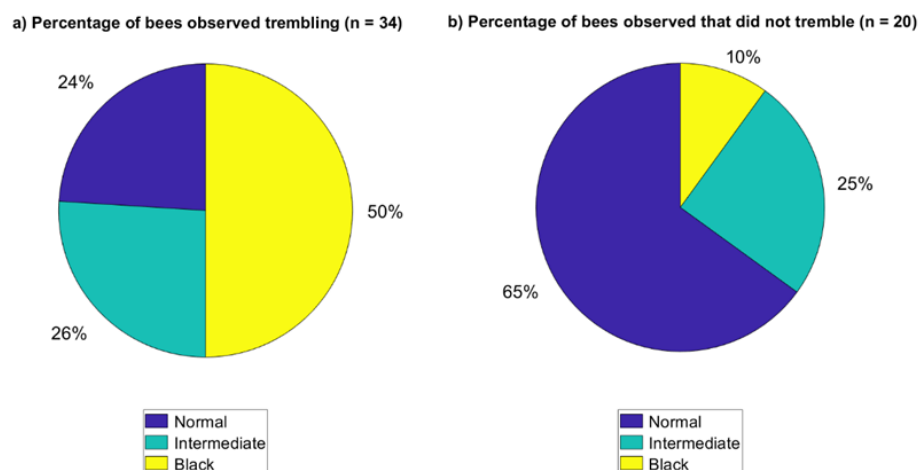


**Figure 4.12:** Two pie charts to indicate the morphology of each bee that was seen to tremble (a) and not tremble (b).

Visually, there also appeared to be differences in the magnitude of trembling. Some bees trembled more strongly than others, i.e., they trembled with a greater angle of movement from their resting position, which also produced an audibly louder vibration on the Petri-dish (see Appendix 3, Video T1). The 54 bees that had stationary periods during their videos were also categorised based on this observation. Bees were listed as (i) non-trembling, (ii) mildly trembling, or (iii) strongly trembling.

#### 4.4.2. The likelihood of observing a CBPV infected bee on the lifted frame of the observation hive

When scrutinising the full frame video recordings, 344 sampling intervals were observed for trembling behaviour and black/hairless bees. In any sampling interval, there was an average of 18 bees in view (i.e., on average, 6192 bees were observed for all 344 sampling intervals, although this is an over-estimation because, in several cases, the same bee will have been sampled multiple times, if it stayed in the observation window for long time periods). Throughout the sampling periods, only one black/hairless bee was seen on the frame (see Appendix 3, Video T8). Remarkably trembling bees were never observed on the frame.

#### 4.4.3. Characterisation of trembling behaviour vibrations

##### 4.4.3.1. Features seen in the first collection of 2DFT images and 2DFT scrolling images

When viewing the 2DFTs of strongly TR and NT bees, some features were identified as being of interest for further analysis. Frequency peaks between 0 and 175 Hz (y axis) and 0 and 30 Hz (x axis) in particular were observed (see Figure 4.8). This area of interest was seen in most bees, regardless of whether they trembled or not. However, on initial investigation the traces appeared to have a lesser magnitude of acceleration in NT bees when compared to TR bees (see Appendix 3, Video T9 and Video T10). A lack of vibrational trace in this frequency bandwidth (0 – 175 Hz, 0 – 30 Hz spectral repetition) can be seen in rare instances ( $n = 2$ ) (see Appendix 3, Video T11). Focus was placed on these frequency ranges for further analysis as it was the area deemed most likely to show accelerometer recording features related to trembling.

##### 4.4.3.2. Features observed in the stacked 2DFT images

The reshaped 'stacked' 2DFT figures that were created from the bee video/accelerometer recordings were investigated for time periods where the bees were stationary. The corresponding areas of the 2DFT figures were then scrutinised for feature differences between NT, mild TR, and strong TR bees.

Unfortunately, no identifiable features were found to correlate with the three categories of trembling. When viewing the stacked 2DFTs of the three bees described in section 4.4.3.1. (see Appendix 3, Video T9, Video T10 and Video T11), this lack of features can be seen (see Figure 4.13). The TR bee produced shaking movements for the entirety of the video and remained in the same position on the Petri-dish, in comparison to the two NT bees whose stationary periods are highlighted between the red lines (see Figure 4.13). When not stationary, the first NT bee (panel 'b', Figure 4.13) frequently groomed or flew/walked around the Petri-dish. The second NT bee (panel 'c', Figure 4.13) ran around the Petri-dish continuously when not stationary. When comparing these three bees, no specific features (in magnitude of acceleration, frequency, or otherwise) could be identified to indicate the TR status of the bee. The same observations were then made for every recorded bee. When compared, there were also no vibrational characteristics specific to trembling behaviour (see also Figure 4.14).

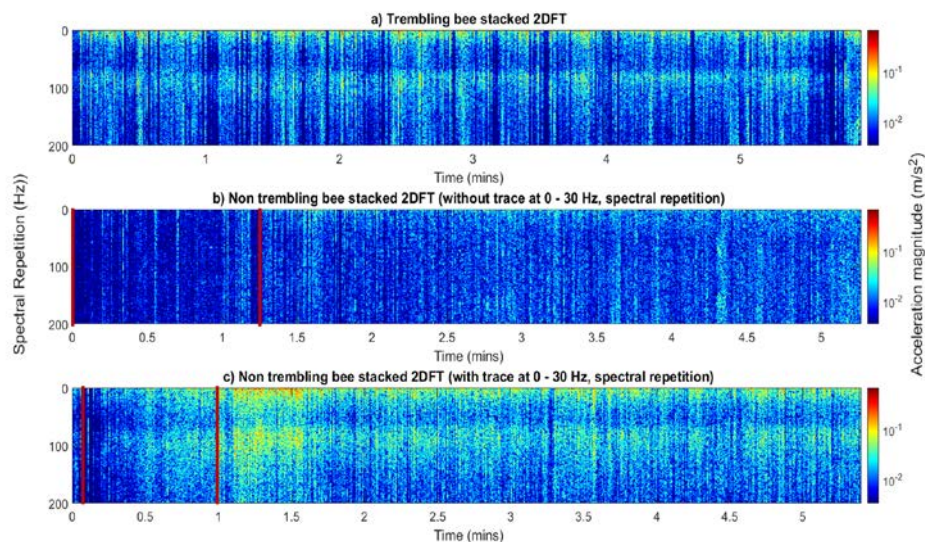


**Figure 4.13:** The stacked 2DFTs for each of the three bees viewed in Video T9 (panel 'a'), Video T10 (panel 'c') and Video T11 (panel 'b'). Only the selected frequencies of interest (0 – 200 Hz) over the full duration of each video (panel 'a' = 5 minutes 55 seconds, panel 'b' = 5 minutes 16 seconds, panel 'c' = 5 minutes 24 seconds) can be seen in this figure. The time periods where each bee is stationary are highlighted between the red lines (except for panel 'a' as the trembling bee in this case was stationary for the entirety of the video). The magnitude of acceleration is logarithmic (to the base 10) scale, where the maximum magnitude is dark red ( $6.8 \times 10^{-1} \text{ m/s}^2$ ), and the minimum is dark blue ( $1/200$  of the maximum). All three panels have been scaled identically to allow comparison. The background vibrations inherent to the recording area have been subtracted from each panel, using the method described in 4.3.5.4.

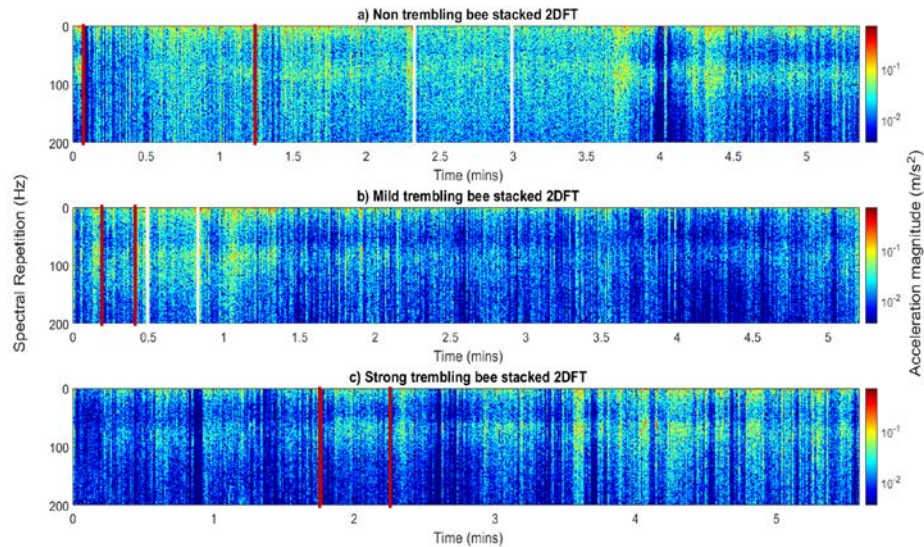


**Figure 4.14:** The stacked 2DFTs for a non-trembling, a mild trembling and a strong trembling bee. The same analysis as seen carried out for Figure 4.13 has been applied here. The time periods where each bee is stationary are highlighted between the red and white lines, which are colour coded to demonstrate the first (red) and second (white) stationary periods for the bees in panels ‘a’ and ‘b’. Panel ‘c’ only has one stationary period, between the red lines. The magnitude of acceleration is logarithmic (to the base 10) scale, where the maximum magnitude is dark red ( $7 \times 10^{-1} \text{ m/s}^2$ ), and the minimum is dark blue ( $1/200$  of the maximum). All three panels have been scaled identically to allow comparison. The background vibrations inherent to the recording area have been subtracted from each panel, using the method described in 4.3.5.4.

There is, however, one feature of particular interest that can be seen in the stacked 2DFTs: a vibrational trace that occurs between approximately 70 and 140 Hz spectral repetition (see Figure 4.15). This trace is likely related to bee activity as it is not seen in the recording of the background noise alone (see Figure 4.15). There appears to be no link between this bandwidth and trembling behaviour as it is observed in most bees, regardless of how symptomatic they were. Overall, 8/54 (15%) bees lacked this frequency band. Of these, five were TR and three were NT. On close inspection of all bee recordings, no specific behavioural trait could be identified as producing this trace, and as it was observed in 85% of individuals, there is strong suggestion that this bandwidth is linked to an element of honey bee physiology.

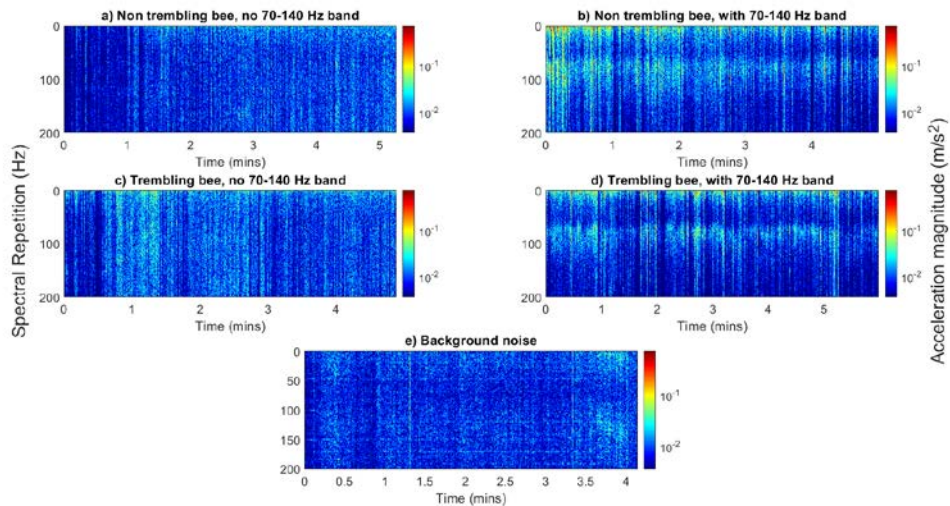


**Figure 4.15:** A set of figures to show the presence and absence of the 70 – 140 Hz frequency band (seen at the centre of the y axis, across the majority of the x axis in panels ‘b’ and ‘d’). Here, the stacked 2DFTs of two NT (panels ‘a’ and ‘b’) and two TR (panels ‘c’ and ‘d’) bees are shown together to demonstrate that the frequency band can be present or absent regardless of trembling status. The lack of frequency band in the background noise panel (‘e’) indicates that this band could be related to the activity of the bee, even though it is not seen in 15% of bees. The magnitude of acceleration is logarithmic (to the base 10) scale, where the maximum magnitude is dark red ( $7.2 \times 10^{-1} \text{ m/s}^2$ ), and the minimum is dark blue ( $1/200$  of the maximum). All panels have been scaled identically to allow comparison. Background subtraction has not been carried out in this instance, as all panels are being directly compared to a recording of background vibrations.

In all figures that exhibit the 70 – 140 Hz band, a corresponding vibrational trace at a lower repetition frequency is also seen (50 Hz). These two bands are systematically seen with one another, and both bands demonstrate a similar magnitude of acceleration (see Figure 4.13, Figure 4.14, Figure 4.15).

#### 4.4.3.3. Inspection of 2DFT images for all bee individuals

Following on from these somewhat disappointing results, where vibrational traces specific to trembling behaviour could not be found, additional 2DFT images for all bee individuals with stationary periods were created for analysis (previously, 2DFT images had only been scrutinised for non-trembling and strongly trembling bees). A larger spectral repetition axis was implemented in this analysis (up to 150 Hz, resulting from the 70 – 140 Hz band identification), to ensure that all potentially relevant frequencies were inspected for vibrational traces of interest. The stacked 2DFTs indicate that there are no frequencies of interest beyond 140 Hz (see Figure 4.13, Figure 4.14, Figure 4.15).

Only two NT bees (4%) demonstrate a lack of vibratory trace across this frequency bandwidth of interest (0 – 175 Hz (y axis), 0 – 30 Hz and 70 – 140 Hz spectral repetition) (see Figure 4.16). All other bees (see Figure 4.17) demonstrate an active 0 – 175 Hz frequency band on the y axis, with varying magnitudes of acceleration that appear to have no link to the strength of trembling (mild or strong) that was seen in the video recordings.

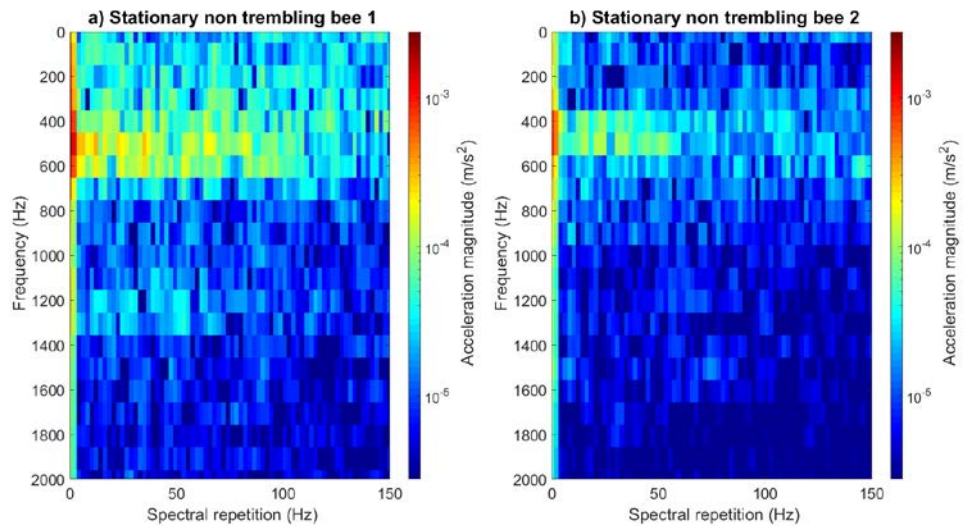


**Figure 4.16:** Data taken from two bee individuals that when stationary, exhibiting a lack of vibrational traces in the frequency bands of interest (0 – 175 Hz y axis, 0 – 30 Hz and 70 – 140 Hz x axis), shown as 2DFTs. Both 2DFTs comprise of 1 second of stationary behaviour. The magnitude of acceleration is logarithmic (to the base 10) scale, where the maximum magnitude is dark red ( $2.8 \times 10^{-3} \text{ m/s}^2$ ), and the minimum is dark blue ( $1/1000$  of the maximum). Both panels have been scaled identically.

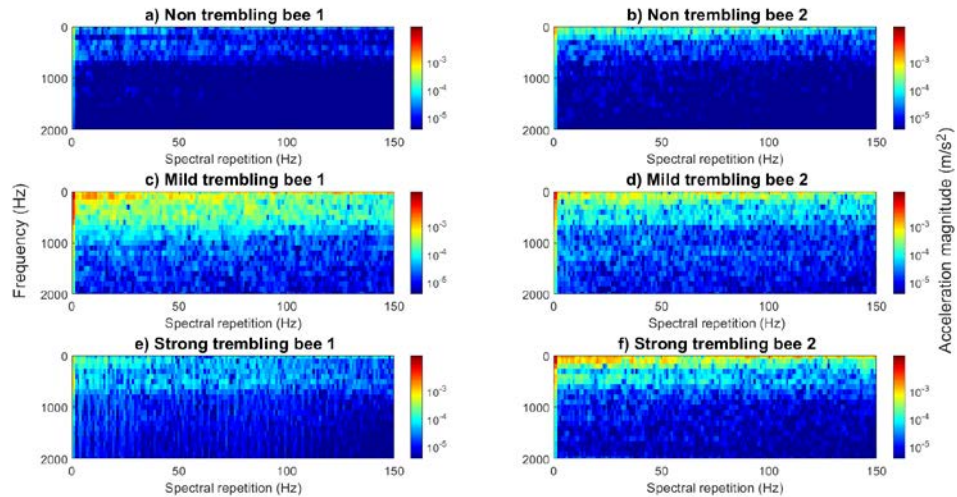


**Figure 4.17:** 2DFT images for 6 randomly selected bees. Each 2DFT is comprised of one second of repeated trembling behaviour. Panels ‘a’ and ‘b’ relate to two non-trembling individuals, panels ‘c’ and ‘d’ related to two mildly trembling individuals, and panels ‘e’ and ‘f’ relate to two strongly trembling individuals. The magnitude of acceleration is logarithmic (to the base 10) scale, where the maximum magnitude is dark red ( $1.8 \times 10^{-2} \text{ m/s}^2$ ), and the minimum is dark blue ( $1/5000$  of the maximum). All panels have been scaled identically.

#### 4.4.4. Principal Component and Discriminant Function analysis of the 2DFT data

The 2DFT images for the NT, mild TR, and strong TR behaviour (analysed in section 4.4.3.3.) were compared. Principal component analysis and discriminant function analysis of this data, again, demonstrated an absence of vibratory features that could discriminate between the three groups (see Figure 4.18).

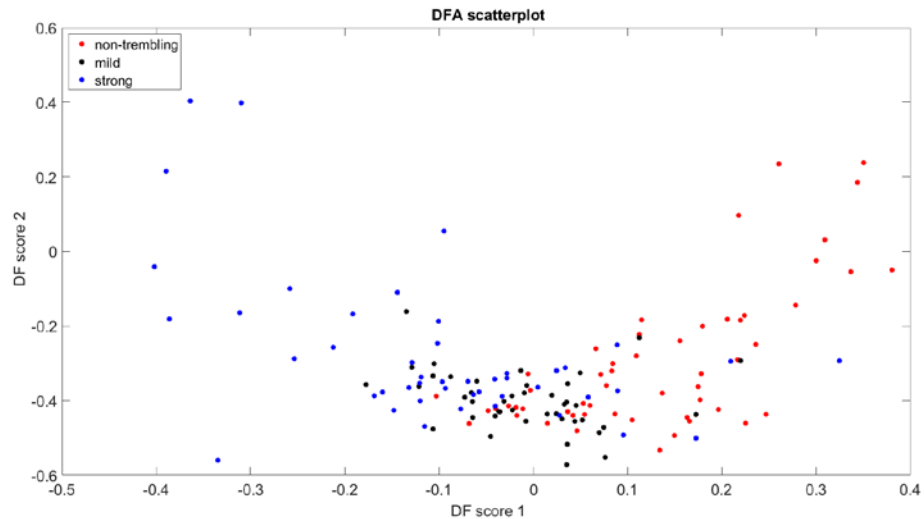


**Figure 4.18:** Discriminant function analysis outcome for feature extraction of the three groups of bee behaviour according to the first 10 principal components. Inclusion of more, or less, principal components did not improve the clustering outcome. There is some discrimination seen between the strong trembling (blue) and non-trembling (red) 2DFT images, but not enough to warrant further investigation.

#### 4.4.5. Investigating the vibrational features in the lowest, missing frequency band

Additional bee accelerometer/video recordings were collected to provide frequency data for the 0 – 15 Hz bandwidth that could not be recorded using the Sony camera. Using a soundcard to record the vibrational activity of bees instead of the camera did turn out to successfully collect these missing frequencies (see Figure 4.19). However, the spectrogram of the accelerometer data revealed no changes over time as the bee moved from an anaesthetised to an awake state (see Appendix 3, Video T12). As a result, I was not able to provide measurable vibrational traces that could potentially be linked to the activity of CBPV related trembling behaviour.

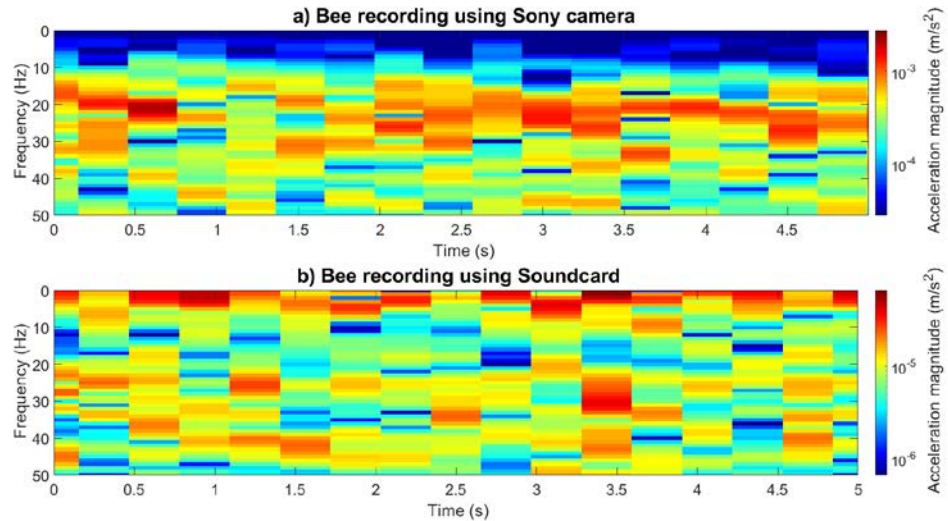


**Figure 4.19:** A plot to demonstrate the inclusion of the 0 – 15 Hz bandwidth when using a soundcard to record accelerometer data. Panel ‘a’ shows five seconds of bee recording using the Sony camera, panel ‘b’ shows five seconds of bee recording using the Alessi io4 soundcard. A high temporal resolution (value of 1) is used to exhibit a data pixel for every frequency value from 0 until 50 Hz. The magnitude of acceleration is logarithmic (to the base 10), where the highest magnitude is dark red ( $2.8 \times 10^{-3} \text{ m/s}^2$  for panel ‘a’ and  $6.6 \times 10^{-5} \text{ m/s}^2$  for panel ‘b’) and the lowest dark blue (1/100 maximum). The two panels could not be scaled identically in this figure due to the two digital accelerometer datasets being stored in different arbitrary units. They are instead scaled individually based on each maximum value, to best demonstrate the inclusion and absence of the 0 – 15 Hz band.

#### 4.5.0. Discussion

This study is, to my knowledge, the first of its kind in attempting to detect and characterise the features of CBPV trembling symptom vibrations. In fact, it appears that no other honey bee virus has been investigated regarding its remote detection, aside from American Foulbrood, where hyperspectral imaging technology was applied (Yones et al., 2019). Previous studies have highlighted the morphological characteristics of CBPV infected bees in detail (Rivière et al., 2010; Dittes et al., 2020b), yet the visible movement of the honey bee body when trembling, and any potential corresponding vibrations, have been neglected in terms of exhaustive description.

In this chapter, I have carefully described both the morphological and visible trembling symptoms of CBPV. When collecting bees from the research hives, it was easy to identify black/hairless and trembling individuals. Clustering occurred at the hive entrance, and apparently healthy workers were observed grabbing or attacking symptomatic bees with

their mandibles and ‘escorting’ them out of the hive entrance. These descriptions are in line with that of previous CBPV observations (Ribi re et al., 2010). The morphological and symptomatic variation observed indicates that both types of CBPV syndrome were present in the sampled colonies (Ribi re et al., 2010). Although morphological type was linked to trembling behaviour in this study, where a greater number of black and shiny bees exhibited trembling than visibly healthy bees, it is likely that both syndromes occurred as there were still several hairy trembling bees, reflecting the descriptions of Type 1 and Type 2 CBPV (Ribi re et al., 2010).

As this is the first time that trembling symptoms have been described in detail, the assessment of the behaviour was made somewhat subjectively, using a list of questions curated from detailed video observation. The only feature of the symptom that appeared to be consistent between individuals was the rocking motion of the body. Aside from this, an assortment of movements and behaviours were observed in trembling honey bees in various combinations. Of these, the Proboscis Extension Reflex (PER) is the only trait described in this work that has also been mentioned elsewhere regarding CBPV, although it is not known whether PER is specifically linked to the virus or not (Dittes et al., 2020a; Dittes et al., 2020b).

#### 4.5.1. The capture of a new honey bee vibration

The 70 – 140 Hz trace that was observed in the majority (85%) of bee stacked 2DFTs has not previously been identified. It is possible that this trace results from some bee-related activity, as it was absent in background noise, and directly corresponded to the lower observed 15 – 50 Hz frequency band that was also present in bee recordings, with both traces demonstrating a similar magnitude. As there was a lack of association between trembling behaviour and this vibration, it is therefore possible to speculate that it is instead inherent to part of the honey bees’ regular physiology.

As some physiological processes, such as respiration and thermoregulation rates, are known to be affected by numerous variables, e.g., body temperature, bee age, and activity level (Allen, 1959; Rothe & Nachtigall, 1989; Stabentheiner et al., 2003; Kovac et al., 2007), this could explain why the trace was seen in some bees, but not others. No further investigation was made into the 70 – 140 Hz trace following its identification as the purpose of this chapter was to pinpoint vibrations that corresponded to CBPV body trembling. However, it would be interesting to follow up this line of investigation in future work, to test the hypothesis that this vibration is somehow linked to a honey bee’s biological state.

#### 4.5.2. Why trembling vibrations may not have been captured in this study

Vibrations specifically produced by trembling were unfortunately not identified in this study. There are a few potential reasons for this. The first is that the trembling frequency bandwidth was not captured by the equipment used. The frequency range that was focussed upon in this research was chosen carefully, based on the information that could be gleaned from the video and 2DFT investigation. Trembling is visible to the human eye; therefore, it was deemed unlikely that a bee would be shaking at a spectral repetition frequency greater than 50 Hz (Brundrett, 1974). Only two clear bandwidths were identifiable in the 2DFT, the first being 0 – 175 Hz and the second around 400 – 600 Hz. The latter band is known to be a naturally occurring resonance of honey bee wing buzzing (Clark et al., 2017), so was disregarded as being linked to body trembling in this case.

Despite the justification for the chosen bandwidth of interest (0 – 175 Hz), on later inspection, it appeared that 0 – 15 Hz was lacking in accelerometer data. Unfortunately, by then, it was not possible to collect CBPV infected bees to record trembling with suitable equipment, as the infected colonies had recovered. Alternatively, healthy bees were collected and observed moving from an unconscious to an awake state in an attempt to identify vibrations, perhaps linked to physiological activities such as heartbeat (known to occur at low frequencies (Schwab et al., 1991; Kaiser et al., 2014)), or respiration (introduction section of Zhao et al., 2019). It was considered that trembling behaviour may partly be an exacerbation of body movements (such as respiration-related abdominal pumping) that are linked to these inherent activities. Therefore, this investigation sought the identification of evidence to support the theory that the 0 – 15 Hz band is where trembling vibrational frequencies might lie. However, no such results were found. Future work must ensure that this bandwidth is captured and that trembling, CBPV infected bees are measured, as this is the only truly viable method to identify if the 0 – 15 Hz band is of interest.

A second reason for lack of trembling vibration capture is possibly caused by the irregular nature of the symptom. Trembling varied between individuals, with differing 'strengths' of shaking motion, alongside the additional combinations of movements previously described (e.g., leg tapping, PER). Simply categorising bees into one of three groups (non-trembling, mild, strong) was necessary for initial identification of any vibrational differences that may have occurred. However, the motion of trembling is perhaps far more complex than this, due to individual differences observed. The symptom has been previously described as 'erratic' in nature (Dittes et al., 2020b), and from my own observations, I can agree with this

statement. That said, it might not be possible for trembling to produce a characteristic vibration with specific, periodic features.

The 2DFT is a useful tool for identifying features specific to repetitive, periodic vibrations. Some honey bee behaviours, like the DVAV (Ramsey et al., 2018) and the honey bee purr (see chapter 5) produce clear features along the spectral repetition axis. Even when this is not the case, the 2DFT can still be helpful for discriminating between different groups of traces, such as Varroa mite walking, bee emergence scratches, and background noise (see chapter 3). Although these three types of vibration lacked strong, specific features, the 2DFTs were still consistent within their groups and identifiable from one another. In the case of CBPV trembling, however, the 2DFTs varied greatly from one another, ranging from strong traces, to no traces at all. The appearance of captured vibrations and their corresponding magnitude occurred randomly from bee to bee, with no indication of what might cause the variation. The individual bee videos also provided a lack of evidence for this.

Additionally, other behaviours such as walking and grooming also exhibited similar, random traces, which made it difficult to define where one behaviour stopped and another started. Like walking and grooming, trembling is a more random, irregular movement that therefore may not produce a well-defined vibration that can easily be identified. This is not to say that trembling cannot be captured by accelerometers. Bees are large enough to produce detectable vibrations (Bencsik et al., 2011; Bencsik et al., 2015; Ramsey et al., 2017; Ramsey et al., 2018; Ramsey et al., 2020), and it is likely that despite a lack of specific characteristics, the vibration was still obtained, unless it does in fact occur within the 0 – 15 Hz area. The potential problem is that the vibration varies too much from bee to bee for it to have an identifiable trace, a feature that is seen in the ‘whooping’ signal and the DVAV signal, for example (Ramsey et al., 2017; Ramsey et al., 2018).

#### 4.5.3. Identifying trembling bees on the frame of the observation hive

In observing the full frame of the observation hive, this study aimed to identify the presence of trembling bees and any corresponding vibrations that may have been captured by the embedded accelerometers. Trembling individuals were never seen on the observed areas of the frame, with only one shiny, black bee identified. It is known that when infected with CBPV, healthy individuals attack those that are ill (Drum & Rothenbuhler, 1983; Ribière et al., 2010; Dittes et al., 2020b), and in this study, they have also been observed expelling those bees from the hive. Although not described for CBPV in the past, forcible removal of infected adults is known to happen in the case of DWV infection (Baracchi et al., 2012), and self-

removal has also been demonstrated to occur when experimentally infected with harmful drugs (Rueppell et al., 2010). As CBPV infected bees cluster at the hive entrance and are known to be rejected by hive mates (Ribi re et al., 2010), it is therefore possible that most unhealthy bees are removed from the hive, leaving few trembling individuals behind on the frames.

It is also conceivable that trembling compromises a bees' ability to hold on to the vertical comb, as they were observed stumbling, falling over and repeatedly grasping at the Petri-dish in this study. This offers another potential explanation for why symptomatic bees are not seen on the frame. With these points in mind, it may not be possible to capture symptom-related vibrations for this particular virus within a honey bee hive. Although, trembling bees have been described as sitting a-top the wooden frames of colonies in CBPV infected hives (Dalmon, 2020), which lends some anecdotal evidence for inability to grasp the comb. This is an avenue that requires further investigation, particularly in terms of the behaviour of infected individuals, as it may be that trembling can be detected by accelerometers if placed in a location more suited to capturing the vibrations of this specific disease (such as on top of the comb).

#### 4.5.4. Future prospects

Despite failing to characterise definitive attributes of trembling-related vibrations as recorded by accelerometers, this work has revealed important information related to the visually observable symptom and its detection. Firstly, the methods implemented in this work have proven to be unexpectedly flawed in that the equipment initially used was unable to detect all potentially meaningful frequencies. Through careful further investigation, I have now rectified this and suggested a new recording technique that is fit for purpose. In losing out on data for this low frequency bandwidth, the results have shed light on the need to focus on this area in the future. The lack of vibrational features captured elsewhere in the data indicate that the 0 – 15 Hz bandwidth could be of particular interest in terms of trembling-related vibrations. Future work can now go ahead with CBPV infected, trembling bees to identify whether this is the case.

Secondly, the detailed video-based observations that were carried out have provided information on the intricate movements that occur as a result of trembling, something that has not previously been done. In understanding the irregular nature of trembling, it has been possible to partially conclude that perhaps the erratic, random nature of the symptom produces a vibration that lacks definitive, detectable features. However, it would now be

advisable to monitor trembling individuals in a more controlled environment, as viral load may have an effect on the different motions seen in this study, e.g., more heavily infected bees may tremble more greatly than those that are less infected. If bees could be infected to the same degree, and be reared and measured under controlled settings, there could be increased potential for identifying specific frequencies and/or spectral repetition frequencies that are linked to the behaviour. However, it is worth noting that infecting bees under standard conditions may prove to be difficult to control as the genomic load of the virus can be extremely high (millions of particles) (Ribi re et al., 2010).. These particles can affect many different areas of the honey bee central nervous system and in differing quantities dependent on bee developmental stage (Ribi re et al., 2010).

Thirdly, the lack of trembling bees seen within the hives has demonstrated the importance of better understanding the behaviour of infected individuals and colonies. It appears worthwhile to investigate the ability of symptomatic bees to hold onto the comb and find out if they gather elsewhere in the hive, such as the tops of the frames. Additionally, it would be interesting to follow and quantify the movements of these bees, in terms of whether they are forced out of the hive by others or remove themselves. In answering these questions, accelerometer placement could be improved to increase the chance of capturing the CBPV vibrations, perhaps at the hive entrance, or the top edges of a frame, where they have been seen to gather (Dalmon, 2020).

#### 4.5.4. Conclusion

This study set out to capture and identify, using accelerometers, any vibrations that may be related to CBPV trembling. Although the aims of this research were largely not achieved, this work has still implemented an investigation into a novel detection method for a well-studied honey bee virus. The results presented here are the first attempts to capture vibrations linked to a colony disease, and through some failures, they have instead performed the purpose of building stronger, future research.

CBPV is just one of more than 20 known honey bee viruses (Dittes et al., 2020a). The application of accelerometer technology could be beneficial in detecting other symptomatic diseases, such as Deformed wing virus, which causes abnormal wing development (de Miranda & Genersch, 2010), and therefore perhaps atypical buzzing. Another application could be the detection of pesticide intoxication, which can lead to irregular motor function such as shaking and tremors etc. (Laurino et al., 2011; Costa et al., 2014; Martinello et al.,

2017). The work demonstrated here is a starting point for accelerometer detection of negative events such as these.

The following chapter is the final results chapter in this thesis and will discuss the vibrational features of a novel honey bee signal, discovered through critical listening of long-term, colony accelerometer data. Although not inextricably linked to the main aims and questions of the thesis (in terms of remote Varroa and disease detection), this final results chapter draws the readers' attention to the importance of understanding a range of honey bee vibrations, which should continue to grow and improve the overall understanding of colony status and events without the need for physical interference.

# Chapter 5: Characterising the features of a novel honey bee vibrational signal

## 5.1.0. Chapter overview

The previous chapter investigated the prospect of detecting a known honey bee virus through the recognition of its main observable symptom – body trembling. Although the implemented method did not successfully capture trembling vibrations, this does not mean that it is unachievable. As a result of this research, it has been possible to identify which aspects of the experimental design were not suitable, and how to overcome these issues for future accelerometer detection of Chronic bee paralysis virus. A thorough description of the observable characteristics of trembling behaviour also provided some insight into why capturing vibrations from infected bees is not a straightforward process.

In this final results chapter, I characterise the features of a novel honey bee vibrational signal. Although the work in the following study does not necessarily tie-in to the remote accelerometer detection of Varroa or honey bee disease, I felt it important to include, nonetheless, for the following reasons: (i) several known honey bee vibrational signals have already been captured and described using accelerometer sensors; (ii) by understanding specific vibrations: their features, their purpose, their temporal characteristics, we can better perceive and interpret what is occurring in accelerometer monitored hives, without the need for visual verification.

The signal that is described in this brief chapter has not been, to our research groups knowledge, previously mentioned in the literature. The following study is a short communication, characterising some of the features of this vibration. As of yet, the behaviour that produces this pulse has not been visually captured, leading to only speculations regarding its function and mechanism.

The main figures in this chapter are listed as Figure 5.1, Figure 5.2, and so on. The supplementary material can be found in Appendix 4, and are referenced as P1, P2 etc. There is some audio and video data associated with this chapter. Audio clips and videos are referred to as P1, P2 etc. in the main text, and their figure legends are found in Appendix 4. The audio clips and videos themselves have DOI links (see page 11) and are also supplied on a USB stick, labelled according to their text reference (P1, P2, and so on).

## 5.2.0. Introduction

Vibrations are particularly important to honey bees as a form of communication (see section 1.3.5.). When monitoring colonies with non-invasive, remote systems, it is then possible to recognise and interpret signals, behaviours and events more thoroughly, sometimes even enabling better beekeeping. The more informative remote measurements are, the better Precision Beekeeping techniques can be (Zacepins et al., 2015).

### 5.2.1. What vibrational signals have already been captured and characterised?

The use of accelerometers has proven that it is possible to determine some hive states based on the contribution of the entire colony's vibration, as well as establish the effects that the loading of the comb have on vibration perception for colony brood state identification (pre-swarming/swarming; brood cycle) (Bencsik et al., 2011; Bencsik et al., 2015; Ramsey et al., 2020). In addition to this, accelerometer sensors have also been used to pull out specific bee vibrational pulses that are of importance to the species ('whooping' signal; dorso-ventral abdominal vibration (DVAV); queen tooting and quacking) (Ramsey et al., 2018; Ramsey et al., 2020). Through correlation of these vibrational pulses and signatures with visual and audible evidence of the behaviour/state that they are linked to, it has been possible to provide a clearer understanding of what the bee/colony is doing when vibrating in a specific way (Bencsik et al., 2011; Bencsik et al., 2015; Ramsey et al., 2017; Ramsey et al., 2018; Ramsey et al., 2020).

Furthermore, the representation of these signals as vibrational waveforms, spectrograms and 2DFTs has allowed automated detection, capturing instances of these pulses/colony vibrational signatures in long-term data sets (Bencsik et al., 2011; Bencsik et al., 2015; Ramsey et al., 2017; Ramsey et al., 2018; Ramsey et al., 2020). When vibrations can be detected automatically, an understanding of their temporal and spatial pattern throughout the season can be established, further providing insight into the function of specific pulses.

The identification and understanding of a larger number of vibrational signals is likely to lead to a more accurate assessment of the colony state, through the provision of more detailed information. Greater accuracy should lead to better informed beekeeping choices and may even allow critical work to be undertaken on a colony before a disruptive/unwanted event, such as disease or swarming, can take hold.

### 5.2.2. Improving the list of known honey bee vibrational signals

A range of honey bee communicatory signals are known but have not yet been characterised in great depth in terms of their vibrational signal. These signals (in addition to the ‘whooping’ signal, DVAV, queen tooting, and queen quacking) are: the waggle dance and round dance (von Frisch, 1946; Dyer, 2002; Couvillon, 2012); the tremble dance (Kirchner, 1993b); the stop signal (previously also referred to as the begging signal, and now also referred to as the ‘whooping’ signal) (Ramsey et al., 2017; Bell et al., 2021); swarm related worker pipes (Seeley & Tautz, 2001); grooming requests (Land & Seeley, 2004); forager laying pipes (Ohtani & Kamada, 1980); the buzz run (Rittschof & Seeley, 2008). There is now the potential to add these vibrational signals to the growing library of well characterised pulses, for future automated detection and better understanding of hive events. Additionally, however, it is highly likely that there are numerous other, yet-to-be-described signals that could also be of importance, due to the complexity of the honey bee colony, and the fact that not all vibrational signals are necessarily visible to the human eye.

In this short chapter, I describe one of these novel signals, a honey bee pulsed vibration, discovered coincidentally through critical listening of long-term colony accelerometer recordings. This pulse, which I refer to as the honey bee ‘purr’, phonetically named due to the cat-like purring sound produced, occurs frequently throughout colony recordings. This chapter aims to describe the features of the purr vibrational signal, in terms of shape, time duration, and frequency. By characterising the elements that define this unique vibration, it should then be possible to move towards its automated detection, allowing a further investigation into its temporal and spatial production patterns. It is further hoped that this study can provide a foundation of knowledge that will benefit and support the future capture of this behaviour visually, for improved understanding of its purpose.

### 5.2.3. Aims of the chapter

The aim of this chapter is as follows:

- Define and describe the features of the honey bee purr vibration.

## 5.3.0. Methods

Accelerometer recordings were taken from a honey bee colony based at Nottingham Trent University Clifton campus. Two accelerometers were embedded in the comb of the central frame of the colony for long-term data acquisition, and the data used for this study was taken from a 24 hour period in June 2021.

Ninety honey bee purrs were extracted from one-hour-long recordings taken from this time period, identified through critical listening. Each purr vibration was transformed into a 2DFT for feature identification and extraction. Purr 2DFTs were characterised based on their frequency, spectral repetition frequency, time duration, and any additional features of interest. Of the collection, a slightly smaller number of high-quality honey bee purrs (76/90) were also analysed for spectral repetition and frequency features. This reduction in pulse numbers was due to signal strength interfering with pulse clarity in some cases. A temporal resolution of 0.016s and a multiplication factor of four were deemed appropriate parameters for viewing honey bee purr 2DFTs, providing a spectral repetition axis with a maximum of 100 Hz.

Histograms for signal spectral repetition frequency and time duration were created using these statistics as a descriptive tool.

#### 5.4.0. Results

The honey bee purr vibration described is a pulsed signal that audibly sounds similar to a high-pitched cat purr (see Appendix 4, Audio P1).

##### 5.4.1. Purr time duration

Purr vibrations ( $n = 90$ ) varied in length from 0.1 – 5 seconds, demonstrating an average length of 0.7 seconds ( $\sigma = 0.94s$ ). Most commonly, purrs occurred over 0.1 seconds (see Figure 5.1 and Figure 5.2). Within the long-term specific accelerometer data that was analysed, rare occurrences of particularly long honey bee purrs were also detected ( $n = 4$ , with time durations of 7s, 7.3s, 10s, and 18s). These instances of lengthy honey bee purrs were quieter with poorer signal-to-noise-ratio (SNR), and the audio was often interrupted by other honey bee vibrations, leading to their exclusion from the analysed main purr collection (see Appendix 4, Audio P2).

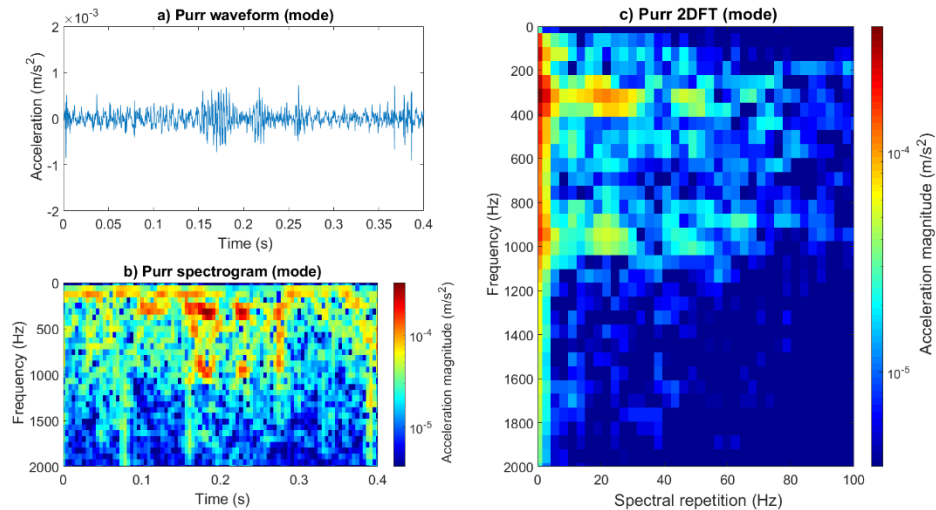


**Figure 5.1:** A representative example of a generic honey bee purr, produced by a bee for 0.1 seconds (the mode time duration of the collection). The waveform of the purr can be seen in panel ‘a’, the spectrogram in panel ‘b’ and the 2DFT in panel ‘c’. The 2DFT and spectrogram have been scaled identically. Magnitude of acceleration is logarithmic (to the base 10), where red is the maximum ( $3.7 \times 10^{-4} m/s^2$ ) and dark blue is the minimum ( $1/100$  of the maximum).

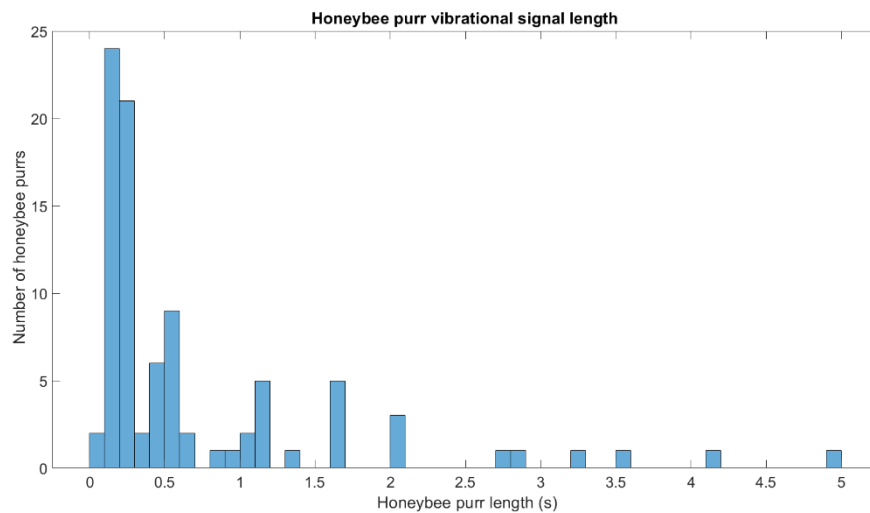


**Figure 5.2:** A histogram to demonstrate the spread of honey bee purr data in terms of pulse time duration ( $n = 90$ ).

#### 5.4.2. Purrr spectral repetition

Purrr vibrations are characterised by a periodically repeating pulse, as is the case for DVAV and queen pipes (Ramsey et al., 2018; Ramsey et al., 2020). A short vibration is produced multiple times sequentially, with a regular periodicity. This repetition can be seen particularly

clearly when viewing signals that are longer than average (see Figure 5.3). Typically ( $n = 76$ ), the spectral repetition of the honey bee purr vibrations was found to be 23 Hz ( $\sigma = 4.72$ ) but ranged from 18 – 37 Hz (see Figure 5.4).

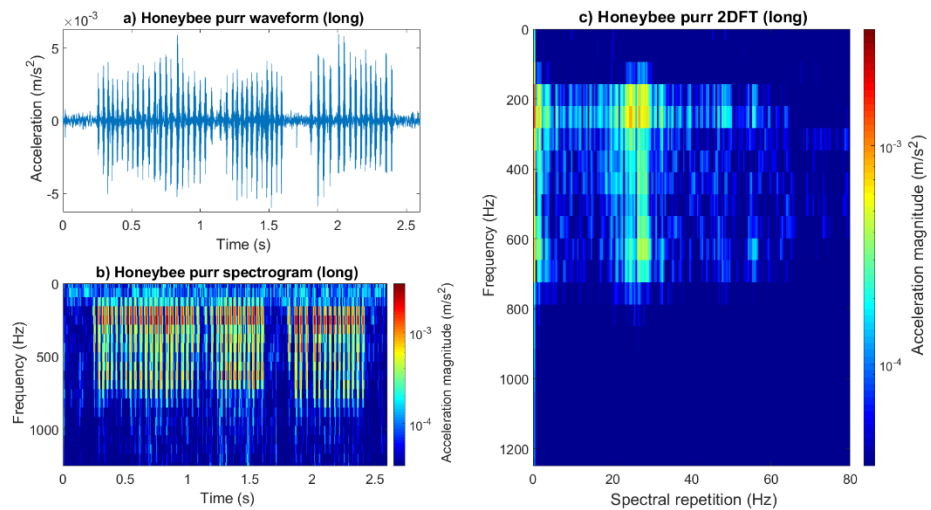


**Figure 5.3:** An example of a honey bee purr that is longer than average, produced by a bee for two seconds. The waveform of the purr can be seen in panel ‘a’, the spectrogram in panel ‘b’ and the 2DFT in panel ‘c’. The 2DFT and spectrogram have been scaled identically. Magnitude of acceleration is logarithmic (to the base 10), where red is the maximum ( $3.4 \times 10^{-3} \text{ m/s}^2$ ) and dark blue is the minimum ( $1/100$  of the maximum).

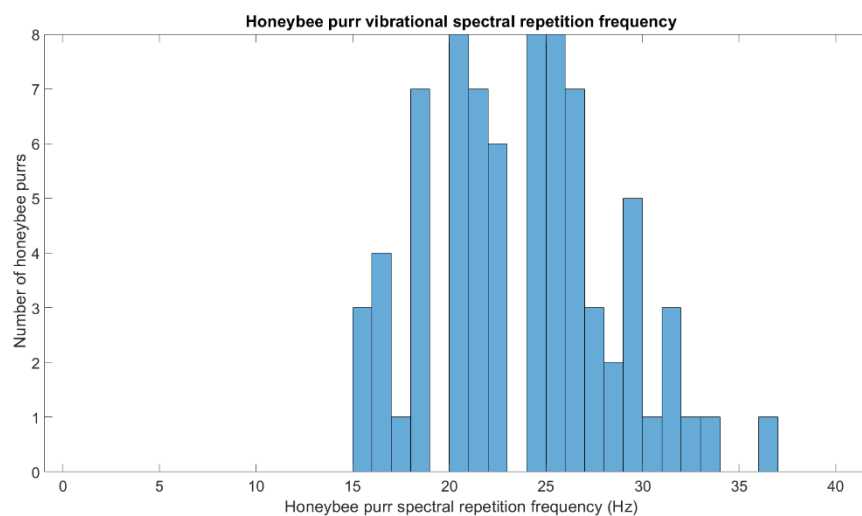


**Figure 5.4:** A histogram to demonstrate the spread of honey bee purr data in terms of pulse spectral repetition ( $n = 76$ ).

### 5.4.3. Purr Frequency

The majority of honey bee purrs exhibited a frequency of 200 – 400 Hz (67% of a population of  $n = 76$  purrs) with two or three additional harmonics. In most cases, these harmonics fell at 600 – 800 Hz (66%) or 1000 – 1200 Hz (49%) (see Figure 5.1 and Figure 5.3), but they were also seen occasionally to occur at 400 – 600 Hz (37%), 1400 Hz (21%), 1600 Hz (37%) and 1800 Hz (13%). No additional frequencies were observed beyond 1800 Hz.

### 5.4.4. Purr additional features

In some cases (13% of a population of  $n = 90$  purrs), honey bee purrs appeared to be linked to a ‘whooping’ signal (see Figure 5.5). Both vibrations instantly follow on from one another, with the whoop always preceding the purr. Audibly, these purr instances sounded as though the same honey bee individual produced both types of vibration sequentially (see Appendix 4, Audio P3).

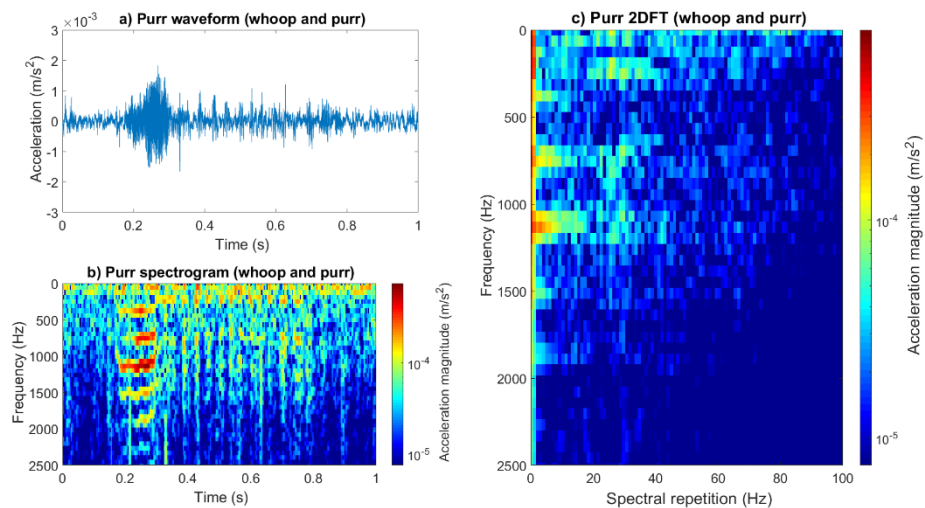


**Figure 5.5:** An example of a ‘whooping’ signal occurring directly before a honey bee purr. The waveform of the purr can be seen in panel ‘a’, the spectrogram in panel ‘b’ and the 2DFT in panel ‘c’. The whoop can be seen between 0.2 and 0.4 seconds in panels ‘a’ and ‘b’, followed by approximately 11 peaks that correspond to the purr vibration. The 2DFT and spectrogram have been scaled identically. Magnitude of acceleration is logarithmic (to the base 10), where red is the maximum ( $3.4 \times 10^{-3} \text{ m/s}^2$ ) and dark blue is the minimum ( $1/100$  of the maximum).

## 5.5.0. Discussion

This is the first time that the vibration, coined the honey bee purr, has been described. Signals that demonstrate a periodically repeating pulse, like the purr, benefit from 2DFT

analysis (Ramsey et al., 2018) which reveals additional vibrational information in the form of spectral repetition. Purr vibrations exhibit commonalities in their features, with the vast majority of the inspected collection demonstrating a time duration 0.1 seconds, main frequency harmonics of 200 – 400 Hz and 600 – 800 Hz, and a spectral repetition frequency of 20 – 27 Hz. As with all biological signals, variation does occur, but overall, the vibration shows promise for automated detection, particularly when viewed as a 2DFT. The commonly produced dorso-ventral abdominal vibration (DVAV), widely accepted as a modulatory signal with the meaning “prepare for greater activity”, is the only known honey bee signal to currently benefit from inspection and automated detection that utilises the 2DFT form (Schneider & Lewis, 2004; Ramsey et al., 2018) (aside from the work done in this thesis). Research into the honey bee purr demonstrates that this type of analysis is not limited to the DVAV anymore.

Through critical listening, the purr signal is easily identifiable, with audibly unique characteristics, and is often heard very clearly above the general noise of the honey bee colony. In fact, it has even been documented by beekeepers, who have recorded instances of honey bee purrs using microphones (on their phones) placed outside hives, although the beekeepers did not know what was causing the sound (see Appendix 4, Audio P4 and related email Figure P5, see also link to Audio P6 (Fleming, 2021)). This further strengthens the possibility of automatic purr detection in long-term accelerometer recordings.

#### 5.5.1. The benefits of characterising honey bee vibrations in detail for future research

This short study, researching the details of the honey bee purr vibrational trace, is a strong starting point for future detection and better understanding of the pulse. Previous investigations into honey bee vibrations demonstrate the advantages that careful, initial analysis has for both novel and known bee signals (Ramsey et al., 2017; Ramsey et al., 2018).

For example, the DVAV is a repeated pulse produced by one bee onto another, for the purpose of shaking the recipient bee and encourage it into implementing hive activities (Schneider & Lewis, 2004). Automated detection of this vibration over the long-term has demonstrated that honey bees produce the signal more frequently in the morning, before foraging begins, and in the evening, following a day of foraging. A lunchtime ‘lull’ occurs where fewer, but louder, DVAVs occur, presumably because foragers are out of the hive gathering resources, and there is less work required until they return (Ramsey et al., 2018). Automated vibration detection in long-term accelerometer recordings have been advantageous for a better understanding of the DVAV. The temporal and spatial patterns of

pulse production, and how this is affected by weather, temperature and time of day has enabled strong conclusions to be drawn on the behaviour. DVAV production is described by the authors as 'stable', and therefore it has been suggested that deviations from usual patterns of production should be easily identifiable in the data. That said, it may be possible to remotely pinpoint variations in colony state as a result of abnormal DVAV signal production (Ramsey et al., 2018).

In this thesis, the honey bee purr has been carefully investigated for its vibrational features, laying a strong foundation for further examination and analysis, such as that seen in DVAV research. Deciphering a larger number of vibrational signals in detail, and discovering new ones, like the honey bee purr, should therefore build a bigger picture of colony state, to the benefit of beekeeping. It is now highly desirable to continue the investigation into the honey bee purr, using this work as a starting point.

#### 5.5.2. What could the function of the honey bee purr be?

There is no visual evidence of a honey bee producing a purr vibration, and therefore the behaviour that the signal is linked to is currently unknown. Some attempts have been made at capturing a purr on video, but these were not successful. Automated detection of the signal would be useful for purr observation, as long-term detection will establish when purr vibrations are more commonly produced and reveal potential patterns or trends in their production over time. This data can then be used to improve the experimental protocol for video-capture of the signal, as the best time of day/time of year for regular purr production may be affirmed, improving chances of capturing the behaviour. Video evidence of purr production could provide key evidence for why some purrs are preceded by a 'whooping' signal, or why some are exceptionally long.

#### 5.5.3. Conclusion

This is the first ever description of a specific honey bee vibration that could be of importance to the species. It is hoped that by showcasing the features of this pulse, it can then be used to search for other instances of purr vibrations in long-term accelerometer recordings, for the benefit of honey bee biological understanding. The discovery of a completely novel signal such as this one demonstrates the value of accelerometer technology in honey bee monitoring. Honey bee research spans over many decades, and yet accelerometers, in recording vibration, a stimulus of importance to the species (see section 1.3.5.), are still allowing us to attain new information that may be hugely beneficial to our understanding of

honey bees. Vibrational data is richly detailed, holding yet-to-be-discovered secrets of the honey bee world, and should continue to be utilised as a highly relevant tool.

# Chapter 6: Contributions, limitations, recommendations

## 6.1.0. Thesis chapter summary

This thesis set out to investigate the use and value of accelerometers and vibration measurements in the detection of Varroa mites within honey bee colonies. Additionally, it sought to identify the potential in capturing honey bee viral symptoms, both as an indirect indicator of Varroa presence, and as a tool for collecting early warning signs of colony ill-health, to reduce its negative effect before other adverse influences (such as mites) take hold and lead to bee demise.

Chapter one covered the literature review for this work, discussing in turn the species of interest (*Varroa destructor*), its influence and effects on honey bees, and how beekeepers currently identify its presence within their colonies. The turn towards a more technological monitoring approach was explored, focussing on present remote honey bee colony management techniques, and introducing the current, early-stage methods of non-invasive Varroa mite monitoring that are being investigated. This chapter finished with a discussion into the specific use of accelerometer sensors in this thesis, covering what they are and how they may benefit remote Varroa measurements.

Chapter two highlighted the exciting, fundamental discovery of the mite jolting behaviour, discussing in detail its characteristic vibrational pulse. The jolting trace was identified as a uniquely strong vibration that differed in features dependent on the substrate on which it was delivered. It was compared to honey bee individual and colony vibrational signals, demonstrating that its magnitude of acceleration is remarkable, and that it offers the potential for mites to be detected within fully populated colonies. The power required by a mite to produce the pulse was also artificially recreated, with results yielding a value high enough to strongly imply that the vibration serves a purpose. I used these findings as the basis for my next exploration, which was to investigate the potential for accelerometer capture of jolting pulses within the capped brood cells, not only as a possible detection method, but also to probe further into why the pulse is produced.

Chapter three encompassed this research. A training database containing Varroa jolting and walking pulses was optimised but produced a less than ideal outcome when attempting to classify the two vibrations. I made the decision to move the research forward with honey

bee emergence and mite walking vibrations instead. I also determined that it was perhaps unlikely that jolting pulses even occur in the reproductive phase, as they were never observed during artificial cell experiments. Bee and mite vibration discrimination was more successful, demonstrating the value of 2DFT images in the analysis. As a result of 2DFT use, I identified the vibrational trace associated with *Varroa* walking gait, further building upon knowledge of mite vibrations. Although not wholly successful in classifying brood-comb samples that did, or did not contain *Varroa* mites, this work promoted understanding of remote detection strategies using accelerometers, leading me to identify potential problems and solutions.

Chapter four focussed on the alternate endeavour of honey bee viral symptom capture by accelerometers. When a colony of *Apis mellifera* were confirmed as being Chronic bee paralysis virus (CBPV) positive, I took the opportunity to explore its typical trembling symptom, and any vibrations that may be associated with it. Again, the 2DFT was deemed to be the most suitable visualisation tool in this study, which revealed a high frequency bandwidth at 70 – 140 Hz that I speculated to be related to honey bee physiological activity. Capture of any specific vibration associated with trembling behaviour was unsuccessful, yet my work again allowed me to pinpoint the possible reasons for this. I drew attention to the most promising routes of future investigation: (i) the low frequency band, and (ii) the importance of further hive-based monitoring.

Finally, chapter five examined the features of a novel honey bee vibrational signal. Once again, the benefits of the 2DFT were highlighted, as the trace of interest was a periodically repetitive pulse. This brief chapter promoted the importance of identifying and characterising new honey bee signals, as they contribute to the understanding of hive life, enabling us to better establish what is normal for a healthy colony, and what signals (their presence, absence, patterns of production) may indicate otherwise.

## 6.2.0. What has this thesis achieved?

### 6.2.1 Answering the core questions

The work carried out in this thesis is pioneering in terms of accelerometer implementation, vibration, and *Varroa* mites. Accelerometers have been utilised successfully in the detection of honey bee vibrational signals, but this is the first time, to my knowledge, that they have been used to capture vibrations originating from *Varroa* individuals. The breadth and scope of accelerometer sensor application has been stretched to encompass the measurement of

a species previously dismissed as 'too small' to be detectable. This has had two main positive repercussions.

Firstly, it has answered one of the core questions in this thesis: can accelerometers be used to detect Varroa? What I once deemed to be a potentially unobtainable achievement has now been realised through exploratory research. The ability to capture mite vibrations has unlocked a plethora of potential new research enquires and avenues. The major sensory systems that are thought to govern mite behaviours and life cycle success (chemical, olfactory, temperature), may not embody the limits of Varroa stimuli perception and transmission. In characterising different mite vibratory traces, we can now delve further into when and why they are produced, which may provide indication that mechanoreception/transmission is of greater importance to the species than previously accepted.

Secondly, it has begun to answer another core question: can mite vibrations be used as an effective search tool in the identification of Varroa in honey bee colonies? There is certainly potential for this, which I will discuss in more detail below.

Additionally, the final core question was pursued: can observable virus symptoms in honey bees be detected by accelerometers, and do the results have the potential to be used as an indirect method of detecting Varroa in colonies? The investigation was the first of its kind, aside from hyperspectral detection of American Foul Brood in honey bee larvae (Yones et al., 2019). Although specific vibratory features could not be found within the accelerometer data for trembling behaviour, there is now scope to build upon this analysis and extend the research to a wider range of symptomatic honey bee diseases.

I now comment on the major benefits of the research conducted in this thesis.

#### 6.2.2. The discovery of the jolting pulse

Prior to my research, it was unknown if Varroa mites produced detectable vibrations. I have here pushed the boundaries of our knowledge in this field, not only identifying that Varroa mites create vibrations that can be captured and analysed, but also discovering a novel mite behaviour that has a corresponding vibration. Without synchronous audio and visual data collection, as implemented in my studies, this finding may not have come to light.

The detailed characterisation and analysis of the jolting pulse has facilitated the prospect that Varroa may in fact purposefully transmit vibration, where previously it was only briefly considered that it may be receptive to this form of stimuli. Many questions now follow. It is

hoped that as a result of this revelation, more interest is granted to the subject of Varroa mechanoreception/transmission. In doing so, it is likely that we will increase our understanding of how this species navigates its life cycle, potentially to the benefit of honey bees, as future discoveries may aid mite management and control.

### 6.2.3. Vibration capture as a remote mite detection strategy

Non-invasive Varroa mite monitoring is a research area that is still in its early stages. The work carried out as part of this thesis has added accelerometers and vibration as a measured parameter to the repertoire of methods already under investigation. It is suggested that a variety of monitoring sensors and media will benefit honey bee colony monitoring (Zacepins et al., 2015), as it would help to paint a more detailed image of colony life, for improved interpretation and management. Vibration sensing can now be considered as a potential tool alongside gas sensors, video monitoring, and audio capture.

This work pursued a novel detection method that had previously only been used to automatically identify and monitor the vibrations of the bees themselves (Bencsik et al., 2011; Bencsik et al., 2015; Ramsey et al., 2017; Bencsik & Newton, 2018; Ramsey et al., 2018; Ramsey et al., 2020). I have here demonstrated that, under certain conditions, it is possible to discriminate the vibrations of a much smaller species that inhabits the colony environment, through the utilisation of detailed vibration data. This highlights the benefit of careful mite pulse characterisation and understanding. We not only gain advantage through increased knowledge of the species' biology and behaviour, but also through automatic detection of similar signals in long-term data.

There is another potential application for the method used in my work, which is the detection and characterisation of the vibrations of other small pests that inhabit the honey bee colony environment, e.g., the small hive beetle, *Aethina tumida* (5.7mm length, 14.2mg (Ellis et al., 2002)). Although not yet found in the UK, this destructive pest has spread from its native country (Africa) to Australia and the USA, and has more recently been detected in Italian honey bee hives (Hood, 2004; Granato et al., 2017). The characterisation and detection of small hive beetle vibrations by accelerometers could be of use for the identification of this species in the countries where it is prevalent and aid early detection in colonies worldwide to help monitor its spread and reduce the chance of infestation spread.

Mite vibration detection has potential as a non-invasive monitoring tool. I here implemented the first steps in this exploration, highlighting the brood-comb as a suitable starting location. In characterising mite walking and jolting pulses, honey bee emergence signals, and

background vibrations, I was able to carefully optimise the training database and identify discriminatory features. This work encompasses the important beginnings of an exciting new research avenue: remote Varroa monitoring via the detection and characterisation of their vibrations.

#### 6.2.4. The implementation of 2DFT images

As mentioned throughout this thesis, the 2DFT has taken the spotlight in much of the analysis. Whilst it has been somewhat neglected as a visualisation tool in animal related vibration/acoustic research, here it has served three out of four of my results chapters. The 2DFT has revealed the unique gait of a Varroa mite, and provided the most favourable discrimination outcome for honey bee, mite, and background vibrations for detection purposes. Although specific features could not be identified in honey bee CBPV 2DFT analysis, this type of visual inquiry has still benefited the investigations, allowing me to narrow down frequency bands of interest and eliminate those that are redundant. It has also revealed a vibrational trace that may be inherent to the physiology of a honey bee. Furthermore, the 2DFT has identified the key features of a novel honey bee signal, in providing the best possible visualisation of this repeated pulse.

### 6.3.0. Limitations to the work carried out in this thesis

#### 6.3.1. The accelerometer

The model of accelerometer used throughout this thesis is the most sensitive available for its size (10mm<sup>3</sup>) and mass (10g). It is highly suitable for capturing the vibrations of honey bees and has done a very good job of detecting honey bee purrs for visualisation and feature extraction. However, vibrations originating from Varroa mites have suffered from poorer signal-to-noise-ratio (SNR) due to the animals' size and mass, and the sensitivity of the accelerometer. This is unavoidable, as the best model of sensor available for this work has been utilised. Accelerometers of higher sensitivity do exist, but there is a trade-off with sensor weight, where higher sensitivity requires a heavier device. The problem with this is that a Varroa mite would not be large enough to subject the sensor to the vibratory force required for detection, and therefore it would not help to use a heavier, more sensitive accelerometer.

#### 6.3.2. The experimental set-up

To confirm the association between behaviour and vibration, synchronous video and accelerometer evidence was first required. For Varroa mites, this meant that observations needed to occur outside of their natural environment (the brood cells, adult honey bees), as

their behaviours and vibrations would have been masked by those of the colony, and/or hidden beneath the capped cells. Furthermore, mites are such small animals, that I was not even sure if they could produce detectable vibrations. For these reasons, it was necessary to remove them from the colony and place them in an easy-to-observe environment, free of background noise interference.

One limitation to this method is that the mites may not have been producing natural, normal behaviours. The experimental design implemented in this thesis, where mites were initially observed on Petri-dish in a sound isolated room was, however, the best possible scenario that I could come up with for identifying whether Varroa vibrations could be captured at all. From this, I have been able to slowly build upon the results, asking new questions about the behaviours and vibrations that were spotted, and designing further experiments around these questions, to find out how natural the behaviours are, and when/where/why they occur.

Mites were always placed within close contact of the accelerometer. This was advantageous for detecting and characterising mite vibrational pulses, but for remote detection purposes, however, the results gathered may not be applicable to the whole colony environment. I have shown that when residing on dense brood-comb, mite vibrations can still reach the accelerometer to a good degree. But more work is needed to establish whether Varroa vibrations can pass through larger sections of comb, considering that currently only two to four accelerometers are placed on an entire frame loaded with brood/honey in a hive for automatic detection purposes (Ramsey et al., 2017; Ramsey et al., 2018). Perhaps it will be that more accelerometers are required for meaningful mite capture.

### 6.3.3. Mite collection method

The mites used in this study were collected from the bottom board of honey bee colonies. There is the risk that these individuals were damaged, nutritionally deprived or suffering from some physiological ill-health as a result of no longer being in the colony, and this may have affected the behaviours observed.

However, Varroa were acquired daily and many were active on the board, indicating that they had not been away from their honey bee hosts for long. They also remained highly active once placed in the recording set-up, and were often long lived, with individuals surviving for at least 24 hours. Collecting mites from the bottom board is also considered to be a viable method (Le Conte, 2019), even though it is not the standard described technique (Dietemann et al., 2013). This is because mites are known to pass from one adult bee to

another, fail to attach to an adult bee during emergence from a brood cell, or are removed via grooming (Le Conte & Arnold, 1987; Martin, 1998). This can therefore lead to a supply of healthy, phoretic mites at the bottom.

Collecting individuals from the bottom board was the most suitable method of collection in terms of gathering numerous individuals for observation. During the autumn months in particular, daily live mite collection regularly reached double figures. Opening capped brood-comb to find and extract mites was carried out as described in chapter 3, for the artificial rearing experiment and was a slow and laborious process that did not provide as many individuals as bottom board collection. As one of the main aims of this thesis was to demonstrate the detectability of Varroa vibrations, stringent control of the mite source was not required. However, for future experiments that involve behavioural manipulation, for example investigating the purpose of the jolting pulse, this would need to be considered more closely.

#### 6.4.0. Future recommendations

This work encompasses a novel scientific pursuit that poses a range of exciting questions and research avenues. I am the first to determine that Varroa mites produce detectable vibrations, and I believe that I have only scratched the surface of Varroa vibration research. Studying the function and mechanism behind jolting pulse production is particularly important, as my work so far indicates that it serves a purpose. In following up this discovery, new and meaningful results could be found that add novel perspectives on the species' sensory systems and life cycle. A stronger understanding of the role that vibration may play could lead, amongst other things, to new management techniques for this pest within honey bee colonies.

Equally, further investigation into alternate mite behaviours could benefit their remote detection. The back-and-forth motion observed on the larvae in the artificial capsule experiment exhibited a strong, detectable vibration (see Appendix 2, Video D26). Characterising and discriminating this pulse could be a better brood-comb detection strategy than focusing on walking pulses that can suffer poor SNR. The most important first step in identifying the potential of this vibration, and perhaps others, is probably to achieve successful rearing of a Varroa and bee larva in a gelatine capsule with synchronous video and accelerometer recording. Additionally, the success of this experiment would also provide stronger evidence for whether jolting pulses do occur in the reproductive phase or not, as the full rearing process would be monitored.

A crucial step towards remote mite detection is the exploration of mite vibration capture on the bottom board. As described in detail in chapter 3 (see section 3.7.4.), this experiment would overcome many of the challenges faced in brood-comb sample detection and has a better chance of achieving discrimination and detection success. It may still be possible to detect mites within the brood cells, as some progress was made particularly in terms of training database optimisation, but the most promising route for this work does appear to be bottom board monitoring, at present.

The characterisation of vibrations linking to CBPV related trembling was not achieved in this case, but I have identified critical areas for further examination, as outlined in chapter 4. Accelerometers could benefit early virus detection in the case of symptomatic diseases such as CBPV and Deformed wing virus, but more controlled experimental methods are required. By providing healthy control individuals and comparing them to groups of bees that have been subject to specific doses of virus in a contained, laboratory setting, the detected vibrations could be better characterised, and this in turn would assist automatic detection. Honey bee trembling symptom feature extraction may also gain advantage from sound isolated recordings, as was demonstrated with Varroa mite vibration capture, where observations benefited from sound isolated recordings.

The identification of the novel honey bee purr signal is also a significant finding that now requires further work. I have determined the features of this vibration and recommend that the next important step is to identify pulse production within the hive. This can be achieved through automatic detection of the signal within long-term recordings, as demonstrated for the honey bee dorso-ventral abdominal vibration and 'whooping' signal (Ramsey et al., 2017; Ramsey et al., 2018). Knowledge of when, and how often, honey bee purr vibrations are produced would begin to indicate function. The more honey bee signals we understand, the better for establishing colony status and events through non-invasive monitoring. The more accurate our monitoring processes are, the easier it will become to implement colony management techniques in a timely and non-disruptive manner, for healthier, productive hives.

### 6.5.0. Conclusion

In this thesis, I have presented novel research that has helped to bridge a gap in knowledge for both Varroa vibration and non-invasive Varroa and honey bee monitoring. Accelerometer sensors have proven to be of great value in the discovery and characterisation of a range of Varroa and honey bee vibrations, demonstrating their use in colony monitoring and the

deeper understanding of the two species' biology and behaviour. It is hoped that this device, which captures such richly detailed data (that consists of the vibrations of many bee individuals over prolonged periods), can be even better appreciated and have wider implementation for its contribution to honey bee and Varroa research.

As with all new discoveries, such as the revelation that Varroa produce detectable vibrations, one of which is new to science, a new gap in knowledge is created that is yearning to be filled. My work here has laid the groundwork for this enterprise, answering some queries, and unearthing new ones. As Karl von Frisch stated: "the life of a bee is like a magic well: the more that you draw from it, the more there is to draw" (Kirchner et al., 2022). There is much to learn about honey bee and Varroa vibration, and I hope that my endeavour in this field can inspire future enthusiasm for exploring this fascinating subject.

# Chapter 7: Appendix 1

**Video S1:** A video demonstrating an individual mite walking, together with the measured vibrations in spectrogram form. The logged coordinates of mite movement allow the individual to be tracked within the field of view which is continuously updated. The right-hand side panel detects the changes between two consecutive images of the original cropped video panel. When motionless the mite remains dark blue in this panel, but the pixels flash red when the mite is walking. The synchronicity between mite movement and the vibrational traces seen on the top spectrogram panel can clearly be seen. This movie soundtrack, which is the accelerometer signal, also demonstrates the audible 'clicking' of mite walking vibrations, which are also synchronous with the movement and spectrogram traces. The spectrogram of the accelerometer data is shown with respect to time, with acceleration magnitude in logarithmic (to the base 10) format, with dark red always forced to be  $6 \times 10^{-3} \text{ m/s}^2$  (for ease of viewing the walking traces) as the highest point of magnitude at any point in time and dark blue as 1/50 of the maximum. This movie and its corresponding audio track are slowed from the original 50 – 25 frames per second for better viewing.

**Video S2:** A short video extract of a Varroa mite performing a gravitational reflex response. The mite in the centre of the Petri-dish is positioned on its back and flips itself into the correct orientation. The vibratory signal coming from this movement can be heard. The soundtrack of the video is the signal coming from the accelerometer that can be seen secured to the Petri-dish.

**Video S3:** A short video extract of three Varroa mites interacting with one another. The cause of this interaction is unknown but has been seen on a handful of occasions where mites come into close contact with one another and appear to become 'stuck' on each other's legs. This causes them to roll around the Petri-dish until they become dislodged from one another. The vibratory signal produced by this interaction can be heard in this video. The soundtrack of the video is, again, the signal coming from the accelerometer that can be seen secured to the Petri-dish.

**Video S4:** A short video extract of Varroa defecation behaviour. The video insert focuses on the mite of interest. This behaviour does not produce a detectable accelerometer trace, in spite of the large periodic displacement the animal exhibits prior to defecation.

**Video S5:** Video showing the accelerometer data in spectrogram format and synchronous displacements of the Varroa individual on Petri-dish. The excerpt demonstrates approximately ten seconds of continuous jolting behaviour slowed down ten times for ease of viewing and hearing of the rapid jolting behaviour. The soundtrack of this video, also slowed by a factor ten, results in the ultra-high frequency (23,000 Hz) jolting pulses to be heard at 2200 Hz. Not all pulses produce an audible signature, but for those that do, the sound could be described as a quiet 'clinking' noise. The

spectrogram shows acceleration magnitude in logarithmic (to the base 10) scale, with dark red showing the highest magnitude and dark blue as the lowest at 1/70 of the maximum. The maximum acceleration magnitude is forced to be that of the Varroa jolting pulses for better viewing. The original video data is shown in panel 'a'. Panel 'b' is a replica of this data, further cropped on the mite and demonstrate simple edge detection by means of the spatial gradient of the pixel intensity. Panel 'c' further shows the temporal changes in pixel intensity in two consecutive frames seen in panel 'b'. When motionless the mite is mostly seen as dark blue in 'c', but when moving the pixels flash red. The sum of the pixel intensities in this panel are then displayed as the white line superimposed on the spectrogram data, demonstrating the remarkable synchronicity between video-detected mite displacement and accelerometer trace.

**Video S6:** Video showing the accelerometer data in spectrogram format and synchronous displacements of the Varroa individual on brood-comb. The processing for all panels in this video has been completed in the same way as for videos S5, S7 and S8, with the video slowed to four times for ease of viewing. The lowest point of acceleration magnitude is here forced to be 1/60 of the maximum. As the mite jolting pulses are more spread out over time on this substrate and the vibrational pulse is inherently of a lower frequency, the frame rate did not need to be slowed as much as it did for video S8. The soundtrack has also been slowed accordingly and still reveals an audible jolting pulse in some instances, this time as a 'knocking' noise. Several jolting instances are included in this video from different points in time to showcase occurrences where the jolt produces a measurable vibrational trace. Although this mite jolted frequently throughout the video, detectable instances of vibration occurred at more irregular intervals. Here too, the synchronicity between mite movement and accelerometer trace can be clearly viewed. Overall, this video amounts to approximately 38 seconds of real-time data.

**Video S7:** Video showing the accelerometer data in spectrogram format and synchronous displacements of the Varroa individual on empty, fully built honeycomb. The processing for all panels in this video has been completed in the same way as for videos S5, S6 and S8, with the video slowed to four times for ease of viewing. The lowest point of acceleration magnitude is here forced to be 1/10 of the maximum. The mite in this video pulses 28 times over a period of approximately four minutes, so the frame rate did not need to be slowed down to five frames-per-second (FPS) as with video S8, where jolting pulses are rapid and continuous. Due to the less regular production of pulses, there are many stretches of time where no jolting pulses occur. To view the synchronicity quickly and easily between mite displacement and accelerometer trace, instances of jolting have been cut together, thereby removing those time periods where no activity occurred. Overall, this video accumulates approximately 24 seconds of mite activity. The soundtrack (i.e., the signal from the accelerometer) has also been included and slowed accordingly. The jolting pulses can be heard in some instances as a 'clapping' noise.

**Video S8:** Video showing the accelerometer data in spectrogram format and synchronous displacements of the Varroa individual on the gelatine capsule. The processing for all panels in this video has been completed in the same way as for videos S5, S6 and S7, with the video slowed to four times for ease of viewing. The lowest point of acceleration magnitude is here forced to be 1/50 of the maximum. As with S7, the mite in this video jolted 28 times over a period of approximately six minutes, so the frame rate did not need to be slowed down to five FPS like it did in S5, where jolting pulses are rapid and continuous. As there are only three jolting pulses that have a visible accelerometer trace, only those three have been included in this video. Time periods in between have been removed, in the same way as for S6 and S7. Overall, this video contains approximately ten seconds of mite activity. The soundtrack has been slowed to match the frame rate of the video. The jolting pulses can here be heard as ‘tapping’ noises.

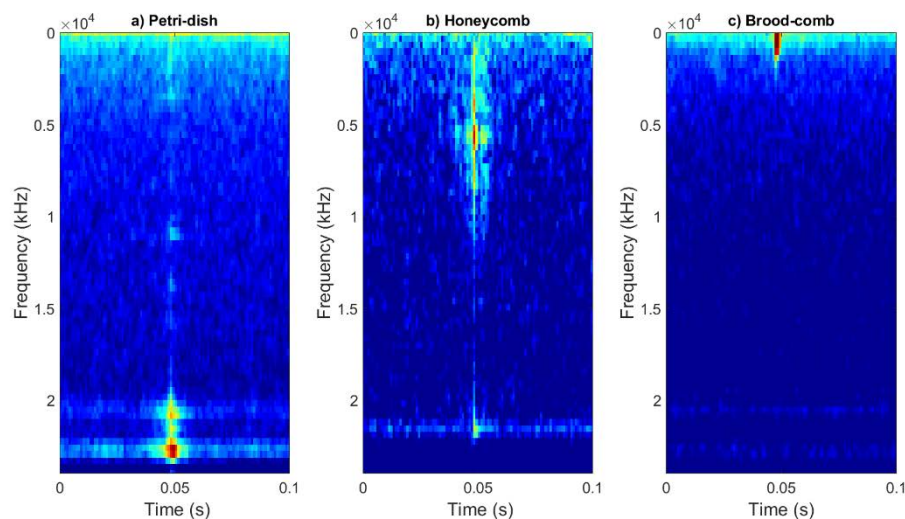


**Figure S9:** A series of spectrograms to demonstrate the filtering parameters chosen for each collection of jolt pulses to improve the alignment process. A selection of pulses from each substrate collection were averaged to produce each panel. This number differed based upon the number of pulses that showcased clarity (Petri-dish = 40, honeycomb = 8, brood-comb = 40). Background frequencies were filtered as follows: 19,000 Hz high-pass (panel ‘a’), 500 Hz high-pass and 12,000 – 19,000 Hz band-stop (panel ‘b’), 500 – 2500 Hz bandpass (panel ‘c’), leaving only the frequencies where strong signal occurs. This then produces cleaner accelerometer data for improved scrutiny of the pulses to identify similarities within each substrate. The colour coding of each spectrogram is not relevant for this figure as it serves only the purpose of substantiating the filtering choices.

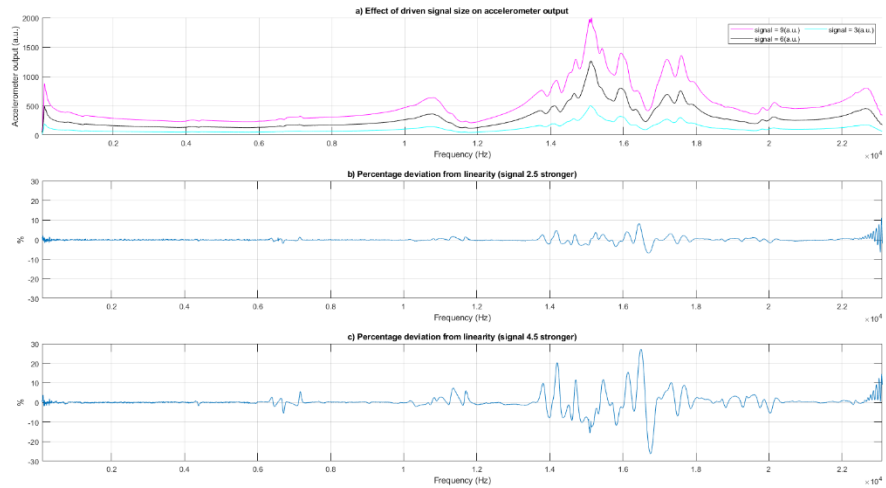


**Figure S10:** Accelerometer sensitivity and linearity with frequency. Artificial vibrations with three different magnitudes were driven with a frequency sweep from 0 – 24,000 kHz, with an electromagnetic shaker. The accelerometer outputs (panel ‘a’) are modulated by both the shaker and the crystal responses. The ratio of any two curves (signal = 6, divided by signal = 3 for (panel ‘b’), and signal = 9, divided by signal = 3 for (panel ‘c’)) allows the estimation of the accelerometer’s linearity alone. These figures demonstrate the remarkable linearity of the sensor, except for the bandwidth between 14,000 – 18,000 Hz and frequencies beyond 23,000 Hz, where up to 10% deviation can be seen. The signals of interest seldom or never overlap with these frequency bands.

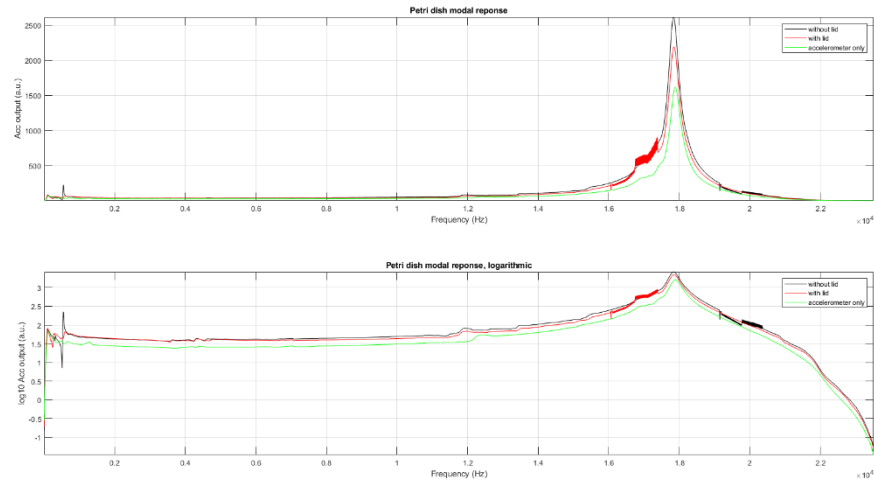


**Figure S11:** Accelerometer modal response, with Petri-dish, Petri-dish and lid, and alone. An artificial vibration was driven at a 25% magnitude of the PC maximum output volume with a frequency sweep from 0 – 24,000 Hz, via an electromagnetic shaker, to the accelerometer (green), accelerometer glued to the Petri-dish (black) and the accelerometer glued to the Petri-dish with the lid placed on (red). These figures demonstrate the linearity of the recording system in both linear and logarithmic scales. A large deviation from linearity is seen at 18,000 Hz, where the signals of interest are seldom seen. The only other discrepancy is seen at 500 Hz, where the Petri-dish exhibits a resonance. The electromagnetic shaker is incapable of vibrating the accelerometer beyond 21,000 Hz, causing the large drop of response seen at ultra-high frequencies.

**Video S12:** A short video extract of *Varroa* jolting behaviour in a Petri-dish. The video insert shows a magnified cropped area for better viewing. The fast left and rightwards displacement of the body can be clearly seen. There is no associated sound with this video as the jolting in this case lacks a detectable accelerometer trace.

**Video S13:** A short video to demonstrate a few instances of jolting behaviour where the mite appears to push its body in an up and down motion by flexing its legs, rather than the more commonly seen side to side motion. Each instance is of the same mite individual during the same filming session, after it has been edited to remove periods of time where this behaviour is not seen.

**Video S14:** Video showcasing the full collection of 250 Petri-dish *Varroa* jolting pulses. Every pulse in the collection is aligned to the centre of the window and presented in decreasing order of strength. The full breadth of variation can be seen between the jolting pulses when viewing them in this way. The magnitude of acceleration is logarithmic (to the base 10) where the highest magnitude is  $2 \times 10^{-3} \text{ m/s}^2$  and the lowest magnitude forced to be 1/40 of the maximum to reduce the contribution of meaningless noise.

**Video S15:** Video showcasing all 189 brood-comb jolting pulse spectrograms. The jolting pulse spectra have undergone the same centring and analysis as in S14 and S16. The magnitude of acceleration is logarithmic (to the base 10), where the highest magnitude is  $2 \times 10^{-3} \text{ m/s}^2$ , and the lowest magnitude set to be 1/40 of the maximum.

**Video S16:** Video showcasing all 28 honeycomb jolting pulse spectrograms. All pulses are showcased in the same way as those seen in S14 and S15 and share the same analysis. The magnitude of acceleration is logarithmic (to the base 10), where the highest magnitude is  $6.5 \times 10^{-4} \text{ m/s}^2$ , and the lowest magnitude set to be 1/40 of the maximum.

**Video S17:** A video to demonstrate a double peak jolt and single peak jolt in quick succession. Video excerpts taken from the brood-comb jolting video (S6) here show instances of a double peak jolt with instances of a single peak jolt. The video and audio are slowed four times both for easier viewing and hearing of the jolting vibration, which is here heard as a 'knocking' sound. A double peak jolt can first be seen near to the 29.655 min time stamp on the x axis, immediately followed by a single peak jolt near to the 29.665 min time stamp. The difference in body motion can be best seen when viewing these jolting instances side-by-side. For the double peak, the mite appears to move its body right and then left, whereas for the single peak the body only moves to the right. This is immediately followed by two consecutive instances of single jolts at time stamps 30.3 min and 30.315 min time stamps where the body only moves in a single downward motion. A second instance of a double peak can then be seen at the 31.84 min time stamp, where the mite appears to move the body in a downward motion followed by movement to the right. Two audible 'knocks' can be clearly heard for the double peaks, in comparison to the one audible 'knock' for the single peaks.

**Video S18:** A video showcasing mite displacement for the jolting pulse with six consecutive peaks. This is a video excerpt taken from the honeycomb jolting video (S7) slowed four times for ease of viewing. The soundtrack, from the accelerometer, which is also slowed accordingly is included and provides the jolting pulses as audible 'clapping' sounds. The jolting pulse that produces the vibrational trace with six consecutive peaks is seen first at the time stamp 12.265 min on the x axis. The mite moves in a rightwards direction before immediately moving the body forwards, unlike the commonly seen singular left or right body displacement. This is followed by a jolting pulse at the time stamp 12.275 min, which showcases this commonly described movement, as a comparison.

## Chapter 8: Appendix 2

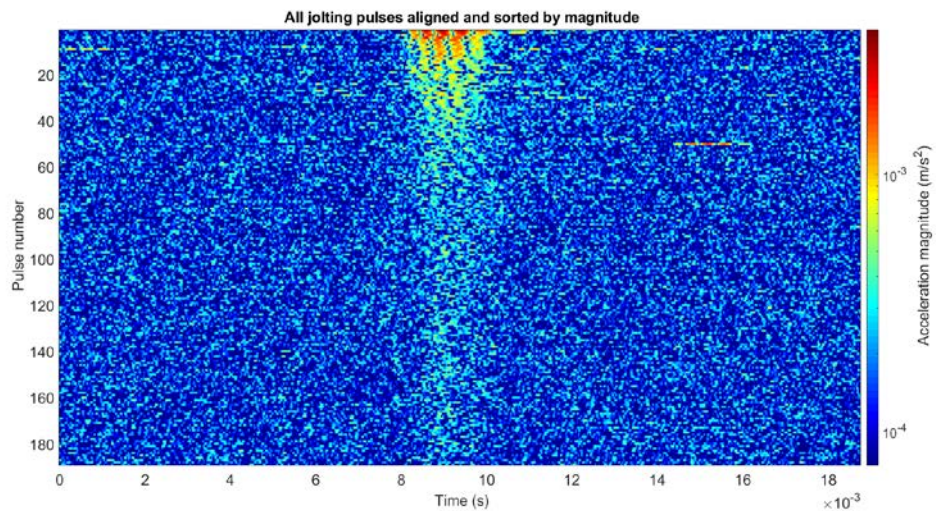


**Figure D1:** The full collection of jolting pulses ( $n = 189$ ) viewed together, following one alignment process using the cross-correlation product. All pulses have been aligned in time to a single reference pulse, using the spectrogram of the pulses for the alignment process. The magnitude of acceleration is logarithmic (to the base 10), where the highest magnitude is dark red ( $3.7 \times 10^{-3} \text{ m/s}^2$ ), and the minimum is dark blue (forced to be  $1/50$  of the maximum). All audio data shown here has been band-pass filtered (500 – 8000 Hz).

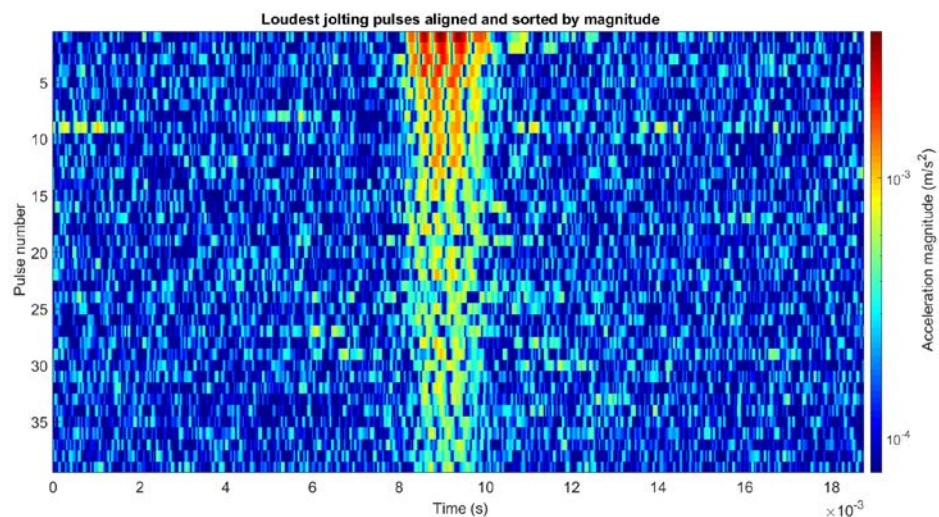


**Figure D2:** The loudest jolting pulses in the collection ( $n = 39$ ) viewed together, following one alignment process using the cross-correlation product. This data is the same as that shown in figure D1, but the window is cropped onto the 39 highest magnitude pulses only.

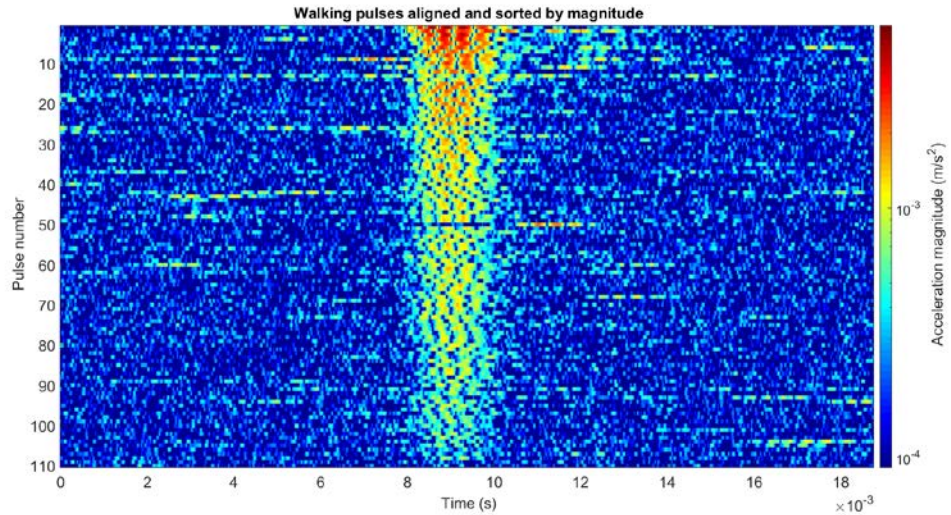


**Figure D3:** The full collection of walking pulses ( $n = 110$ ) viewed together, following one alignment process using the cross-correlation product. All pulses have been aligned in time to a single reference pulse, using the spectrogram of the pulses for the alignment process. The magnitude of acceleration is logarithmic (to the base 10), where the highest magnitude is dark red ( $5.4 \times 10^{-3} \text{ m/s}^2$ ) and the minimum is dark blue (forced to be  $1/60$  of the maximum). All audio data shown here has been band-pass filtered (500 – 8000 Hz).

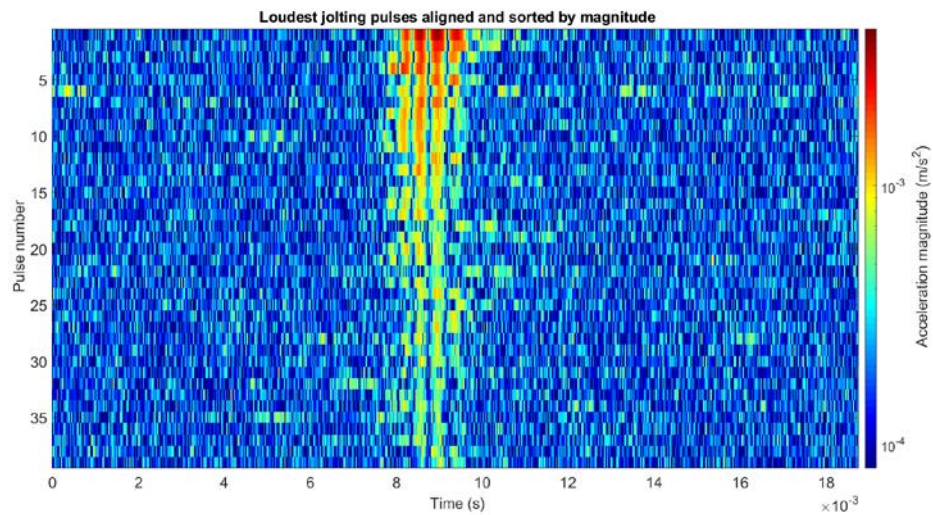


**Figure D4:** The final collection of jolting pulses for the training database, aligned to one another in time. The magnitude of acceleration is logarithmic (to the base 10), where the highest magnitude is dark red ( $3.7 \times 10^{-3} \text{ m/s}^2$ ) and the minimum is dark blue (forced to be  $1/50$  of the maximum). All audio data shown here has been high-pass filtered (500 Hz).

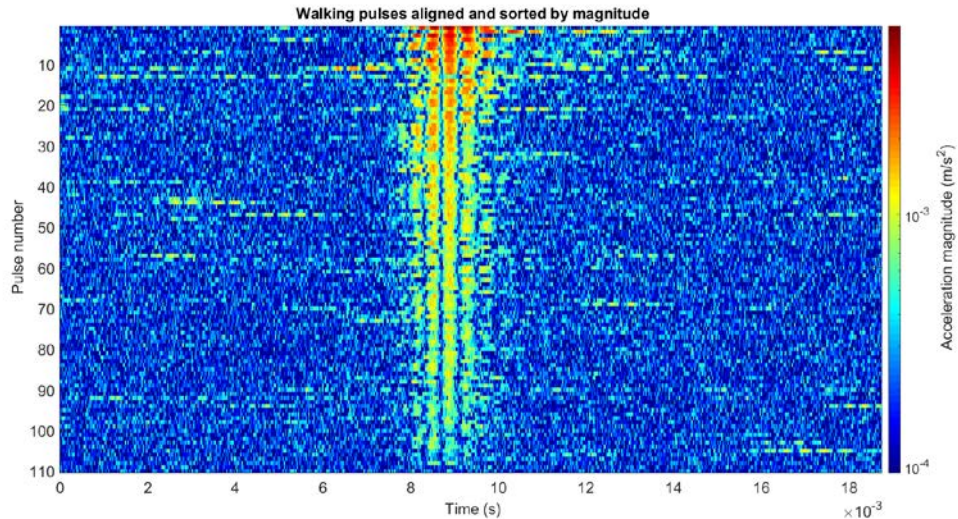


**Figure D5:** The final collection of walking pulses for the training database, aligned to one another in time. The magnitude of acceleration is logarithmic (to the base 10), where the highest magnitude is dark red ( $5.4 \times 10^{-3} \text{ m/s}^2$ ) and the minimum is dark blue (forced to be  $1/60$  of the maximum). All audio data shown here has been high-pass filtered (500 Hz).

**Figure D6:** Method 2: Training database creation and discrimination of temporal features specific to mite jolting and walking vibrational traces

Initially, the raw accelerometer waveform data was used to calculate the second order time differential. Points of steep, negative inflection were indicative of pulse presence in the data. However, the waveform data was not suitable for this analysis as too many negative inflection points were identified in each time window that was tested.

Instead, the accelerometer data was transformed into a spectrogram, and the same analysis was carried out. Four different functions and five different parameters were tweaked and tested to find the optimum pulse search tool.

Parameters:

1. The time window length. Initially this was identified as a 0.1 second time window, with the pulse at the centre of the window. Walking pulses demonstrated a number of satellite pulses either side of the centred vibrational trace, whereas the majority of jolting pulses did not. The time window was tweakable, to increase or decrease the amount of time either side of the centred pulse, therefore also increasing or decreasing the number of satellites (for jolting pulses, the window needed to cut-off before a new, unrelated jolting pulse was produced).
2. The multiplication factor of the spectrogram. Altering the multiplication factor value caused an increase or decrease in the number of interleaving datapoints along the x axis (time). The vibrational data along the horizontal axis in turn became more or less detailed visually.

3. The temporal resolution of the spectrogram. Altering the temporal resolution value caused an increase or decrease in the number of datapoints seen on the y axis (frequency). This changed the detail seen in the vibrational data vertically.
4. The threshold value. A threshold value was chosen to identify steep points of negative inflection. If a point fell beyond this threshold, it was identified as a walking or jolting pulse. This threshold could be altered to allow the capture of more or fewer points.
5. Normalisation of the data. The data was tested when normalised, and when not.

Functions:

1. Function 1: simply counting the number of negative inflection points that fell beyond the threshold.
2. Function 2: calculating the mean of the second order time differential of the spectrogram and identifying if there was a difference in the average of walking and jolting time windows.
3. Function 3: finding differences in the spectrum of the second order time differential (threshold not required in this case).
4. Function 4: plotting a histogram of the second order time differential of the spectrogram (threshold not required in this case).

Function 1 produced the best outcome for discriminating between the two groups. The optimum parameters were identified as a time window of 0.11 seconds, a threshold value of  $-5 \times 10^{-6}$ , a multiplication factor of four, and a temporal resolution of 0.0005s.

When viewing the data, generally it appeared that walking pulses fell at a value of five (i.e., five negative inflection points per window) or above, and jolting pulses fell at a value of four (i.e., four negative inflection points per window) or below (see Figure D7). To identify the optimum parameters required for good discrimination, this critically assessed boundary of five was used. The best outcome was chosen based on the number of walking pulses that fell at five or above and the number of jolting pulses that fell at four or below. The parameters that worked together to produce the best discrimination based on this boundary were chosen as the optimum.

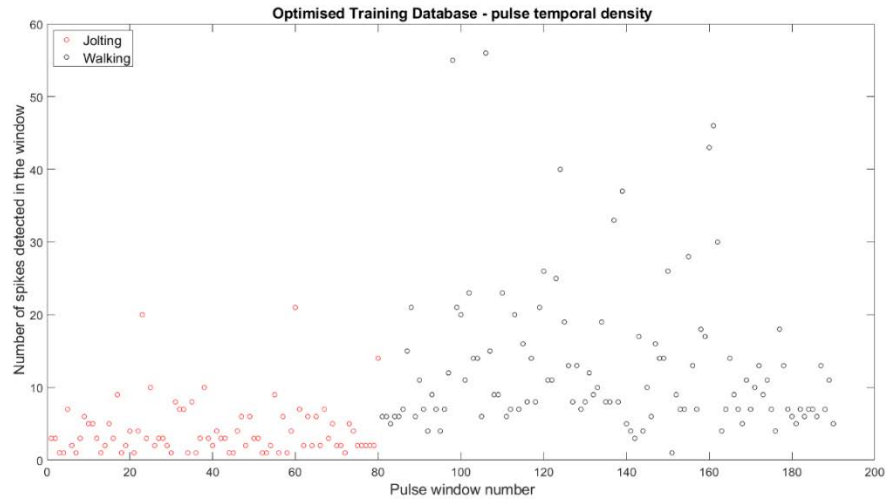


**Figure D7:** Discrimination of the temporal density of walking and jolting pulses within time windows of 0.11 seconds of data. This plot demonstrates the outcome of the optimum parameters that influenced the discrimination between jolting and walking. Each point on the plot represents one time window containing walking (black) or jolting (red) data. The two groups are well discriminated, with little overlap. The number of walking pulses found per window mostly falls at  $\geq 5$ , and the number of jolting pulses found per window mostly falls at  $\leq 4$ . Pulse windows where the genuine, centred jolting pulse was not detected, but satellite traces were (i.e., false positives) ( $n = 65$ ) have been omitted from this plot for the purpose of showing genuine detection successes only.

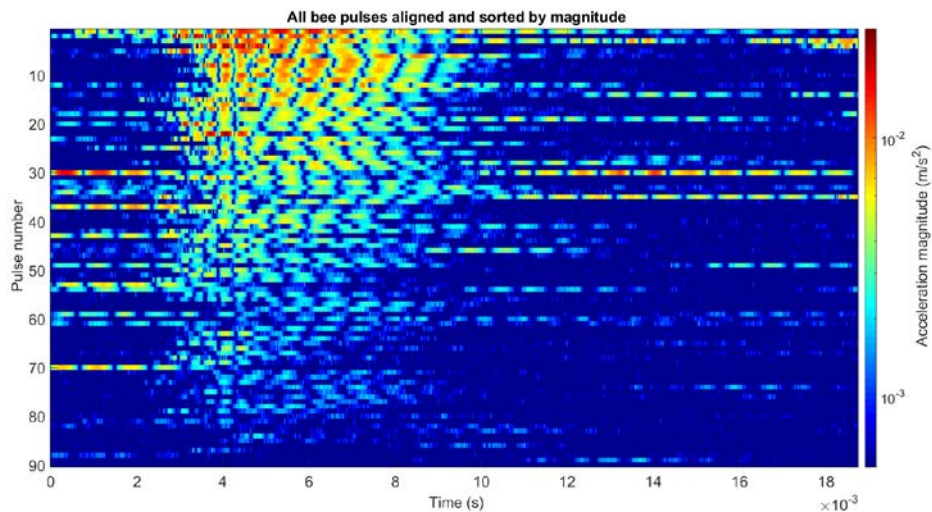


**Figure D8:** All honey bee emergence pulses aligned and sorted by magnitude. A large number of satellite bee pulses occur at either side of the central pulses, as emergence vibrations are repeated regularly within a short time period. The magnitude of acceleration is logarithmic (to the base 10), where the highest magnitude is dark red ( $2.6 \times 10^{-2} \text{ m/s}^2$ ) and the minimum is dark blue (forced to be 1/50 of the maximum). All audio data shown here has been high-pass filtered (500 Hz).

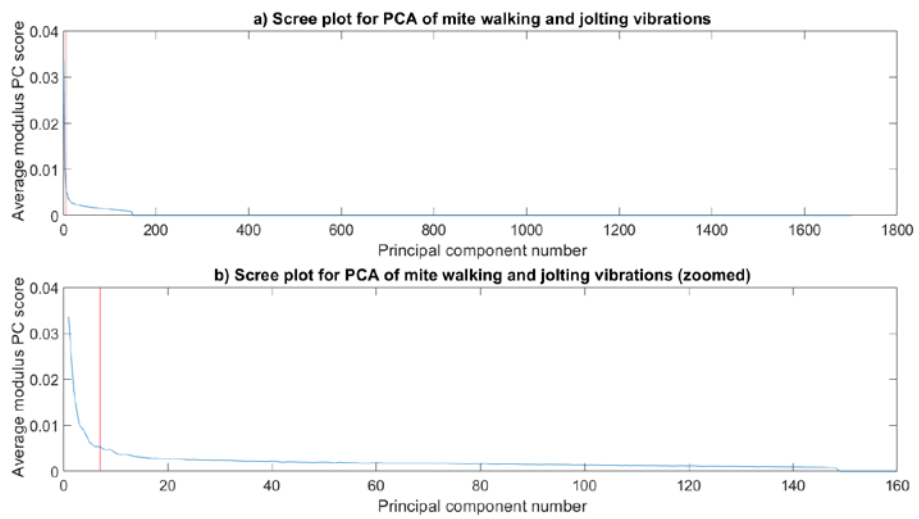


**Figure D9:** A scree plot to demonstrate the number of principal components identified as most appropriate for mite walking and jolting spectrogram discrimination. Panel ‘a’ shows all possible principal components along the x axis, panel ‘b’ shows a cropped version of this figure, to better showcase the principal components of importance. The data below the curve, to the left of the red line are those principal components chosen for discrimination (PC score = 7, percentage deviations 26%).

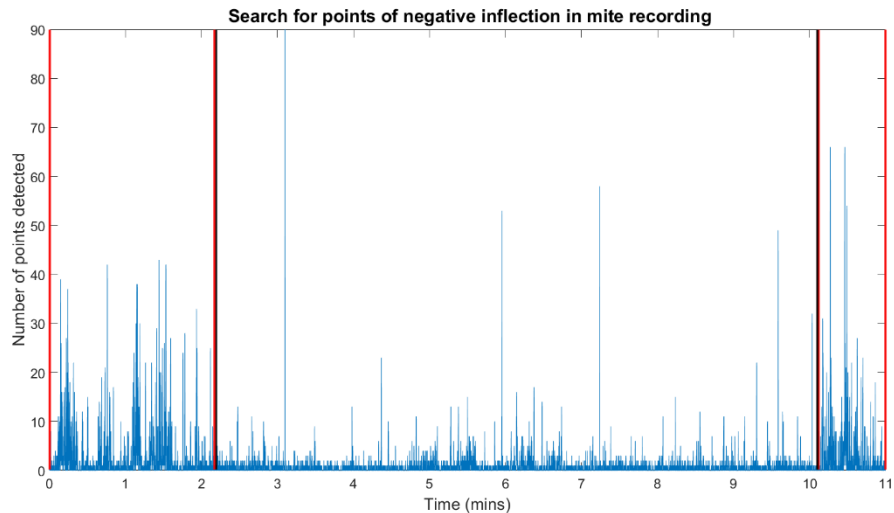


**Figure D10:** Here, 11 minutes of accelerometer data containing Varroa activity was scanned for points of negative inflection. The Varroa was always in view. Using optimised parameters (see Figure D6) the accelerometer data was scanned every 0.11 seconds to count the number of spikes in each time window. The number of spikes exceeds what was expected of this analysis. The data seen between the red bars at the start and end of the plot (0 – 138 seconds and 611 – 660 seconds) relate to Varroa walking activity, with various periods of immobility dispersed throughout. Between the black bars (139 – 610 seconds), the Varroa was jolting and immobile in between consecutive jolts. Because of the very high number of stationary mite periods that were interspersed with activity, there are no bars indicating when the mite was not moving.

**Audio D11:** An audio clip of bee emergence vibrations.

**Audio D12:** An audio clip of mite walking vibrations.

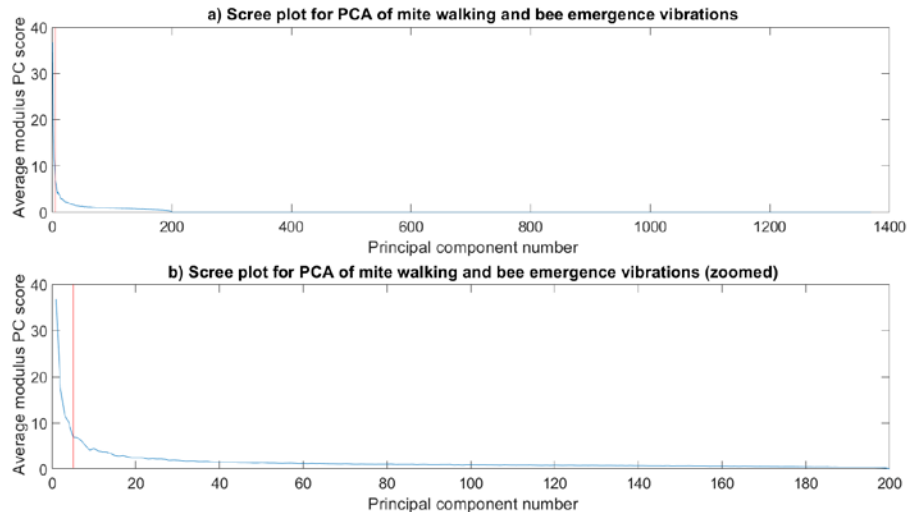


**Figure D13:** A scree plot to demonstrate the number of principal components identified as most appropriate for mite walking and bee emergence spectrogram discrimination. Panel ‘a’ shows all possible principal components along the x axis, panel ‘b’ shows a cropped version of this figure, to better showcase the principal components of importance. The data below the curve, to the left of the red line are those principal components chosen for discrimination (PC score = 5, percentage deviations = 27%).

**Video D14:** A video to demonstrate the unique gait of a Varroa mite, captured as a 2DFT image. Here, the video first shows a bee emerging from her cell, followed by a Varroa mite walking and resting on brood-comb (panel ‘a’). These two concatenated videos run synchronously in time with the accelerometer recording taken from this footage (panel ‘b’). The accelerometer data is transformed into a 2DFT that updates with time, showcasing the frequency (Hz) and spectral repetition (Hz) of the vibrations produced by the bee, the mite and the background as they occur. The accelerometer recording has here been cropped (200 – 4000 Hz) and high-pass filtered (0 – 500 Hz) to best visualise the data of interest. The bottom panel ‘c’ showcases DF space, based on the PCA/DFA results of the 2DFT TDB, which are detailed later in section 3.5.4. The centroid of each of the three TDB DF clusters can be seen (bee = blue, mite = black, background = cyan). The red circle with black ‘tail’ represents the journey taken by the video-related accelerometer data in DF space, in relation to the PCA/DFA TDB results. This panel also runs synchronously in time with both panels ‘a’ and ‘b’. When the bee produces vibrations, the red circle remains in DF space near to the bee centroid, when the mite walks, the red circle moves to the vicinity of the mite centroid, and when the mite is stationary the red circle is found near the background centroid.

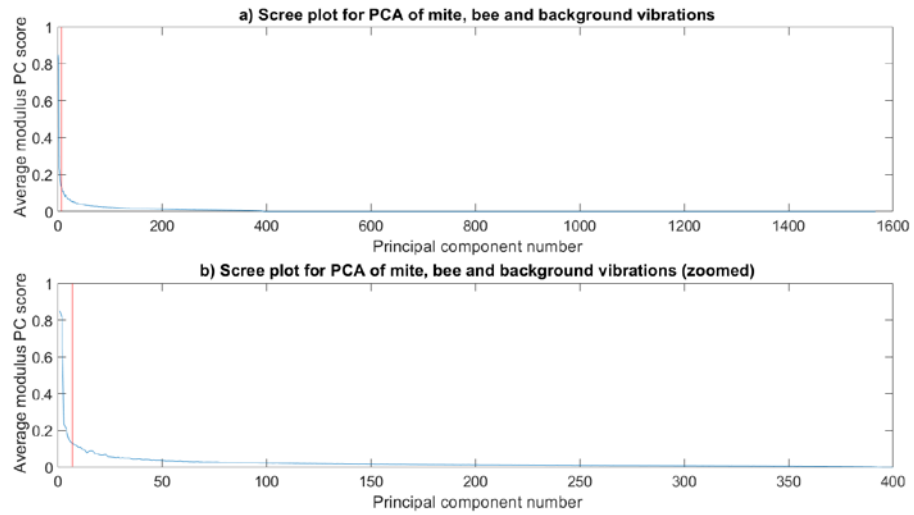


**Figure D15:** A scree plot to demonstrate the number of principal components identified as most appropriate for mite walking, bee emergence and background 2DFT discrimination. Panel ‘a’ shows all possible principal components along the x axis, panel ‘b’ shows a cropped version of this figure, to better showcase the principal components of importance. The data below the curve, to the left of the red line are those principal components chosen for discrimination (PC score = 6, percentage deviations = 25%).

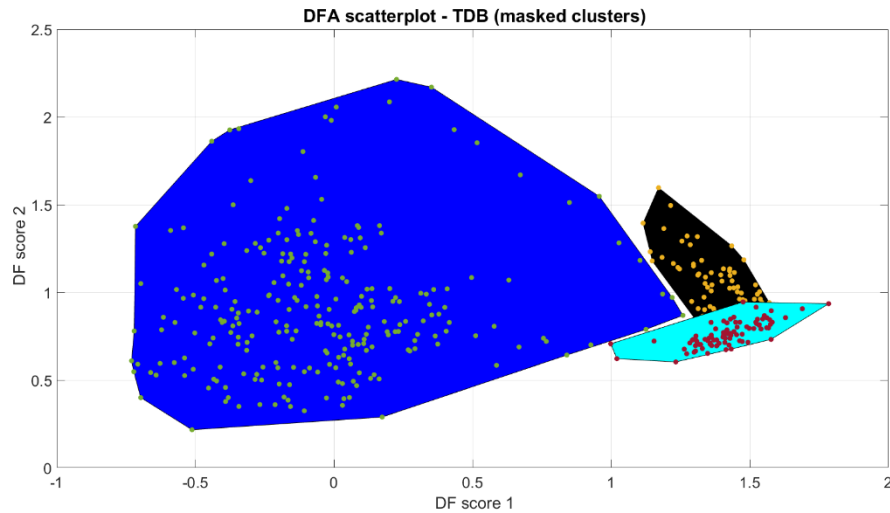


**Figure D16:** The DFA scatterplot outcome with colour-filled ‘masks’. The masked areas incorporate the clustered datapoints for each group (bee = blue, mite = black, background = cyan). The area of each mask is determined by the peripheral datapoints of each cluster. Those that contributed to the TDB are highlighted in alternate colours (bee = green, mite = yellow, background = red). The bee cluster was extended beyond the shape achieved in the original scatterplot (see Figure 3.18). When projecting the full recording of honey bee only brood-comb samples (that contributed to the TDB) onto the scatterplot, there was strong clustering in DF space between the mite and bee mask. All these points were deemed to be honey bee vibrations through critical listening, and as such, the bee mask was extended to include those peripheral points, providing a better representation of the DF space that bee vibrations inhabit.

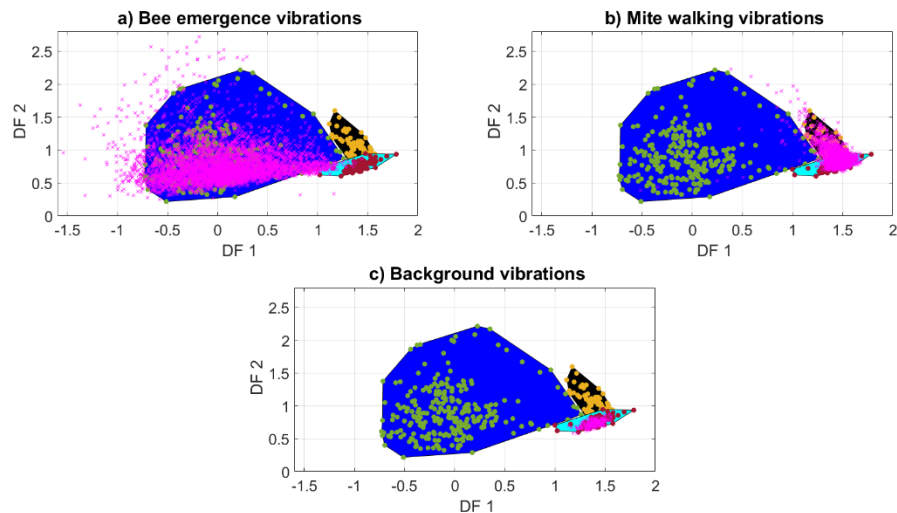


**Figure D17:** A plot to demonstrate the classification of datapoints that were taken from carefully selected time periods within the recordings that contributed to the TDB (pink crosses). Each plot contains a time duration of accelerometer data that represents each group of vibrations represented in the TDB (panel 'a' = bee, 20 minutes; panel 'b' = mite, 12 minutes; panel 'c' = background, 50 seconds). The masked areas incorporate the clustered datapoints for each TDB group (bee = blue, mite = black, background = cyan). The area of each mask is determined by the peripheral datapoints of each cluster. Those that contributed to the TDB are highlighted in alternate colours (bee = green, mite = yellow, background = red). Panel 'b' is representative of mite activity, where the individual walked intermittently for short bursts of approximately one second. As such, background vibrations could not be completely omitted from this data as its purpose is to showcase multiple seconds of mite-related activity.

**Audio D18:** An audio clip of the accelerometer data that contributed to the points falling into the bee mask (see Figure D17). Here, one minute of data has been extracted from the full dataset to evidence the presence of only honey bee vibrations (and some unavoidable background noise) in this cluster. The audio file contains the accelerometer data for 60 points (one point on the DF space plot = one second accelerometer data) that are concatenated for ease of listening.

**Audio D19:** An audio clip of the accelerometer data that contributed to the points falling into the mite mask. This data has undergone the same preparation as Figure D18.

**Audio D20:** An audio clip of the accelerometer data that contributed to the points falling into the background mask. This data has undergone the same preparation as Figure D18 and Figure D19.

**Audio D21:** Audio clip of the vibrations produced by the honey bee in the anomalous recording.

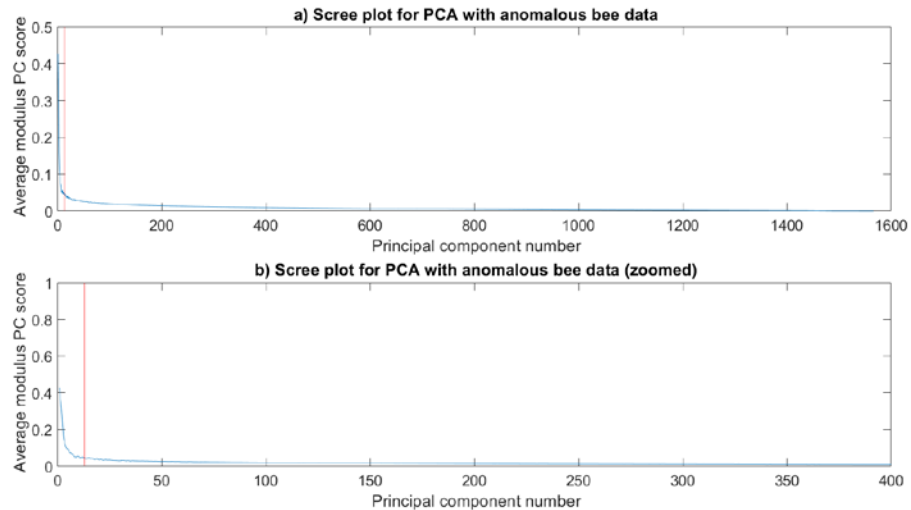


**Figure D22:** A scree plot for the TDB with the fourth category containing anomalous bee vibrations. A suitable number of principal components to include was identified as 13.

**Video D23:** A video to demonstrate the walking pulses on the capsule when the larva is alive. The accelerometer data is here shown in spectrogram format (panel 'a'). Panel 'b' shows the original video of the mite, cropped to zoom-in on the specimen. As the mite moves, the pixels corresponding to the body of the mite flash red (panel 'c'). When the pixels remain blue, the mite is motionless. The soundtrack to this movie is included to demonstrate the audible 'clicking' of the mite walking vibrations that are synchronous with the movement of the mite and the spectrogram traces. The three larger bandwidth peaks at the beginning of the video correspond to a 'clunking' sound made by the incubator and are not related to the mite. The video begins after this vibration is detected, but it is still visible due to the nature of the video building software, which shows the one second of data that precedes the beginning of the video. Both the video and the audio have been slowed four times (down from 50 to 12.5 frames-per-second (FPS)) for easier viewing. The spectrogram of the accelerometer data is shown with respect to time, with acceleration magnitude in logarithmic (to the base 10) format. The maximum (dark red) is forced to be that of the loudest walking pulse of those seen in this video ( $3.5 \times 10^{-4} \text{ m/s}^2$ ) and the minimum (dark blue) is  $1/20$  of the maximum.

**Video D24:** A video to demonstrate the walking pulses on the capsule when the larva is deceased. The analysis used to create video D23 has also been used for this video. There is a period of mite walking that isn't audible or detected as vibrational traces (between time stamps 67.88 and 67.92), showing that not all walking pulses are detectable by accelerometer, although the vast majority can be seen in the spectrogram. The movie soundtrack is included with this video, which demonstrates the audible 'clicking' of mite walking vibrations that are synchronous with the movement and spectrogram traces. Both the video and the audio have been slowed four times (from 50 to 12.5 FPS) for easier viewing. The spectrogram of the accelerometer data is shown with respect to time, with acceleration magnitude in logarithmic (to the base 10) format. Here the maximum (dark red) is forced to be that

of the loudest walking pulse of those seen in this video ( $3.3 \times 10^{-4} \text{ m/s}^2$ ) and the minimum (dark blue) is 1/20 of the maximum.

**Video D25:** A video of a honey bee larva in the capsule with its corresponding accelerometer track viewed as a spectrogram. Here, the Varroa mite is deceased, to showcase evidence that the accelerometer traces seen in the spectrogram are produced only by the larva. Thirty seconds of accelerometer and video data are shown at 50 FPS. In the spectrogram panel, the magnitude of acceleration is logarithmic (to the base 10), where the highest magnitude (dark red) is forced to be that of the loudest larval 'click' ( $0.25 \text{ m/s}^2$ ) and the minimum is 1/200 of the maximum (dark blue). The spectrogram panel runs synchronously in time with both the video and audio recordings. The zoomed in panel to the bottom left-hand corner of the video serves the purpose of better showcasing the movements of the larva.

**Video D26:** A video of the behaviour of interest that produces the Varroa multiple peak vibration.

Recording	% points in mite mask	% points in bee mask	% points in background mask	% points falling outside of masks
Honey bee 1	0.07	80	13	7
Honey bee 2	0.01	62	15	23
Mite 1	11	0.7	62	26
Mite 2	12	5	61	22

**Table 1:** The classification outcome for each recording that contributed to the TDB. Percentage overlap of points into each cluster is shown.

Recording number (Varroa present)	% overlap Varroa mask
1	0.4
2	1.3
3	0.3
4	0.04
5	0.7
6	0
7	0.02
8	0.07
Recording number (Varroa absent)	% overlap Varroa mask
1	0
2	0.04
3	0.04
4	0.07
5	10
6	0
7	0.03
8	0

**Table 2:** Percentage overlap of datapoints in the mite mask, seen for each brood-comb recording.

Recording number (Varroa present)	% overlap Varroa mask
1	0.13
2	0.3
3	0.02
4	0
5	0.1
6	0
7	0
8	0.02
Recording number (Varroa absent)	% overlap Varroa mask
1	0
2	0.04
3	0
4	0.04
5	7.2
6	0
7	0.03
8	0

**Table 3:** Percentage overlap of datapoints in the mite mask, seen for each brood-comb recording when the TDB was tweaked to contain 1.5 second accelerometer extracts.

Recording number (Varroa present)	% overlap Varroa mask
1	0
2	0.5
3	0.004
4	0
5	0.08
6	0
7	0
8	0.07
Recording number (Varroa absent)	% overlap Varroa mask
1	3
2	0
3	0
4	0
5	0.01
6	0
7	0

**Table 4:** Percentage overlap of datapoints in the ‘mite only’ area of the mite mask for Varroa present and absent recordings when projected onto the 4 category TDB. Here, 7/10 of the Varroa absent recordings are shown, as three contributed to TDB creation.

## Chapter 9: Appendix 3

**Video T1:** A video to demonstrate a lack of visible trembling, followed by trembling that has been assessed as ‘mild’ and then ‘strong’.

**Figure T2:** The method for the alternative background removal process.

Method 1: The stacked 2DFT of the honey bee recording was sorted by magnitude so that the vertical element that contained the strongest magnitude of acceleration was placed at the beginning of the figure, followed by the second strongest and so on, until all elements were arranged this way. The area of the figure that exhibited the lowest magnitude was expected to include only the background vibrations that were inherent to the room at the time (i.e., periods where the honey bee was motionless). This area was selected and averaged for subtraction (300 vertical elements) (see Figure T3). This method was not used because although the artefact (seen in the chosen background removal method (see section 4.3.5.4)) was not present in this case, the honey bee vibrational traces were not as well defined.

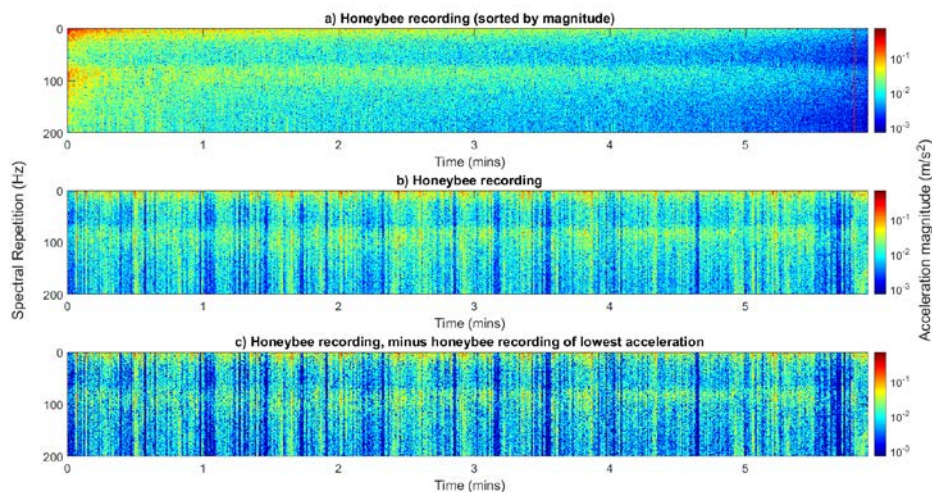


**Figure T3:** The subtraction of the lowest area of magnitude in the honey bee recording. The honey bee recording (panel ‘b’) is sorted by magnitude in panel ‘a’, in the same way that the background recording was in Figure 4.11. A red line indicates the area that was chosen for averaging and subtracting. The honey bee recording minus this area of low magnitude (panel ‘c’) demonstrates a lack of artefact, but there is less definition to the honey bee vibrational traces themselves. The magnitude of acceleration is logarithmic (to the base 10), where dark red is the maximum ( $1 \times 10^{-3}$  m/s<sup>2</sup>), and dark blue is the minimum ( $1/1000$  of the maximum). All panels are scaled identically.

It was also possible to see two frequency bandwidths (0 – 50 Hz, 70 – 140 Hz) across the entirety of the figure, when it was sorted by magnitude (see Figure T3). This perhaps indicated that although the bee was expected to be motionless at the lowest magnitude area of the figure, the bee may have been producing some low-level vibrations that were related to its physiology in some way. Therefore, the averaged area that was subtracted may have included honey bee vibrations as well as background vibrations, biasing the outcome.

**Method 2:** For this attempt at background subtraction, the background recording was averaged and subtracted as it was in the chosen method (see section 4.3.5.4.), but in this case, any pixels that were of a higher magnitude than those seen in the honey bee recording were forced to be zero. In doing so, the artefact seen in the chosen method was removed (see Figure T4).

However, this method was not chosen as there was a disadvantage. By forcing the value of some of the background noise to be a particular, chosen magnitude, it was no longer accurate to the vibrations that were originally recorded. This biased the final outcome of the subtraction, as it had been artificially tweaked to suit my requirements.

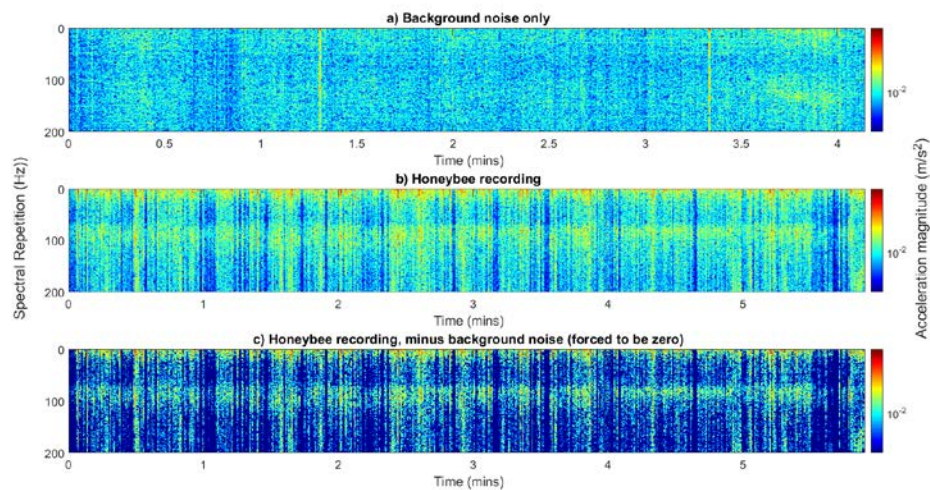


**Figure T4:** The subtraction of the background noise where higher magnitude pixels are forced to be zero. Here, the background recording (panel ‘a’) is averaged and subtracted from the honey bee recording (panel ‘b’). Any pixels in panel ‘a’ that exhibited a higher magnitude of acceleration than those found in panel ‘b’, were forced to be zero to artificially remove the artefact. The magnitude of acceleration is logarithmic (to the base 10), where dark red is the maximum ( $1.2 \times 10^{-3} \text{ m/s}^2$ ), and dark blue is the minimum (1/1000 of the maximum). All panels are scaled identically.

**Video T5:** A video demonstrating a variety of behaviours seen in trembling bee individuals.

**Video T6:** A video demonstrating a trembling bee with head and antennae shaking motions.

**Video T7:** A video demonstrating a trembling bee that is repeatedly stretching its legs out onto the Petri-dish, possibly as a way of attempting to maintain stability.

**Video T8:** The only instance of a black, hairless bee observed on the lifted frame of the CBPV infected observation hive. Unfortunately, the quality of this video is not ideal, but the black bee can be seen in the middle.

**Video T9:** A video of a bee that trembled with its corresponding 2DFT scrolling with respect to time. The 2DFT shows frequency on the y axis, and spectral repetition (the number of frequency revolutions of each spectral component per second) on the x axis. The 2DFT is programmed to run synchronously with the bees' movements in the video. This demonstrates the 2DFT area of interest (0 – 175 Hz, 0 – 30 Hz spectral repetition). The 0 – 175 Hz and 400 – 600 Hz frequency ranges on the y axis peak regularly throughout this video. The 400 – 600 Hz peak is a vibration that naturally occurs from the buzzing of the bees' wings and is not related to CBPV. The 0 – 175 Hz area, which is seen to peak at differing points on the spectral repetition axis between 0 and 30 Hz was chosen for further investigation as a feature of trembling behaviour. The maximum magnitude of acceleration is logarithmic (to the base 10), seen as dark red (and forced to be  $1 \times 10^3 \text{ m/s}^2$  for every frame of the video, for consistency), with the minimum being dark blue (1/200 of the maximum). This video is scaled identically with T10 and T11 for comparison between the three bees.

**Video T10:** A video of a bee that did not tremble with its corresponding 2DFT scrolling with respect to time. This video underwent the same analysis as T9. The maximum magnitude of acceleration is logarithmic (to the base 10), seen as dark red (and forced to be  $1 \times 10^3 \text{ m/s}^2$  for every frame of the video, for consistency), with the minimum being dark blue (1/200 of the maximum). This video is scaled identically with T9 and T11 for comparison between the three bees. Video T9 demonstrated the maximum magnitude of acceleration out of the three compared videos; hence the maximum forced value (red) relates to this.

**Video T11:** A video of a bee that did not tremble, that lacked the frequency bandwidths of interest, with its corresponding 2DFT scrolling with respect to time. This video underwent the same analysis as T9 and T10. The maximum magnitude of acceleration is logarithmic (to the base 10), seen as dark red (and forced to be  $1 \times 10^3 \text{ m/s}^2$  for every frame of the video, for consistency), with the minimum being dark blue (1/200 of the maximum). This video is scaled identically with T9 and T10 for comparison between the three bees. Video T9 demonstrated the maximum magnitude of acceleration out of the three compared videos; hence the maximum forced value (red) relates to this.

**Video T12:** A video of a non-trembling bee moving from an un-conscious to a conscious state. This video demonstrates the inclusion of the 0 – 15 Hz frequency bandwidth that could not be captured with the Sony camera. The top scrolling window shows the accelerometer data as a spectrogram, captured by an Alessi io4 soundcard. The spectrogram scrolls synchronously with the video of the bee.

This top window shows only the frequency bandwidth of interest (0 – 20 Hz). The second window shows the same data, but with a larger frequency range (0 – 200 Hz). The bottom window shows the bee 'waking up' over five minutes. Magnitude of acceleration is logarithmic (to the base 10) where the highest magnitude is dark red ( $0.2 \text{ m/s}^2$ ) and the lowest dark blue ( $1/100$  of the maximum). Both spectrogram windows are scaled identically.

## Chapter 10: Appendix 4

**Audio P1:** An audio clip of a honey bee purr.

**Audio P2:** An audio clip of an exceptionally long honey bee purr.

**Audio P3:** An audio clip of a purr with a preceding 'whooping' signal.

**Audio P4:** An audio clip of what is believed to be a honey bee purr, recorded by Carol Williamson (see related email, Figure P5). Included with permission.

**From:** E C Williamson <[wsbka@yahoo.co.uk](mailto:wsbka@yahoo.co.uk)>  
**Sent:** Wednesday, July 22, 2020 12:59 PM  
**To:** Bencsik, Martin <[martin.bencsik@ntu.ac.uk](mailto:martin.bencsik@ntu.ac.uk)>  
**Subject:** Re: West Suffolk Beekeeping Association winter programme of talks 2020 - 2021

Dear Martin

Thank you for your quick reply. We're really disappointed but I have to agree with your comments: Zoom is just not quite the same as face-to-face and much can be lost by the lack of contact and interaction. I'll certainly be in touch again when conditions improve.

On a personal note, when I googled your name I found that you have researched bees' vibrations so I wonder what you make of the attached clip - I hope it transfers properly. I have WBCs and noticed over the middle two weeks of August 2018 that there was an odd purring noise coming from their direction, so loud that I thought it was a bird in the nearby hedge. I pinpointed a particular hive, queenright, vigorous and productive - the noise was sporadic and loudest under the hive, hence the dubious visuals. They showed no inclination to swarm.

Kind regards

Carol Williamson  
Secretary, WSBKA

**Figure P5:** Email from Carol Williamson, describing the sound that is believed to be a honey bee purr(s).

**Audio P6:** An audio clip of what is believed to be a honey bee purr, recorded by Stephen Fleming. Included with permission. <https://soundcloud.com/bee-craft-magazine/hive-whodunnit>

# Reference List

- Adedeji, A.A., et al., 2020. Non-destructive technologies for detecting insect infestation in fruits and vegetables under postharvest conditions: A critical review. *Foods*, **9**(7), 10.3390/foods9070927.
- Allen, M.D., 1959. Respiration rates of worker honey bees of different ages and at different temperatures. *Journal of Experimental Biology*, **36**(1), 10.1242/jeb.36.1.92.
- Altmann, J., 1974. Observational study of behaviour: Sampling methods. *Behaviour*, **49**(3-4), 10.1163/156853974X00534.
- Ammar, K.N.A.E., 2015. Ultra-structural study of the bee louse *Varroa destructor* Anderson and Trueman 2000 (Acari: Varroidae) with resistance models from *Apis mellifera*. *Journal of the Egyptian Society of Parasitology*, **45**(2), pp.375-384.
- Anderson, D.L., and Trueman, J.W.H., 2000. *Varroa jacobsoni* (Acari: Varroidae) is more than one species. *Experimental and Applied Acarology*, **24**(3), 10.1023/A:1006456720416.
- Annoscia, D., et al., 2020. Neonicotinoid Clothianidin reduces honey bee immune response and contributes to Varroa mite proliferation. *Nature*, **11**(1), pp.1-7.
- Anwarul, S., and Dahiya, S., 2020. A comprehensive review on face recognition methods and factors affecting facial recognition accuracy. In: *Lecture Notes in Electrical Engineering*, 10.1007/978-3-030-29407-6\_36.
- Aumeier, P., 2001. Bioassay for grooming effectiveness towards *Varroa destructor* mites in Africanized and Carniolan honey bees. *Apidologie*, **32**(1), 10.1051/apido:2001113.
- Ayodele, T.O., 2010. Machine learning overview. *New Advances in Machine Learning*, **2**, pp.9-18.
- Azandémè-Hounmalon, G.Y., et al., 2016. Visual, vibratory, and olfactory cues affect interactions between the red spider mite *Tetranychus evansi* and its predator *Phytoseiulus longipes*. *Journal of Pest Science*, **89**(1), 10.1007/s10340-015-0682-y.
- Babic, Z., et al., 2016. Pollen bearing honey bee detection in hive entrance video recorded by remote embedded system for pollination monitoring. *ISPRS Annals of Photogrammetry, Remote Sensing and Spatial Information Sciences*, III-7, 10.5194/isprsannals-iii-7-51-2016.
- Bailey, L., 1965. Paralysis of the honey bee, *Apis mellifera* Linnaeus. *Journal of Invertebrate Pathology*, **7**(2), 10.1016/0022-2011(65)90024-8.
- Bailey, L., and Ball, B.V. 1991. *Honey bee pathology (2<sup>nd</sup> Ed.)*. Academic Press, London, UK.
- Bailey, L., Gibbs, A.J., and Woods, R.D., 1963. Two viruses from adult honey bees (*Apis mellifera* Linnaeus). *Virology*, **21**(3), 10.1016/0042-6822(63)90200-9.
- Bak, B., et al., 2020. Diagnosis of varroosis based on bee brood samples testing with use of semiconductor gas sensors. *Sensors*, **20**(14), 10.3390/s20144014.

- Banga, K.S., Kotwaliwale, N., Mohapatra, D., and Giri, S.K., 2018. Techniques for insect detection in stored food grains: An overview. *Food Control*, **94**, 10.1016/j.foodcont.2018.07.008.
- Baracchi, D., and Cini, A., 2014. A socio-spatial combined approach confirms a highly compartmentalised structure in honey bees. *Ethology*, **120**(12), 10.1111/eth.12290.
- Baracchi, D., Fadda, A., and Turillazzi, S., 2012. Evidence for antiseptic behaviour towards sick adult bees in honey bee colonies. *Journal of Insect Physiology*, **58**(12), 10.1016/j.jinsphys.2012.09.014.
- Barlow, V.M., and Fell, R.D., 2006. Sampling methods for Varroa mites on the domesticated honey bee. *Department of Entomology, Virginia Tech., US. Virginia Cooperative Extension. Publication 444-103*.
- Beer, R.D., and Chiel, H.J., 2003. Locomotion, invertebrate. *CORTEX*, **11**, pp.384–399.
- Beetsma, J., Boot, W.J., and Calis, J., 1999. Invasion behaviour of Varroa *jacobsoni* Oud: from bees into brood cells. *Apidologie*, **30**(2-3), 10.1051/apido:19990204.
- Bell, H., Kietzman, P., and Nieh, J., 2021. The complex world of honey bee vibrational signalling: A response to Ramsey et al. (2017). 10.13140/RG.2.2.28012.82562/1.
- Bencsik, M., et al., 2011. Identification of the honey bee swarming process by analysing the time course of hive vibrations. *Computers and Electronics in Agriculture*, **76**(1), 10.1016/j.compag.2011.01.004.
- Bencsik, M., et al., 2015. Honey bee colony vibrational measurements to highlight the brood cycle. *PLoS ONE*, **10**(11), 10.1371/journal.pone.0141926.
- Bencsik, M., and Newton, M.I., 2018. Honey bee vibration monitoring using the 805M1 accelerometer. *Proceedings*, **4**(1), 10.3390/ecsa-5-05637.
- Bergland, G. D., 1969. A guided tour of the fast Fourier Transform. *IEEE Spectrum*, **6**(7), 10.1109/MSPEC.1969.5213896.
- Bieńkowska, M., and Konopacka, Z., 2001. Assessment of honey bee colonies infestation by the mite *Varroa destructor* based on its natural mortality during the summer season. *Journal of Apicultural Science*, **45**, pp.129-141.
- Bilik, S., et al., 2021. Visual diagnosis of the *Varroa destructor* parasitic mite in honey bees using object detector techniques. *Sensors*, **21**(8), 10.3390/s21082764.
- Birch, M.C. and Keenlyside, J.J., 1991. Tapping behaviour is a rhythmic communication in the death-watch beetle, *Xestobium rufovillosum* (Coleoptera: Anobiidae). *Journal of Insect Behaviour*, **4**(2), pp.257-263.
- Bjerge, K., et al., 2019. A computer vision system to monitor the infestation level of *Varroa destructor* in a honey bee colony. *Computers and Electronics in Agriculture*, **164**, 10.1016/j.compag.2019.104898.
- Blanken, L.J., van Langevelde, F., and van Dooremalen, C., 2015. Interaction between *Varroa destructor* and imidacloprid reduces flight capacity of honey bees. *Proceedings of the Royal Society B: Biological Sciences*, **282**(1820), 10.1098/rspb.2015.1738.

- Boecking, O., 1999. Sealing up and non-removal of diseased and *Varroa jacobsoni* infested drone brood cells is part of the hygienic behaviour in *Apis cerana*. *Journal of Apicultural Research*, **38**(3-4), 10.1080/00218839.1999.11101006.
- Boot, W.J., Driessen, R.G., Calis, J.N., and Beetsma, J., 1995. Further observations on the correlation between attractiveness of honey bee brood cells to *Varroa jacobsoni* and the distance from larva to cell rim. *Entomologia Experimentalis et Applicata*, **76**(3), 10.1111/j.1570-7458.1995.tb01966.x.
- Boot, W.J., et al., 1997. Reproductive success of *Varroa jacobsoni* in brood of its original host, *Apis cerana*, in comparison to that of its new host, *A. mellifera* (Hymenoptera: Apidae). *Bulletin of Entomological Research*, **87**(2), 10.1017/s0007485300027255.
- Bowen-Walker, P.L., Martin, S.J., and Gunn, A., 1997. Preferential distribution of the parasitic mite, *Varroa jacobsoni* Oud. on overwintering honey bee (*Apis mellifera* L.) workers and changes in the level of parasitism. *Parasitology*, **114**(2), 10.1017/S0031182096008323.
- Bozek, K., Hebert, L., Portugal, Y., Mikheyev, A.S., and Stephens, G.J., 2021. Markerless tracking of an entire honey bee colony. *Nature Communications*, **12**(1), 10.1038/s41467-021-21769-1.
- Braga, A.R., et al., 2020. A method for mining combined data from in-hive sensors, weather and apiary inspections to forecast the health status of honey bee colonies. *Computers and Electronics in Agriculture*, **169**, 10.1016/j.compag.2019.105161.
- Branco, M.R., Kidd, N.A.C., and Pickard, R.S., 2006. A comparative evaluation of sampling methods for *Varroa destructor* (Acari: Varroidae) population estimation. *Apidologie*, **37**(4), 10.1051/apido:2006010.
- Bratek, P., and Dziurdzia, P., 2021. Energy-efficient wireless weight sensor for remote beehive monitoring. *Sensors*, **21**(18), 10.3390/s21186032.
- Broad, G.R., and Quicke, D.L.J., 2000. The adaptive significance of host location by vibrational sounding in parasitoid wasps. *Proceedings of the Royal Society B: Biological Sciences*, **267**(1460), 10.1098/rspb.2000.1298.
- Brüel and Kjær, *Product data: piezoelectric accelerometer types 4507 and 4508*. Available from: *Type 4507-B-006 Piezoelectric CCLD Accelerometer*, Brüel & Kjær (bksv.com) [accessed 20/09/2021].
- Brundrett, G.W., 1974. Human sensitivity to flicker. *Lighting Research & Technology*, **6**(3), 10.1177/096032717400600302.
- Calderón, R.A., Chaves, G., Sánchez, L.A., and Calderón, R., 2012. Observation of *Varroa destructor* behaviour in capped worker brood of Africanized honey bees. *Experimental and Applied Acarology*, **58**(3), 10.1007/s10493-012-9579-0.
- Calderón, R.A., Fallas, N., Zamora, L.G., van Veen, J.W., and Sánchez, L.A., 2009. Behaviour of *Varroa* mites in worker brood cells of Africanized honey bees. *Experimental and Applied Acarology*, **49**(4), 10.1007/s10493-009-9266-y.

- Caldwell, M.S., 2014. Interactions between airborne sound and substrate vibration in animal communication. In: Cocroft, R.B., Wessel, A., eds. *Studying Vibrational Communication*. Heidelberg: Springer, 2014, pp.65-92.
- Calis, J.N.M., Boot, W.J., and Beetsma, J., 2006. Attractiveness of brood cells from different honey bee races (*Apis mellifera*) to Varroa mites. *Behavioural Ecology*, **17**, pp.55.
- Carr, A.L., and Roe, M., 2016. Acarine attractants: Chemoreception, bioassay, chemistry and control. *Pesticide*, **131**, 10.1016/j.pestbp.2015.12.009.
- Carreck, N.L., Ball, B.V., and Martin, S.J., 2010. Honey bee colony collapse and changes in viral prevalence associated with *Varroa destructor*. *Journal of Apicultural Research*, **49**(1), 10.3896/IBRA.1.49.1.13.
- Casas, J., Magal, C., and Sueur, J., 2007. Dispersive and non-dispersive waves through plants: Implications for arthropod vibratory communication. *Proceedings of the Royal Society B: Biological Sciences*, **274**(1613), 10.1098/rspb.2006.0306.
- Cecchi, S., et al., 2019. Multi-sensor platform for real time measurements of honey bee hive parameters. In: *IOP Conference Series: Earth and Environmental Science*. IOP Publishing, pp.012016.
- Cecchi, S., Spinsante, S., Terenzi, A., and Orcioni, S., 2020. A smart sensor-based measurement system for advanced beehive monitoring. *Sensors (Switzerland)*, **20**(9), 10.3390/s20092726.
- Chambino, L.L., Silva, J.S., and Bernardino, A., 2020. Multispectral facial recognition: A review. *IEEE Access*, **8**, 10.1109/ACCESS.2020.3037451.
- Chantawannakul, P., et al., 2006. A scientific note on the detection of honey bee viruses using real-time PCR (TaqMan) in Varroa mites collected from a Thai honey bee (*Apis mellifera*) apiary. *Journal of Invertebrate Pathology*, **91**(1), 10.1016/j.jip.2005.11.001.
- Chazette, L., Becker, M., and Szczerbicka, H., 2016. Basic algorithms for beehive monitoring and laser-based mite control. In: *2016 IEEE Symposium Series on Computational Intelligence (SSCI)*. IEEE, pp.1–8.
- Chen, Y.P., and Siede, R., 2007. Honey bee viruses. *Advances in Virus Research*, **70**, pp.33-80.
- Cividini, S., and Montesanto, G., 2020. Biotremology in arthropods. *Learning and Behaviour*. **48**(3), 10.3758/s13420-020-00428-3.
- Clark, C.J., Mountcastle, A.M., Mistick, E., and Elias, D.O., 2017. Resonance frequencies of honey bee (*Apis mellifera*) wings. *Journal of Experimental Biology*, **220**(15), 10.1242/jeb.154609.
- Coineau, Y., Theron, P.D., and Valette, C., 1997. Une association de phanères, constituant probablement un système de communication sonore original chez les acariens. *Acarologia*, **38**(2), pp.111-116.
- Colin, T., et al., 2021. Effects of late miticide treatments on foraging and colony productivity of European honey bees (*Apis mellifera*). *Apidologie*, **52**(2), 10.1007/s13592-020-00837-3.

- Le Conte, Y., 2019. Personal communication.
- Le Conte, Y., et al., 2015. *Varroa destructor* changes its cuticular hydrocarbons to mimic new hosts. *Biology Letters*, **11**(6), 10.1098/rsbl.2015.0233.
- Le Conte, Y., and Arnold, G., 1987. Influence de l'âge des abeilles (*Apis mellifica* L.) et de la chaleur sur le comportement de *Varroa jacobsoni* Oud. *Apidologie*, **18**(4), pp.305-320.
- Le Conte, Y., and Arnold, G., 1988. Etude du thermopréférendum de *Varroa jacobsoni* Oud. *Apidologie*, **19**(2), 10.1051/apido:19880205.
- Le Conte, Y., Ellis, M., and Ritter, W., 2010. Varroa mites and honey bee health: Can Varroa explain part of the colony losses? *Apidologie*, **41**(3), pp.353-363.
- Costa, E.M., et al., 2014. Toxicity of insecticides used in the Brazilian melon crop to the honey bee *Apis mellifera* under laboratory conditions. *Apidologie*, **45**(1), 10.1007/s13592-013-0226-5.
- Couvillon, M.J., 2012. The dance legacy of Karl von Frisch. *Insectes sociaux*, **59**(3), 10.1007/s00040-012-0224-z.
- Crailsheim, K., Hrasnigg, N., and Stabentheiner, A., 1996. Diurnal behavioural differences in forager and nurse honey bees (*Apis mellifera carnica* Pollm). *Apidologie*, **27**(4), pp.235-244.
- Dalmon, A., 2020. Personal communication.
- Dietemann, V., et al., 2013. Standard methods for Varroa research. *Journal of Apicultural Research*, **52**(1), 10.3896/IBRA.1.52.1.09.
- Dillier, F.X., Fluri, P., and Imdorf, A., 2006. Review of the orientation behaviour in the bee parasitic mite *Varroa destructor*: Sensory equipment and cell invasion behaviour. *Revue Suisse de Zoologie*, **113**(4), 10.5962/bhl.part.80381.
- Dittes, J., Aupperle-Lellbach, H., Schäfer, M.O., Mülling, C. K., and Emmerich, I. U., 2020a. Veterinary diagnostic approach of common virus diseases in adult honey bees. *Veterinary Sciences*, **7**(4), 10.3390/vetsci7040159.
- Dittes, J., Schäfer, M.O., Aupperle-Lellbach, H., Mülling, C. K., and Emmerich, I. U., 2020b. Overt infection with Chronic bee paralysis virus (CBPV) in two honey bee colonies. *Veterinary Sciences*, **7**(3), 10.3390/vetsci7030142.
- Diyes, G.C.P., and Rajakaruna, R. S., 2017. Life cycle of Spinose ear tick, *Otobius megnini* (Acari: Argasidae) infesting the racehorses in Nuwara Eliya, Sri Lanka. *Acta Tropica*, **166**, 10.1016/j.actatropica.2016.11.026.
- Donzé, G., et al., 1998. Aliphatic alcohols and aldehydes of the honey bee cocoon induce arrestment behaviour in *Varroa jacobsoni* (Acari: Mesostigmata), an ectoparasite of *Apis mellifera*. *Archives of Insect Biochemistry and Physiology: Published in Collaboration with the Entomological Society of America*, **37**(2), pp.129-145.
- Donzé, G., and Guerin, P.M., 1994. Behavioural attributes and parental care of Varroa mites parasitizing honey bee brood. *Behavioural Ecology and Sociobiology*, **34**(5), 10.1007/BF00197001.

- Donzé, G., and Guerin, P.M., 1997. Time-activity budgets and space structuring by the different life stages of *Varroa jacobsoni* in capped brood of the honey bee, *Apis mellifera*. *Journal of Insect Behaviour*, **10**(3), 10.1007/BF02765605.
- van Dooremalen, C., et al., 2012. Winter survival of individual honey bees and honey bee colonies depends on level of *Varroa destructor* infestation. *PLoS ONE*, **7**(4), 10.1371/journal.pone.0036285.
- Dowling, A., 2015. The evolution of parasitism and host association in mites. In: Morand, S., Krasnov, B. R., Littlewood, T. J., eds. *Parasite Diversity and Diversification*. Cambridge: Cambridge University Press, 2015, pp.265-288.
- Drum, N.H., and Rothenbuhler, W.C., 1983. Non-stinging aggressive responses of worker honey bees to hive mates, intruder bees and bees affected with chronic bee paralysis. *Journal of Apicultural Research*, **22**(4), 10.1080/00218839.1983.11100596.
- Duysens, J., Clarac, F., and Cruse, H., 2000. Load-regulating mechanisms in gait and posture: Comparative aspects. *Physiological Reviews*. 10.1152/physrev.2000.80.1.83.
- Dyer, F.C., 2002. Visually mediated odometry in honey bees. *The Journal of Experimental Biology*, **200**(19), 10.1146/annurev.ento.47.091201.145306.
- Eliash, N., et al., 2014. Can we disrupt the sensing of honey bees by the bee parasite *Varroa destructor*? *PLoS ONE*, **9**(9), 10.1371/journal.pone.0106889.
- Elizondo, V., Briceño, J. C., Trvieso, C.M., and Alonso, J.B., 2013. Video monitoring of a mite in honey bee cells. In: *Advanced Materials Research*, **664**, 10.4028/www.scientific.net/AMR.664.1107.
- Ellis, J.D., Delaplane, K.S., and Hood, W.M., 2002. Small hive beetle (*Aethina tumida* Murray) weight, gross biometry, and sex proportion at three locations in the southeastern United States. *American Bee Journal*, **142**(7), pp.520-522.
- Elzen, P.J., et al., 1999. Detection of resistance in US *Varroa jacobsoni* oud. (Mesostigmata: Varroidae) to the acaricide fluvalinate. *Apidologie*, **30**(1), 10.1051/apido:19990102.
- Escalante, I., Badger, M.A., and Elias, D.O., 2019. Variation in movement: Multiple locomotor gaits in neotropical harvestmen. *Biological Journal of the Linnean Society*, **127**(2), 10.1093/biolinnean/blz047.
- Es'Kov, E.K., Lykhin, D., Maslennikova, V., Toropstev, A., and Yaroshvich, G., 2003. Effectiveness of the acoustic method in the detection of mites (Acari) in sealed bee brood. *Agricultural Biology*, **38**(6), pp.123-125.
- Evans, G.O., and Till, W.M., 1979. Mesostigmatic mites of Britain and Ireland (Chelicerata: Acari-Parasitiformes): An introduction to their external morphology and classification. *The Transactions of the Zoological Society of London*, **35**(2), 10.1111/j.1096-3642.1979.tb00059.x.
- Evans, J.D., and Cook, S.C., 2018. Genetics and physiology of Varroa mites. *Current Opinion in Insect Science*, **26**, 10.1016/j.cois.2018.02.005.
- Fakhimzadeh, K., Ellis, J.D., and Hayes, J.W., 2011. Physical control of Varroa mites (*Varroa destructor*): The effects of various dust materials on Varroa mite fall from adult honey

- bees (*Apis mellifera*) in vitro. *Journal of Apicultural Research*, **50**(3), 10.3896/IBRA.1.50.3.04.
- Ferrari, S., Silva, M., Guarino, M., and Berckmans, D., 2008. Monitoring of swarming sounds in beehives for early detection of the swarming period. *Computers and Electronics in Agriculture*, **64**(1), 10.1016/j.compag.2008.05.010.
- Fleming, S., 2021. Hive Whodunnit. *Bee Craft Magazine*.
- Frey, E., Odemer, R., Blum, T., and Rosenkranz, P., 2013. Activation and interruption of the reproduction of *Varroa destructor* is triggered by host signals (*Apis mellifera*). *Journal of Invertebrate Pathology*, **113**(1), 10.1016/j.jip.2013.01.007.
- Fries, I., Huazen, W., Wei, S., and Jin, C.S., 1996. Grooming behaviour and damaged mites (*Varroa jacobsoni*) in *Apis cerana cerana* and *Apis mellifera ligustica*. *Apidologie*, **27**(1), 10.1051/apido:19960101.
- Fuangarworn, M., 2012. *Sphaerolichus lekprayoonae* n. sp. (Acari: Sphaerolichida: Sphaerolichidae), a new species of leaf-litter inhabiting mite from Thailand. *Tropical Natural History*, **12**(2), pp.245-256.
- Fukuse, K., and Yano, S., 2019. Delayed mite hatching in response to mechanical stimuli simulating egg predation attempts. *Scientific Reports*, **9**(1), 10.1038/s41598-019-50007-4.
- Gardner, J. W. and Bartlett, P. N., 1994. A brief history of electronic noses. *Sensors and Actuators*, **18-19**, pp.211-220.
- Gashout, Hanan A., Guzman-Novoa, E., Goodwin, P.H., and Correa-Benitez, A., 2020a. Impact of sublethal exposure to synthetic and natural acaricides on honey bee (*Apis mellifera*) memory and expression of genes related to memory. *Journal of Insect Physiology*, **121**, 10.1016/j.jinsphys.2020.104014.
- Gashout, H. A, Guzman-Novoa, E., and Goodwin, P.H., 2020b. Synthetic and natural acaricides impair hygienic and foraging behaviours of honey bees. *Apidologie*, **51**(6), pp.1155-1165.
- Gerula, D., Węgrzynowicz, P., Panasiuk, B., and Bieńkowska, M., 2017. Testing a CO<sub>2</sub> counter for assessment of phoretic *Varroa* mites in bee colonies. In: *Proceedings of the 13th COLOSS Conference*. Athens, p.26.
- Glavan, G., Novak, S., Božič, J. and Kokalj, A.J., 2020. Comparison of sublethal effects of natural acaricides carvacrol and thymol on honey bees. *Pesticide Biochemistry and Physiology*, **166**, 10.1016/j.pestbp.2020.104567.
- Goetz, B., and Koeniger, N., 1993. The distance between larva and cell opening triggers brood cell invasion by *Varroa jacobsoni*. *Apidologie*, **24**(1), 10.1051/apido:19930108.
- Granato, A., et al., 2017. Introduction of *Aethina tumida* (Coleoptera: Nitidulidae) in the regions of Calabria and Sicily (southern Italy). *Apidologie*, **48**(2), 10.1007/s13592-016-0465-3.
- Gregorc, A., Knight, P.R., and Adamczyk, J., 2017. Powdered sugar shake to monitor and oxalic acid treatments to control *Varroa* mites (*Varroa destructor* Anderson and

- Trueman) in honey bee (*Apis mellifera*) colonies. *Journal of Apicultural Research*, **56**(1), 10.1080/00218839.2017.1278912.
- Gregorc, A., and Sampson, B., 2019. Diagnosis of Varroa mite (*Varroa destructor*) and sustainable control in honey bee (*Apis mellifera*) colonies: A review. *Diversity*, **11**(12), 10.3390/D11120243.
- Gronenberg, W., 1996. Fast actions in small animals: Springs and click mechanisms. *Journal of Comparative Physiology A: Sensory, Neural, and Behavioural Physiology*, **178**(6), 10.1007/BF00225821.
- Guzman-Novoa, E., et al., 2012. First detection of four viruses in honey bee (*Apis mellifera*) workers with and without deformed wings and *Varroa destructor* in Mexico. *Journal of Apicultural Research*, **51**(4), 10.3896/IBRA.1.51.4.08.
- Harrison, J.M., 1987. Roles of individual honey bee workers and drones in colonial thermogenesis. *Journal of Experimental Biology*, **129**, pp.53-61.
- Häußermann, C.K., Ziegelmann, B., Bergmann, P., and Rosenkranz, P., 2015. Male mites (*Varroa destructor*) perceive the female sex pheromone with the sensory pit organ on the front leg tarsi. *Apidologie*, **46**(6), 10.1007/s13592-015-0367-9.
- Hepburn, H.R., 1998. Reciprocal interactions between honey bees and combs in the integration of some colony functions in *Apis mellifera* L. *Apidologie*, **29**(1-2), 10.1051/apido:19980103.
- Higes, M. Higes, M., Martín-Hernández, R., Hernández-Rodríguez, C.S., and González-Cabrera, J., 2020. Assessing the resistance to acaricides in *Varroa destructor* from several Spanish locations. *Parasitology Research*, **119**(11), 10.1007/s00436-020-06879-x.
- Hill, P.S.M., 2009. How do animals use substrate-borne vibrations as an information source? *Naturwissenschaften*, **96**(12), 10.1007/s00114-009-0588-8.
- Hill, P.S.M., and Wessel, A., 2016. Biotremology. *Current Biology*, **26**(5), pp.187-191.
- Hood, W.M., 2004. The small hive beetle, *Aethina tumida*: A review. *Bee World*, **85**(3), pp.51-59.
- Hooker, W.A., 1912. *The life history and binomics of some North American ticks*. Washington D. C., U.S. Department of Agriculture, Bureau of Entomology.
- Hopp, S.L., Owren, M.J., and Evans, C.S., eds, 1998. *Animal acoustic communication: Sound analysis and research methods*. Springer Science & Business Media.
- Houck, M.A., and O'Connor, B.M., 1991. Ecological and evolutionary significance of phoresy in the Astigmata. *Annual review of entomology*. **36**, 10.1146/annurev.ento.36.1.611.
- Howard, D., Duran, O., and Hunter, G., 2018. A low-cost multi-modal sensor network for the monitoring of honey bee colonies/hives. *Intelligent Environments*, 10.3233/978-1-61499-874-7-69.
- Hrnčir, M., Barth, F.G., and Tautz, J., 2005. Vibratory and airborne-sound signals in bee communication (hymenoptera). In: Drosopoulos, S., Claridge, M. F., eds. *Insect Sounds*

*and Communication: Physiology, Behaviour, Ecology, and Evolution*. Boca Raton: CRC Press, 2005, p.421.

- Imoize, A.L., Odeyemi, S.D., and Adebisi, J. A., 2020. Development of a low-cost wireless bee-hive temperature and sound monitoring system. *Indonesian Journal of Electrical Engineering and Informatics*, **8**(3), 10.11591/ijeei.v8i3.2268.
- Kaiser, W., Weber, T., Otto, D., and Miroshnikow, A., 2014. Oxygen supply of the heart and electrocardiogram potentials with reversed polarity in sleeping and resting honey bees. *Apidologie*, **45**(1), 10.1007/s13592-013-0229-2.
- Kamler, M., Nesvorna, M., Stara, J., Erban, T., and Hubert, J., 2016. Comparison of tau-fluvalinate, acrinathrin, and amitraz effects on susceptible and resistant populations of *Varroa destructor* in a vial test. *Experimental and Applied Acarology*, **69**(1), 10.1007/s10493-016-0023-8.
- Kather, R., Drijfhout, F.P., Shemilt, S., and Martin, S. J., 2015a. Evidence for passive chemical camouflage in the parasitic mite *Varroa destructor*. *Journal of Chemical Ecology*, **41**(2), 10.1007/s10886-015-0548-z.
- Kather, R., Drijfhout, F.P., and Martin, S.J., 2015b. Evidence for colony-specific differences in chemical mimicry in the parasitic mite *Varroa destructor*. *Chemoecology*, **25**(4), 10.1007/s00049-015-0191-8.
- Kershenbaum, A., et al., 2016. Acoustic sequences in non-human animals: A tutorial review and prospectus. *Biological Reviews*, **91**(1), 10.1111/brv.12160.
- Kilpinen, O., 2001. Activation of the poultry red mite, *Dermanyssus gallinae* (Acari: Dermanyssidae), by increasing temperatures. *Experimental and Applied Acarology*, **25**(10-11), 10.1023/A:1020409221348.
- Kilpinen, O., 2005. How to obtain a bloodmeal without being eaten by a host: The case of poultry red mite, *Dermanyssus gallinae*. *Physiological Entomology*, **30**(3), 10.1111/j.1365-3032.2005.00452.x.
- Kim, B., et al., 2019. Detection of Chronic bee paralysis virus using ultra-rapid PCR and nested ultra-rapid PCR. *Journal of Apicultural Research*, **58**(1), 10.1080/00218839.2018.1517999.
- Kimchi, T., Reshef, M., and Terkel, J., 2005. Evidence for the use of reflected self-generated seismic waves for spatial orientation in a blind subterranean mammal. *Journal of Experimental Biology*, **208**(4), 10.1242/jeb.01396.
- Kimura, T., Ohashi, M., Okada, R., and Ikeno, H., 2011. A new approach for the simultaneous tracking of multiple honey bees for analysis of hive behaviour. *Apidologie*, **42**(5), 10.1007/s13592-011-0060-6.
- Kirchner, W.H., 1993a. Lichtsinn und Vibrationssinn der Varroa-Milbe. *Apidologie*, **24**(5), pp.490-492.
- Kirchner, W.H., 1993b. Vibrational signals in the tremble dance of the honey bee, *Apis mellifera*. *Behavioural Ecology and Sociobiology*, **33**(3), 10.1007/BF00216597.

- Kirchner, W.H., Hager, F.A., and Krausa, K., 2022. Vibrational behaviour in honey bees. In: *Biotremology: Physiology, Ecology and Evolution*. Springer, 2022, pp.387-410.
- Knoll, S., Pinna, W., Varcasia, A., Scala, A., and Cappai, M.G., 2020. The honey bee (*Apis mellifera* L., 1758) and the seasonal adaptation of productions. Highlights on summer to winter transition and back to summer metabolic activity. A review. *Livestock Science*, **235**, 10.1016/j.livsci.2020.104011.
- König, A., 2021. First results of the BeE-nose on mid-term duration hive air monitoring for Varroa infestation level estimation. *Sensors & Transducers*, **250**(3), pp.39-43.
- König, A., 2022. An in-hive soft sensor based on phase space features for Varroa infestation level estimation and treatment need detection. *Journal of Sensors and Sensor Systems*, **11**(1), 10.5194/jsss-11-29-2022.
- Kovac, H., Stabentheiner, A. and Brodschneider, R., 2009. Contribution of honey bee drones of different age to colonial thermoregulation. *Apidologie*, **40**, pp.82-95.
- Kovac, H., Stabentheiner, A., Hetz, S.K., Petz, M., and Crailsheim, K., 2007. Respiration of resting honey bees. *Journal of Insect Physiology*, **53**(12), 10.1016/j.jinsphys.2007.06.019.
- Kralj, J., Fuchs, S., 2006. Parasitic *Varroa destructor* mites influence flight duration and homing ability of infested *Apis mellifera* foragers. *Apidologie*, **37**(5), 10.1051/apido:2006040.
- Kraus, B., 1993. Preferences of *Varroa jacobsoni* for honey bees (*Apis mellifera* L.) of different ages. *Journal of Apicultural Research*, **32**(2), pp.57-64.
- Kraus, F.B., Neumann, P., Scharpenberg, H., Praagh, J.V. and Moritz, R.F.A., 2003. Male Fitness of honey bee colonies (*Apis mellifera* L.). *Journal of Evolutionary Biology*, **16**(5), pp.914-920.
- Kraus, B., Velthuis, H.H.W., and Tingek, S., 1998. Temperature profiles of the brood nests of *Apis cerana* and *Apis mellifera* colonies and their relation to varroosis. *Journal of Apicultural Research*, **37**(3), 10.1080/00218839.1998.11100969.
- Kridi, D.S., de Carvalho, C. G. N., and Gomes, D. G., 2016. Application of wireless sensor networks for beehive monitoring and in-hive thermal patterns detection. *Computers and Electronics in Agriculture*, **127**, 10.1016/j.compag.2016.05.013.
- Kriegbaum, H., 1997. Grasshopper reproductive strategies measured in the field: A trade-off between age at maturity and egg production per day. *Naturwissenschaften*, **84**(4), 10.1007/s001140050370.
- Kuenen, L.P.S., and Calderone, N.W., 1997. Transfers of Varroa mites from newly emerged bees: Preferences for age- and function-specific adult bees (Hymenoptera: Apidae). *Journal of Insect Behaviour*, **10**(2), 10.1007/BF02765554.
- Kuenen, L.P.S., and Calderone, N.W., 1998. Positive anemotaxis by Varroa mites: Responses to bee odour plumes and single clean-air puffs. *Physiological Entomology*, **23**(3), 10.1046/j.1365-3032.1998.233085.x.

- Kuennen, L.P.S., and Calderone, N. W., 2000. Varroa mite infestations in elevated honey bee brood cells: Effects of context and caste. *Journal of Insect Behaviour*, **13**(2), 10.1023/A:1007784130228.
- Kviesis, A., Komasilovs, V., Komasilova, O., and Zacepins, A., 2020a. Application of fuzzy logic for honey bee colony state detection based on temperature data. *Biosystems Engineering*, **193**, 10.1016/j.biosystemseng.2020.02.010.
- Kviesis, A., Zacepins, A., Fiedler, S., Komasilovs, V., and Laceklis-Bertmanis, J., et al., 2020b. Automated system for bee colony weight monitoring. *AGROFOR*, **5**(2), 10.7251/agreng2002044k.
- Land, B.B., and Seeley, T.D., 2004. The grooming invitation dance of the honey bee. *Ethology*, **110**(1), 10.1046/j.1439-0310.2003.00947.x.
- Laurino, D., Porporato, M., Patetta, A., and Manino, A., 2011. Toxicity of neonicotinoid insecticides to honey bees: Laboratory tests. *Bulletin of Insectology*, **64**(1), pp.107-113.
- Leclercq, G., Pannebakker, B., Gengler, N., Nguyen, B. K., and Francis, F., 2017. Drawbacks and benefits of hygienic behaviour in honey bees (*Apis mellifera* L.): A review. *Journal of Apicultural Research*, **56**(4), pp.366-375.
- Lecocq, A., Kryger, P., Vejsnaes, F., and Bruun Jensen, A., 2015. Weight watching and the effect of landscape on honey bee colony productivity: Investigating the value of colony weight monitoring for the beekeeping industry. *PLoS ONE*, **10**(7), 10.1371/journal.pone.0132473.
- Levin, C.G., Collison, C.H., and Collison, C.H., 1990. Brood nest temperature differences and their possible effect on drone brood production and distribution in honey bee colonies. *Journal of Apicultural Research*, **29**(1), 10.1080/00218839.1990.11101195.
- Li, S., Yu, X., and Feng, Q., 2019. Fat body biology in the last decade. *Annual Review of Entomology*, **64**, 10.1146/annurev-ento-011118-112007.
- Li, Z., et al., 2016. Drone and worker brood microclimates are regulated differentially in honey bees, *Apis mellifera*. *PLoS ONE*, **11**(2), 10.1371/journal.pone.0148740.
- Lin, Z. et al., 2016. Go east for better honey bee health: *Apis cerana* is faster at hygienic behaviour than *A. mellifera*. *PLoS One*, **11**(9), p.e0162647.
- Liu, T.P., 1988. The morphology of the tarsal sensilla in the female mite *Varroa jacobsoni*. *Pan-Pacific Entomologist*, **64**(3), pp.261-265.
- Liu, T.P., and Peng, Y.S, 1990. Palpal tarsal sensilla of the female mite, *Varroa jacobsoni* oudemans (Acari: Varroidae). *The Canadian Entomologist*, **122**(2), 10.4039/Ent122295-3.
- Macedo, P.A., Wu, J., and Ellis, M.D., 2002. Using inert dusts to detect and assess Varroa infestations in honey bee colonies. *Journal of Apicultural Research*, **41**(1-2), 10.1080/00218839.2002.11101062.

- Maggi, M.D., et al., 2010a. Brood cell size of *Apis mellifera* modifies the reproductive behaviour of *Varroa destructor*. *Experimental and Applied Acarology*, **50**(3), 10.1007/s10493-009-9314-7.
- Maggi, M.D., Ruffinengo, S. R., Negri, P., and Eguaras, M. J., 2010b. Resistance phenomena to amitraz from populations of the ectoparasitic mite *Varroa destructor* of Argentina. *Parasitology Research*, **107**(5), 10.1007/s00436-010-1986-8.
- Magnier, B., Ekszterowicz, G., Laurent, J., Rival, M., and Pfister, F., 2018. Beehive traffic monitoring by tracking bee flight paths. In: *13th International Joint Conference on Computer Vision, Imaging and Computer Graphics Theory and Applications*. Funchal, pp.563-571.
- Markl, H., 1967. Die Verständigung durch Stridulationssignale bei Blattschneiderameisen. Die biologische Bedeutung der Stridulation. *Zeitschrift für Vergleichende Physiologie*, **57**(3), 10.1007/BF00303001.
- Martin, C., et al., 2001. Variations in chemical mimicry by the ectoparasitic mite *Varroa jacobsoni* according to the developmental stage of the host honey bee *Apis mellifera*. *Insect Biochemistry and Molecular Biology*, **31**(4-5), pp.365-379.
- Martin, S.J., 1998. A population model for the ectoparasitic mite *Varroa jacobsoni* in honey bee (*Apis mellifera*) colonies. *Ecological Modelling*, **109**(3), 10.1016/S0304-3800(98)00059-3.
- Martin, S.J., 2004. Acaricide (pyrethroid) resistance in *Varroa destructor*. *Bee World*, **85**(4), 10.1080/0005772X.2004.11099632.
- Martinello, M., et al., 2017. Spring mortality in honey bees in north-eastern Italy: detection of pesticides and viruses in dead honey bees and other matrices. *Journal of Apicultural Research*, **56**(3), 10.1080/00218839.2017.1304878.
- McMenamin, A.J., Genersch, E., 2015. Honey bee colony losses and associated viruses. *Current Opinions in Insect Science*, **8**, 10.1016/j.cois.2015.01.015.
- Mendes, C.S., Bartos, I., Akay, T., Márka, S., and Mann, R. S., 2013. Quantification of gait parameters in freely walking wild type and sensory deprived *Drosophila melanogaster*. *eLife*, **2**, 10.7554/eLife.00231.
- Metallo, C., Mukherjee, R., and Trimmer, B. A., 2020. Stepping pattern changes in the caterpillar *Manduca sexta*: The effects of orientation and substrate. *Journal of Experimental Biology*. **14**, jeb220319.
- Mezquida, D.A., Martinez, J.L., 2009. Short communication. Platform for beehives monitoring based on sound analysis. A perpetual warehouse for swarm's daily activity. *Spanish Journal of Agricultural Research*, **7**(4), pp.824-828.
- Michelsen, A., 2014. Physical Aspects of Vibrational Communication. In: *Studying Vibrational Communication*. Springer, Berlin, Heidelberg, 10.1007/978-3-662-43607-3\_11.
- Michelsen, A., and Elsner, N., 1999. Sound emission and the acoustic far field of a singing acridid grasshopper (*Omocestus viridulus* L.). *Journal of Experimental Biology*, **202**(12), 10.1242/jeb.202.12.1571.

- Michelsen, A., Fink, F., Gogala, M., and Traue, D., 1982. Plants as transmission channels for insect vibrational songs. *Behavioural Ecology and Sociobiology*, **11**(4), 10.1007/BF00299304.
- Michelsen, A., Kirchner, W.H., and Lindauer, M., 1986. Sound and vibrational signals in the dance language of the honey bee, *Apis mellifera*. *Behavioural Ecology and Sociobiology*, **18**(3), 10.1007/BF00290824.
- Milani, N., 1999. The resistance of *Varroa jacobsoni* Oud. to acaricides. *Apidologie*, **30**(-3), 10.1051/apido:19990211.
- de Miranda, J.R., and Genersch, E., 2010. Deformed wing virus. *Journal of Invertebrate Pathology*, **103**, pp.S48-S61.
- Modirrousta, H., and Moharrami, M., 2015. First molecular detection of Chronic bee paralysis virus (CBPV) in Iran. *Archives of Razi Institute*, **70**(4), pp.229-235.
- Morfin, N., Goodwin, P.H., and Guzman-Novoa, E., 2020. Interaction of *Varroa destructor* and sublethal clothianidin doses during the larval stage on subsequent adult honey bee (*Apis mellifera* L.) health, cellular immunity, deformed wing virus levels and differential gene expression. *Microorganisms*, **8**(6), 10.3390/microorganisms8060858.
- Morimoto, T., et al., 2012. Molecular identification of Chronic bee paralysis virus infection in *Apis mellifera* colonies in Japan. *Viruses*, **4**(7), 10.3390/v4071093.
- Mortimer, B., 2017. Biotremology: Do physical constraints limit the propagation of vibrational information?. *Animal Behaviour*, **130**, 10.1016/j.anbehav.2017.06.015.
- Murillo, A.C., and Mullens, B.A., 2017. A review of the biology, ecology, and control of the northern fowl mite *Ornithonyssus sylviarum* (Acari: Macronyssidae). *Veterinary Parasitology*, **246**, 10.1016/j.vetpar.2017.09.002.
- Murphy, F.E., Magno, M., Whelan, P., and Vici, E.P., 2015. B+ WSN: Smart beehive for agriculture, environmental, and honey bee health monitoring - Preliminary results and analysis. In: *2015 IEEE Sensors Applications Symposium (SAS)*, IEEE, pp.1-6.
- Nation, J.L., Sanford, M.T., and Milne, K., 1992. Cuticular hydrocarbons from *Varroa jacobsoni*. *Experimental and Applied Acarology*, **16**(4), 10.1007/BF01218575.
- Nazzi, F., and Le Conte, Y., 2016. Ecology of *Varroa destructor*, the major ectoparasite of the western honey bee *Apis mellifera*. *Annual Review of Entomology*, **61**(1), 10.1146/annurev-ento-010715-023731.
- Nganso, B.T., Mani, K., Altman, Y., Rafaeli, A., and Soroker, V., 2020. How crucial is the functional pit organ for the Varroa mite? *Insects*, **11**(6), 10.3390/insects11060395.
- Ngo, T.N., Wu, K.C., Yang, E.C., and Lin, T.T., 2019. A real-time imaging system for multiple honey bee tracking and activity monitoring. *Computers and Electronics in Agriculture*, **163**, 10.1016/j.compag.2019.05.050.
- Ngo, T.N., Rustia, D.J.A., Yang, E.C., and Lin, T.T., 2021. Automated monitoring and analyses of honey bee pollen foraging behaviour using a deep learning-based imaging system. *Computers and Electronics in Agriculture*, **187**, 10.1016/j.compag.2021.106239.

- Nirody, J. A., Duran, L. A., Johnston, D., and Cohen, D. J., 2021. Tardigrades exhibit robust interlimb coordination across walking speeds and terrains. *Proceedings of the National Academy of Sciences*. **118**(35), e2107289118.
- Noël, A., le Conte, Y., and Mondet, F., 2020. *Varroa destructor*: How does it harm *Apis mellifera* honey bees and what can be done about it? *Emerging Topics in Life Sciences*, **4**(1), pp.45-57.
- Nolasco, I., et al., 2019. Audio-based identification of beehive states. In: IEEE, ed. *ICASSP 2019-2019 IEEE International Conference on Acoustics, Speech and Signal Processing (ICASSP)*. pp.8256-8260.
- Ohtani, T., and Kamada, T., 1980. 'Worker piping': The piping sounds produced by laying and guarding worker honey bees. *Journal of Apicultural Research*, **19**(3), 10.1080/00218839.1980.11100016.
- Oršolić, N., 2010. A review of propolis antitumour action *in vivo* and *in vitro*. *Journal of ApiProduct and ApiMedical Science*, **2**(1), 10.3896/IBRA.4.02.1.01.
- Ortiz, G., Frizzera, D., Seffin, E., Annoscia, D., and Nazzi, F., 2019. Honey bees use various criteria to select the site for performing the waggle dances on the comb. *Behavioural Ecology and Sociobiology*, **73**(5), 10.1007/s00265-019-2677-9.
- Otten, H., Wäckers, F., Battini, M., and Dorn, S., 2001. Efficiency of vibrational sounding in the parasitoid *Pimpla turionellae* is affected by female size. *Animal Behaviour*, **61**(3), 10.1006/anbe.2000.1639.
- Owen, J.P., and Mullens, B.A., 2004. Influence of heat and vibration on the movement of the northern fowl mite (Acari: Macronyssidae). *Journal of Medical Entomology*, **41**(5), 10.1603/0022-2585-41.5.865.
- Page, R.E., and Metcalf, R.A., 1984. A population investment sex ratio for the honey bee (*Apis mellifera* L.). *American Naturalist*, **124**(5), 10.1086/284306.
- Patek, S.N., Dudek, D.M., and Rosario, M.V., 2011. From bouncy legs to poisoned arrows: Elastic movements in invertebrates. *Journal of Experimental Biology*, **214**(12), 10.1242/jeb.038596.
- Peck, D.T., Smith, M.L., and Seeley, T.D., 2016. *Varroa destructor* mites can nimbly climb from flowers onto foraging honey bees. *PLoS ONE*, **11**(12), 10.1371/journal.pone.0167798.
- Peng, Y.S., Fang, Y., Xu, S., and Ge, L., 1987. The resistance mechanism of the Asian honey bee, *Apis cerana* Fabr., to an ectoparasitic mite, *Varroa jacobsoni* Oudemans. *Journal of Invertebrate Pathology*, **49**(1), pp.54-60.
- Pérez, N., et al., 2016. Continuous monitoring of beehives' sound for environmental pollution control. *Ecological Engineering*, **90**, 10.1016/j.ecoleng.2016.01.082.
- Pernal, S.F., Baird, D.S., Higo, H.A., Slessor, K.N., and Winston, M.L., 2005. Semiochemicals influencing the host-finding behaviour of *Varroa destructor*. *Experimental and Applied Acarology*, **37**(1-2), 10.1007/s10493-005-1117-x.

- Pettis, J.S., 2004. A scientific note on *Varroa destructor* resistance to coumaphos in the United States. *Apidologie*, **35**(1), 10.1051/apido:2003060.
- Piccirillo, G.A., and de Jong, D., 2003. The influence of brood-comb cell size on the reproductive behaviour of the ectoparasitic mite *Varroa destructor* in Africanized honey bee colonies. *Genetics and Molecular Research*, **2**(1), pp.36-42.
- del Piccolo, F., Nazzi, F., Della Vedova, G., and Milani, N., 2010. Selection of *Apis mellifera* workers by the parasitic mite *Varroa destructor* using host cuticular hydrocarbons. *Parasitology*, **137**(6), 10.1017/S0031182009991867.
- Picek, L., Novozamsky, A., Frydrychova, R.C., Zitova, B. and Mach, P., 2022. Monitoring of *Varroa* infestation rate in beehives: a simple AI approach. In *2022 IEEE International Conference on Image Processing (ICIP)*, pp. 3341-3345.
- Pietropaoli, M., et al., 2021. Evaluation of two commonly used field tests to assess *Varroa destructor* infestation on honey bee (*Apis mellifera*) colonies. *Applied Sciences (Switzerland)*, **11**(10), 10.3390/app11104458.
- Pinnelli, G.R., Singh, N.K., Soroker, V., and Plettner, E., 2016. Synthesis of enantiopure alicyclic ethers and their activity on the chemosensory organ of the ectoparasite of honey bees, *Varroa destructor*. *Journal of Agricultural and Food Chemistry*, **64**(45), 10.1021/acs.jafc.6b03492.
- Piou, V., 2020. Personal communication.
- Piou, V., Tabart, J., Urrutia, V., Hemptinne, J.L., and Vétillard, A., 2016. Impact of the phoretic phase on reproduction and damage caused by *Varroa destructor* (Anderson and Trueman) to its host, the European honey bee (*Apis mellifera* L.). *PLoS ONE*, **11**(4), 10.1371/journal.pone.0153482.
- Piou, V., Tabart, J., Hemptinne, J.L., and Vétillard, A., 2018. Effect of pollen extract supplementation on the varroa tolerance of honey bee (*Apis mellifera*) larvae reared in vitro. *Experimental and Applied Acarology*, **74**(1), 10.1007/s10493-017-0198-7.
- Piou, V., Urrutia, V., Laffont, C., Hemptinne, J.L., and Vétillard, A., 2019. The nature of the arena surface affects the outcome of host-finding behaviour bioassays in *Varroa destructor* (Anderson & Trueman). *Parasitology Research*, **118**(10), 10.1007/s00436-019-06435-2.
- Piou, V., and Vétillard, A., 2020. *Varroa destructor* rearing in laboratory conditions: importance of foundress survival in doubly infested cells and reproduction of laboratory-born females. *Apidologie*, **51**(6), 10.1007/s13592-020-00775-0.
- Plettner, E., Eliash, N., Singh, N.K., Pinnelli, G.R., and Soroker, V., 2017. The chemical ecology of host-parasite interaction as a target of *Varroa destructor* control agents. *Apidologie*, **48**(1), 10.1007/s13592-016-0452-8.
- Pritchard, D.J., 2016. Grooming by honey bees as a component of *Varroa* resistant behaviour. *Journal of Apicultural Research*, **55**(1), pp.38-48.

- Proctor, H.C., 1991. Courtship in the water mite *Neumania papillator*: Males capitalize on female adaptations for predation. *Animal Behaviour*, **42**(4), 10.1016/S0003-3472(05)80242-8.
- Proctor, H.C., 1992a. Mating and spermatophore morphology of water mites (Acari: Parasitengona). *Zoological Journal of the Linnean Society*, **106**(4), 10.1111/j.1096-3642.1992.tb01250.x.
- Proctor, H.C., 1992b. Sensory exploitation and the evolution of male mating behaviour: a cladistic test using water mites (Acari: Parasitengona). *Animal Behaviour*, **44**(4), 10.1016/S0003-3472(05)80300-8.
- Proctor, H.C., and Pritchard, G., 1989. Neglected predators: water mites (Acari: Parasitengona: Hydrachnellae) in freshwater communities. *Journal of the North American Benthological Society*, **8**(1), pp.100-111.
- Proctor, H.C., and Pritchard, G., 1990. Prey detection by the water mite *Unionicola crassipes* (Acari: Unionicolidae). *Freshwater Biology*, **23**(2), 10.1111/j.1365-2427.1990.tb00271.x.
- Qandour, A., Ahmad, I., Habibi, D., and Leppard, M., 2014. Remote beehive monitoring using acoustic signals. *Acoustics Australia*, **42**(3), 10.1007/s40857-015-0016-5.
- Ramírez, M., Prendas, J.P., Travieso, C.M., Calderón, R., and Salas, O., 2012. Detection of the mite *Varroa destructor* in honey bee cells by video sequence processing. In: *2012 IEEE 16th International Conference on Intelligent Engineering Systems (INES)*. IEEE, pp.103-108.
- Ramirez, W.B., and Malavasi, J.G., 1991. Conformation of the ambulacrum of *Varroa jacobsoni* Oudemans (Mesostigmata: Varroidae): A grasping structure. *International Journal of Acarology*, **17**(3), 10.1080/01647959108683903.
- Ramsey, M.T., 2018. *The Ethology of Honeybees (Apis mellifera) Studied Using Accelerometer Technology*. Nottingham: Nottingham Trent University.
- Ramsey, M., Bencsik, M., and Newton, M.I., 2017. Long-term trends in the honey bee 'whooping signal' revealed by automated detection. *PLoS ONE*, **12**(2), 10.1371/journal.pone.0171162.
- Ramsey, M., Bencsik, M., and Newton, M.I., 2018. Extensive vibrational characterisation and long-term monitoring of honey bee dorso-ventral abdominal vibration signals. *Scientific Reports*, **8**(1), 10.1038/s41598-018-32931-z.
- Ramsey, M.T., et al., 2020. The prediction of swarming in honey bee colonies using vibrational spectra. *Scientific Reports*, **10**(1), 10.1038/s41598-020-66115-5.
- Ramsey, S.M., et al., 2019. *Varroa destructor* feeds primarily on honey bee fat body tissue and not haemolymph. *Proceedings of the National Academy of Sciences*, **116**(5), pp.1792-1801.
- Ramsier, M.A., and Dominy, N.J., 2012. Receiver bias and the acoustic ecology of aye-eyes (*Daubentonia madagascariensis*). *Communicative and Integrative Biology*, **5**(6), 10.4161/cib.21509.

- Rath, W., 1999. Co-adaptation of *Apis cerana* Fabr. and *Varroa jacobsoni* oud. *Apidologie*, **30**(2-3), pp.97-110.
- Reeping, D., and Reid, K., 2016. *Introductory Engineering Mathematics*. Momentum Press.
- Ribbands, C.R., 1950. Changes in the behaviour of honey bees following their recovery from anaesthesia. *The Journal of experimental biology*, **27**(3-4), 10.1242/jeb.27.3.302.
- Ribièrè, M., et al., 2002. Molecular diagnosis of Chronic bee paralysis virus infection. *Apidologie*, **33**(3), 10.1051/apido:2002020.
- Ribièrè, M., Olivier, V., and Blanchard, P., 2010. Chronic bee paralysis: A disease and a virus like no other?. *Journal of Invertebrate Pathology*, **103**, 10.1016/j.jip.2009.06.013.
- Rinderer, T., de Guzman, L., and Sylvester, H.A., 2004. Re-examination of the accuracy of a detergent solution for Varroa mite detection. *American Bee Journal*, **144**(7), pp.560-562.
- Rittschof, C.C., and Seeley, T.D., 2008. The buzz-run: How honey bees signal "Time to go!" *Animal Behaviour*, **75**(1), 10.1016/j.anbehav.2007.04.026.
- Robles-Guerrero, A., Saucedo-Anaya, T., González-Ramírez, E., and De La Rosa-Vargas, J.I., 2019. Analysis of a multiclass classification problem by Lasso Logistic Regression and Singular Value Decomposition to identify sound patterns in queen less bee colonies. *Computers and Electronics in Agriculture*, **159**, 10.1016/j.compag.2019.02.024.
- Robles-Guerrero, A., Saucedo-Anaya, T., González-Ramírez, E., and Galván-Tejada, C.E., 2017. Frequency analysis of honey bee buzz for automatic recognition of health status: A preliminary study. *Research in Computing Science*, **142**(1), 10.13053/rcs-142-1-9.
- Roces, F., and Hölldobler, B., 1994. Leaf density and a trade-off between load-size selection and recruitment behaviour in the ant *Atta cephalotes*. *Oecologia*, **97**(1), 10.1007/BF00317902.
- Rosenkranz, P., Aumeier, P., and Ziegelmann, B., 2010. Biology and control of *Varroa destructor*. *Journal of Invertebrate Pathology*, **103**, 10.1016/j.jip.2009.07.016.
- Rosenkranz, P., and Garrido, C., 2004. Volatiles of the honey bee larva initiate oogenesis in the parasitic mite *Varroa destructor*. *Chemoecology*, **14**(3), pp.193-197.
- Rothe, U., and Nachtigall, W., 1989. Flight of the honey bee - IV. Respiratory quotients and metabolic rates during sitting, walking, and flying. *Journal of Comparative Physiology B*, **158**(6), 10.1007/BF00693012.
- Rueppell, O., Hayworth, M.K., and Ross, N.P., 2010. Altruistic self-removal of health-compromised honey bee workers from their hive. *Journal of Evolutionary Biology*, **23**(7), 10.1111/j.1420-9101.2010.02022.x.
- Ruvinga, S., Hunter, G.J., Duran, O., and Nebel, J.C., 2021. Use of LSTM networks to identify "queen-less-ness" in honey bee hives from audio signals. In: *2021 17th International Conference on Intelligent Environments, IE 2021 – Proceedings*, 10.1109/IE51775.2021.9486575.

- Sammataro, D., Untalan, P., Guerrero, F., and Finley, J., 2005. The resistance of Varroa mites (acari: Varroidae) to acaricides and the presence of esterase. *International Journal of Acarology*, **31**(1), 10.1080/01647950508684419.
- Sandeman, D.C., Tautz, J., and Lindauer, M., 1996. Transmission of vibration across honeycombs and its detection by bee leg receptors. *Journal of Experimental Biology*, **199**(12), 10.1242/jeb.199.12.2585.
- Santer, R.D., and Hebets, E.A., 2011. The sensory and behavioural biology of whip spiders (Arachnida, Amblypygi). In: *Advances in Insect Physiology*, **41**, 10.1016/B978-0-12-415919-8.00001-X.
- Schmerge, J.D., Riese, D.J., and Hasiotis, S.T., 2013. Vinegaroon (arachnida: Thelyphonida: Thelyphonidae) trackway production and morphology: Implications for media and moisture control on trackway morphology and a proposal for a novel system of interpreting arthropod trace fossils. *Palaios*, **28**(2), 10.2110/palo.2012.p12-012r.
- Schmolz, E., Kösece, F., and Lamprecht, I., 2005. Energetics of honey bee development: Isoperibol and combustion calorimetric investigations. *Thermochimica Acta*, **437**(1-2), 10.1016/j.tca.2005.06.001.
- Schneider, S.S., and Lewis, L.A., 2004. The vibrational signal, modulatory communication and the organisation of labour in honey bees (*Apis mellifera*). *Apidologie*, **35**(2), 10.1051/apido:2004006.
- Schurr, F., et al., 2019. Validation of quantitative real-time RT-PCR assays for the detection of six honey bee viruses. *Journal of Virological Methods*, **270**, 10.1016/j.jviromet.2019.04.020.
- Schwab, E.R., Chilson, R.A., and Eddleman, C.D., 1991. Heartbeat rate modulation mediated by the ventral nerve cord in the honey bee, *Apis mellifera*. *Journal of Comparative Physiology B*, **161**(6), 10.1007/BF00260751.
- Schwartz, K.R., et al., 2020. The neonicotinoid imidacloprid alone alters the cognitive behaviour in *Apis mellifera* L. and the combined exposure of imidacloprid and *Varroa destructor* mites synergistically contributes to trial attrition. *Journal of Apicultural Research*, **60**(3), 10.1080/00218839.2020.1866233.
- Seeley, T.D., and Tautz, J., 2001. Worker piping in honey bee swarms and its role in preparing for lift-off. *Journal of Comparative Physiology - A Sensory, Neural, and Behavioural Physiology*, **187**(8), 10.1007/s00359-001-0243-0.
- Serridge, M., and Licht, T.R., 1987. Piezoelectric accelerometers and vibration preamplifiers: Theory and application handbook.
- Shamble, P.S., Hoy, R.R., Cohen, I., and Beatus, T., 2017. Walking like an ant: A quantitative and experimental approach to understanding locomotor mimicry in the jumping spider *Myrmarachne formicaria*. *Proceedings of the Royal Society B: Biological Sciences*, **284**(1858), 10.1098/rspb.2017.0308.
- Sharif, M.Z., Jiang, X., and Puswal, S.M., 2020. Pests, parasitoids, and predators: Can they degrade the sociality of a honey bee colony, and be assessed via acoustically monitored systems. *Journal of Entomology and Zoology Studies*, **8**, pp.1248-1260.

- Siefert, P., Buling, N., and Grünewald, B., 2021. Honey bee behaviours within the hive: Insights from long-term video analysis. *PLoS ONE*, **16**(3), 10.1371/journal.pone.0247323.
- Siefert, P., Hota, R., Ramesh, V., and Grünewald, B., 2020. Chronic within-hive video recordings detect altered nursing behaviour and retarded larval development of neonicotinoid treated honey bees. *Scientific Reports*, **10**(1), 10.1038/s41598-020-65425-y.
- Singh, N.K., et al., 2015. The effect of DEET on chemosensing of the honey bee and its parasite *Varroa destructor*. *Apidologie*, **46**(3), 10.1007/s13592-014-0330-1.
- Smith, M.L., and Chen, P.C., 2017. Larger but not louder: bigger honey bee colonies have quieter combs. *Behavioural Ecology and Sociobiology*, **71**(11), pp.1-7.
- Soler Cruz, M.D., et al., 2005. Scanning electron microscopy of foreleg tarsal sense organs of the poultry red mite, *Dermanyssus gallinae* (DeGeer) (Acari:Dermanyssidae). *Micron*, **36**(5), 10.1016/j.micron.2005.03.003.
- Sonenshine, D.E., et al., 2022. Histological Atlas of the Internal Anatomy of Female *Varroa destructor* (Mesostigmata: Varroidae) Mites in Relation to Feeding and Reproduction. *Annals of the Entomological Society of America*, **115**(2), 10.1093/aesa/saab043.
- Spagna, J.C., and Peattie, A.M., 2012. Terrestrial locomotion in arachnids. *Journal of Insect Physiology*, **58**(5), 10.1016/j.jinsphys.2012.01.019.
- Stabentheiner, A., Vollmann, J., Kovac, H., and Crailsheim, K., 2003. Oxygen consumption and body temperature of active and resting honey bees. *Journal of Insect Physiology*, **49**(9), 10.1016/S0022-1910(03)00148-3.
- Stec, D., and Kuszewska, K., 2020. CO<sub>2</sub> narcosis influences the memory of honey bees. *Journal of Apicultural Research*, **59**(4), 10.1080/00218839.2019.1710028.
- Sterling, E.J., and McCreless, E.E., 2006. Adaptations in the aye-aye: A review. In: *Lemurs*, 10.1007/978-0-387-34586-4\_8.
- Szczurek, A., et al., 2020a. The effectiveness of *Varroa destructor* infestation classification using an e-nose depending on the time of day. *Sensors*, **20**(9), 10.3390/s20092532.
- Szczurek, A., et al., 2020b. Gas sensor array and classifiers as a means of varroosis detection. *Sensors*, **20**(1), 10.3390/s20010117.
- Tautz, J., 1996. Honey bee waggle dance: Recruitment success depends on the dance floor. *Journal of Experimental Biology*, **199**(6), 10.1242/jeb.199.6.1375.
- Tautz, J., Casas, J., and Sandeman, D., 2001. Phase reversal of vibratory signals in honeycomb may assist dancing honey bees to attract their audience. *Journal of Experimental Biology*, **204**(21), 10.1242/jeb.204.21.3737.
- Tautz, J., and Lindauer, M., 1997. Honey bees establish specific sites on the comb for their waggle dances. *Journal of Comparative Physiology A*, **180**(5), 10.1007/s003590050070.

- Tentcheva, D., et al., 2004. Prevalence and seasonal variations of six bee viruses in *Apis mellifera* L. and *Varroa destructor* mite populations in France. *Applied and Environmental Microbiology*, **70**(12), 10.1128/AEM.70.12.7185-7191.2004.
- Terenzi, A., Cecchi, S., Spinsante, S., Orcioni, S., and Piazza, F., 2019a. Real-time system implementation for beehives weight measurement. In: *019 IEEE International Workshop on Metrology for Agriculture and Forestry (MetroAgriFor)*. IEEE, pp.231-236.
- Terenzi, A., Cecchi, S., Orcioni, S., and Piazza, F., 2019b. Features extraction applied to the analysis of the sounds emitted by honey bees in a beehive. In: IEEE, ed. *019 11th International Symposium on Image and Signal Processing and Analysis (ISPA)*. pp.3-8.
- Terenzi, A., Cecchi, S., and Spinsante, S., 2020. On the importance of the sound emitted by honey bee hives. *Veterinary Sciences*, **7**(4), 10.3390/vetsci7040168.
- Terenzi, A., Ortolani, N., Nolasco, I., Benetos, E., and Cecchi, S., 2022. Comparison of feature extraction methods for sound-based classification of honey bee activity. *IEEE/ACM Transactions on Audio Speech and Language Processing*, **30**, 10.1109/TASLP.2021.3133194.
- Tewarson, N.C., Singh, A., and Engels, W., 1992. Reproduction of *Varroa jacobsoni* in colonies of *Apis cerana indica* under natural and experimental conditions. *Apidologie*, **23**(2), 10.1051/apido:19920209.
- Tihelka, E., 2018. Effects of synthetic and organic acaricides on honey bee health: A review. *Slovenian Veterinary Research*, **55**(3), pp.114-140.
- Toufaily, A.I., Evison, S.E., Hughes, W.O., and Ratnieks, F.L., 2018. Both hygienic and non-hygienic honey bee, *Apis mellifera*, colonies remove dead and diseased larvae from open brood cells. *Philosophical Transactions of the Royal Society B: Biological Sciences*, **373**(1751), 10.1098/rstb.2017.0201.
- Traynor, K.S., et al., 2020. *Varroa destructor*: a complex parasite, crippling honey bees worldwide. *Trends in Parasitology*, **36**(7), pp.592-606.
- Trouiller, J., Arnold, G., Chappe, B., Le Conte, Y., and Masson, C., 1992. Semiochemical basis of infestation of honey bee brood by *Varroa jacobsoni*. *Journal of Chemical Ecology*, **18**(11), pp.2041-2053.
- Trouiller, J., and Milani, N., 1999. Stimulation of *Varroa jacobsoni* Oud. oviposition with semiochemicals from honey bee brood. *Apidologie*, **30**(1), 10.1051/apido:19990101.
- Tustain, R.C.R., and Faulke, J., 1979. Effect of carbon dioxide anaesthesia on the longevity of honey bees in the laboratory. *New Zealand Journal of Experimental Agriculture*, **7**(3), pp.327-329.
- Underwood, B., and Tashakkori, R., 2022. Detecting anomalies in honey bee hives using their audio recordings. In: *SoutheastCon 2022*. IEEE, pp.173-177.
- vanEngelsdorp, D., et al., 2009. Colony collapse disorder: A descriptive study. *PLoS ONE*, **4**(8), 10.1371/journal.pone.0006481.

- von Frisch, K., 1946. *Die Tänze der Bienen*. First Edition, Österreichische Zoologische Zeitschrift, Wien Springer, Germany.
- Wäckers, F.L., Mitter, E., and Dorn, S., 1998. Vibrational sounding by the pupal parasitoid *Pimpla (Coccygomimus) turionellae*: An additional solution to the reliability-detectability problem. *Biological Control*, **11**(2), 10.1006/bcon.1997.0592.
- Wang, S., et al., 2020. Reproduction of ectoparasitic mites in a coevolved system: *Varroa* spp.—Eastern honey bees, *Apis cerana*. *Ecology and Evolution*, **10**(24), 10.1002/ece3.7038.
- Weihmann, T., Brun, P., & Pycroft, E., (2017). Speed dependent phase shifts and gait changes in cockroaches running on substrates of different slipperiness. *Frontiers in Zoology*. **14**, <https://doi.org/10.1186/s12983-017-0232-y>
- Winston, M.L., 1987. *The Biology of the Honeybee, Apis Mellifera*. Harvard University Press, Cambridge, Massachusetts.
- Wolff, J.O., 2021. Locomotion and kinematics of arachnids. *Journal of Comparative Physiology*, **207**(2), 10.1007/s00359-021-01478-2.
- Wu, Y.Y., et al., 2015. Multiple virus infections and the characteristics of Chronic bee paralysis virus in diseased honey bees (*Apis mellifera* L.) in China. *Journal of Apicultural Science*, **59**(2), 10.1515/JAS-2015-0026.
- Xie, X., Huang, Z.Y., and Zeng, Z., 2016. Why do Varroa mites prefer nurse bees? *Scientific Reports*, **6**, 10.1038/srep28228.
- Yang, C., and Collins, J., 2019. Deep learning for pollen sac detection and measurement on honey bee monitoring video. In: *2019 International Conference on Image and Vision Computing New Zealand (IVCNZ)*. IEEE, pp.1-6.
- Yones, M.S., Ma'moun, S.A., Farag, R.M., and Abd El-Raouf, M.M., 2019. Hyperspectral application for early diagnosis of American foulbrood disease in the honey bee (*Apis mellifera* L.) larvae. *Egyptian Journal of Remote Sensing and Space Science*, **22**(3), 10.1016/j.ejrs.2019.05.002.
- Yu, B., et al., 2022. Beehive sound: Can it indicate the response of honey bees to chemicals in or out of the beehive?. Preprint, 10.21203/rs.3.rs-1302604/v1.
- Zacepins, A., Brusbardis, V., Meitalovs, J., and Stalidzans, E., 2015. Challenges in the development of Precision Beekeeping. *Biosystems Engineering*, **130**, 10.1016/j.biosystemseng.2014.12.001.
- Zacepins, A., Kviesis, A., Stalidzans, E., Liepniece, M., and Meitalovs, J., 2016. Remote detection of the swarming of honey bee colonies by single-point temperature monitoring. *Biosystems Engineering*, **148**, 10.1016/j.biosystemseng.2016.05.012.
- Zacepins, A., Pecka, A., Osadcuks, V., Kviesis, A., and Engel, S., 2017. Solution for automated bee colony weight monitoring. *Agronomy Research*, **15**(2), pp.585-593.
- Zakaria, M., and Allam, S., 2009. New acarine setal receptors of *Varroa Destructor*. *Acarines: Journal of the Egyptian Society of Acarology*, **3**(1), 10.21608/ajesa.2009.4962.

- Zgank, A., 2020. Bee swarm activity acoustic classification for an iot-based farm service. *Sensors*, **20**(1), 10.3390/s20010021.
- Zgank, A., 2021. Iot-based bee swarm activity acoustic classification using deep neural networks. *Sensors*, **21**(3), 10.3390/s21030676.
- Zhao, J., et al., 2019. Abdominal pumping involvement in the liquid feeding of honey bee. *Journal of Insect Physiology*, **112**, 10.1016/j.jinsphys.2018.11.002.
- Zhao, Y., et al., 2021. Based investigate of beehive sound to detect air pollutants by machine learning. *Ecological Informatics*, **61**, 10.1016/j.ecoinf.2021.101246.
- Ziegelmann, B., Lindenmayer A, Steidle J, and Rosenkranz P., 2013. The mating behaviour of *Varroa destructor* is triggered by a female sex pheromone: Part 1: Preference behaviour of male mites in a laboratory bioassay. *Apidologie*, **44**(3), 10.1007/s13592-012-0182-5.